GDAŃSK UNIVERSITY OF TECHNOLOGY

The author of the PhD dissertation: Andam Mustafa
Scientific discipline: Environmental Engineering, Mining and Energy

DOCTORAL DISSERTATION

Title of PhD dissertation: Urban flash flood hazard identification and assessment applying geospatial techniques and hydrodynamic modeling; Erbil city case study, Kurdistan Region of Iraq.

Title of PhD dissertation (in Polish): Identyfikacja i ocena zagrożenia powodziami błyskawicznymi w miastach z wykorzystaniem technik geoprzestrzennych i modelowania hydrodynamicznego; Studium przypadku miasta Erbil, Region Kurdystanu w Iraku.

Supervisor   Signature
dr hab. inż. Michał Szydłowski, prof. Gdańsk Tech

Gdańsk, 2023

GDAŃSK UNIVERSITY OF TECHNOLOGY

STATEMENT

The author of the PhD dissertation: Andam Mustafa

I, the undersigned, declare that I am aware that in accordance with the provisions of Art. 27 (1) and (2) of the Act of 4th February 1994 on Copyright and Related Rights (Journal of Laws of 2021, item 1062), the university may use my doctoral dissertation entitled:
"Urban flash flood hazard identification and assessment applying geospatial techniques and hydrodynamic modeling; Erbil city case study, Kurdistan Region of Iraq." for scientific or didactic purposes.[1]

Gdańsk, 05th April 2023 …….……....…….
signature of the PhD student

Aware of criminal liability for violations of the Act of 4th February 1994 on Copyright and Related Rights and disciplinary actions set out in the Law on Higher Education and Science (Journal of Laws 2021, item 478), as well as civil liability, I declare, that the submitted doctoral dissertation is my own work.
I declare, that the submitted doctoral dissertation is my own work performed under and in cooperation with the supervision of dr hab. inż. Michał Szydłowski, prof. Gdańsk Tech.

This submitted PhD dissertation has never before been the basis of an official procedure associated with the awarding of a PhD degree.
All the information contained in the above dissertation which is derived from written and electronic sources is documented in a list of relevant literature in accordance with art. 34 of the Copyright and Related Rights Act.
I confirm that this PhD dissertation is identical to the attached electronic version.

Gdańsk, 05th April 2023 …….……....…….
signature of the PhD student

I, the undersigned, agree to include an electronic version of the above PhD dissertation in the open, institutional, digital repository of Gdańsk University of Technology.

Gdańsk, 05th April 2023 …….……....…….
signature of the PhD student

---

[1] Art 27. 1. Educational institutions and entities referred to in art. 7 sec. 1 points 1, 2 and 4–8 of the Act of 20 July 2018 – Law on Higher Education and Science, may use the disseminated works in the original and in translation for the purposes of illustrating the content provided for didactic purposes or in order to conduct research activities, and to reproduce for this purpose disseminated minor works or fragments of larger works.

2. If the works are made available to the public in such a way that everyone can have access to them at the place and time selected by them, as referred to in para. 1, is allowed only for a limited group of people learning, teaching or conducting research, identified by the entities listed in paragraph 1.

GDAŃSK UNIVERSITY OF TECHNOLOGY

DESCRIPTION OF DOCTORAL DISSERTATION

The Author of the PhD dissertation: M.Sc. Eng. Andam Mustafa

Title of PhD dissertation: Urban flash flood hazard identification and assessment applying geospatial techniques and hydrodynamic modeling; Erbil city case study, Kurdistan Region of Iraq.

Language of PhD dissertation: English

Supervision: dr hab. inż. Michał Szydłowski, prof. Gdańsk Tech

Date of doctoral defence:

Keywords of PhD dissertation in English: urban flash floods; extreme rainfall events; LULC; hydrological modeling; hydrodynamic modeling; numerical simulation; Erbil; flood hazard maps

Keywords of PhD dissertation in Polish: miejskie powodzie błyskawiczne; ekstremalne opady deszczu; LULC; modelowanie hydrologiczne; modelowanie hydrodynamiczne; symulacja numeryczna; Irbil; mapy zagrożenia powodziowego

Summary of PhD dissertation in English: This dissertation aims to investigate the factors behind flash flooding in Erbil's central district, located in the Kurdistan Region of Iraq, and develop a methodology for assessing flood hazards in the city, despite limited data accessibility. In this thesis, each factor was investigated, including analyzing extreme precipitation events in the last two decades, including their spatial and temporal distribution of rainfall, intensity, and exceedance probability, and examines the impact of changes in Land Use and Land Cover (LULC) on the hydrological response of the Erbil basin. The hydrodynamic model's input data were generated using GIS-based modeling interface. HEC-RAS 2-D software package's suitability was ensured by evaluating two building representation techniques and two mathematical models (Diffusion-Wave Equations (DWE) and Shallow-Water Equations (SWE)) using the Toce River urban flood experimental model. The study utilized a two-dimensional hydrodynamic model (HEC-RAS 2-D) to assess the susceptibility, vulnerability, and socioeconomic impact of flooding in the study area. Using the model, flood hazard maps were created to show the extent of potential flooding in the study area during various rainfall events and return periods. Ultimately, the study concludes that without essential engineering measures, there is an increased probability of flooding in the center of Erbil.

Summary of PhD dissertation in Polish: Rozprawa ma na celu zbadanie czynników będących przyczyną gwałtownych powodzi w centralnej dzielnicy Erbil w Regionie Kurdystanu w Iraku oraz opracowanie metodyki oceny zagrożenia powodziowego w mieście przy ograniczonej dostępności danych. W pracy przeanalizowano ekstremalne opady atmosferyczne z ostatnich dwóch dekad, w tym ich przestrzenny i czasowy rozkład, intensywność i prawdopodobieństwo przekroczenia, a także zbadano wpływ zmian w użytkowaniu gruntów i pokryciu terenu (ang. LULC) na przebieg procesów hydrologicznych w zlewni Erbil. Dane do hydrodynamicznego modelu powodzi zostały opracowane przy użyciu narzędzi GIS. Prawidłowość wykorzystania oprogramowania HEC-RAS 2-D została potwierdzona przez zastosowanie dwóch technik reprezentacji budynków i dwóch modeli matematycznych (fali dyfuzyjnej [ang. DWE] i równań wody płytkiej [ang. SWE]) do analizy powodzi miejskiej na fizycznym modelu rzeki Toce. W badaniach wykorzystano dwuwymiarowy model hydrodynamiczny (HEC-RAS 2-D) do oceny podatności, wrażliwości i społeczno-ekonomicznych skutków powodzi na badanym obszarze. Korzystając z modelu, utworzono mapy zagrożenia powodziowego, w celu określenia zasięgu potencjalnej powodzi na badanym obszarze podczas opadów różnych okresach powtarzalności. Z badań wynika, że bez podjęcia niezbędnych działań inżynierskich istnieje zwiększone prawdopodobieństwo powodzi w centrum Erbil.

GDAŃSK UNIVERSITY OF TECHNOLOGY

M.Sc. Eng. Andam Mustafa

URBAN FLASH FLOOD HAZARD IDENTIFICATION AND ASSESSMENT APPLYING GEOSPATIAL TECHNIQUES AND HYDRODYNAMIC MODELING; ERBIL CITY CASE STUDY, KURDISTAN REGION OF IRAQ

Identyfikacja i ocena zagrożenia powodziami błyskawicznymi w miastach z wykorzystaniem technik geoprzestrzennych i modelowania hydrodynamicznego; Studium przypadku miasta Erbil, Region Kurdystanu w Iraku.

DOCTORAL DISSERTATION

Supervisor:
dr hab. inż. Michał Szydłowski, prof. Gdańsk Tech

GDAŃSK 2023

No individual raindrop ever considers itself responsible for the flood.

"John Ruskin"

This dissertation is dedicated to my lovely wife, Nsar, and our children, Zheer and Zhelia. Throughout my academic career, their unwavering love and support have been indispensable!

Dedicated to the most wonderful parents in the world.

Acknowledgements

I would like to express my sincere appreciation to my supervisor, Professor Michał Szydłowski, for providing me with the opportunity to pursue a doctoral degree. His never-ending efforts helped me stay on track. I was motivated to become an effective researcher by his unwavering support. During the course of my research, I was fortunate enough to receive guidance on how to create a strong network from a seasoned professional.

"Behind every successful man, there is a strong woman", according to this popular proverb, I would want to emphasize that my wife and life partner (Nsar Garari) is the main reason for my accomplishment in obtaining a PhD degree. Doctoral study would have been difficult for me without her assistance. She is a supportive wife, a master's degree holder, a professional employee, and a powerful woman in my eyes.

In addition, I would want to express my gratitude to my lovely children (Zheer and Zhelia). During the course of my PhD study, I frequently found that I did not have enough time to spend with them. I hope that my achieving this degree will make them proud and that in the future I will be capable of compensating for those days.

I would like to thank my parents for all of the support they have given me and the great amount of patience they have shown throughout the five years. My aunt and my siblings have, like they always have, offered me their steadfast support, and because of this, a straightforward expression of thanks on my behalf is also insufficient.

I would like to express my sincere gratitude to the Presidency of the Erbil municipality, Ministry of Municipalities and Tourism - Kurdistan Regional Government (KRG), for generously granting me the opportunity to pursue a PhD degree. This incredible chance allowed me to continue my academic pursuits and contribute to the advancement of my field. I am deeply honored and grateful for this support.

Special thanks to my academic colleagues from our Department of Geotechnical and Hydraulic Engineering, Faculty of Civil and Environmental Engineering, Gdansk University of Technology, who have helped me in different stages of this journey. These academic colleagues include Dr. Tomasz Kolerski, Dr. Katarzyna Weinerowska-Bords, Dr. Wojciech Artichowicz.

Finally, I would like to extend my gratitude to everyone who assisted me in successfully completing my PhD study and I would also like to apologize for the fact that I did not name everyone who assisted me in this endeavor.

Funding and research

This research did not receive any specific grant from funding agencies in the public, commercial, or not-for-profit sectors.

Table of Contents

List of Figures

List of Tables

Nomenclature and Abbreviations

Abbreviations	Description
2-D	Two-Dimensional
3-D	Three-Dimensional
A.S.L	Above Sea Level
AIDR	Australian Institute for Disaster Resilience
AMS	American Meteorology Society
AP	Anisotropic Porosity
BB	Building Block
BH	Building Hole
BP	Building Porosity
BR	Building Resistance
CFSR	Climate Forecast System Reanalysis
cm	Centimeter
CN	Curve Number
CN-SCS	Curve Number-Soil Conservation Service
D	Depth
DEM	Digital Elevation Model
DTM	Digital Terrain Model
DW	Diffusion Wave
DWE	Diffusion Wave Equations
ETM+	Enhanced Thematic Mapper Plus
FAO	Food and Agriculture Organization
FME	Feature Manipulation Engine
GDMS	General Directorate of Meteorology and Seismology
GDP	Gross Domestic Product
GIS	Geographic Information System
HEC-HMS	Hydrologic Engineering Center-Hydrologic Modeling System
HEC-RAS	Hydrologic Engineering Center-River Analysis System
hr	Hour/s
HSG	Hydrologic Soil Groups
IDF	Intensity-Duration-Frequency
IMD	Indian Meteorological Department
KRG	Kurdistan Regional Government
KRI	Kurdistan Region of Iraq
KRSO	Kurdistan Region Statistics Office
LDCM	Landsat Data Continuity Mission
LPT	Log-Pearson Type III
LULC	Land Use Land Cover
m	Meter
MENA	Middle East and North Africa
min	Minutes
MLC	Maximum Likelihood Classifier
mm	Milimeter
MSS	Multispectral Scanner
PM	Porosity Model
PPMCC	Pearson Product-Moment Correlation Coefficient

RMSE	Root Mean Square Error
RS	Remote Sensing
s	Seconds
SRTM	Shuttle Radar Topography Mission
SWE	Shallow Water Equations
SWE-ELM	Shallow Water Equations-Eulerian-Lagrangian Method
TM	Thematic Mapper
V	Velocity
ZI	Diffusion Model

Summary

Floods are a type of natural disaster that is responsible for a significant number of deaths and property damage. Cities in general have become locations that are more prone to be flooded as a result of continued urbanization and population growth. In addition, the consequences of climate change contribute to variation of the hydrological cycle. More damage is caused by this phenomenon in developing countries than in developed countries. Historically speaking, though, flooding in Erbil, Kurdistan Region of Iraq (KRI), is not an uncommon occurrence. However, during the past two decades, the frequency of floods has grown, causing concern among city residents.

In this thesis, a comprehensive review of the research efforts conducted in the study area has been carried out. It has been found that this work will constitute the first step in dealing with the issue of urban flooding in Erbil. Therefore, it was essential to approach this research in a methodical manner, beginning with the collection of rainfall data and the development of hydrological models, and then proceeding to the development of hydrodynamic models with the assistance of Remote Sensing (RS) data and geospatial techniques. The research process as a whole was plagued by several challenges and difficulties, the most significant of which was the absence or poor quality of data. In particular, the rainfall data series had gaps in recording, and the data were recorded on a 24-hour (hr) basis, which could influence the model's outcomes. No Digital Elevation Models (DEMs) with high resolution were available for the research area, and there were no high-quality satellite images available. Drainage network maps for the city and many others were also unavailable, which made carrying out the research a challenge. The purpose of this dissertation is to identify, evaluate, and simulate urban flash floods in the central district of Erbil Province. Additionally, the utilitarian goal of the work is to assess the flood hazard in the city by developing flood hazard maps.

In the first phase, a detailed evaluation and analysis of extreme precipitation events that have occurred in the last two decades was conducted, focusing on spatial and temporal rainfall distribution, intensity rate, and exceedance probability. In addition, Intensity-Duration-Frequency (IDF) curves for the city center of Erbil were derived using daily rainfall depth measurements from the Erbil meteorological station. Furthermore, empirical formulas were developed to estimate precipitation intensity for different return periods and durations.

In the following phase, the aim was to prepare the hydrological model, which involved evaluating, identifying, and categorizing changes in LULC in the central district of Erbil Province. To effectively manage hydro-structures and monitor environmental changes, particular attention was paid to the impact of rapid urban expansion on the central part of the city. Using data from RS and various

geospatial techniques in the study area, changes in LULC were examined and analyzed in five different periods, starting from 1984, 1994, 2004, 2014, and 2019. Subsequently, the hydrological model was developed using the Hydrologic Engineering Center-Hydrologic Modeling System (HEC-HMS), based on the data obtained from LULC. This allowed for the comparison of alternative scenarios and evaluation of the transformation and development in the examined area.

Then, it was decided to begin developing a hydrodynamic model. However, as stated earlier, the absence or poor quality of data posed obstacles to the process of preparing a comprehensive model. As a result, it was decided to first test a previously prepared physical model (available in the literature) with Hydrologic Engineering Center-River Analysis System HEC-RAS 2-D to ensure that this software could be used to achieve the objectives of this research. Specifically, the purpose of this study is to evaluate the potential and capabilities of HEC-RAS 2-D in investigating the accuracy of various building representation techniques for modeling inundation processes within heterogeneous floodplains, as well as the computational efficiency of the models in terms of different grid resolutions and roughness coefficients.

In the final phase, the data and information collected throughout the research were used to develop a hydrodynamic model of urban flooding in Erbil using HEC-RAS 2-D. To ensure the quality of the data used in flood modeling, different precision DEMs were utilized, and the output of the DEM was studied in terms of low and high-resolution models. The aim was to identify areas that were vulnerable to flooding and address some of the gaps left by previous research on stormwater management in Erbil.

It is important to note that uncertainty is a natural part of any modeling process and can arise from various sources such as data quality, assumptions made during modeling, and limitations of the numerical methods used. This uncertainty can impact the accuracy of the flood model's results and their ability to reflect reality. Despite these challenges, the findings and results of this dissertation are still significant and valuable for both scientific and practical applications. While there may be limitations to the accuracy of the model due to data limitations and other factors, the approach and methodology used in this study can serve as a foundation for future research and improvements in flood modeling in Erbil and other areas prone to urban flooding.

The analysis of the likelihood of exceeding the maximum rainfall in Erbil indicated that rainfalls with probabilities of 1%, 10%, and 20% are relatively high. They come out to 113.45, 71.16 and 59.45 mm, respectively. It is crucial to determine the reasons for flash floods in the studied area, including terrain, urban growth, the sewer system, and awareness, as well as the intensity rate and temporal

distribution of rainfall. Between 1984 and 2004, bare land and built-up areas consistently increased, whereas between 2004 and 2019, built-up areas increased dramatically by about 245%. From 1984 to 2019, permeable areas such as agricultural land and vegetation declined steadily. One of the main causes of flooding is the transformation of the topsoil layer, which limits the absorption of rain. Due to the obstruction of natural drainage and decreasing permeability, hydrological simulations have demonstrated that urbanization may significantly exacerbate flooding induced by a particular storm.

The HEC-RAS 2-D model can simulate unsteady urban flooding using two building representation techniques, Building-Block (BB) and Building-Resistance (BR). The BR technique accurately represents building units in numerical simulations by employing high Manning coefficients. One remarkable and powerful aspect of BR is that predictions of velocity and water depth are highly sensitive to the value of the Manning coefficient used for developed building units. BR is a good option when detailed building geometry data or DEMs are not available and can be used with any kind of computational mesh resolution.

The HEC-RAS 2-D hydrodynamic model was utilized to estimate the extent of flooding in the studied area under various flooding events with different return periods. The results showed that the inundated areas and water accumulation zones in Erbil were consistent with those identified in the numerical simulations. However, efforts were made to create flood hazard maps to provide both short-term and long-term solutions for the study area.

پوختەی توێژینەوە

لافاو دیاردەیەکی سروشتییە، هەندێک جار کارەساتی لێدەکەوێتەوە. وەهەرەوها لافاو باوترین و بەربڵاوترین کارەساتی سروشتیە کە پەیوەندیداربێت بە گۆڕانی ئاو و هەوا. بە گشتی، کە لە شارەکان ڕووبدات قەبارەی زیانە گیانی و مادیەکانی گەورەتر دەبن، چونکە لە شارەکاندا چڕی دانیشتووان زۆرترە. زیانەکانی لافاو لە وڵاتانی تازەپێگەیشتوودا زیاترە بە بەراورد بە وڵاتانی پێشکەوتوو. چونکە لە شارەکاندا، کاتێک ڕێڕەوە ئاوییە سروشتییەکان دەگۆڕدرێن، کەمتر ڕەچاوی جڵەوگیری و گلدانەوەی لافاو دەکرێت. لە مێژووی هەوڵێری پایتەختی هەرێمی کوردستانی عێراقدا، لافاو ڕووداوێکی نامۆ نییە. بەڵام لە ماوەی دوو دەیەی ڕابردوودا، ژمارەی لافاوەکان زیادی کردووە، ئەمەش بۆ گۆڕینی هەڕەمەکیی ڕێڕەوە ئاوییە سروشتییەکان دەگەڕێتەوە.

لەم تێزەدا پێداچوونەوەیەکی گشتگیر بە تێو ئەو هەوڵە زانستیانەدا کراوە کە لە ڕابردوودا لەو بوارەدا ئەنجامدراون. وا دەردەکەوێت کە ئەم کارە هەوڵی یەکەمی مامەڵەکردن بێت لەگەڵ پرسی لافاو لە شاری هەوڵێر. بۆیە زۆر گرنگ بوو کە بە شێوەیەکی میتۆدی کار لەسەر ئەم لێکۆڵینەوەیە بکرێت. سەرەتا بە کۆکردنەوەی زانیاری و داتای بارانبارین و پەرەپێدانی مۆدێلی هایدرۆلۆجی دەست پێکرا، پاشان بەردەوامی بە کارەکان درا بۆ پەرەپێدانی مۆدێلی هایدرۆداینامیکی، بە سوود وەرگرتن لە داتاکانی هەستکردن لە دوورەوە (RS) و تەکنیکە جیۆفەزاییەکان (GIS). پرۆسەی توێژینەوەکە بە گشتی بە دەست چەندین ئاڵنگاری و کێشەوە گیرۆدە بوو، کە سەختترینیان نەبوونی زانیاریی ورد و گشتگیربوو. بە تایبەتی لە زنجیرە داتاکانی بارانبارینداء، کەم و کوڕی لە تۆمارکردنیاندا هەبوو، بە جۆرێک داتاکان لەسەر بنەمای ٢٤ سەعات تۆمارکراون، ئەمەش دەتوانێت کاریگەری لەسەر دەرئەنجامەکانی مۆدێلەکە هەبێت. هیچ مۆدێلێکی بەرزونزمی دیجیتاڵی (DEM) بە ڕوونییەکی تەواو، بۆ ناوچەی توێژینەوەکە لەبەردەستدا نەبوو، هەروەها هیچ وێنەیەکی کوالیتیی بەرزی مانگی دەستکرد لەبەردەستدا نەبوو. دیسانەوە نەخشەی تۆڕەکانی ئاوەڕۆ بۆ شارەکە و چەندین نەخشەی دیکە بەردەست نەبوون. ئەمانەش وایانکرد ئەنجامدانی توێژینەوەکە ببێتە تەحەدایەک. مەبەست لەم تێزی دکتۆرایە دەستنیشانکردن و هەڵسەنگاندن و هاوشێوەکردنی لافاوە لە قەزای ناوەندی پارێزگای هەوڵێر. سەرەڕای ئەوەش، ئامانجی سوودمەندانەی کارەکە هەڵسەنگاندنی مەترسیی لافاوە لە شارەکەدا بە ئامادەکردنی نەخشەی مەترسیی لافاو.

لە قۆناغی یەکەمدا هەڵسەنگاندن و شیکارییەکی وردی ڕووداوەکانی بارانبارینی بەخۆر کە لە بیست ساڵی ڕابردوودا ڕوویانداوە ئەنجامدرا، کە تیایدا تیشک خرایە سەر دابەشبوونی زەمەنی و جوگرافیی بارانبارین، ڕێژەی توندی و ئەگەری بارینی زۆرترین باران لە ڕۆژێکدا. جگە لەوەش، هێڵەکانی توندی-ماوە-فرێکوێنسی (IDF) بۆ سەنتەری شاری هەوڵێر بە بەکارهێنانی بڕی بارانبارینی ڕۆژانە لە وێستگەی کەشناسیی هەوڵێرەوە ئامادەکراون. جگە لەوەش، هاوکێشەی ئەزموونی پەرەی پێدرا بۆ خەملاندنی توندی بارانبارین بۆ ماوەی جیاوازی باران بارین.

لە قۆناغی دواتردا ئامانج ئامادەکردنی مۆدێلی هایدرۆلۆجی بوو، کە بریتیبوو لە هەڵسەنگاندن و دەستنیشانکردن و پۆلێنکردنی گۆڕانکارییەکان لە ڕووپۆشی زەوی (LULC) لە قەزای ناوەندیی پارێزگای هەوڵێر. بۆ بەڕێوەبردنێکی کاریگەرانەی پرۆژەکانی تایبەت بە سەرچاوەکانی ئاو و چاودێریکردنی گۆڕانکارییە ژینگەییەکان، گرنگییەکی تایبەت درا بە کاریگەرییەکانی فراوانبوونی خێرای سەنتەری شاری هەوڵێر. بە بەکارهێنانی داتاکانی هەستکردن لە دوورەوە و تەکنیکە جیۆفەزاییە جیاوازەکان لە ناوچەی لێکۆڵینەوەلێکراودا، گۆڕانکارییەکان لە ڕووپۆشی زەوی لە پێنج قۆناغی جیاوازدا پشکنران و شیکرانەوە، کە لە ساڵانی 1984، 1994، 2004، 2014، و2019. دواتر مۆدێلی هایدرۆلۆجی بە بەکارهێنانی بەرنامەی (HEC-HMS) ئامادەکرا، بە پشتبەستن بەو زانیاریانەی کە لە شیکردنەوەی ڕووپۆشی زەوی وەرگیراون. ئەمەش ڕێگەخۆشکەر بوو بۆ بەراوردکردنی سیناریۆ جیاوازەکان و هەڵسەنگاندنی گۆڕانکاری و گەشەکردنەکان لە ناوچەی لێکۆڵینەوەلێکراودا.

پاشان، بڕیاردرا دەست بە ئامادەکردنی مۆدێلێکی هایدرۆداینامیکی بکرێت، بەڵام وەکو لە پێشتر ئاماژەمان پێدا، نەبوونی یان کوالیتیی خراپی داتاکان، بەربەستی لەبەردەم پرۆسەی ئامادەکردنی مۆدێلێکی گشتگیردا دروستکرد. بۆیە لەم سۆنگەیەوە بڕیار درا سەرەتا مۆدێلێکی فیزیکی پێشتر ئامادەکراو (لە وتارەکاندا بەردەستە) بە بەکارهێنانی پرۆگرامی HEC-RAS 2-D تاقیبکرێتەوە بۆ دڵنیابوون لەوەی کە دەتوانرێت ئەم پرۆگرامە بەکاربهێنرێت بۆ گەیشتن بە ئامانجەکانی ئەم توێژینەوەیە. بە تایبەتی ئامانجی ئەم توێژینەوەیە هەڵسەنگاندنی تواناکانی HEC-RAS 2-D لە لێکۆڵینەوە لە وردی تەکنیکە جیاوازەکانی نوێنەرایەتیکردنی بینا بۆ مۆدێلکردنی پرۆسەکانی لافاو. هەروەها کارایی حیساباتی مۆدێلەکە لە ڕووی بەکارهێنانی تۆڕی جیاواز و ڕێژەی زبری.

لە قۆناغی کۆتاییدا، ئەو داتا و زانیارییانەی کە بە درێژایی توێژینەوەکە کۆکراونەتەوە، بەکارهێنران بۆ پەرەپێدانی مۆدێلێکی هایدرۆداینامیکی بۆ ئامادەکردنی مۆدێلی لافاوی شاری هەولێر بە بەکارهێنانیHEC-RAS 2-D . بۆ دڵنیابوون لە کوالیتیی ئەو زانیاریانەی کە لە مۆدێلکردنی لافاودا بەکارهێنراون، (DEM) بە وردی جیاواز بەکارهێنرا، وە ئەنجامەکان لە ڕووی مۆدێلی ڕوونی نزم و بەرزەوە لێکۆڵینەوەی لەسەر کرا. ئامانج لێی دەستنیشانکردنی ئەو ناوچانە بوو کە بەرکەوتەی لافاو بوون و پڕکردنەوەی بەشێک لەو بۆشاییانە بوو کە لێکۆڵینەوەکانی پێشووتر لەسەر بەڕێوەبردنی ئاوی باران لە هەولێر بەجێیان هێشتووە.

بەگرنگی دەزانین ئاماژە بەوەش بکەین کە نادڵنیایی بەشێکی سروشتی هەر پرۆسەیەکی مۆدێلکردنە و دەتوانێت لە سەرچاوە جیاوازەکانەوە سەرهەڵبدات وەک جۆرایەتیی زانیاریەکان، گریمانەکانی کە لە کاتی مۆدێلکردندا دەکرێن، و سنووردارى شێوازە ژمارەییەکانی بەکارهێناو. ئەم نادڵنیاییە دەتوانێت کاریگەری لەسەر وردی ئەنجامەکانی مۆدێلی لافاو و توانای ڕەنگدانەوەی واقیعیان هەبێت. سەرەڕای ئەم ئاڵنگارییانە، دۆزینەوە و ئەنجامەکانی ئەم تێزە هێشتا گرنگ و بەنرخن بۆ هەردوو بەکارهێنانی زانستی و پراکتیکی. لە کاتێکدا ڕەنگە سنووردارىبوون لە وردبینیی مۆدێلەکەدا هەبێت بەهۆی سنووردارىبوونی داتا و هۆکارەکانی دیکە، بەڵام ئەو ڕێباز و میتۆدۆلۆژیایەی لەم توێژینەوەیەدا بەکارهێناوە دەتوانێت ببێتە بناغەیەک بۆ لێکۆڵینەوەکانی داهاتوو و باشترکردنی مۆدێلی لافاو لە هەولێر و ناوچەکانی دیکە کە تووشی لافاو دەبن.

شیکاری ئەگەری تێپەڕاندنی زۆرترین بڕی بارانبارین لە هەولێر نیشانی ئەوە دەدا کە بارانبارین بە ئەگەری 1%، 10%، و 20% تارادەیەک زۆرە. کە یەکسانە بە 113.45 و 71.16 و 59.45 ملم یەک لە دوای یەک. دیاریکردنی هۆکارەکانی لافاوی بەخوڕ لەو ناوچانەی لێکۆڵینەوەیان لێ کراوە، زۆر گرنگە، لەوانە بەرز و نزمیی زەوی، گەشەی شارەکە، سیستەمی ئاوەڕۆ و هۆشیاریی گشتی، هەروەها ڕێژەی توندی و دابەشبوونی زەمەنی بارانبارین. لە نێوان ساڵانی ١٩٨٤ بۆ ٢٠٠٤، خاکە ڕووتەکان و ناوچە بنیاتنراوەکان بە بەردەوامی زیادیان کردووە، لە کاتێکدا لە نێوان ساڵانی ٢٠٠٤ بۆ ٢٠١٩، ڕووبەری ناوچە بنیاتنراوەکان بە ڕێژەی نزیکەی ٢٤٥% زیادی کردووە. لە ساڵی ١٩٨٤ تا ٢٠١٩ ئەو زەویانەی کە توانای هەڵمژینیان هەیە وەکو زەویی کشتوکاڵی و سەوزاییەکان، بە شێوەیەکی بەردەوام ڕێژەکەیان دابەزینی بەخۆوە بینیوە. یەکێک لە هۆکارە سەرەکییەکانی لافاو گۆڕانی چینی سەرەوەی خاکە، کە دەبێتە هۆی سنووردارکردنی هەڵمژینی باران. بەهۆی ڕێگریکردن لە ئاوەڕۆی سروشتی و کەمبوونەوەی توانای هەڵمژین. هاوشێوەکردنی هایدرۆلۆجی دەریخستووە کە شارنشینی ڕەنگە بە شێوەیەکی بەرچاو ئەو لافاوانەی کە بەهۆی بارانێکی بەخوڕ دروست دەبێت، بەهێزتر بکاتەوە.

مۆدێلی HEC-RAS 2-D دەتوانێت لافاوێکی ناجێگیر(unsteady) شارەکان هاوشێوە بکات بە بەکارهێنانی دوو تەکنیک بۆ نوێنەرایەتیکردنی بینا، (BB) و(BR). دەرکەوت کە تەکنیکی (BR) بە وردی یەکەکانی بینا لە هاوشێوەکردنی ژمارەییدا نیشان دەدات بە بەکارهێنانی ڕێژەیەکی بەرزی زبری کە ناسراوە بە (Manning Coefficient). لایەنێکی سەرنجڕاکێش و بەهێزی (BR) ئەوەیە کە پێشبینییەکانی خێرایی و قوواڵیی ئاو زۆر هەستیارن بە بەهای (Manning Coefficient) کە بۆ یەکەکانی بینا دروستکراو بەکاردەهێنرێت. (BR) بژاردەیەکی باشە کاتێک داتای ووردی دابەشبوونی ئەندازەیی بینا و باڵەخانەکان یان DEM بەردەست نییە و دەتوانرێت لەگەڵ هەر جۆرە ڕوونییەکی تۆری حیساباتی بەکاربهێنرێت.

مۆدێلی هایدرۆداینامیکی بە بەکارهێنانی HEC-RAS 2-D بەکارهێنرا بۆ خەملاندنی فراوانیی لافاو بۆ دیوەی ناوەوەی شەقامی ١٢٠ مەتری هەولێر لە ژێر ڕووداوە جۆراوجۆرەکانی بارانی بە خوڕ بە ئەگەری دووبارەبوونەوەی جیاواز. ئەنجامەکان دەریانخست کە ناوچە ژێرئاوکەوتووەکان و ئەو ناوچانەی کە ئاوی باران تێیاندا لە هەولێر کۆدەبێتەوە لەگەڵ ئەوانەی لە هاوشێوەکردنی ژمارەییدا دەستنیشانکراون یەکدەگرنەوە. لەگەڵ ئەوشدا هەوڵ درا بۆ دروستکردنی نەخشەی مەترسیی لافاو بۆ دابینکردنی چارەسەریی کورتخایەن و درێژخایەن بۆ ناوچەی لێکۆڵینەوەکە.

Streszczenie

Powodzie są rodzajem klęski żywiołowej, która jest odpowiedzialna za znaczną liczbę ofiar śmiertelnych i szkód materialnych. Ogólnie rzecz biorąc, miasta stały się miejscami, które są bardziej podatne na powodzie w wyniku ciągłej urbanizacji i wzrostu liczby ludności. Ponadto skutki zmian klimatu przyczyniają się do modyfikacji cyklu hydrologicznego. Zjawisko to powoduje więcej szkód w krajach rozwijających się, niż w krajach rozwiniętych. Jednak historycznie rzecz biorąc, powódź w Erbil, w irackim regionie Kurdystanu, nie jest zjawiskiem rzadkim. Ponadto w ciągu ostatnich dwóch dekad częstotliwość powodzi wzrosła, wywołując niepokój wśród mieszkańców miast.

W niniejszej rozprawie dokonano kompleksowego przeglądu stanu wiedzy na temat badań, które zostały przeprowadzone na rozpatrywanym obszarze. Według wiedzy Autora, praca ta jest pierwszą próbą kompleksowej oceny przyczyn i potencjalnych skutków powodzi miejskich w Erbil. Dlatego istotne było podejście do przeprowadzonych badań w sposób metodyczny, począwszy od zebrania danych o opadach i opracowania modeli hydrologicznych, a następnie przystąpienie do opracowania modeli hydrodynamicznych z wykorzystaniem danych teledetekcyjnych i technik geoprzestrzennych. Proces badawczy jako całość był obarczony kilkoma wyzwaniami i trudnościami, z których najważniejszym był brak lub niska jakość potrzebnych danych. W szczególności, serie danych dotyczących opadów mają luki w zapisie, a dane pomiarowe były często rejestrowane tylko w trybie 24-godzinnym, co mogło wpłynąć na wyniki modelowania. Ponadto, dla obszaru badawczego nie były dostępne cyfrowe modele terenu (DEM) o wysokiej rozdzielczości. Nie było również dostępnych zdjęć satelitarnych wysokiej jakości. Mapy sieci melioracyjnej oraz kanalizacji także były niedostępne. Z tego powodu przeprowadzenie badań było dużym wyzwaniem.

Celem naukowym tej rozprawy jest identyfikacja przyczyn, symulacja występowania oraz ocena potencjalnych hydraulicznych skutków miejskich powodzi błyskawicznych w centralnej dzielnicy prowincji Erbil. Ponadto utylitarnym celem pracy jest ocena zagrożenia powodziowego w mieście, poprzez opracowanie map zagrożenia powodziowego.

W pierwszej fazie dokonano szczegółowej oceny i analizy ekstremalnych zdarzeń opadowych, które wystąpiły w ostatnich dwóch dekadach pod kątem przestrzennego i czasowego rozkładu opadów, ich natężenia oraz prawdopodobieństwa przekroczenia. Ponadto, na podstawie dziennych pomiarów wysokości opadów ze stacji meteorologicznej Erbوwil, wyznaczono krzywe intensywności, czasu trwania i częstotliwości (IDF) dla centrum miasta Erbil. Opracowano również wzory empiryczne do szacowania intensywności opadów dla różnych okresów i czasów ich trwania.

W kolejnej fazie, w celu przygotowania modelu hydrologicznego, podjęto próbę oceny, identyfikacji i kategoryzacji zmian w pokryciu i zagospodarowaniu terenu (ang. LULC) w centralnym okręgu prowincji Erbil. Aby właściwie zarządzać urządzaniami wodnymi w mieście i monitorować zmiany w środowisku, pomocne byłoby zwrócenie szczególnej uwagi na to, jak szybko ekspansja urbanistyczna wpływa na centralną część miasta. Wykorzystując dane z RS i różne techniki geoprzestrzenne, na badanym obszarze zbadano i przeanalizowano zmiany LULC w pięciu różnych okresach. Etapy czasowe rozpoczęły się w latach 1984, 1994, 2004, 2014 i 2019. Następnie, korzystając z danych uzyskanych z LULC, stworzono model hydrologiczny typu opad-odpływ dla zlewni Erbil, przy użyciu Systemu Modelowania Hydrologicznego Centrum Inżynierii Hydrologicznej (HEC-HMS). Zrobiono to w celu porównania alternatywnych scenariuszy procesu transformacji opadu w odpływ ze zlewni oraz oceny wpływu zmian pokrycia terenu na ten proces na badanym obszarze.

Następnie postanowiono wykonać model hydrodynamiczny dla badanego obszaru. Jednak brak danych lub ich słaba jakość stanowiły przeszkodę w procesie przygotowania kompleksowego modelu w programie HEC-RAS 2-D. W związku z tym, zdecydowano, że najpierw program obliczeniowy zostanie przetestowany na dostępnych w literaturze danych, dotyczących modelowania fizycznego powodzi w dolinie rzeki Toce. Zrobiono to, aby upewnić się, że oprogramowanie może być wykorzystane do osiągnięcia celów pracy badawczej. W szczególności celem pierwszych analiz byłą ocena możliwości programu HEC-RAS 2-D w zakresie wykorzystania różnych technik reprezentacji budynków w modelowaniu powodzi, dokładności reprezentacji przebiegu zalewów powodziowych w heterogenicznych obszarach zalewowych oraz wydajności obliczeniowej modeli (DWE, SWE) w odniesieniu do różnych rozdzielczości siatki i współczynników szorstkości.

Na ostatnim etapie dane i informacje, które zostały przygotowane w trakcie wcześniejszych badań, zostały wykorzystane do opracowania w programie HEC-RAS 2-D hydrodynamicznego modelu powodzi miejskich w Erbil. Podjęto starania, aby ocenić jakość wyników uzyskiwanych z modelowania powodzi w zależności od dokładności DEM. Wyniki zostały ocenione pod kątem wykorzystania w modelu hydrodynamicznym DEM o niskiej i wysokiej rozdzielczości. Szczegółowo zbadano i omówiono wyniki otrzymane w wyniku zastosowania DEM o dobrej rozdzielczości. Oprócz badań nad modelowaniem miejskich powodzi w oprogramowaniu HEC-RAS 2-D, praktycznym celem pracy była próba zlokalizowania w Erbil obszarów szczególnie narażonych na powodzie deszczowe. Pozwoliło to na uzupełnienie luk, które pozostawiły wcześniejsze badania dotyczące zarządzania wodami opadowymi w Erbil.

Rodzaj i jakość danych oraz typy modeli matematycznych i metod numerycznych znacząco wpływają na niepewność wyników modelowania powodzi. Ze względu na to, że uzyskane w ramach

pracy doktorskiej ustalenia opierają się na ograniczonych danych, wyniki analiz nie do końca odpowiadają rzeczywistości. Jednak końcowy rezultat przeprowadzonych badań można ocenić jako zadowalający w ramach akceptowalnych ograniczeń i możliwy do wykorzystania jako podejście naukowe i w praktyce.

Analiza prawdopodobieństwa przekroczenia maksymalnych opadów w Erbil wykazała, że opady z prawdopodobieństwem 1%, 10% i 20% są relatywnie wysokie. Ich wysokości wynoszą odpowiednio 113,45, 71,16 i 59,45 mm. Kluczowe znaczenie ma określenie przyczyn gwałtownych powodzi na badanym obszarze, które obejmują ukształtowanie terenu, zabudowę miejską, system kanalizacyjny i świadomość czynników warunkujących dynamikę spływu, a także intensywność i rozkład czasowy opadów. W latach 1984-2004 liczba gruntów niezabudowanych i obszarów zabudowanych stale rosła, podczas gdy w latach 2004-2019 obszar zabudowany wzrósł drastycznie o około 245%. W latach 1984-2019 obszary przepuszczalne, takie jak grunty rolne i roślinność, stale się zmniejszały. Stąd ustalono, że jedną z głównych przyczyn powodzi jest przekształcenie wierzchniej warstwy gleby w taką, która ogranicza wchłanianie deszczu. Symulacje hydrologiczne wykazały, że ze względu na blokowanie naturalnego drenażu i zmniejszającą się przepuszczalność, urbanizacja może znacznie nasilić powodzie wywołane przez ekstremalny epizod opadowy.

Model HEC-RAS 2-D może odtwarzać nieustalone powodzie miejskie, wykorzystując dwie techniki reprezentacji budynków, którymi są BB i BR. W przypadku BR, technika ta odwzorowuje pojedyncze budynki lub ich zespoły przez wykorzystanie wysokich współczynników Manninga w rejonie zabudowy. Ciekawą i w rzeczywistości pożądaną cechą techniki BR jest to, że obliczane prędkości przepływu wody, a także głębokości są bardzo wrażliwe na wartość współczynnika Manninga, stosowanego do imitowania obecności zabudowy. Jest to dobra opcja, gdy szczegółowe dane geometrii budynku lub wystarczająco dokładny DEM nie są dostępne. Ponadto technika ta może być używana z dowolną rozdzielczością siatki obliczeniowej.

Model hydrodynamiczny HEC-RAS 2-D wykorzystano do oszacowania, jaka część badanego obszaru zostałaby zalana w wyniku różnych zdarzeń powodziowych z różnymi okresami powtarzalności. Ustalenia potwierdziły, że obszary zalane lub obszary, na których zgromadziła się woda w Erbil w czasie rzeczywistych powodzi, są takie same, jak te zidentyfikowane w symulacjach numerycznych. Niemniej jednak podjęto wysiłek przygotowania map zagrożenia powodziowego, aby zapewnić tymczasowe i długoterminowe rozwiązania w ramach zarządzania ryzykiem powodziowym na badanym obszarze.

1. Introduction

Floods are one of the leading causes of death, as well as the relocation of communities and damage to agriculture and infrastructure [1-3]. Rain is a naturally occurring phenomenon that provides a boon to life on Earth, but it also has the potential to be a major cause of catastrophic events and widespread devastation. The flood is the cause of the transformation of rain from a boon to a calamity. In 2021, a total of 432 catastrophes were reported, which is significantly more than the average of 357 catastrophes per year from 2001 to 2020. Floods dominated these events with 223 occurrences, an increase from the average of 163 yearly flood occurrences reported between 2001 and 2020 [4]. The intensity of both extremely wet and extremely dry events will rise as the climate continues to warm [5]. Floods are regarded as one of the natural disasters that are increasing in frequency as a consequence of climate change [6,7]. In 2019, 40% of natural disasters occurred in Asia, resulting in 45% of disaster-related deaths and 74% of the impacted population [8]. This indicates that the frequency and severity of floods are greater in developing countries than in developed countries. In fact, Asia is second only to Africa in the number of developing countries [9]. It is a fact that population, land area, urbanization rate, Gross Domestic Product (GDP), and forest coverage rate can influence the spatiotemporal variation of flood disasters in different countries [10,11].

The effects of climate change in the Middle East will be felt most strongly, especially in Iraq, Syria, and Iran, among other countries in the region. This includes drought, an increase in the frequency of dusty days, and extreme rainfalls for a short time [4]. This has had a negative impact on the escalation of water resource conflicts in the region, particularly in the countries in the Tigris and Euphrates river basins [12]. Notably, Iraq is located downstream of the basin, and Iran and Turkey mainly manage the basin's resources and discharge a lesser amount of water into Iraqi territory [13]. There are two opposing phenomena: floods and droughts. According to EM-DAT, in 2021, about seven million Iraqis were affected by drought [4]. On the other hand, according to Wang, *et al.* [14], Iraq is one of the countries where flash floods were the most prevalent flood disasters. Therefore, scientific efforts are required to mitigate the effects of these two contradictory natural occurrences in Iraq. In the preceding paragraph, floods were referred to as a catastrophe, however, they can be managed scientifically and technically to become a reliable water source.

The bordering countries of Iraq were investigated, including Turkey, Iran, Saudi Arabia, Jordan, and Kuwait, and it was observed that the frequency of floods is also increasing. Ercüment Beyhun, *et al.* [15] conducted research on the floods that were officially recorded in Turkey and observed that the number is increasing. The expansion of urban areas in the province of Bodrum in Turkey had a

significant influence on the rise in the frequency of urban flash floods, which led to an increase in the total land area that was vulnerable to flooding [16]. Almazroui, *et al.* [17] investigated the effect of climate change on hydro-structures in Turkey and Saudi Arabia. Significantly, future project decisions in the semi-arid region of Turkey should account for an average 5% increase in precipitation intensity, but the similar figure for the dry region of Saudi Arabia is between 15% and 20% [17]. Modarres, *et al.* [18] concluded that the increase in flood magnitude and drought severity in Iran can be partially attributed to land use changes, a decreasing trend in annual rainfall, an increasing trend in maximum rainfall, and inappropriate water resources management strategies. In spite of its generally dry climate, Saudi Arabia has had a number of devastating floods in recent years. Researchers across many regions of Saudi Arabia have employed RS technology and Geographic Information Systems (GIS) to identify and evaluate urban floods [19-23]. Even close to the southern Iraqi border, the state of Kuwait experienced strong rainstorms in the winters of 2018 and 2020, followed by catastrophic flooding not seen in Kuwait since 1976 [24].

The Kurdistan Region is a federal region located in the north of the Federal Republic of Iraq, with Erbil, Sulaymaniyah, and Duhok as its three major cities (see Figure 1). According to the Iraqi constitution in 2005, "shall recognize the region of Kurdistan, along with its existing authorities, as a federal region" [25], but the region existed after the Gulf War in 1991 as a de facto autonomous entity. Erbil is the region's capital and is regarded as its political, commercial, social, and religious center. In a broad sense, the history of the Kurdistan Region can be divided into two distinct time frames: the first one spanning from 1991 to 2003, ending with the collapse of the former Iraqi regime, and the second phase starting in 2004 and continuing to the present day. The purpose of this division is to highlight the progress made in the region during these two distinct periods. During the first phase, Iraq was subject to international sanctions, making it a challenging time period, and the country's pace of economic growth was low. In contrast, the second phase marks the beginning of a new era in the region's history, with Erbil, the capital of the KRI, becoming the focal point of development in the region after the invasion of Iraq by coalition forces in April 2003. Erbil is now regarded as an important political, economic, and administrative center not only for Iraq but also for neighboring countries [26]. Since 2009, the Kurdistan Regional Government (KRG) has been working to expand its capacity and prepare for a gradual transition to independence by developing its oil and gas industry and attracting investment from foreign oil corporations. These are among the actions they have taken [27]. Thus, it is evident that the past two decades have been marked by and witnessed remarkable progress on various fronts [28].

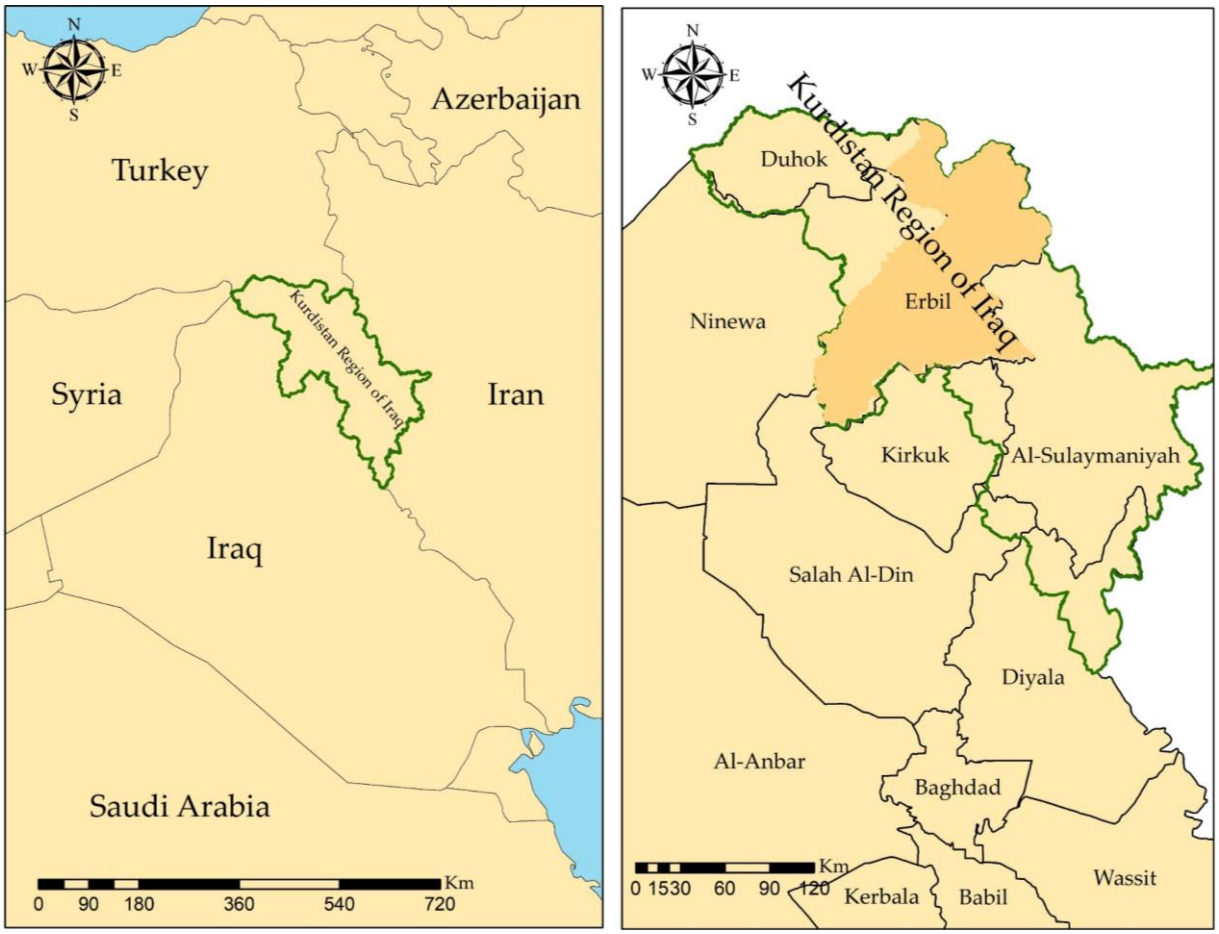

Figure 1. Iraq and Kurdistan Region map.

In spite of the fact that the number of floods that have occurred in Erbil over the first two decades of this century has been on the rise due to a variety of factors [29], this phenomenon is not unusual in Erbil's history [30]. After all, floods in Erbil that took place in the 1930s have been described in a variety of works of literature, particularly novels [31]. Flooding has occurred in a number of older neighborhoods of Erbil, including Tayrawa, Saydawa, Khanaqah, and Taajil, amongst others. A picture of a map that was drawn in the early 20th century can be found on the official website of the governorate of Erbil; however, the exact date of the map is uncertain [32]. Interestingly, the map clearly shows that a natural waterway runs through the city. This is proof that the effects of this waterway could continue and certainly have (see Figure 2). Waterways have historically played a significant role in shaping human societies and cultures. They have served as sources of water for drinking, irrigation, and transportation, as well as sites for religious and cultural activities. In many cases, the presence of a waterway has influenced the location of settlements, trade routes, and agricultural practices. Furthermore, the waterway could continue to have an impact on the city's development and sustainability in the future.

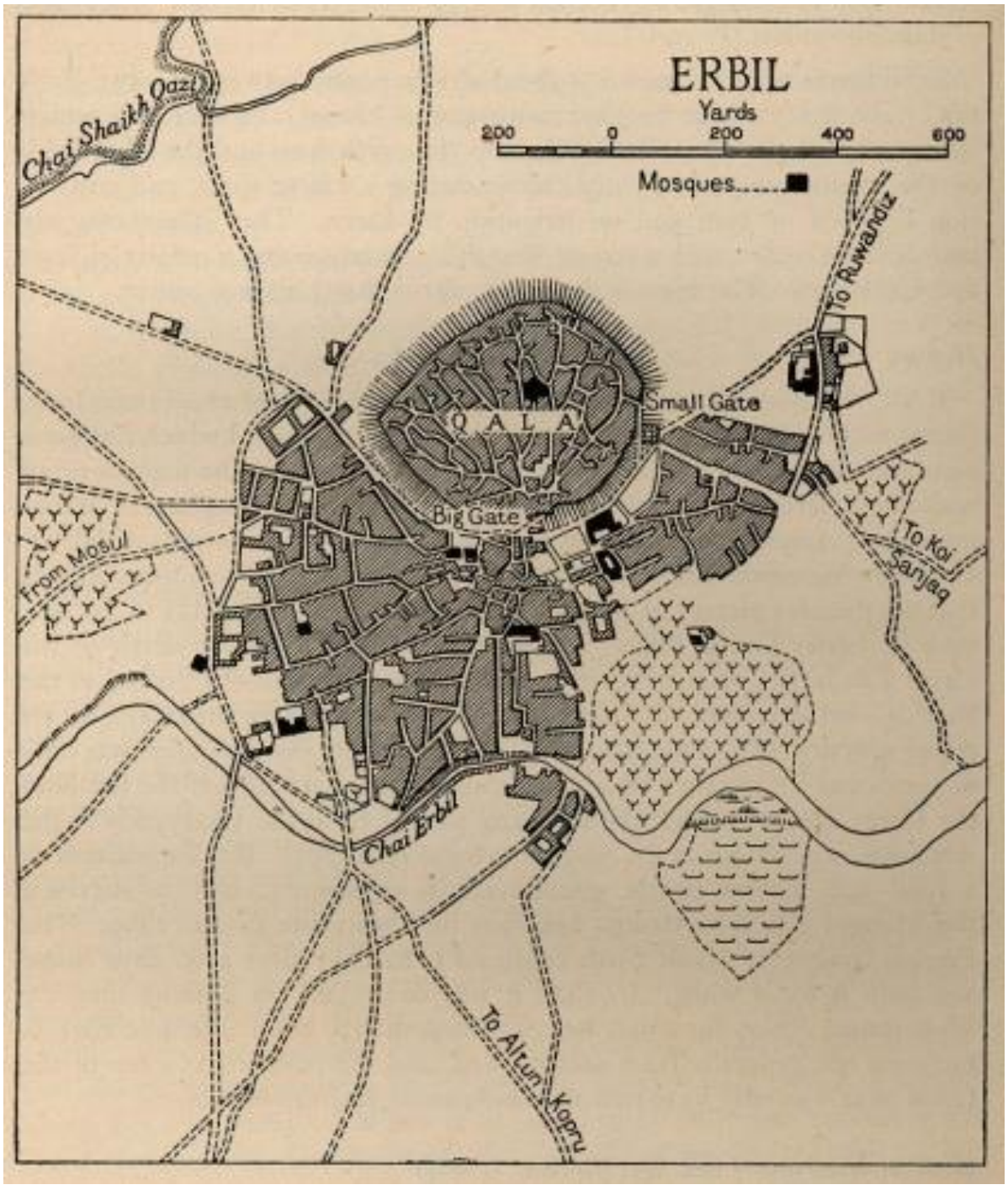

Figure 2. Historical map of Erbil [32].

In their research on the strategy framework for sustainable management of sewage systems in semi-arid cities, Nanekely, Scholz and Al-Faraj [30] focused on Erbil and used archives from the Erbil province to present historical photographs of the city during floods in the 1930s, 1960s, and 1970s (see Figure 3).

Figure 3. Flood history in Erbil: (**a**) Khanah quarter 1936; (**b**) Tayrawa main street 1960; (**c**) Tayrawa 1967; and (**d**) Tayrawain main street 1970 [30].

As can be seen, Erbil has been hit by flooding in the past, which has had a negative impact on the residents of the city. The number of floods that have occurred in the center of Erbil over the course of the previous two decades of this century has significantly increased, as indicated by a study that used rainfall and meteorological data [29]. As a result, the residents of the city are concerned, to varying degrees. Figure 4 shows flooding both during and after some of the floods that have occurred throughout this century. It should be noted that each of these floods resulted in a different degree of property damage, economic losses, and social unrest. The flooding also resulted in an increase in the number of power outages because many local and smaller power generators were affected [30]. Generally, floods will have an effect on the transport system as well; but, in the KRI, in particular, the transport system is dependent on private cars and taxis. Therefore, as a result of this, citizens have been

arriving late to work, which has resulted in increased levels of traffic congestion. On general, there are various locations that experience difficulties with traffic during floods. Such places like Kurdistan street (known as 60 meter street) become inundated, particularly in the vicinity of the underpasses, causing traffic to stop. Close to the Saydawa bridge, the Tayrawa Bazar, and the intersection where the Council of Ministers is located is a vulnerable area, which is known as Barzani Namr street. The street known as Peshawa Qazi street the vulnerable area is located near the main street of Shaqlawa.

Figure 4. Flooding devastating consequences in Erbil in two separate events at the end of 2021 [33,34] (continued on next page).

Figure 4. Flooding devastating consequences in Erbil in two separate events at the end of 2021 [33,34].

People living in developing countries have become accustomed to the idea that during the rainy season, they will experience flooding as a normal occurrence. Since the number of floods in the region is on the rise, it is necessary to make efforts to either mitigate their severity or find ways to adapt to the trend. Therefore, in this regard, the problem of flooding is likely to receive more attention. Experts in this field have intensified their efforts to apply their recommendations, opinions, and arguments according to the region in the service of presenting solutions. Utilizing hydrodynamic models is often necessary to build detailed flood inundation maps. Since the beginning of the 21st century, various

techniques and methods for the building of such models have been developed [35-39]. Due to developments in processing capacity and the availability of global terrain datasets, large-scale hydraulic analyses have received increased attention in recent years [35,40].

The assessment of flood hazards, including their quantification, is a necessary step in the preparation of emergency plans and mitigation strategies. In light of this, there is an obvious need for large-scale flood hazard maps to be created using precise topographic data, and there is also a clear requirement for high-quality benchmark data collections of equivalent spatial coverage to evaluate flood-prone areas. The flood hazard is characterized by the physical characteristics of the flood occurrences (e.g., inundation extent, water depth, and flow velocity) with an associated probability of exceedance or return period [41]. Commonly, flood risk is determined by combining the likelihood of a flood of a particular intensity occurring in a specific location over a given time period with the potential consequences (flood losses) [42,43]. Additionally, vulnerability consists of two components: exposure and susceptibility to damage. Exposure relates to the question "Who or what will be affected?", while susceptibility addresses the question "How will the affected items be damaged?" [44]. Different studies have determined that the depth of flooding is a direct measure of the damage caused [45,46]. It is possible to extend this measure with additional flood factors such as flow velocity, duration, water temperature, water contamination, and warning time in order to provide additional measurements of the negative effects [47]. A map like this will be an important factor in supporting the relevant authorities in the event of extreme rainfall, helping to prevent and reduce the damage caused by flooding in the center of Erbil. This will make it abundantly clear that efforts can be directed towards decreasing the consequences of flooding in places that have been identified on the map as vulnerable zones. In fact, floods in late 2021 and early 2022 inflicted significant damage on both the people of Erbil and the city itself. As a result, preventing the occurrence of similar disasters is an unavoidable task, and it is imperative that all available scientific, technical, and material capacities be utilized.

2. Objective and Scope

The overall objective of the research was to identify and assess the hazard of urban flash flooding on a city scale and investigate the factors that contribute to the occurrence of such events. To achieve this, various approaches and procedures were developed and utilized in a case study of the city center of Erbil. The investigation focused on several issues as subjects of the research, including: (1) Gathering necessary data on rainfall and its effects on flash flooding in the study area. (2) Preparing IDF curves to use in developing hydrodynamic models. (3) Evaluating the LULC in the study area over an extended period to determine its impact on hydrological transformation and increase in the frequency of flooding. (4) Selecting a technique that can be used in regions with limited data to develop flood hydrodynamic models. (5) Developing a hydrodynamic model to analyze and identify potential flash flood hazards in the study area.

The doctoral dissertation is divided into four main parts, labeled I through IV, that correspond to the five overarching concerns explained earlier. Figure 5 shows the divisions into parts. In each part of the dissertation, the following specific concerns are addressed:

Part I:

- Collection of rainfall data for Erbil Province, particularly the city center.
- Evaluation and analysis in detail of the extreme rainfall events that have occurred over the past few decades with regard to the spatial and temporal distribution of rainfall, the intensity rate of rainfall, and the exceedance probability.
- Development of IDF curves for the city center of Erbil using the daily rainfall depth measurements collected at the meteorological station in Erbil.

Part II:

- Analysis, recognition, and categorization of the changes that have occurred in LULC in Erbil Province, particularly with regard to how rapid urban expansion has affected the center of the city.
- Recognition of the effects of this transformation on the hydrological response in the studied area.
- Hydrological simulations were performed in HEC-HMS to compare different scenarios and evaluate the transformation and development of the researched area.

Part III:

- Finding the impact of the choice of building representation techniques and hydrodynamic models on urban flood simulations using HEC-RAS 2-D.
- Analysis and comparison of the results of the urban flood simulations performed mainly using two different mathematical models (2-D Saint-Venant and 2-D Diffusion Wave (DW)).
- Investigating the impact that different numerical mesh resolutions have on the outcomes.

Part IV:

- The development of a hydrodynamic model for urban flash floods specifically for the central area of Erbil.
- The social and economic impact that the floods had on society in general.
- Identification of flood-prone zones in the central district of Erbil and flood hazard mapping.

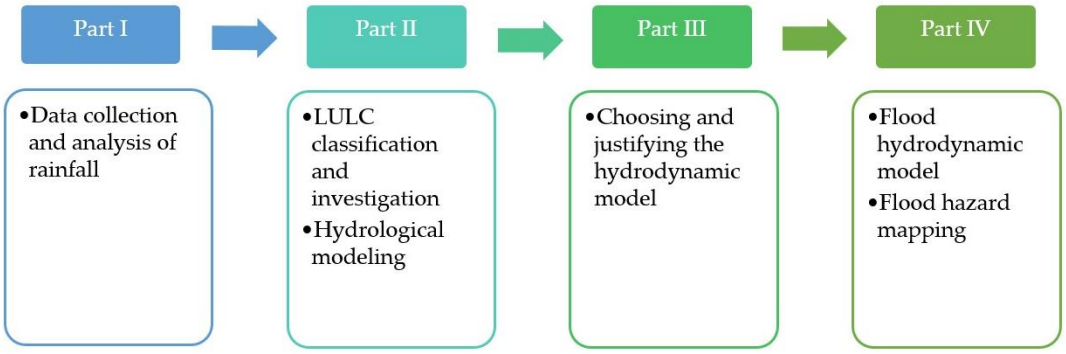

Figure 5. Breakdown of the Ph.D. dissertation into sections.

A partial results of the research were described by the author in the following publications:

Mustafa Andam, Muhammed Hadi, Szydłowski Michał (2019). Extreme rainfalls as a cause of urban flash floods; a case study of the Erbil-Kurdistan region of Iraq, ***Acta Scientiarum Polonorum Formatio Circumiectus***, 18(3), 113-132, https://doi.org/10.15576/ASP.FC/2019.18.3.113

Kareem Dalshad, M Amen Aumed, Mustafa Andam, Yuce Mehemt Ishak, Szydłowski Michał (2022), Comparative Analysis of Developed Rainfall Intensity–Duration–Frequency Curves for Erbil with Other Iraqi Urban Areas, ***Water***, 14(3), 419, https://doi.org/10.3390/w14030419

Mustafa Andam, Szydłowski Michał (2020). The Impact of Spatiotemporal Changes in Land Development (1984–2019) on the Increase in the Runoff Coefficient in Erbil, Kurdistan Region of Iraq, ***Remote Sensing***, 12(8), 1302, https://doi.org/10.3390/rs12081302

Mustafa Andam, Szydłowski Michał (2021). Application of different building representation techniques in HEC-RAS 2-D for urban flood modeling using the Toce River experimental case, ***PeerJ***, 9, e11667, https://doi.org/10.7717/peerj.11667

3. Study Area

Erbil is the capital of the Iraqi Kurdistan Region, in Kurdish called (Hewlêr). Erbil is a historic city in the region, and its history dates back thousands of years due to the presence of the Shanadar cave in the Bradost mountain region, which is considered the cradle of humanity [48]. Additionally, Erbil's historic castle dates back to the Assyrian era and thousands of years B.C [26]. According to the Kurdistan Region Statistics Office's (KRSO) annual report for 2021, the population of the city was approximately 2.25 million. The central district of the city is home to more than one million residents. Interestingly, almost 80% of the population resides in metropolitan areas [49]. Erbil Province covered an area of 14,873.68 km². It is located at 36.11'28'' degrees of latitude and 44.00'33'' degrees of longitude, and it has an average elevation of 406 m Above Sea Level (A.S.L) [29] (see Figure 6). Because of its geographic location, Erbil Province has a climate that is classified as semi-arid continental, with summers that are very hot and dry and winters that are particularly cold and wet.

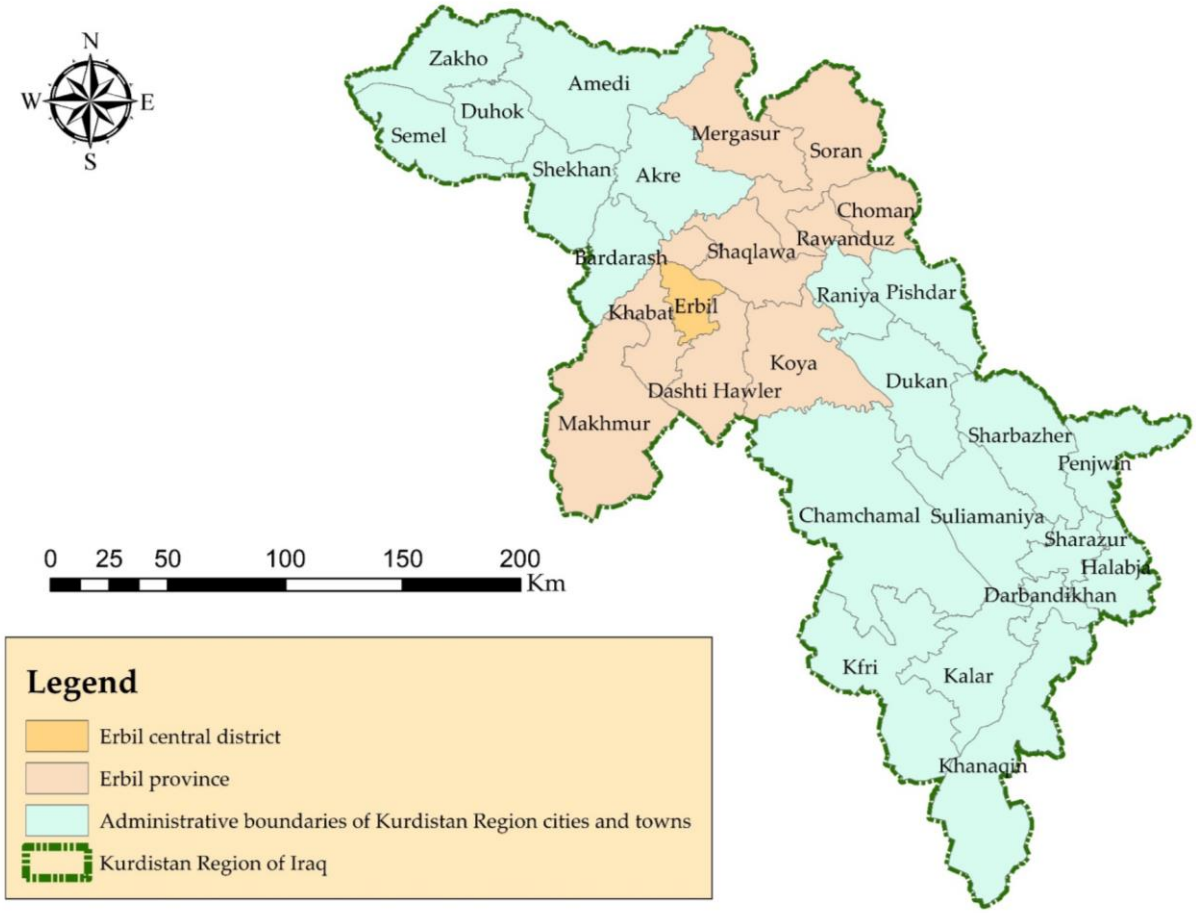

Figure 6. Administrative borders of Iraq's Kurdistan region and location of Erbil's central district.

Throughout the course of this research, different maps and outlines of boundaries were drawn up. Figure 7a illustrates the hydrological sub-basins in Erbil that were created using DEM data with a resolution of 30 m. As well as it presents the area subjected to hydrological analysis. Because Erbil is such a large area, the analysis was limited to sub-basins located in the center district and surrounding districts. During the process of developing the hydrodynamic model, the main focus was on the area that lies within Erbil's 120 m ring road (see Figure 7b).

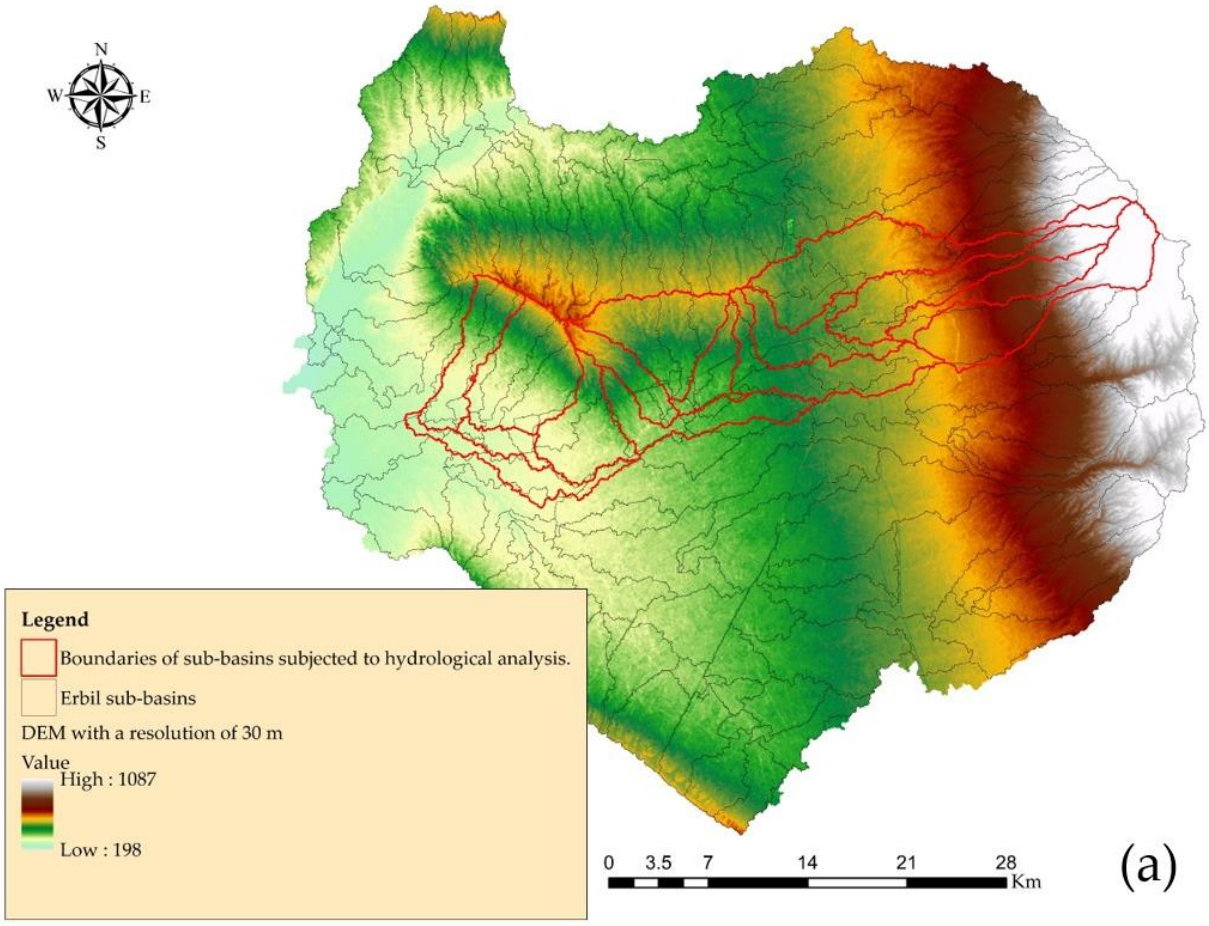

Figure 7. Study area: (a) Hydrological boundary of Erbil sub-basins (continued on next page).

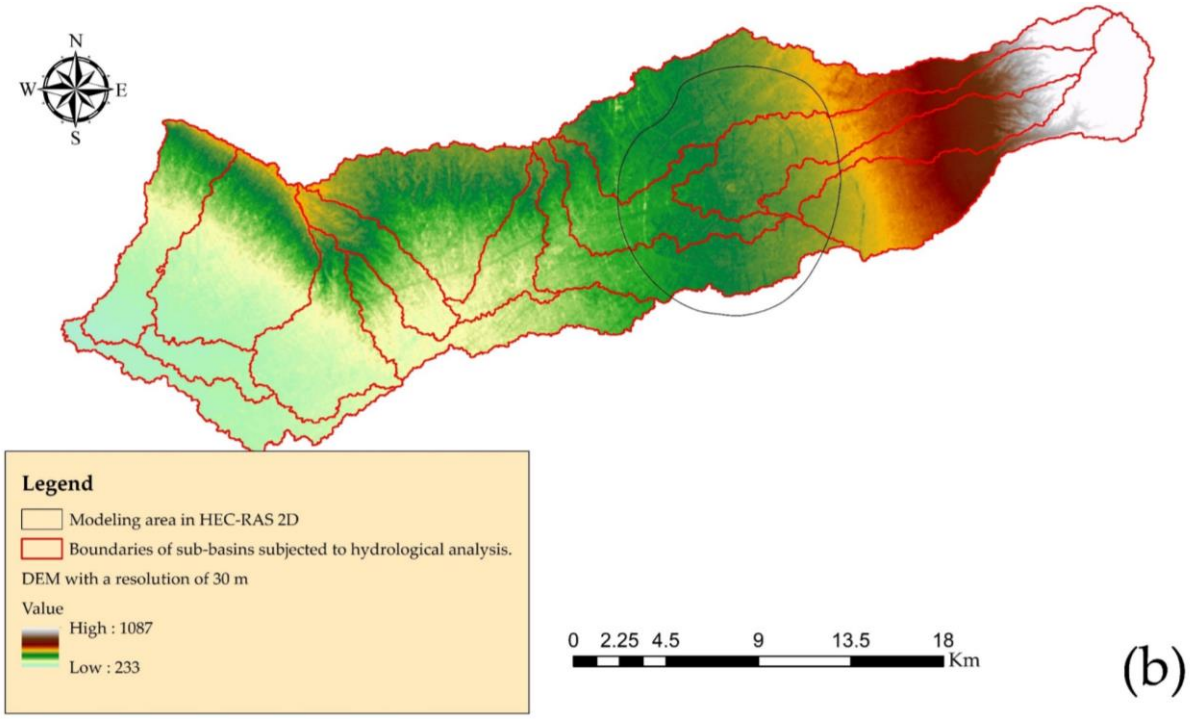

Figure 7. Study area: (**b**) Boundary of sub-basins subjected to hydrological and LULC analysis and the boundary of modelling area in HEC-RAS 2-D.

4. Part I: Precipitation Analysis

4.1 State of Art

Rain plays a vital role in providing fresh water on Earth through the hydrologic cycle, but it can also be a cause of natural disasters such as floods. Failing to analyze, assess, and consider these types of disasters can result in significant losses and damage to infrastructure like housing, roads, bridges, and industrial areas. Globally, flooding is one of the most frequently occurring natural hazards [50]. Worldwide, there has been an increase in pluvial flooding caused by extreme rainfall events within a limited time frame. The reasons for this vary from country to country, but the primary cause is associated with the growth of the population and urban development. These factors result in significant changes in land cover, and they are compounded by the effects of climate change. Each of these factors plays a role in flooding events. Failure to consider these aspects could result in an increase in population and urban development, leading to greater surface runoff and significant economic and social losses. Furthermore, climate change will have a crucial role in intensifying and accelerating the hydrologic cycle [51,52]. In addition to the factors mentioned earlier, ten Veldhuis, *et al.* [53] and Ashley, *et al.* [54] identified another cause of flooding, which is ageing infrastructure. Furthermore, other contextual factors, such as behavioural patterns, demographics, and the timing and day of the week the storm occurs, may also have a particular effect on the magnitude and type of damage, as noted by Miceli, *et al.* [55]. The effects of extreme hydrologic events, such as intense rainfalls or unexpected snow melts, not only make the infrastructure of developed cities vulnerable but also pose a significant threat to their citizens [56].

In recent years, the increased risk of flooding due to climate change has prompted several countries to focus on climate change adaptation planning. One of the most significant storms on record hit Copenhagen, Denmark, in July 2011, resulting in precipitation intensities higher than 2000-year return periods [57]. Gdańsk, Poland, was also severely impacted by flooding in 2001 and 2016, causing economic and social losses [58]. France has also experienced an increase in extreme rainfall events, with one particularly intense episode in June 2010 [59]. Flash flooding has been a costly and deadly problem in the United States, causing the most fatalities and damage compared to any other weather-related hazard [60]. India has also been affected by urban flash flooding during high-intensity rainfall events, with an increasing trend in urban flood catastrophes observed since the beginning of the twenty-first century [61]. In Seoul, South Korea, an extreme rainfall event in 2010 destroyed 17,645 houses during resulting urban flash floods [62].

In November 2009, Jeddah, which serves as the capital city of Saudi Arabia, encountered a severe downpour lasting for only three hours. Despite its short duration, the rainfall resulted in catastrophic flooding that caused significant harm to infrastructure and properties, as well as the loss of over 113 lives and injuries to numerous people. According to Youssef, *et al.* [63], more than 10,000 homes and industrial properties were destroyed. Similarly, in Ikitelli, a district located in Istanbul, Turkey, a neighboring country north of the study area, a flash flood in 2009 resulted in the death of 20 individuals and the destruction of a commercial district, as per Ávila, *et al.* [64]. According to Al-Amri and Subyani [65], designing water projects in arid regions poses a challenge due to the unpredictable and inconsistent nature of rainfall, which is also true for semi-arid regions. Managing water resources becomes difficult because precipitation levels can vary significantly from year to year [66].

Rainfall IDF relationships are graphical representations of the amount of precipitation that falls over a certain period in catchment areas [67]. Rainfall IDF curves are important for preventing flooding and reducing the loss of life, property, and costs associated with water damage insurance and weather-related risk assessments. These graphical representations of the amount of water that falls within a given period of time in catchment areas have been estimated in developed countries since 1932, but the lack of accurate and long-term rainfall data in many developing countries is a major obstacle in their construction [68]. Researchers worldwide have developed IDF curves and empirical formulas to address this issue [69-74]. For example, Lima, *et al.* [75] proposed a new method to estimate IDF curves using the scaling-invariant property of rainfall duration versus intensity, and Kristvik, *et al.* [76] used scale invariance to downscale the distribution of extreme precipitation to derive local-scale IDF curves for future precipitation. Other studies have looked at how satellite-based precipitation data can be used to estimate IDF curves [77,78]. Researchers in arid regions such as Saudi Arabia, Iraq, and Turkey have also developed IDF relationships with different return periods in different parts of the countries [65,79-91].

This part of the study highlights the issue of extreme rainfall events in Erbil, Iraq, and the lack of research and data on this subject. The study aims to fill this gap by conducting a detailed analysis of extreme rainfall events over the past decade, focusing on spatial and temporal rainfall distribution, intensity rate, and exceedance probability. The study also examines the effects of each analyzed aspect on the resulting flash floods in the Erbil Centre district.

The significance of this study is high, as it contributes to the development of knowledge about hydrology in Iraq and helps to understand the causes and effects of urban flash floods in Erbil. The results of this study can be used to improve the city's infrastructure and drainage systems, as well as

to develop effective flood management strategies. Overall, the study provides valuable insights into the causes and effects of urban flash floods in Erbil and can help to inform policies and strategies for managing and mitigating the impacts of extreme weather events in the region.

It is clear that the other important objective of this study is to develop IDF curves and empirical formulas for Erbil city center using daily rainfall depth measurement data from the Erbil meteorological station. These curves and formulas are important tools in the management of water resources and the design and operation of stormwater management systems. The study aimed to fill a gap in the availability of such data for the location, which could assist authorities in implementing strategies and making good decisions. While the methods and equations used in the study may be standard, the novelty of the work lies in the development of IDF curves and formulas for a location where such data is not available. The results of the study could have significant practical applications in improving water resource management in local urban areas. The results of the study were also published in articles [29,92].

4.2 Material and Methods

4.2.1 Rainfall data collection

The rainfall data used in the study was gathered from three different sources. Between 1980 and 1991, data was obtained from the Climate Forecast System Reanalysis (CFSR) of the National Centre for Environmental Prediction. During this period, the studied region was insecure, and officials from meteorological stations could not regularly record the weather data. However, such dataset has been used by other researchers in the past [30,93,94]. From 1992 to 2018, the General Directorate of Meteorology and Seismology in Kurdistan region/Iraq (GDMS) provided the dataset, which was recorded daily and consistently using a standard classic rain gauge in Erbil. The remaining data was obtained from the Directorate of Irrigation/Erbil and General Directorate of Agriculture/Erbil, both of which have automatic meteorological stations in the Centre district of Erbil.

Due to limited sources from which rainfall data could be collected, an estimate was required to proceed. Table 1 presents the meteorological stations located in Erbil Province that have been used for this study, along with the corresponding periods for which their data was collected [29].

Figure 8 presents the maximum daily rainfall recorded in the Centre district of the Erbil Province between 1980 and 2018. During the 20th century, the daily rainfall varied between 20 mm and 80 mm, and the highest recorded amount during that period was 79 mm on November 21, 1992. However, in the first decade of the 21st century, there was a sudden increase in the fluctuation of daily rainfall, with

the highest amount of 102.3 mm recorded on February 2, 2006. This is the highest amount recorded within the mentioned period and should be taken into account in the design of hydraulic structures and sewer systems.

Table 1. Meteorological stations in Erbil Province [29].

No.	Name of the station	Longitude E	Latitude N	Period (years)	Elevation A.S.L (m)	Note
1	Khabat Station	43.65000	36.26610	2001-2006	252	
2	Qushtapa Station	44.03190	36.00390		398	
3	Irrigation Directorate/Erbil, Station	44.00942	36.16150	2008-2018	406	Located in the target area
4	General Directorate of Agriculture/Erbil, station	44.01452	36.17183		411	
5	CFSR Station	44.04000	36.19500	1980-1991	414	
6	Erbil Meteorological Station	44.03890	36.19500	1992-2018	420	
7	Ankawa Station	44.01190	36.22060	2001-2006	434	
8	Rawandoz Station	44.53390	36.61690		677	
9	Soran Station	44.54280	36.65810		679	
10	Khalifan Station	44.40060	36.60390		687	
11	Harir Station	44.35500	36.54750		724	
12	Shaqlawa Station	44.32140	36.40560		975	
13	Sidakan Station	44.67110	36.79830		1020	
14	Salahaddin Station	44.20860	36.37810		1087	
15	Choman Station	44.88080	36.62780		1090	
16	Mergasor Station	44.30080	36.84000		1204	

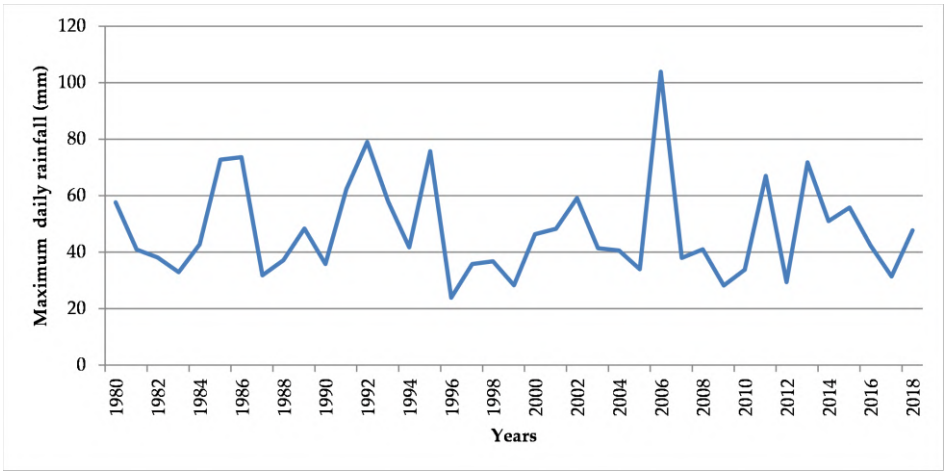

Figure 8. Maximum daily rainfall measured in two different stations: CFSR from 1980 to 1991, and Erbil meteorological station from 1992 to 2018 [29].

Figure 9 illustrates the changing pattern of annual rainfall in the Centre district of Erbil Province over time. Despite some fluctuations, there was a general decline observed between 1980 and 2017. However, in 2018, the amount of rainfall soared, reaching a value of 721.30 mm, which was not recorded in the Erbil meteorological station for the previous 24 years. It is worth noting that the maximum daily rainfall did not necessarily correlate with the annual rainfall. For instance, the year with the maximum annual rainfall was 1992, whereas the maximum daily rainfall in that year was 79 mm. Nonetheless, in general, the maximum daily rainfall contributed to an increase in annual precipitation, as seen in 2006, the year with the highest maximum daily rainfall in 39 years.

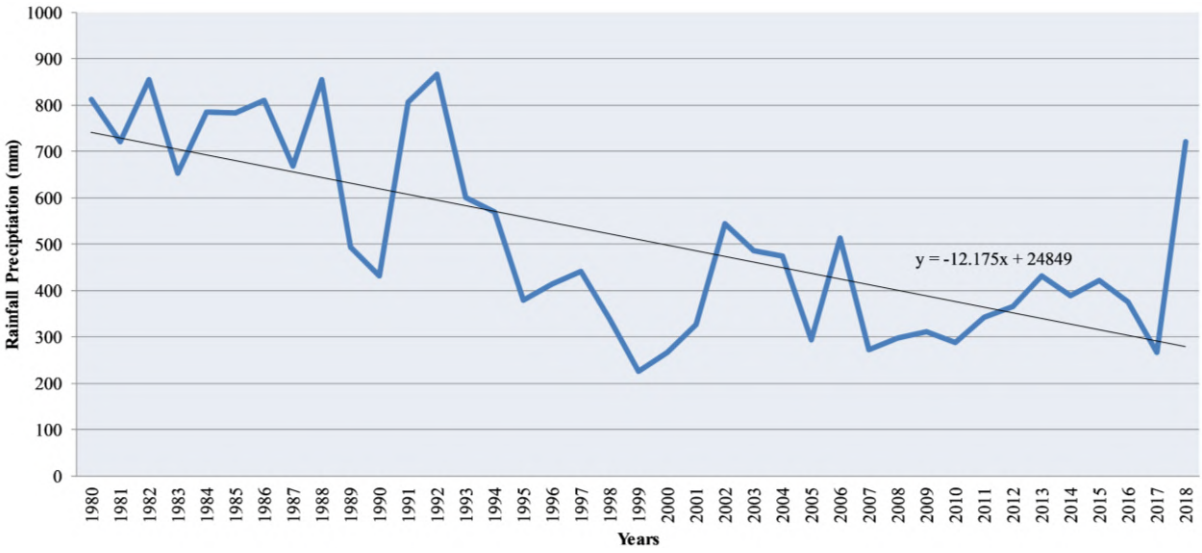

Figure 9. Annual rainfall in the studied area measured in two different stations: CFSR from 1980 to 1991, then Erbil meteorological station from 1992 to 2018 [29].

4.2.2 Rainfall spatial distribution

The physical features and landscape of the Erbil Province greatly impact how precipitation is distributed across the region, which is influenced by air temperature. Higher altitudes are more likely to experience precipitation compared to lower altitudes. Figure 10 displays the geomorphology of the Erbil Province and highlights that areas in the north and northeast of Erbil have higher elevations A.S.L, with some areas reaching an average of 3000 m. However, the altitude decreases in the Centre district, reaching approximately 500 meters. This means that the amount of precipitation also decreases in the Centre district compared to other areas, resulting in variations in the type and quantity of precipitation.

The Mergasur area is located 158 km away from the Centre district, has an altitude of 1204 m A.S.L, and experiences a yearly precipitation of 1307.9 mm. Rawanduz, on the other hand, receives an annual rainfall of 783.8 mm and is situated at an altitude of 677 m A.S.L Qushtapa sub-district, which is only

23 km away and located in the southern part of the Centre district, receives a total of 398 mm of rainfall per year.

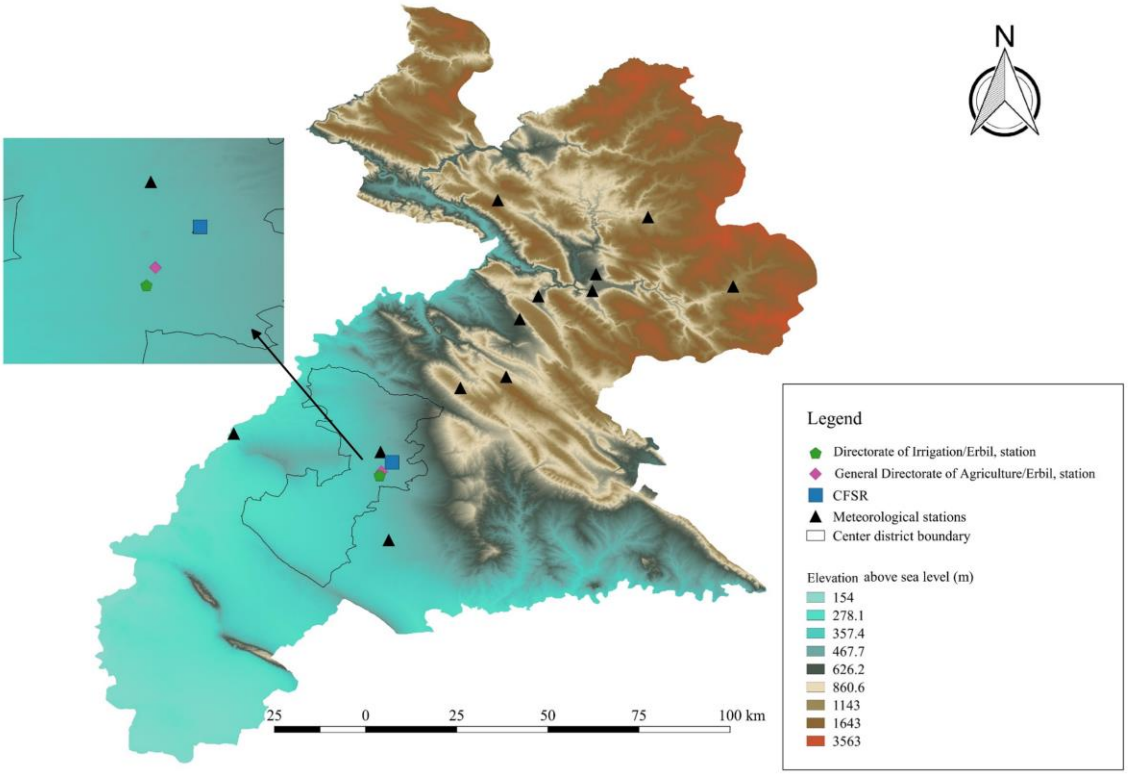

Figure 10. Erbil topography and the location of meteorological stations [29].

4.2.3 Temporal rainfall distribution

Since hourly precipitation data was only available for the Erbil Centre district between 2008 and 2018, the investigation of maximum daily rainfall episodes was limited to this time period.

- One such episode occurred on April 22, 2011 and covered all of Erbil Province. However, the amount of rainfall varied across stations. For example, Mergursur district, a mountainous area with an altitude of 1204 m A.S.L, recorded 96.2 mm of rainfall, while Qushtapa sub-district, a more or less flat terrain at an altitude of 398 m A.S.L, recorded 22.3 mm. In the Centre district, the Erbil meteorological station recorded 67 mm of rainfall. The automatic station of the Erbil Directorate of Irrigation, located in the Centre of Erbil, reported a total of 48.9 mm of rainfall, which occurred between 2:00 am and 10:00 pm with the main part of the rainfall occurring between 6:00 pm and 10:00 pm, as depicted in Figure 11a.

- The highest amount of rainfall recorded by the Erbil meteorological station in the second decade of the twenty-first century occurred on January 28, 2013, at 71.8 mm. The episode lasted for 27 hr, with the first phase from 2:00 am to 6:00 am, followed by a 10-hr break, and then another phase from 4:00 pm to 12:00 am on January 29, 2013. The last phase started just one hour later at 2:00 am, and the majority of rainfall was recorded by 2:00 pm, resulting in 69.5 mm of recorded rainfall. This extreme weather event was observed across all stations in Erbil Province between January 27 and 29, 2013, with Mergasur district, a mountainous area, recording 362.2 mm of rainfall in three days, and Qushtapa sub-district recording 45.8 mm on January 28, 2013 (see Figure 11b).

- On January 28, 2014, the Erbil meteorological station recorded 51 mm of rainfall, while the Erbil Directorate of Irrigation station recorded 44.3 mm. The episode was divided into two parts, with 41.9 mm of rainfall falling in 13-hr from 1:00 am to 1:00 pm in the first and most significant part. In the second part of the event, the rain started again after a 5-hr break, and within an hour, 2.4 mm of rainfall was observed, as shown in Figure 11c.

- The final day of 2015 and the first day of 2016 were marked by rainfall in Erbil Province. The meteorological officials stationed in Erbil's central district recorded a substantial rainfall of 55.8 mm within a span of 15 hr. The event began at noon on December 31, 2015, and lasted until 2:00 am on January 1, 2016, as indicated in Figure 11d by the Directorate of Irrigation.

- On March 28, 2016, a sporadic episode of intense rainfalls was recorded in Erbil Province. Within an hour, 12.2 mm of rainfall was observed at 6:00 pm, followed by 8.3 mm at 10:00 pm. However, the total amount recorded by the Erbil meteorological station was 42.2 mm, as shown in Figure 11e.

- The last event occurred on November 22 and 23, 2018, Erbil experienced another rainy day, with a total of 47.7 mm of rainfall recorded by the meteorological station in 10 hr. The event started at 11:00 pm on November 22, 2018, and lasted until 8:00 am the following day, as shown in Figure 11f by the Directorate of Irrigation.

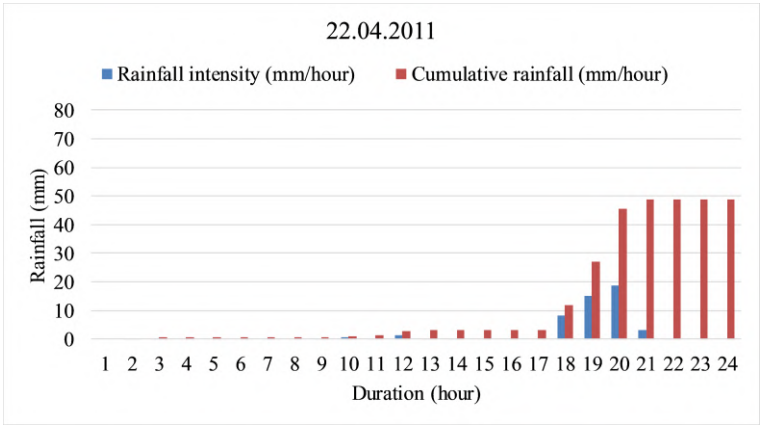

(**a**)

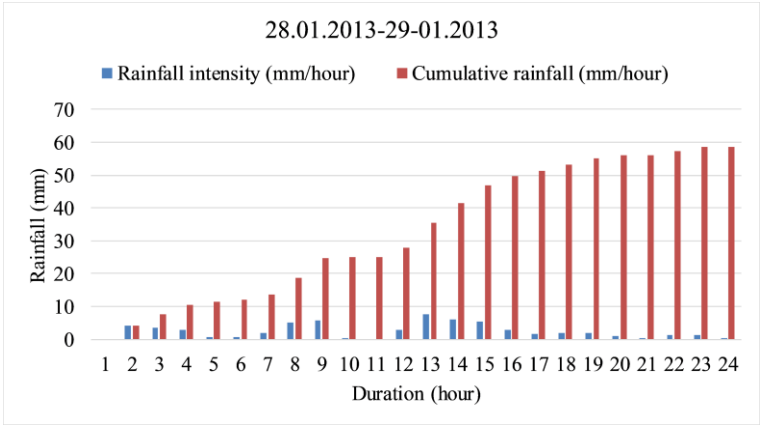

(**b**)

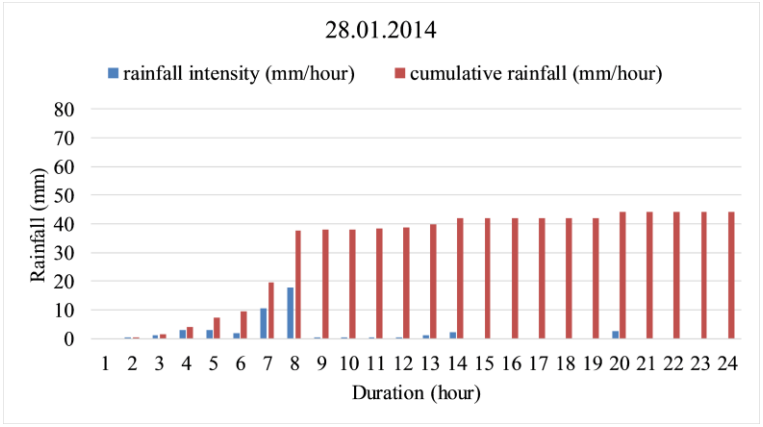

(**c**)

Figure 11. Temporal rainfall distribution, measured in the automated meteorological station of the directorate of Irrigation/Erbil (**a**) Temporal rainfall distribution of 22.04.2011. (**b**) Temporal rainfall distribution of 28.01.2013-29-01.2013. (**c**) Temporal rainfall distribution of 28.01.2014 [29] (continued on next page).

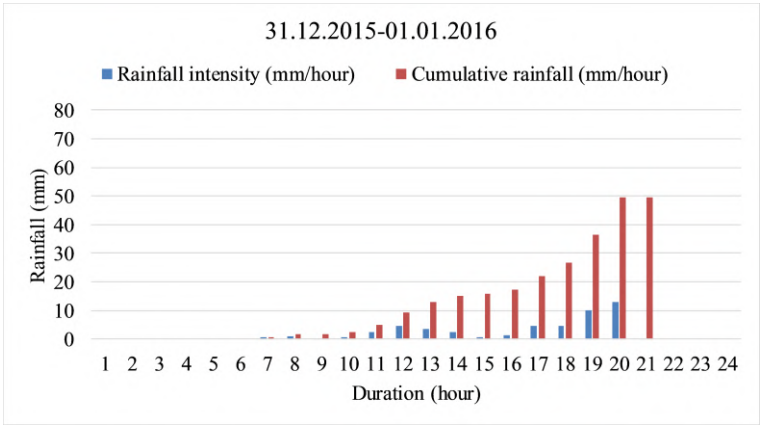

(**d**)

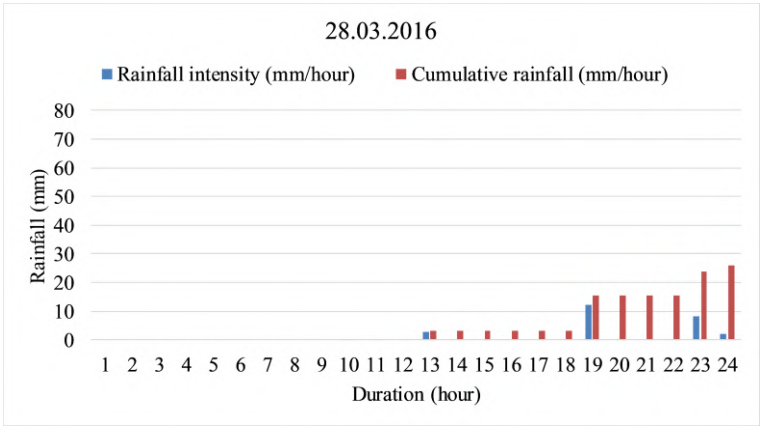

(**e**)

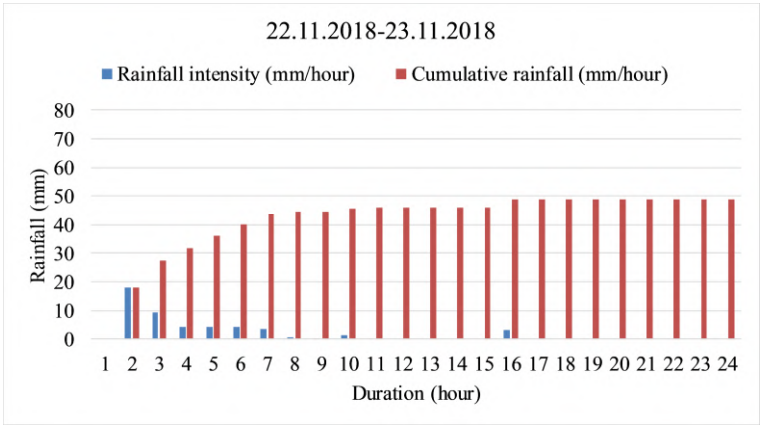

(**f**)

Figure 11. Temporal rainfall distribution, measured in the automated meteorological station of the directorate of Irrigation/Erbil (d) Temporal rainfall distribution of 31.12.2015-01.01.2016. (e) Temporal rainfall distribution of 28.03.2016. (f) Temporal rainfall distribution of 22.11.2018–23.11.2018 [29].

4.2.4 Huff curves

Huff [95] proposed a set of dimensionless, synthetic rainfall time distribution patterns based on data from watersheds in the mid-western USA. These correlations are applicable to regions with similar climate and topography, including the Midwest in the USA. The rainfall episodes were divided into four quartiles based on when the peak rainfall intensity occurs during the storm duration. Within each quartile, the distribution was plotted for different probabilities of occurrence. The first quartile indicates that half of the total depth is observed in the first 25% of the storm duration. The second quartile shows that half of the depth is between 25% and 50% of the total time. The third quartile indicates that half of the total depth occurs between 50% and 75% of the rainfall duration, while the fourth quartile shows that half of the total depth is observed between 75% and 100% of the total rainfall duration (see Figure 12).

Numerous studies have used Huff curves to model temporal rainfall distributions in various parts of the world, including the study by Nascimento, *et al.* [96], which modelled rainfall time distribution using a dimensionless hyetograph. Additionally, Bezak, *et al.* [97] studied the impact of duration and temporal rainfall distribution on hydraulic flood modelling results in the Glinscica stream catchment in Slovenia using the Huff curves. In this study, the quartiles and curves are used as a classification for rainfall time distribution, to compare the temporal rainfall distribution of extreme rainfall episodes in the studied area.

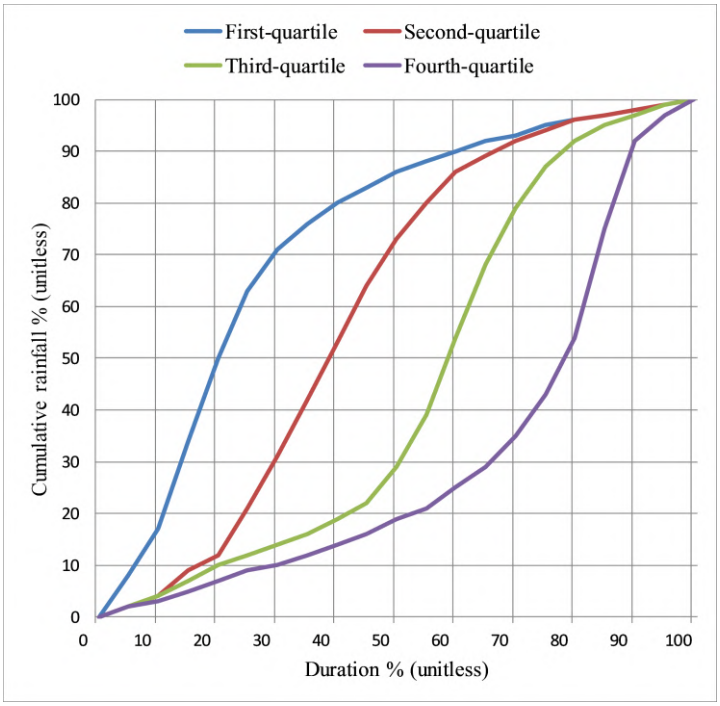

Figure 12. Storm-quartile classifications by Huff [95].

Due to the wide variability of rainfall intensity from site to site and the lack of research focusing on the analysis of rainfall and its characteristics in the studied area. Consequently, the rainfall events mentioned above are compared to an American scale formulated by the American Meteorology Society (AMS) Glickman [98] (glossary of meteorology), which subdivides the intensity of rainfall into four groups, as shown in Table 2.

Table 2. Classification of rainfall intensity, according to the AMS [98].

Type of rainfall intensity	Amount in one hour (mm)
Light rain < 2.5	Light rain < 2.5
Moderate rain > 2.5 and < 7.6 or 10	Moderate rain > 2.5 and < 7.6 or 10
Heavy rain > 7.6 or between 10 and 50	Heavy rain > 7.6 or between 10 and 50
Violent rain > 50	Violent rain > 50

4.2.5 Statistical analysis of rainfall

During the first stage of the analysis, the sequences were arranged in order from the most significant episode to the smallest. Then, the empirical exceedance probability was calculated for the dataset covering the period of 1980 to 2018, using the Weibull equation [99].

$$p(i) = \frac{r}{N+1} \tag{1}$$

where p is the exceedance probability, r represents the location of a specific episode in the rainfall distribution series, and N is the size of the series.

The precipitation probability distribution function was modeled using the lognormal distribution, with parameter estimation performed via the maximum likelihood method as recommended by the Polish Hydrologists Association [100]. The values of $P_{max,p}$ indicating the maximum daily annual rainfall with a given probability of an excess of p were calculated using the following equation:

$$P_{max,p} = \epsilon + \exp\left(\mu + \sigma . u_p\right) \tag{2}$$

where the lowest amount of maximum daily rainfall is denoted by ϵ; whereas μ, σ indicate the distribution criteria determined using the maximum likelihood estimation;

Where ϵ can be calculated based on the below equation Stedinger [101]:

$$\epsilon = \frac{P_{\max(1)}P_{\max(N)} - \left(median_{i=1,2,\ldots,N}(P_{\max,i})\right)^2}{P_{\max(1)} + P_{\max(N)} - 2median_{i=1,2,\ldots,N}(P_{\max,i})} \tag{3}$$

Where $P_{\max(1)}P_{\max(N)}$ are maximum and minimum values of $P_{\max,i}$ in the precipitation time series $i = 1, 2, \cdots, N$

μ – distribution parameter calculated using the method of maximum likelihood, from the formula:

$$\mu = \frac{1}{N}\sum_{i=1}^{N} \ln\left(P_{\max,i} - \epsilon\right) \tag{4}$$

σ – distribution parameter calculated using the method of maximum likelihood, from the formula:

$$\sigma = \sqrt{\frac{1}{N-1}\sum_{i=1}^{N}\left[\ln\left(P_{\max,i} - \epsilon\right) - \mu\right]^2} \tag{5}$$

And u_p is the quantile of the p order in standardized normal distribution.

For the series of data, the hypothesis was verified using the Kolmogorov test. The p_{value} of the test was 0.92, and there was no principle for rejecting the hypothesis that the distribution of maximum rainfall is a lognormal distribution.

4.2.6 Development of IDF curves and formulas

The rainfall IDF relationships that are widely used in water infrastructure design and construction. Because the rainfall data collected from each source were 24-hr rainfall data, it was necessary to downscale the data to shorter periods such as annual maximum rainfall data for standard periods of 10, 20, 30, 60, 120, 180, 360, and 720 minutes. This was done so that the data could be used more effectively. The dataset consists of annual maximum daily (24hr) rainfall (mm/h); over 39 years from 1980 to 2018 (see Table 3).

Table 3. Maximum daily rainfall for duration of 1980-2018 [29,92].

No.	Year	24-hr precipitation (mm)	No.	Year	24-hr precipitation (mm)
1	1980	57.6	21	2000	46.4
2	1981	40.9	22	2001	48.3
3	1982	38.1	23	2002	59.2
4	1983	32.9	24	2003	41.4
5	1984	42.7	25	2004	40.6
6	1985	72.7	26	2005	34
7	1986	73.6	27	2006	103.9
8	1987	31.8	28	2007	38
9	1988	37.2	29	2008	41
10	1989	48.4	30	2009	28.2
11	1990	35.8	31	2010	33.8
12	1991	62.4	32	2011	67
13	1992	79	33	2012	29.4
14	1993	57.9	34	2013	71.8
15	1994	41.7	35	2014	51
16	1995	75.7	36	2015	55.8
17	1996	23.9	37	2016	42.4
18	1997	35.8	38	2017	31.4
19	1998	36.8	39	2018	47.7
20	1999	28.3			

There are two methods to create IDF curves for standard periods. One approach involves acquiring rainfall data on short timescales from meteorological stations equipped with automatic rain gauges. The second method involves downsizing daily maximum rainfall from conventional rain gauges to shorter durations. Due to the lack of these standard times, the Indian Meteorological Department (IMD) utilized an equation to determine the rainfall data for periods shorter than 24-hr [102].

$$P_i = P_{24}[\frac{t}{24}]^{(\frac{1}{3})} \tag{6}$$

where P_i is the required precipitation depth for a duration less than 24-hr in mm, P_{24} is the daily precipitation depth in mm and t is the required duration time in hours.

4.2.7 Gumbel distribution

The Gumbel method, developed by the German mathematician Emil Gumbel, has been commonly employed in hydrology and other fields to model extreme events [103,104]. This approach was selected for the flood probability analysis because it has become the most popular distribution for IDF. As noted by Elsebaie [84], the Gumbel method is a straightforward and uncomplicated method that can be utilized for extreme events, such as peak rainfalls or maximum values. To calculate the frequency of precipitation P_T (in mm) for each duration with a specific return period T (in years), the following equation is used:

$$P_T = P_{ave} + K \times S \tag{7}$$

K is the Gumbel frequency factor, which can be found by:

$$K = -\frac{\sqrt{6}}{\pi}\left[0.577 + ln\left[ln\left[\frac{T}{T-1}\right]\right]\right] \tag{8}$$

where P_{ave} is the average of the maximum precipitation corresponding to a specific duration.

The arithmetic average in Equation (6) is used when using the Gumbel distribution.

$$P_{ave} = \frac{1}{n}\sum_{i=n}^{n} P_i \tag{9}$$

The individual extreme value of rainfall is P_i, and the number of events or years of record is n. The following equation is used to calculate the standard deviation:

$$S = \left[\frac{1}{n-1}\sum_{i=1}^{n}(P_i - P_{ave})^2\right]^{1/2} \tag{10}$$

where S is the standard deviation of P_T data. The frequency factor (K), which is a function of the return period and sample size, when multiplied by the standard deviation gives the departure from

the average rainfall of a desired return period. The rainfall intensity I_T (mm/hr) for the return period T_d is then calculated as follows:

$$I_T = \frac{P_T}{T_d} \tag{11}$$

where T_d is the duration in hours.

4.2.8 Log-Pearson Type III (LPT III)

LPT III involves taking the logarithm of the measured values, and then determining the mean and standard deviation based on the logarithmically transformed data. The precipitation frequency is calculated in the same way as the Gumbel method using the LPT III technique. The following is a simplified expression for the latter distribution:

$$P^* = log\ (P_i) \tag{12}$$

$$P_T^* = P_{ave}^* + K_T S^* \tag{13}$$

$$P_{ave}^* = \frac{1}{n}\sum_{i=n}^{n} P^* \tag{14}$$

$$S^* = \left[\frac{1}{n-1}\sum_{i=1}^{n}(P^* - P_{ave}^*)^2\right]^{1/2} \tag{15}$$

P_T^*, P_{ave}^*, and S^* are the same as before, but based on logarithmically transformed P_i values; i.e. P^* of Equation (12). The Pearson frequency factor K_T is determined by the return period (T) and the skewness coefficient (C_s).

The frequency factor for this distribution must be computed using the skewness coefficient C_s. Equation (16) calculates the skewness coefficient:

$$C_s = \frac{n\sum_i^{ni}(P^* - P_{ave}^*)^3}{(n-1)(n-2)(S^*)^3} \tag{16}$$

K_T values can be obtained from tables in many sources of hydrologic data; such as [105]. By knowing the skewness coefficient and the recurrence interval, the frequency factor K_T for the LPT III distribution can be extracted. The antilog of the solution in Equation (13) represents the estimated extreme value for the given return period.

4.2.9 Derivation of IDF empirical formula

The IDF empirical formula describes the relationship between rainfall intensity (I), rainfall duration (t), and return period (T). Both the Gumbel distribution method and the LPT III method can

utilize this formula. To establish an equation for calculating rainfall intensity (I) in a particular region for a specific recurrence interval and rainfall period, several steps must be taken based on the results obtained from the IDF curves. The following steps are used to derive the equation:

$$I = \frac{CT^m}{t^a} \tag{17}$$

where I is the intensity of rainfall (mm/h), t is the duration of rainfall (minutes), T is the return period (years), and the constants (C, m, and a) are empirical parameters that are dependent on precipitation data, and the shape, size, and location of the study area, and can be obtained by using the logarithmic transformation of Equation (17). After performing a logarithmic transformation on Equation (14), Equation (18) can be obtained:

$$logI = log(CT^m) - a\ logt \tag{18}$$

Assuming ($CT^m = K$), Equation (15) can be rewritten as in Equation (16):

$$logI = log(K) - alogt \tag{19}$$

Plotting the logarithm of precipitation intensity ($logI$) value against the logarithm of time ($logt$) value will present a linear relationship. To find the linear relationship's slope (the average value of constant a for all return periods), solve Equation (18), where represents the constant a, and $log(K)$ in equation (19) represents the intercept from each return period's plot. The linear relationship's slope will be displayed.

Finding C and m is as simple as plotting the logarithmic intercept ($logCT^m$) against the logarithmic return period ($logT$) in a new graph in Equation (21).

Assuming that:

$$K = CT^m \tag{20}$$

taking the log of both sides of Equation (20) will result in the following Equation (21):

$$logK = logC - mlogT \tag{21}$$

Plotting $logK$ and $logT$ in Equation (21), a linear equation of the plot can be obtained, then the m value can be found, which represents the slope of the linear relationship. The value of the anti-log of the intercept from the plotted curve represents the *C* coefficient for Equation (17).

4.2.10 Goodness of fit

With this test, it is possible to determine how well the observed frequency of occurrence in a sample corresponds to the expected frequencies obtained from the hypothesized distributions in a

sample. It is possible to perform a goodness-of-fit test between observed and expected frequencies using the chi-square quantity, which is expressed as:

$$\chi^2 = \sum_{i=1}^{k} (O_i - E_i)^2 / E_i \tag{22}$$

The variable χ^2 follows a chi-square sampling distribution, and is used to test how well the observed frequencies in a histogram match the expected frequencies, denoted as O_i and E_i respectively, for k class intervals. A small χ^2 value indicates a good fit between the observed and expected frequencies, while a large χ^2 value indicates a poor fit. If the null hypothesis is accepted, then the fit is considered good; if it is rejected, the fit is considered bad. The critical region is located in the right tail of the chi-square distribution, and its boundaries are determined by a critical value that can be found using standard chi-square tables. In this case, the critical region is defined by $\chi^2 >$ [80,84,106].

4.3 Results and Discussion

4.3.1 Extreme rainfalls

The climate of the Kurdistan region can be described as semi-arid continental, with summers that are extremely hot and dry, and winters that are quite cold and wet. The dataset covering the past 39 years has been analyzed, and it was observed that the highest maximum daily rainfall occurred in the first decade of the 21st century, specifically in 2006. Out of the nine largest episodes between 1980 and 2018, four of them occurred in this century, accounting for 44% of the total during this period. The remaining episodes occurred in the previous century, with a total daily rainfall not exceeding 79 mm (see Table 4). Therefore, the rainfall that occurred on February 3, 2006, was the highest ever recorded in the history of the Erbil meteorological station since the establishment of the KRG in 1992 and since the Iraq-Iran war between 1980 and 1988.

Table 4. Comparison of maximum daily rainfall episodes: at the end of the 20th century, and at the beginning of the 21st century, recorded at Erbil meteorological station and CFSR– in 1980–2018 [29].

The 20th century 1980-2000 (21 years)	The occurrence of rainfall episodes with the largest annual daily precipitation	The 21st century 2001-2018 (18 years)
1992 – 79mm 1995 – 75.7mm	The three largest episodes	2006 - 103.9mm
1992 – 79mm 1995 – 75.7mm 1986 – 73.6mm 1985 – 72.7mm	The six largest episodes	2006 - 103.9mm 2013 – 71.8mm
1992 – 79mm 1995 – 75.7mm 1986 – 73.6mm 1985 – 72.7mm 1991 – 62.4mm	The nine largest episodes	2006 - 103.9mm 2013 – 71.8mm 2011 – 67mm 2002 – 59.2mm

4.3.2 Analysis of rainfall distribution patterns over space and time

The results provided more evidence that the topography of the study area has an effect on both the total amount of rainfall and its spatial distribution. It was observed that the yearly rainfall is higher to the north and northwest of Erbil because these areas are located at a high elevation A.S.L For example, there are locations that reach higher than 3000 m A.S.L, and it should come as no surprise that these areas receive, on average, more precipitation than the city center of Erbil. For instance, in the direction of the town of Kasnazan, the altitude is more than 200 m A.S.L with the center of Erbil, which is only around 11 km away from the city center. This has resulted in two effects: first, there is a difference in the amount of rainfall that occurs in these two locations, and second, the runoff that occurs in this area of Kasnazan flows toward the central part of the city. This inevitably leads to flooding and water accumulation in low-lying areas.

The initial set of analyses focused on examining the time distribution and intensity of each event. The first event occurred on April 22, 2011 and lasted for approximately 20 hr, divided into three phases with a pause in between. The first two phases did not show any notable trends, but in the third phase, which started at 6:00 pm and lasted for five hours until 10:00 pm, 90% of the total rainfall was recorded in 60% of the time, which was comparable to the second quartile of the Huff method (see Figure 13a). During the first three hours of the third phase, the rainfall intensity was measured at 8.4, 15.3, and 18.6 mm/hr, respectively, all of which were classified as heavy rainfall by the AMS glossary.

The second event occurred on January 28 and 29, 2013, and recorded a total of 69.5 mm of rainfall at the Directorate of Irrigation/Erbil station. This event lasted 37 hr, with a break in between resulting

in two phases. The first phase did not exhibit any significant points, while the second phase observed a total of 58.6 mm of rainfall over 23 hr, with no intense rainfall during this period. The intensity ranged from 0.1-7.6 mm/hr, classified as moderate and light rain, with only one hour exceeding this range by 0.1 mm, thereby categorized as heavy rain. The second phase was comparable to the second quartile of the Huff method (see Figure 13b).

The event on January 28, 2014, lasted 13 hr, with light rainfall at the onset up to 40% of the time, followed by a heavy rainfall with about 90% of the total amount for the next 40-60% of the total duration of the rainfall. This phase was also comparable to the second quartile of the Huff method (see Figure 13c). The significant point occurred in the middle of the event when the intensity was 10.4 and 17.8 mm/hr, both classified as heavy rainfall by the AMS.

The episode of December 31, 2015, to January 1, 2016, was a rainfall lasting 15-hr continuously; at the beginning, rain intensity was light and moderate, then at the range of 90% of the total rainfall observed during 90% of the rainfall duration, which was the same as the fourth quartile of the Huff method (see Figure 13d). It was difficult to compare this episode to any of the quartiles of the Huff method due to its irregularity. Nevertheless, the rainfall intensity was considered heavy due to the two aforementioned hours exceeding the AMS heavy rainfall range of 7.6 mm/hr.

On November 22-23, 2018, the rainfall episode was different from the previously mentioned ones. It started immediately with heavy rains reaching an intensity of 18.2 and 9.3 mm/hr, respectively. Within the first two hours, which was 30% of the total rainfall duration, 70% of cumulative rainfall was observed. The shape of the curve was similar to the first quartile of the Huff method (see Figure 13e).

The key point to note is that out of the six episodes analyzed, five of them were classified as heavy rainfall events. Heavy rainfall is a critical factor that contributes to the occurrence of flash floods, along with other factors such as topography, urban development, sewer systems, and awareness. Based on reports by municipality officials and media photos investigating the aftermath of the rainfall events, flash floods were observed in all cases for several hours before the situation returned to normal the following day.

Comparison of the rainfall episodes in the study area with the Huff quartiles revealed that three of the events were similar to the second quartile, where half of the rainfall occurred between 25 and 50% of the total duration. Additionally, two of the episodes were identical to the first and fourth quartiles, while one of the events could not be compared due to its irregularity.

The study found that some of the rainfall episodes were classified as heavy rainfalls, but the duration of these phases is an important factor that needs to be taken into account. For example, during

the rainfall that occurred on November 22-23, 2018, the rainfall intensity reached 18.2 mm and 9.3 mm in the first two hours, but then decreased to light and moderate rainfall ranges. This demonstrates that flash floods are more likely to occur when the rainfall intensity is sustained over a longer duration, rather than just a short period of time. In a case study from Gdańsk, Poland on July 9, 2001, the rainfall continued for 17 hr, with the intensity being more than 15 mm/hr for four hours, before decreasing to light and moderate ranges [58]. However, it is believed that the duration of this intense rainfall was still short, and that there are other factors, such as urban development and changes in land use/land cover, that contribute to flash floods in the studied area.

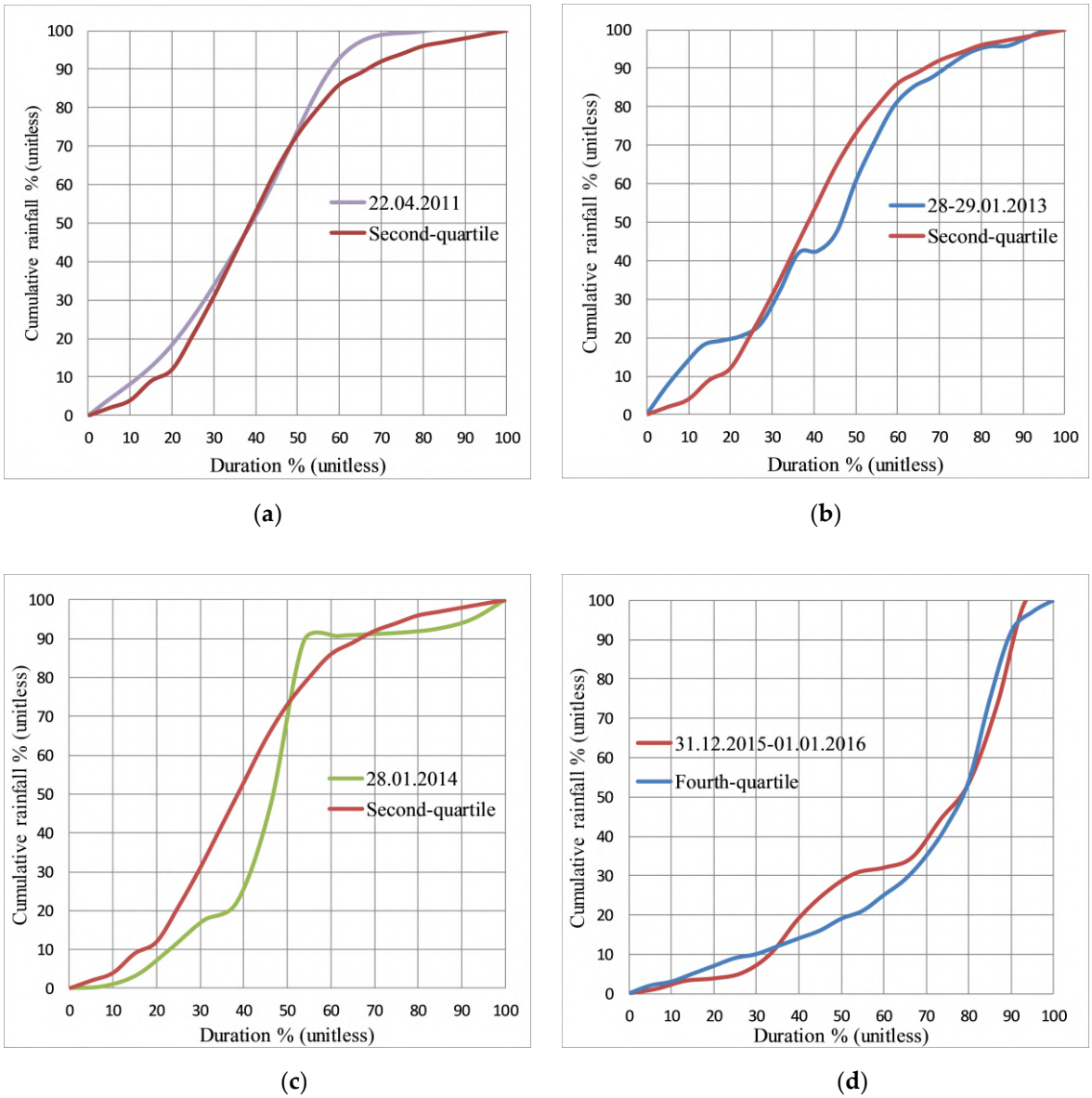

Figure 13. Comparison of the unitless time distribution of extreme rainfall events, measured in the automated meteorological station (continued on next page) [29].

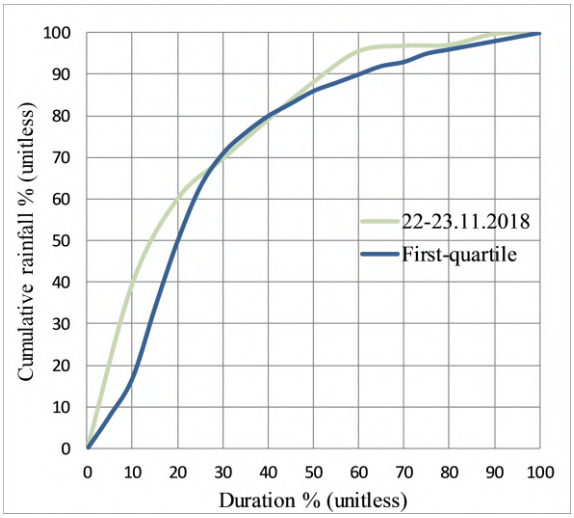

(**e**)

Figure 13. Comparison of the unitless time distribution of extreme rainfall events, measured in the automated meteorological station of the directorate of Irrigation/Erbil (a) the episode of 22.04.2011 compared with the second quartile of the Huff method. (b) the episode of 28–29.01.2013 compared with the second quartile of the Huff method. (c) the episode of 28.01.2014 compared with the second quartile of the Huff method. (d) the episode of 31.12.2015–01.01.2016 compared with the fourth quartile of the Huff method. (e) the episode of 22–23.11.2018 compared with the first quartile of the Huff method [29].

4.3.3 Exceedance probability

The Figure 14 illustrates the probability distribution of daily maximum rainfall totals based on a 39-year dataset (1980-2018) using a lognormal distribution. Four events had an occurrence probability between 1-10%, while the occurrence probability of the other events was between 10-100%. The events on April 22, 2011, January 28-29, 2013, January 28, 2014, December 31, 2015-January 1, 2016, March 28, 2016, and November 22-23, 2018 had an occurrence probability of 17.5%, 15%, 32.5%, 30%, 47.5%, and 40%, respectively.

Regarding the probability of exceedance, the theoretical probability of 1% increase in the maximum value of the annual daily total of rainfall has a small probability of 113.45 mm, compared to the highest rainfall recorded between 1980 and 2018 at 103.9 mm, which had an empirical probability of 2.5%. The theoretical probability of 10% is equivalent to 71.16 mm of rainfall, which was the amount of rainfall observed in the January 28, 2013 episode. The theoretical probability of 20% is equivalent to 59.45 mm of rainfall, which could occur frequently. Engineers and governmental authorities concerned should consider these calculated occurrence probabilities when designing and planning hydraulic structures.

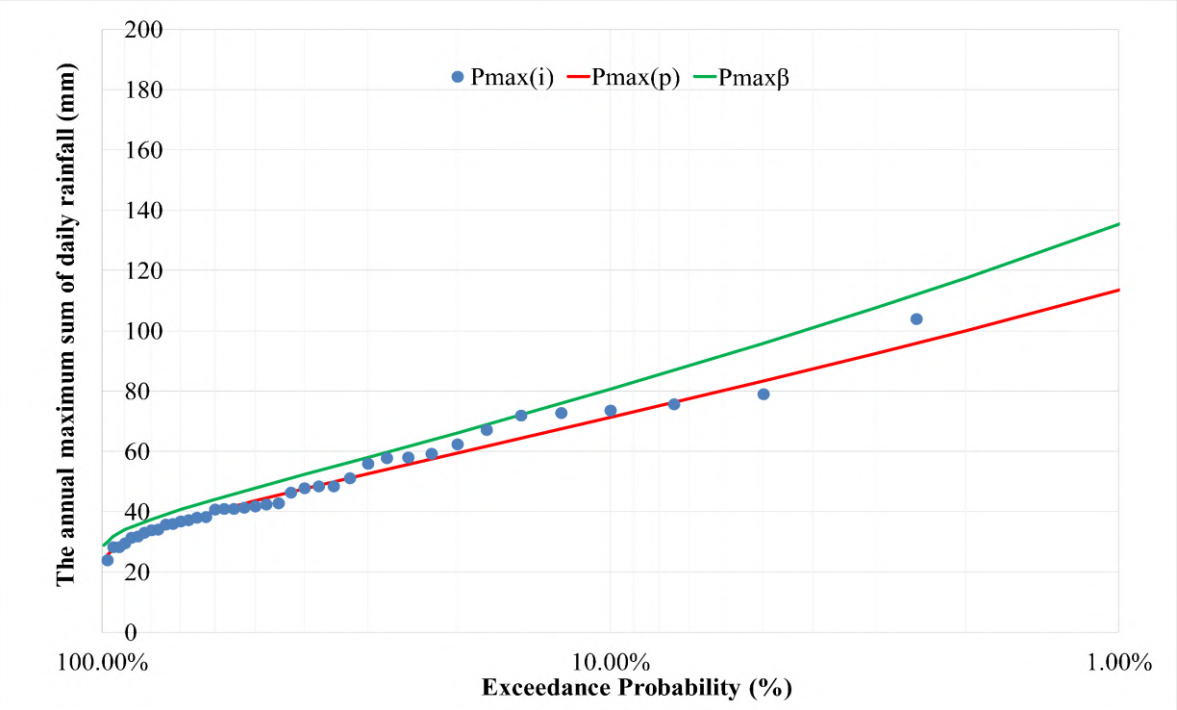

Figure 14. The exceedance probability curve according to lognormal distribution with the maximum likelihood estimation (MLE) and the 85% confidence interval limit – $P_{max(p)\beta}$. $P_{max(i)}$ denoting the empirical probability of the occurrence of annual maximum daily rainfall, $P_{max(p)}$ denoting the theoretical probability of the occurrence of annual maximum daily rainfall [29].

Box plots were used for statistical analysis in this study, as they provide a powerful tool for understanding the data and identifying patterns of distribution, including the median, outliers, and variance. Although the box plots were not all symmetrical, the box plot for February was comparatively symmetrical (see Figure 15b). However, the rainfall data for January and March were positively skewed, with the majority of the data falling within the lower quartile. This indicates a high level of mutual consonance for these months. The box plot shape allows us to visualize both the similarity and variance in the data set. Despite the high consonance, all box plots had outlier values, which could affect their appearance. The descriptive statistical analysis for maximum annual precipitation revealed a maximum value of 103.9 mm, a minimum value of 23.9 mm, and mean and standard deviation values of 47.81 mm and 17.42 mm, respectively. The lines in the boxes represented the median of the distribution for each month, while the bounds of the boxes represented the 25th and 75th percentiles. The whiskers extended to the edges of 1.5 times the interquartile range, and individual points outside of those bounds were shown (see Figure 15a and b).

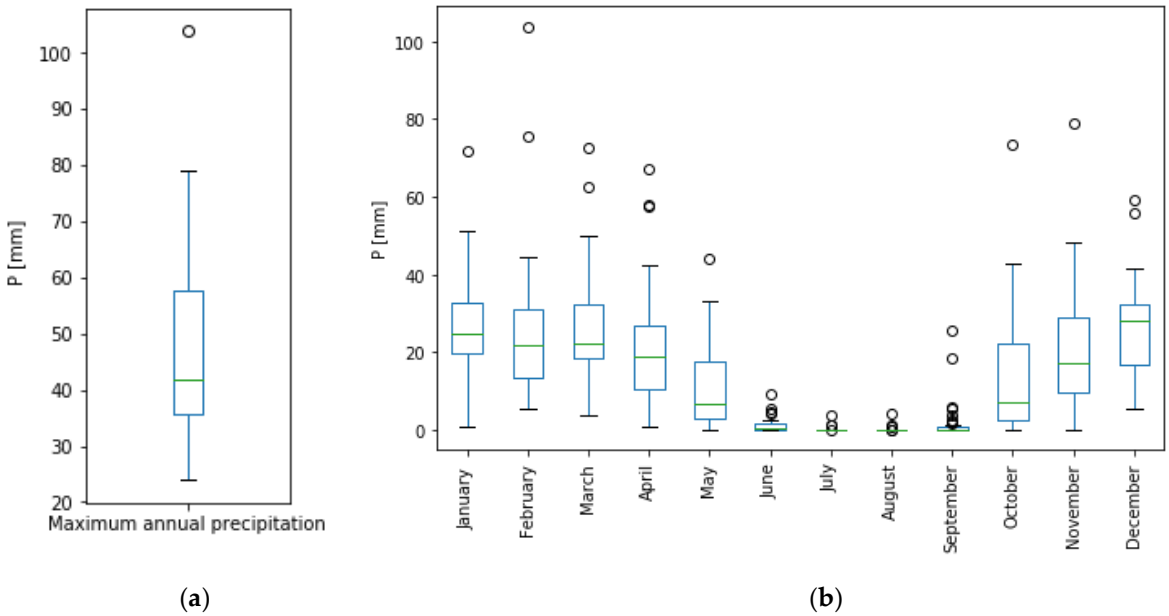

(**a**) (**b**)

Figure 15. (**a**) Box plot representing the distribution of maximum annual daily precipitation for the 39 years' data set (**b**) Box plot representing the distribution of maximum precipitation in each month for the 39 years' data set [29].

4.3.4 Developed IDF curves and formulas

As there has been no research in the studied area focusing on the analysis of rainfall and its characteristics, IDF curves have not been created or made available. IDF curves and empirical IDF formulas for the city of Erbil were developed for the first time using the annual maximum rainfall data for a period of 39 years (1980–2018), which is the only accessible recorded data. IDF curves and IDF empirical formulas were developed for rainfall durations of 10, 20, 30, 60, 120, 180, 360, 720, and 1440 minutes for return periods of 2, 5, 10, 25, 50, and 100 years for the city of Erbil in the KRI [92].

Table 5 presents the results of the Gumbel method used in this study. The findings indicate a consistent decrease in rainfall intensity as rainfall duration increases for the same return period, and an increase in rainfall intensity with an increase in return period. The IDF curves, displayed in Figures 16 and 17 on both ordinary and log-log scales, illustrate this relationship for different return periods (2, 5, 10, 25, 50, and 100 years). The study's results were compared to previous research, revealing that Erbil's rainfall intensity calculated using the Gumbel method for various return periods is lower than that of Sulaymaniyah and higher than that of Baghdad and Basrah [86,88,89]. For instance, at a duration of 60 minutes and a two-year return period, Erbil's rainfall intensity was 15.583 mm/hr, while Sulaymaniyah's intensity was 20.21 mm/hr, Baghdad's intensity was approximately 11 mm/hr, and Basrah's intensity was even lower.

Table 5. Rainfall intensities calculated using the Gumbel method for various standard time scales and return periods [92].

	10 min			20 min			30 min		
	P_{ave}=9.121		S=3.326	P_{ave}=11.492		S=4.190	P_{ave}=13.155		S=4.796
Tr (years)	K	P_T	I_T	K	P_T	I_T	K	P_T	I_T
2	-0.164	8.576	51.454	-0.164	10.805	32.414	-0.164	12.368	24.736
5	0.719	11.513	69.080	0.719	14.506	43.518	0.719	16.605	33.210
10	1.305	13.459	80.757	1.305	16.958	50.874	1.305	19.412	38.824
25	2.044	15.918	95.506	2.044	20.055	60.165	2.044	22.957	45.915
50	2.592	17.742	106.451	2.592	22.353	67.060	2.592	25.588	51.176
100	3.137	19.552	117.313	3.137	24.634	73.903	3.137	28.199	56.398
	60 min			120 min			180 min		
	P_{ave}=16.574		S=6.043	P_{ave}=20.882		S=7.614	P_{ave}=23.904		S=8.715
	K	P_T	I_T	K	P_T	I_T	K	P_T	I_T
2	-0.164	15.583	15.583	-0.164	19.633	9.817	-0.164	22.475	7.492
5	0.719	20.921	20.921	0.719	26.359	13.180	0.719	30.174	10.058
10	1.305	24.458	24.458	1.305	30.815	15.407	1.305	35.274	11.758
25	2.044	28.924	28.924	2.044	36.442	18.221	2.044	41.716	13.905
50	2.592	32.239	32.239	2.592	40.619	20.309	2.592	46.497	15.499
100	3.137	35.529	35.529	3.137	44.763	22.382	3.137	51.241	17.080
	360 min			720 min			1440 min		
	P_{ave}=30.117		S=10.981	P_{ave}=37.945		S=13.835	P_{ave}=42.638		S=16.877
	K	P_T	I_T	K	P_T	I_T	K	P_T	I_T
2	-0.164	28.316	4.719	-0.164	35.676	2.973	-0.164	39.870	1.661
5	0.719	38.016	6.336	0.719	47.898	3.991	0.719	54.779	2.282
10	1.305	44.442	7.407	1.305	55.994	4.666	1.305	64.655	2.694
25	2.044	52.559	8.760	2.044	66.220	5.518	2.044	77.131	3.214
50	2.592	58.582	9.764	2.592	73.809	6.151	2.592	86.388	3.599
100	3.137	64.560	10.760	3.137	81.340	6.778	3.137	95.576	3.982

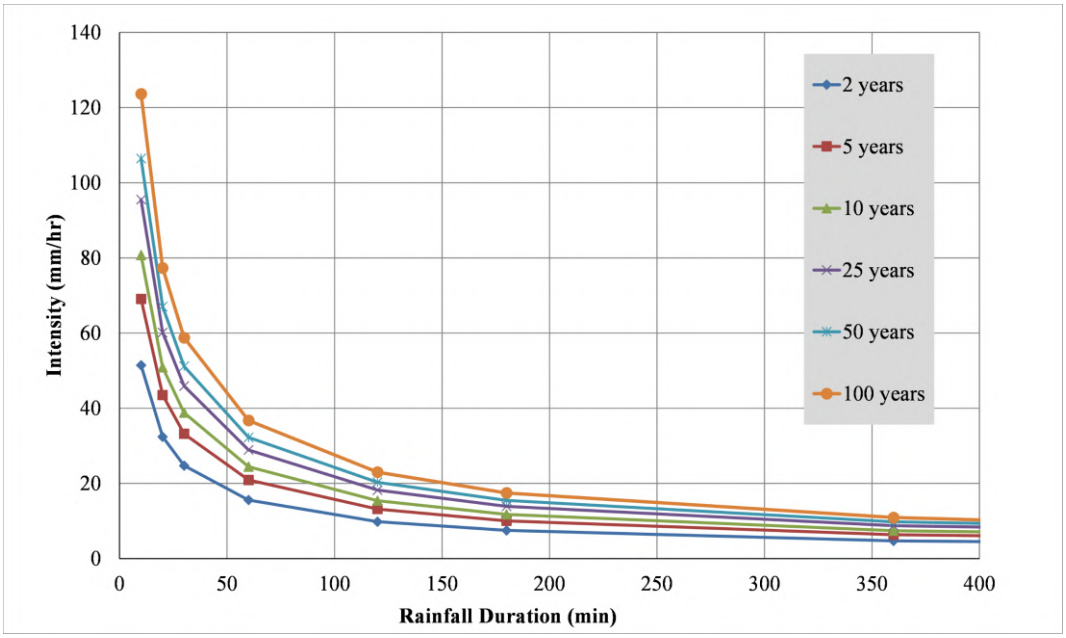

Figure 16. IDF curves generated using the Gumbel method on an ordinary scale [92].

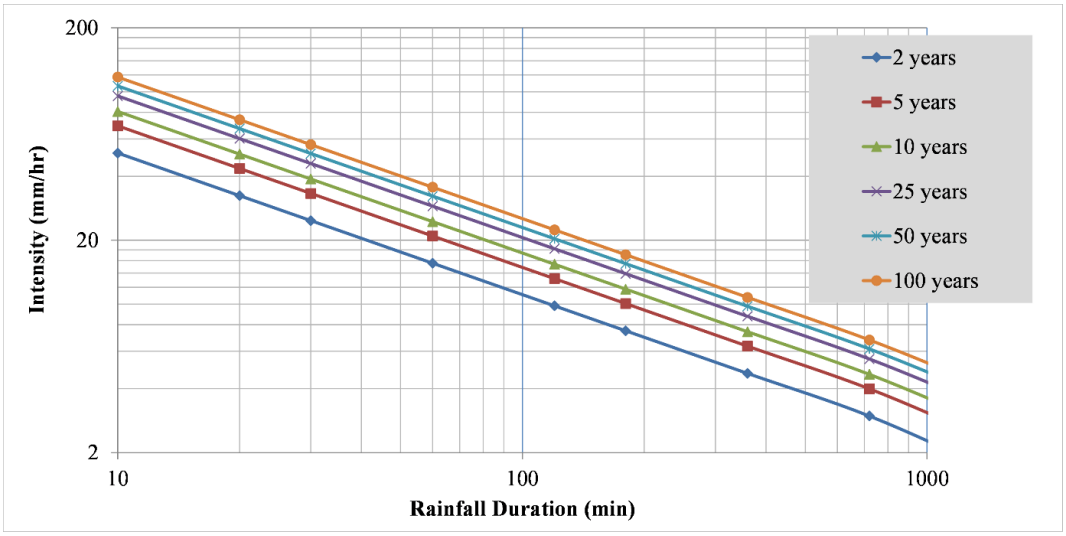

Figure 17. IDF curves generated using the Gumbel method on log-log scale [92].

It is possible that the varying climates and elevations above sea level of different locations may explain the results observed. In Iraq, the average annual rainfall is 154 mm but can vary significantly across the country, ranging from less than 100 mm in the south to over 1200 mm in the northeast. The rainy season occurs from October to April. Researchers Salman, *et al.* [107] divided Iraq into four climate zones based on topography and climate: Zone I includes the mountainous north and northeast regions with a Mediterranean climate; Zone II encompasses the undulating south and west with a steppe climate; Zone III covers the western plateau in the west, which is an extension of the Syrian and Arabian

deserts and has a continental desert climate; and Zone IV encompasses the great Mesopotamian plain in the center and south with a subtropical semi-arid climate [92]. According to Al-Ansari [13], Iraq is shaped like a basin on the topographic map and contains the great Mesopotamian plains of the Tigris and Euphrates rivers. The climate is predominantly continental, subtropical, and semi-arid, with a Mediterranean climate in the north and northeastern mountainous regions. The climate divisions of Iraq have an impact on the annual rainfall in each province. For example, Erbil and Sulaymaniyah provinces are located in Zone I with a Mediterranean climate, and their average annual rainfall is approximately 419.2 mm and varies between 328 mm and 848 mm, respectively [86]. Baghdad, located in the middle of Iraq, receives around 280 mm of rainfall annually [88]. The mean annual precipitation in the central district of Nasiriyah and Basrah provinces, located in Zone IV with a subtropical semi-arid climate, is 117.64 mm and 131.65 mm, respectively. Al-Ansari [108] classified Iraq into four regions based on the land's topography, namely the Mountain Region, Plateau and Hills Regions, the Mesopotamian plain, and Jazera and Western Plateau. While Erbil city center is located in the Plateau and Hills Regions, the northern and northeastern parts of Erbil Province are considered to be in the Mountain Region, according to Al-Ansari's classification [92].

The results obtained using the LPT III method, which were found to be similar to those obtained from the Gumbel method (see Table 6). The results indicated that as the return period increased, the rainfall intensity also increased, while an increase in rainfall duration led to a decrease in rainfall intensity for the same return period. Although there were some small differences between the results obtained from the two methods, the LPT III method was considered to be more accurate due to its ability to consider the skewness of the data distribution. Specifically, the Gumbel method produced slightly higher results than LPT III for short return periods such as 2, 5, and 10 years, but this situation became contradictory when the return period increased to 25, 50, or 100 years, as the LPT III method produced slightly higher results than the Gumbel method [92].

Table 6. Rainfall intensities calculated using the LPT III method for various standard time scales and return periods [92].

		10 minutes			20 minutes			30 minutes		
		P_{ave}=9.121		S=3.326	P_{ave}=11.492		S=4.190	P_{ave}=13.155		S = 4.796
Tr (years)	K	P_T^*	P_T	I_T	P_T^*	P_T	I_T	P_T^*	P_T	I_T
2	-0.073	0.924	8.399	50.393	1.025	10.582	31.745	1.083	12.113	24.226
5	0.852	1.060	11.477	68.861	1.160	14.460	43.380	1.219	16.552	33.105
10	1.319	1.128	13.436	80.613	1.229	16.928	50.783	1.287	19.377	38.755
25	1.890	1.212	16.291	97.745	1.312	20.525	61.575	1.371	23.495	46.991
50	2.280	1.269	18.582	111.495	1.369	23.412	70.237	1.428	26.801	53.601
100	2.640	1.322	20.983	125.898	1.422	26.437	79.311	1.481	30.263	60.525
		60 minutes			120 minutes			180 minutes		
		P_{ave}=16.574		S=6.043	P_{ave}=20.882		S=7.614	P_{ave}= 23.904		S=8.715
	K	P_T^*	P_T	I_T	P_T^*	P_T	I_T	P_T^*	P_T	I_T
2	-0.073	1.184	15.262	15.262	1.284	19.228	9.614	1.343	22.011	7.337
5	0.852	1.319	20.855	20.855	1.420	26.275	13.138	1.478	30.078	10.026
10	1.319	1.388	24.414	24.414	1.488	30.760	15.380	1.547	35.211	11.737
25	1.890	1.471	29.602	29.602	1.572	37.297	18.648	1.630	42.694	14.231
50	2.280	1.528	33.767	33.767	1.629	42.543	21.272	1.688	48.700	16.233
100	2.640	1.581	38.129	38.129	1.682	48.039	24.020	1.740	54.991	18.330
		360 minutes			720 minutes			1440 minutes		
		P_{ave}=30.117		S=10.981	P_{ave}=37.945		S=13.835	P_{ave}=42.638		S=16.877
2	-0.073	1.443	27.732	4.622	1.543	34.940	2.912	1.644	44.022	1.834
5	0.852	1.579	37.896	6.316	1.679	47.746	3.979	1.779	60.156	2.506
10	1.319	1.647	44.363	7.394	1.747	55.894	4.658	1.848	70.422	2.934
25	1.890	1.731	53.791	8.965	1.831	67.773	5.648	1.931	85.388	3.558
50	2.280	1.788	61.358	10.226	1.888	77.306	6.442	1.989	97.400	4.058
100	2.640	1.841	69.284	11.547	1.941	87.293	7.274	2.041	109.982	4.583

AlHassoun [81] recommended that when accuracy is required in storm design studies, the results of the LPT III method be used. Figures 18 and 19 show the intensity–duration–frequency (IDF) curves using the LPT III method on an ordinary scale and on the log-log scale (for T = 2, 5, 10, 25, 50, 100 years). The findings of that study are consistent with the findings of previous studies conducted in some parts of the study area and neighboring countries, according to the researchers.

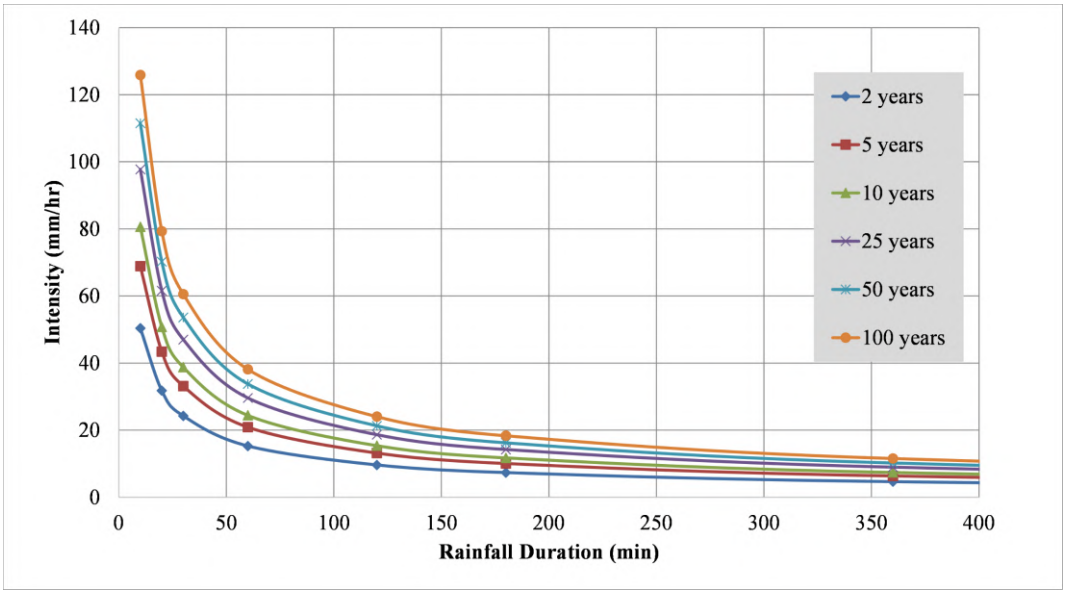

Figure 18. IDF curves generated using the LPT III method on an ordinary scale [92].

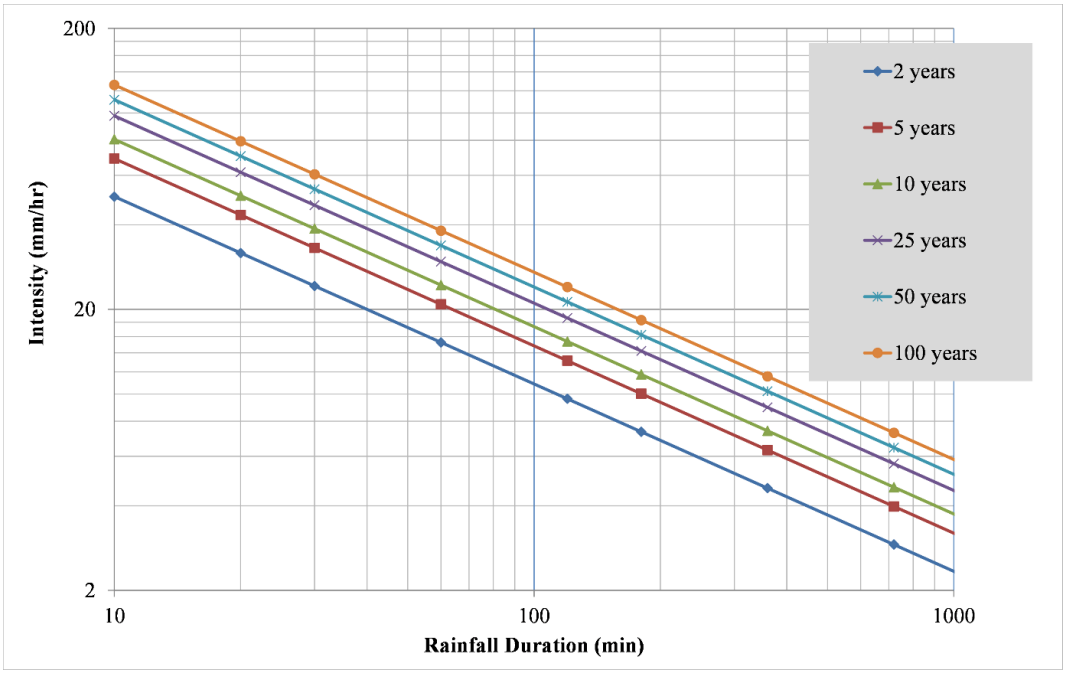

Figure 19. IDF curves generated using the LPT III method on a log-log scale [92].

Table 7 displays the parameter values resulting from analyzing the IDF data with the two methods. These values are utilized to formulate equations for the study area. The parameters of the IDF equations, namely (C, m and a) obtained from both distributions are relatively close, except for the C parameter from the Gumbel Theory distribution, which was slightly higher than the other distribution's C parameter (refer to Table 7). Additionally, the parameters (C, m and a) of other Iraqi Provinces are

presented, indicating that the developed IDF equations of all mentioned Governorates have slightly different (m and a) parameters, while the parameter C varies significantly. Sulaymaniyah and Erbil have the highest C values of 288.4 and 234.020, respectively, using the Gumbel method, whereas in Baghdad, Nasiriyah, and Basrah, the value of the C parameter decreased to 9.074, 8.283, and 7.95, respectively. This variation in parameter values among different Iraqi cities is a testament to the distinct climatic conditions in each city, as previously explained in this section.

Table 7. The values of the parameters used in the development of formulas in different cities of Iraq [82,86,88,89].

Region	Parameter	Gumbel method	LPT III method
Erbil	C	234.020	212.790
	m	0.200	0.228
	a	0.681	0.667
Sulaymaniyah	C	288.4	
	m	0.191	
	a	0.666	
Baghdad	C	9.074	7.044
	m	0.318	0.422
	a	0.667	0.667
Nasiriyah	C	8.283	7.565
	m	0.301	0.350
	a	0.674	0.674
Basrah	C	7.95	
	m	0.298	
	a	0.667	

In the process of developing the IDF empirical formulas, a logarithmic conversion was implemented to the precipitation parameters in both methods. This conversion helped transform the relationship into a linear equation, enabling the calculation of all associated parameters. The empirical equation parameters (Equations 23 and 24) obtained for the Gumbel and LPT III distribution methods, respectively, are presented in Table 7.

$$I = \frac{234.020T^{0.200}}{t^{0.681}} \tag{23}$$

$$I = \frac{212.790T^{0.228}}{t^{0.667}} \tag{24}$$

Additionally, various goodness-of-fit tests were conducted to determine the most suitable statistical distribution. The results of the chi-square goodness-of-fit test conducted on an annual series of rainfall data are presented in Table 8. The table indicates that there is no statistically significant

difference between the rainfall intensity values for all return periods, as shown by the chi-square test results performed on the dataset. This discovery reinforces the utility of developing local IDF formulas rather than one general equation for the entire country. As previously mentioned, rainfall is unpredictable and erratic in both time and space, and therefore, localized formulas are better suited to capture the unique characteristics of each region.

Table 8. The results of the chi-square goodness-of-fit test on the annual maximum rainfall [92].

Chi square (χ^2)		
Return periods (year)	Gumbel method	LPT III method
2	0.255	0.095
5	0.023	0.092
10	0.080	0.103
25	0.037	0.049
50	0.006	0.0002
100	0.167	0.098

4.4 Conclusions

Erbil, one of the Iraqi cities, frequently experiences extreme rainfall events leading to urban flash flooding in the Centre district. The Centre district of Erbil is characterized by flat terrain with elevations ranging between 390 and 425 meters A.S.L. According to the GDMS, the amount of annual rainfall in Erbil Province ranges from 350 to 1300 mm, depending on the elevation above sea level. The greatest total daily rainfall amount recorded in the analyzed 39-year period did not exceed 103.9 mm. Out of the six episodes analyzed, three were similar to the second quartile of the Huff quartiles, indicating that the second quartile of the Huff method could be used as the synthetic rainfall distribution in the studied area and as input data for future hydrological modeling works.

However, five out of the six analyzed episodes were characterized by heavy rainfalls of short duration, leading to flash floods. Therefore, the design criteria for the sewer system must be revised, and a new synthetic rainfall distribution must be created. An important conclusion from the analysis of the probability of exceeding the maximum rainfall in Erbil is that the rainfalls with a probability of 1%, 10%, or 20% are relatively high, with values of 113.45 mm, 71.16 mm, and 59.45 mm, respectively. It is important to note that designers often use such rainfall values in developing drainage systems. However, high rainfall has returned almost every year in the last two decades of the twenty-first century, which is not consistent with design assumptions. Therefore, incorporating these changes in design should be a priority to reduce the impact of floods in cities.

Moreover, the study derived IDF curves and empirical formulas for rainfall durations and return periods specific to Erbil city in Iraq, using the Gumbel and LPT III methods. The results showed that there was no significant difference between the methods and that the IDF curves were suitable for predicting rainfall intensity for design purposes. The study highlights the importance of having IDF curves specific to each province in Iraq due to differences in topography and climate. However, the study's validity was limited by the lack of recorded data on shorter-duration rainfall events, and the analysis only examines statistical relationships between variables and does not reveal physical mechanisms.

5. Part II: Investigation the Hydrological Response to Urbanization

5.1 State of Art

Since the latter half of the 20th century, RS has become a popular method for detecting changes in LULC. RS imagery has been widely used for environmental analysis and urban expansion, with various functional and sophisticated strategies being developed [109]. The classification of LULC plays a crucial role in research on physical and social sciences concerning urbanization and soil mapping [110]. LULC is an essential parameter for detecting natural changes due to climate change and human activities. The detection of LULC changes is valuable for a broad range of subjects, including urban development, coastal dynamics, deforestation monitoring, shoreline changes, and river transportation, which uses multitemporal satellite images [111-113]. Human beings seeking to meet different needs such as residential, agricultural, industrial, mining, and other infrastructural facilities, cause changes in LULC, which are main concerns linked with the economic and sustainable development of a region. The timely and precise detection and identification of changes in the Earth's surface provide a foundation for a deeper understanding of human-nature interactions and correlations [114-117]. In the past, in situ data was used for studying LULC; however, such data are insufficient in spatial and temporal extent. It is also difficult, if not impossible, to collect data from unreachable areas. Therefore, data collection is time-consuming and often expensive, and such data are not reliable for effective planning and decision-making. Satellite images are a valuable source of information on LULC, as they provide swift, cyclic, and precise data acquisition from the RS system [118]. Multitemporal RS data, mainly time-series Multispectral Scanner (MSS), Thematic Mapper (TM), Enhanced Thematic Mapper Plus (ETM+), and Landsat Data Continuity Mission (LDCM) images, have been widely used for detecting LULC changes since the launch of the Landsat satellite in the early 1970s [119-121]. Researchers have widely used Landsat images because they are relatively inexpensive, accessible, and have a long history.

The expansion of built-up areas has a significant impact on the climate and natural resources, as urban sprawl transforms natural land cover into man-made land cover to meet human needs. This results in the establishment of an unacceptable climate in terms of air quality and the depletion of natural resources [122]. Investigating the spatial and temporal forms of urban development has become one of the critical challenges in monitoring and analyzing present and future directions of urban growth issues [123]. For the last 300 years, the trend of LULC has been characterized by deforestation and the expansion of agricultural land globally [124]. However, in recent decades, developing countries have experienced a reduction in rural land and an expansion of urban areas through urbanization [125-128]. Urban growth phenomena have become unsustainable in many cities worldwide [129]. In fact,

urbanization itself is a globally concerning topic, where people are leaving rural areas and moving to big cities [130].

The expansion of impermeable areas caused by urbanization is widely recognized as a major contributor to increased flood risk [131]. As cities grow, hydrologic and hydraulic processes are altered, resulting in decreased drainage capacity and an increased occurrence of flash floods in urban areas [132,133]. This increase in flood risk is due to the larger volume and faster rate of runoff caused by impermeable surfaces such as concrete and asphalt. Therefore, it is important to understand the extent and location of land use and land cover changes, as they have significant impacts on various aspects of urban planning and the environment, such as land management, air quality, and flood probability [134-137]. Many studies have investigated the effects of LULC changes on urban flash floods, such as the increase in peak discharge and shorter time to peak in the Konar catchment in India and the step-up in peak discharge in Riyadh, Saudi Arabia [138,139]. Similarly, in Poland, increased catchment impermeability has been shown to be connected to an increase in maximum flows over time [131].

From 2003 until the present day, the KRI has experienced significant development and expansion. This growth has been driven by the region's relative safety and strong economy, which have led to increased demand for property investment. The KRG has also encouraged local and international investors to build residential and industrial areas. However, this expansion has also led to changes in the land use and land cover (LULC) patterns of Erbil, the capital city of the KRI, particularly in the central district. A study by Hameed [140] found that built-up areas and bare land have expanded while vegetation and farmlands have decreased dramatically. Unfortunately, this rapid urban development has also increased the probability of urban flash floods in Erbil Province. Since 2010, the number of urban flash floods has increased, leading to overflowing sewer pipes and sewage mixing with stormwater [29]. These floods have also caused power outages as local power generators were flooded.

Given these changes, it is important to urgently map the LULC transformations in Erbil Province to aid in land development planning, flood control, and resource management. Identifying and classifying LULC changes in the city can help manage hydro-structures and monitor environmental changes. This knowledge can also assist authorities in making better decisions.

In this part of the study, LULC changes have been analyzed in the studied area in five phases from 1984 to 2019. With the aim to answer four research questions regarding LULC changes and their impact on the runoff coefficient, which is used to determine the amount of rainfall runoff. The questions included: (1) How did LULC change every ten years during this period? (2) How did economic, social, and political situations influence LULC changes? (3) How did these changes affect hydrological

response? and (4) Is the probability of urban flash floods increasing? The results of the study were also published in article [141].

5.2 Material and Methods

5.2.1 RS data

In order to analyze changes in LULC in the center of Erbil Province, various LULC cover types were generated using remotely sensed data. Satellite images from Landsat 4-5 (TM) (1982–2011), Landsat 7 ETM+ (1999–present), and Landsat 8 OLI (2013–present) were obtained from the LandsatLook viewer (https://landsatlook.usgs.gov/viewer.html), with each image selected based on quality and seasonal similarity (between June and August). To delineate the watershed boundary of the study area, a DEM of the Shuttle Radar Topography Mission (SRTM) (http://dwtkns.com/srtm30m/) was obtained at a resolution of 1 arc-second (30 m). Additionally, higher resolution true-color satellite and aerial imagery were obtained from Google Maps and HERE WeGo (wego.here.com). A soil map for the area was created using a basin boundary from the digital soil map of Iraq prepared by the Food and Agriculture Organization (FAO) (see Figure 20).

Table 9. Source and details of Landsat images used for classification [141].

Satellite	Sensor_ID	path/row	No. Bands	Date of acquisition	Grid cell size (m)
Landsat 4-5 TM C1 Level-1	LT51690351984167XXX02	169/35	7	June 15, 1984	30
Landsat 4-5 TM C1 Level-1	LT51690351994226RSA00	169/35	7	August 14, 1994	30
Landsat 7 ETM+ C1 Level-1	LE71690352004198ASN01	169/35	9	July 16, 2004	30
Landsat 8 OLI/TIRS C1 Level-1	LC81690352014201LGN01	169/35	11	July 20, 2014	30
Landsat 8 OLI/TIRS C1 Level-1	LC81690352019183LGN00	169/35	11	July 02, 2019	30

5.2.2 Image pre-processing

Extensive pre-processing was carried out, specifically involving geo-referencing, layer stacking, extraction, and image enhancement. To obtain multi-composite images for further analysis, layers were stacked using Erdas Imagine 2014, and then the study area was extracted from the stacked satellite image using the "extract by mask" function in ArcGIS 10.5.1, with the Erbil basin boundary as the mask. Using Erdas Imagine 2014 again, the resolution of the images was enhanced twice by applying the convolution function in spatial tools and the subset function in subset and chip tools. This enhancement

process was necessary to obtain a clear image for the subsequent classification and accuracy assessment stage.

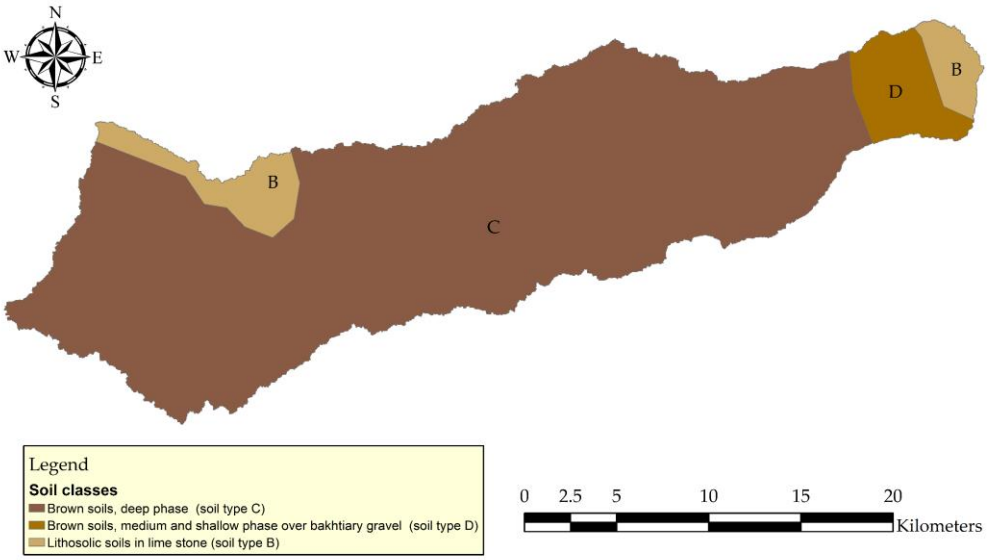

Figure 20. The soil classes in the study area [141].

5.2.3 Image classification

Image classification and change identification are commonly used techniques for observing changes in LULC in urban areas. The process is complex and requires careful consideration of multiple factors to achieve accurate results. The basin was classified into five different LULC classes, which include water, built-up areas, bare land, agriculture, and vegetation. To perform this study, supervised classification using Erdas Imagine 2014 was used. In supervised classification, the software user creates spectral signatures of known classes, and then the software identifies the cover type of each pixel in the image based on its most similar spectral signature [142]. The Maximum Likelihood Classifier (MLC) is a widely used parametric classification algorithm [143-145]. In the beginning of the classification process, a false-color composite was created by combining three bands (bands 5, 4, and 3) for each LULC class in each satellite image. Google Maps and HERE WeGo were used to accurately define the training sites [141]. The training sites varied in pixel size and were used as areas of interest to train the images. These trained images were later merged into one signature for a given LULC category and used for the classification.

5.2.4 Image post-processing

The LULC maps produced were noisy due to the similarities in spectral responses of certain land cover classes, such as pasture/scrubland and built-up areas. To ensure accuracy, the classified image was compared to reality, and an accuracy assessment analysis was conducted to verify the classification results. The purpose of the accuracy assessment was to quantitatively evaluate the degree to which the pixels were classified into the LULC categories. The accuracy of the classified images for 1984, 1994, 2004, 2014, and 2019 was evaluated using randomly generated points in Erdas Imagine 2014. The number of reference points used for accuracy assessment varies based on the size of the study area [146,147].

5.2.5 Hydrological modeling

To better manage water resources, it is crucial to understand how changes in the environment affect hydrological processes. A hydrological model to demonstrate the impact of land surface changes on the hydrological response of the basin, specifically the relationship between rainfall and runoff. The Hydrologic Engineering Center (HEC) developed the Hydrologic Modeling System (HMS) for this purpose, and it is widely used due to its simplicity and limited number of parameters [148,149]. The hydrological model consists of three main components: the basin model (see Figure 21), the meteorological model, and the control specification, which describe the hydrological processes. The HEC-GeoHMS tool in ArcMap was used to develop the basin model parameters. The Curve Number (CN) approach developed by the Soil Conservation Service (CN-SCS) was used to calculate precipitation losses [149], and the SCS-Unit hydrograph approach was used for transformation. The Muskingum–Cunge method was used for river routing [150,151]. Analyzed long-term series of maximum daily rainfall data were used in this study and within them, a probability distribution of 10%, which is equal to 71.16 mm [29], which was presented in Part I of this thesis.

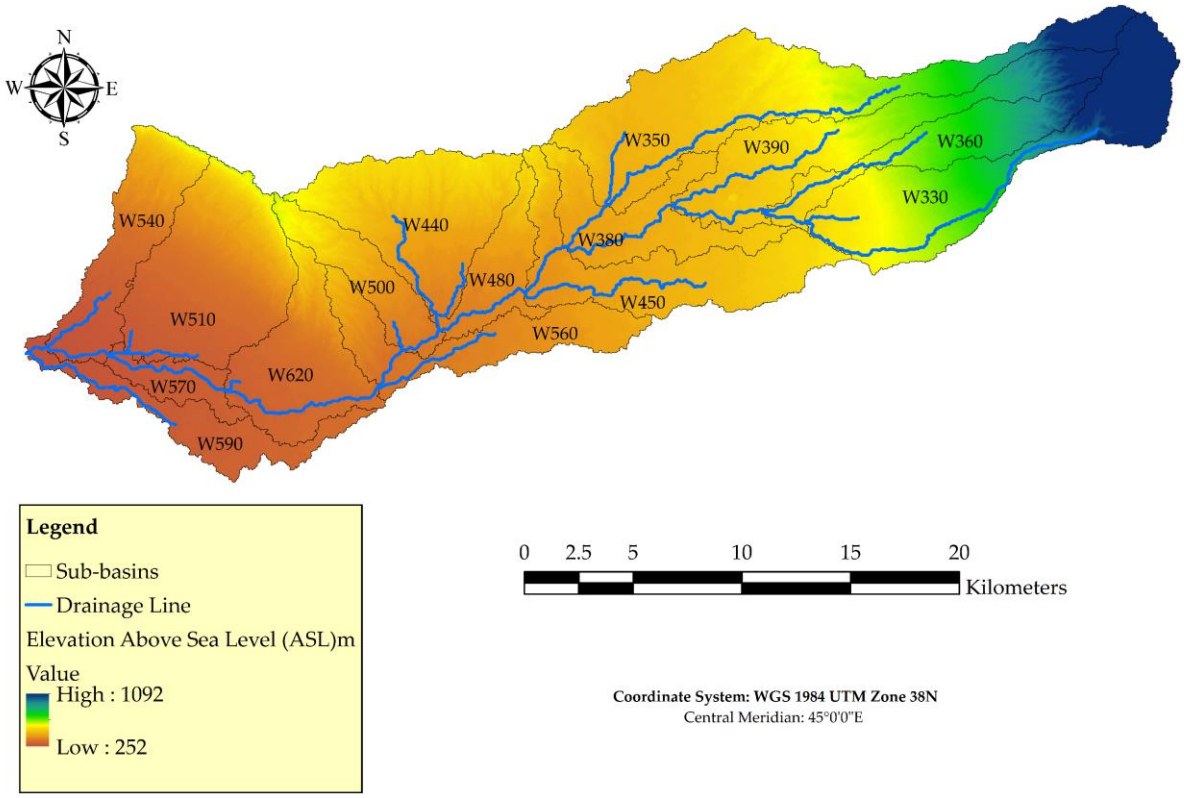

Figure 21. Topography and delineated sub-basins over the study area [141].

5.3 Results and Discussion

5.3.1 LULC accuracy assessment

The evaluation of the classification accuracy for the prepared LULC change maps was conducted, which involved assessing both producer's accuracy and user's accuracy. Producer's accuracy is calculated by dividing the number of correctly classified reference points of a specific class by the total number of reference points for that category, indicating the error of omission [152]. User's accuracy, on the other hand, measures individual category accuracy by dividing the number of correctly classified reference points of a specific class by the total number of points classified as that category, indicating the error of commission [153]. The accuracy assessment was performed on the results of five images, and the overall classification accuracy was determined to be 85.60% [141]. It is worth noting that each image was analyzed and evaluated independently, and different satellite images were used in this study (see Table 10). The accuracy rate is dependent on the quality of the RS data, such as the resolution, available bands, and image quality.

Table 10. Accuracy assessment for the 1984, 1994, 2004, 2014 and 2019 classified images based on the error matrix [141].

	Years	Water	Built-up	Bare land	Agriculture	Vegetation
Producer's Accuracy (%)	1984	100	98.88	62.99	78.69	94.74
User's Accuracy (%)		86.00	88.00	80.00	96.00	72.00
Overall Classification Accuracy (%)					84.40	
Kappa Statistics (%)					80.50	
Producer's Accuracy (%)	1994	100	98.80	57.25	80.70	97.73
User's Accuracy (%)		77.00	82.00	79.00	92.00	86.00
Overall classification Accuracy (%)					83.20	
Kappa Statistics (%)					79.00	
Producer's Accuracy (%)	2004	-	99.04	68.21	81.02	99.07
User's Accuracy (%)		-	82.40	82.40	88.80	85.60
Overall Classification Accuracy (%)					84.80	
Kappa Statistics (%)					79.73	
Producer's Accuracy (%)	2014	-	95.28	83.85	77.78	93.69
User's Accuracy (%)		-	80.80	87.20	95.20	83.20
Overall Classification Accuracy (%)					86.60	
Kappa Statistics (%)					82.13	
Producer's Accuracy (%)	2019	-	95.37	83.21	84.83	95.45
User's Accuracy (%)		-	82.40	91.20	98.40	84.00
Overall Classification Accuracy (%)					89.00	
Kappa Statistics (%)					85.33	

However, it is essential to acknowledge that this study has limitations when examining the accuracy of classified maps due to the nature of LULC changes, which can vary according to different regional conditions. Additionally, there was a lack of availability of ground values that could have provided more accurate results.

5.3.2 LULC results and change detection

Figure 22a-e displays the land use and land cover (LULC) maps produced for the study area for the years 1984, 1994, 2004, 2014, and 2019. In both 1984 and 1994, the water class accounted for only 0.50% of the basin, and surface waters disappeared in the years following this period. However, if there is sufficient precipitation, seasonal streams still flow in the area. For instance, in 2018, the annual precipitation level reached 721.3 mm, which was higher than the levels recorded in Erbil city center since 1992. Consequently, some seasonal streams reappeared.

(**a**) 1984

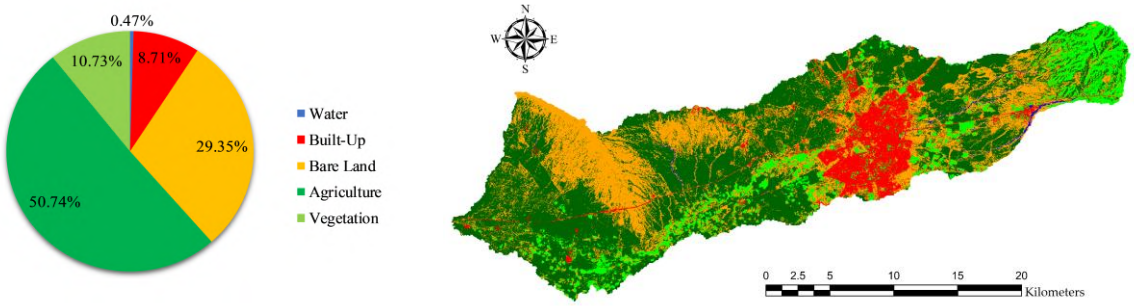

(**b**) 1994

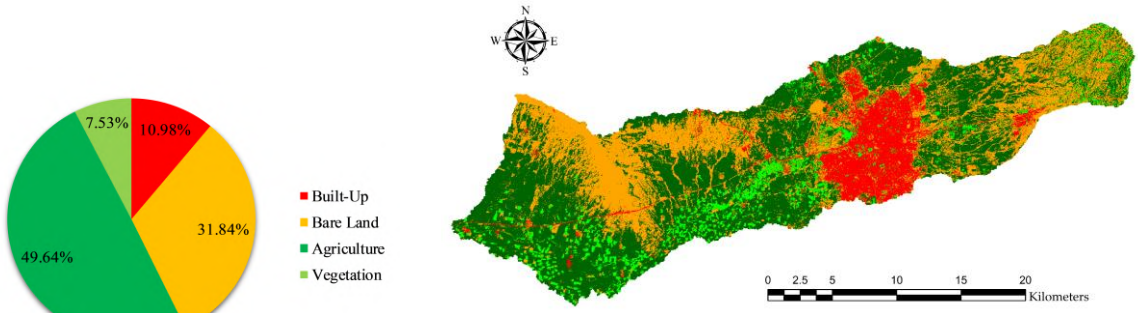

(**c**) 2004

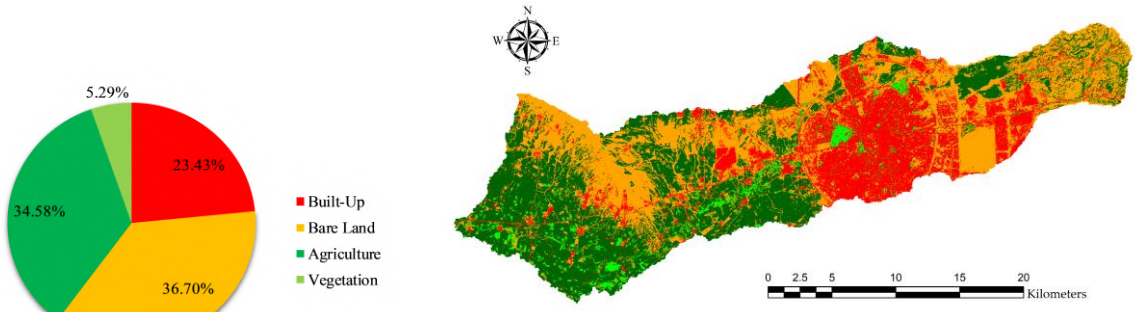

(**d**) 2014

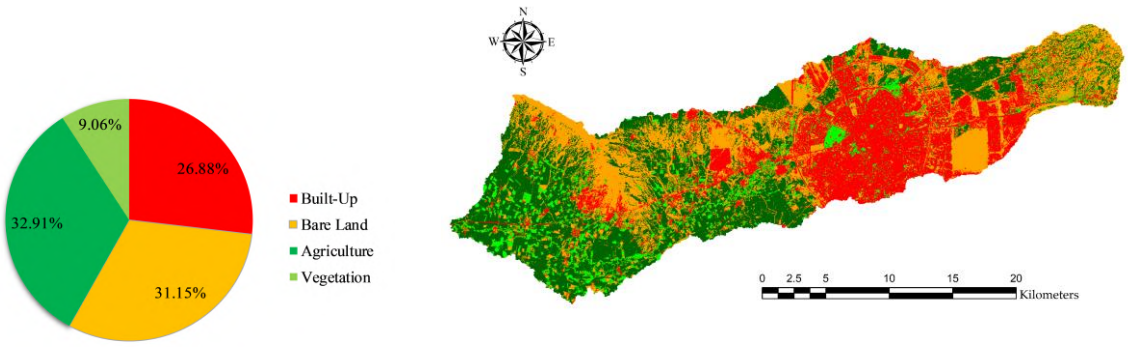

(**e**) 2019

Figure 22. Land Use/Land Cover (LULC) maps of the studied area for the years (**a**) 1984, (**b**) 1994, (**c**) 2004, (**d**) 2014 and (**e**) 2019 [141].

Between 1984 and 2014, there was a significant decrease in the areas of agriculture and vegetation, while built-up areas steadily increased from 30.751 km² in 1984 to 119.101 km² in 2014. Specifically, agricultural areas accounted for 54% of the total area in 1984 but decreased to 33% in 2019. The range of vegetation also decreased from approximately 14% in 1984 to 5% in 2014. The LULC transformation from 1984 to 2004 was observed to be steady compared to that between 2004 and 2014. The latter period saw a significant transformation and ultimately, development in the urban area.

In 2019, built-up areas covered 136.658 km², and there was a reduction in bare land compared to 2014. The area of vegetation, which had been decreasing in previous decades, increased to around 46.054 km² in 2019. The table provided in the study (Table 11) highlights the changes in land cover and land use in the area.

Table 11. LULC categories; their corresponding areas for 1984, 1994, 2004, 2014 and 2019 [141].

LULC Category	1984	1994	2004	2014	2019
	Area (km²)				
Water	2.537	2.387	-	-	-
Built-up	30.751	44.283	55.823	119.101	136.658
Bare land	129.337	149.191	161.863	186.572	158.347
Agriculture	276.966	257.919	252.363	175.781	167.288
Vegetation	68.756	54.568	38.298	26.893	46.054

The evolution of the land cover in the area is divided into two different time periods, as determined by the analysis. The first time period begins prior to 2004, while the second time period begins after that year. Therefore, it can be claimed that the year 2004 is a year that may be designated as a distinguishing point between two periods where changes in LULC are quite different from one another. The allies' successful overthrow of Saddam Hussein's dictatorship in Iraq in March 2003 and

the country's subsequent re-engagement with the rest of the world are the primary contributors to this divergence. Throughout the first phase, the economic situation in Iraq largely collapsed, and there was no development of the kind being discussed here. Iraq was also involved in a number of wars, including the conflict that lasted a decade and took place between Iraq and Iran from the early to the late 1980s. Then Iraq's invasion of Kuwait broke out, which was followed by the Gulf War. As a result, Iraq was subjected to a prolonged economic and political blockade. All of these circumstances had a cumulatively bad effect on the population and increased the burden they carried. The growth rate in the built-up area class is relatively slow between the years 1984 and 2004, in comparison to the years that followed

The city of Erbil has experienced significant changes in urbanization across different time periods, driven by factors such as legislation, politics, and socio-economic determinants. From 1984 to 2003, the region experienced slow economic growth due to several wars, but after 2004, Erbil witnessed considerable growth and development, particularly in the built-up areas. The increase in built-up areas between 1984 and 2004 was about 25 km², equivalent to 1.25 km² per year, while between 2004 and 2014, the increase was about 63 km², equivalent to 6.3 km² per year. This rapid urban growth can be attributed to oil production and real estate investment, which led to an economic boom. The population of Erbil Province also grew significantly during this period [141]. The study shows that increasing urban development in floodplain zones can lead to a higher peak discharge, reduced time to peak, and increased runoff volume, which has been supported by previous research in the area. Figure 23 shows the evolution of built-up areas from 1984 to 2019.

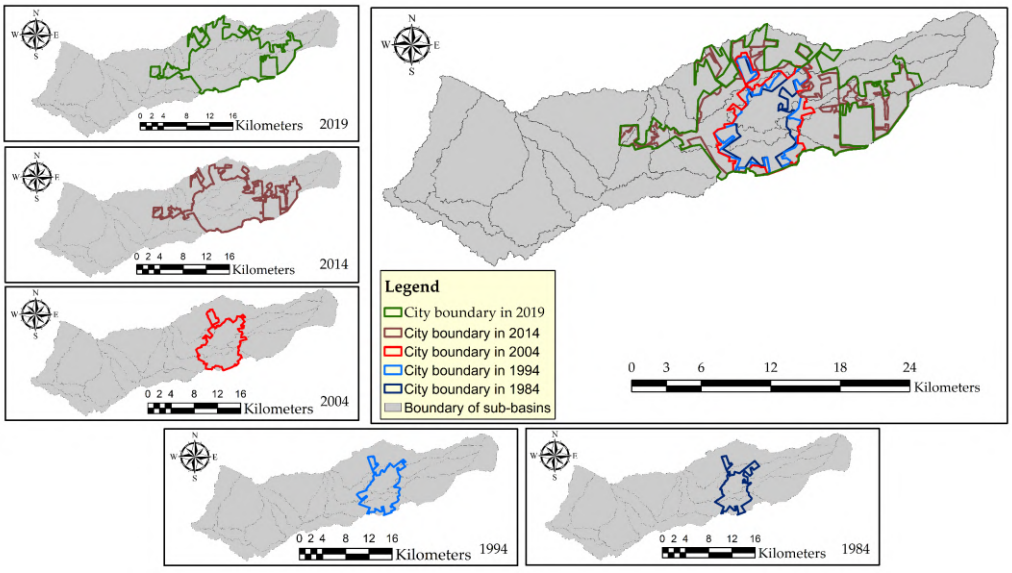

Figure 23. The evolution of built-up areas from 1984 to 2019 [141].

5.3.3 The Impact of urbanization on the hydrological response and potential for flash floods

The objective of this study is to analyze the impact of urban development on flood peak discharge, runoff coefficient, and flood hydrograph, using rainfall-runoff hydrological modeling. The modeling was conducted for a storm rainfall depth with a probability distribution of 10%, which is equivalent to 71.16 mm, and land use conditions from 1984, 1994, 2004, 2014, and 2019. The runoff was calculated using the SCS-CN loss method in the HEC-HMS model, which takes into account the soil group, land use, and hydrological conditions of the land cover to compute the CN. The soil and land use maps were combined, and the hydrological soil group was determined based on the soil cover. The assigned CN values, which are relevant to the hydrological soil group and land use cover, are listed in Table 12. The composite CN for each sub-basin was computed and used as input for the SCS-CN modeling in HEC-HMS (see Table 13).

Table 12. Runoff CN for the integration of different land cover and hydrological soil groups [141].

LULC category	Runoff CN for different soil groups			
	A	B	C	D
Water	100	100	100	100
Built Up	77	85	90	92
Bare Land	68	79	86	89
Agriculture	65	76	84	88
Vegetation	43	65	76	82

Table 13. Calculated runoff CN based on the unified soil groups layer and LULC layer of the sub-basins in the studied area using HEC-GeoHMS [141].

Sub-Basins	Years				
	1984	1994	2004	2014	2019
W330	81.12	81.81	83.74	86.14	86.15
W350	83.89	83.99	84.57	86.07	86.10
W360	84.39	85.58	86.15	87.74	87.84
W380	84.84	85.26	85.62	87.02	86.96
W390	85.03	86.31	87.07	87.52	87.44
W440	83.49	83.53	83.68	84.06	83.83
W450	84.92	85.15	85.70	87.21	87.20
W480	82.95	83.71	83.44	85.01	85.23
W500	82.21	82.28	82.17	82.68	82.44
W510	84.20	84.38	84.18	84.39	83.79
W540	83.55	83.64	83.51	83.73	83.19
W560	83.10	83.71	83.47	84.52	84.21
W570	82.37	83.44	83.12	83.59	82.83
W590	82.75	82.97	82.79	83.18	82.93
W620	83.21	83.89	83.82	84.32	83.96

The use of hydrological modeling has shown that urban growth has a greater impact on flash flooding caused by more frequent rainfall events, rather than larger storm events, which have a smaller probability distribution [29]. Erbil's urban expansion is evident due to its flat terrain and the urban model shaped by the form and height of the Erbil Citadel, resulting in concentric rings with a radial axis in peripheral areas [26]. Although many land parcels were distributed within the city master plan, some of them have not been developed due to a lack of municipal services and facilities. However, the category of the land has changed, from agricultural to residential, such as in the neighborhood of Hasarok 8. Residential areas are mostly concentrated on the east, north-east, and south-east of the city. On the other hand, the other part of the city is more developed in terms of architecture and urban design, with wealthy quarters, exclusive compounds, office buildings, and business centers. Erbil has become the most developed city in the region due to its status as the capital of the KRI, and the presence of KRG ministries, the parliament, international organizations, the airport, diplomatic representatives, international companies, and political infrastructure. Erbil has now more than ninety different quarters, compared to only eight in 1950 [154]. The upper sub-basins (W330, W350, W360, W380, W390, and W450) show a significant increase in built-up areas, particularly in W330, which grew by about 2178% between 2004 and 2019. Also, built-up areas in sub-basins such as W350 and W360 grew by 465.14% and 1029.29%, respectively. In contrast, the lower sub-basins (440, 480 and 500, 510, 540, 560, 570, 590, and 620) experienced slower development between 1984 and 2004, but development began after 2004 [141]. However, the size of development in these areas was not as significant as that in the upper sub-basins.

Analyzing the land cover over such a long period of time was done with the intention of translating these changes into the hydrological response of the basin to these changes and determining the influence that urbanization has on the potential for flash floods. The results sheds light on both urban development and its impact on the flood peak discharge, in addition to the runoff coefficient and the flood hydrograph. It does this by employing the rainfall-runoff hydrological modeling for a storm rainfall depth with the probability distribution of 10%, which is equal to 71.16 mm, and the land use conditions of 1984, 1994, 2004, 2014, and 2019 (see Figure 24). The runoff coefficient for the Erbil basin was increased as a direct result of the LULC transformation that took place. The hydrological modeling that was done using HEC-HMS revealed that the runoff coefficient for the Erbil basin in 1984 was only 0.39. The rate grew to 0.40 and 0.41, respectively, in 1994 and 2004, and the rate reached 0.44 in 2014, which could be considered a high rate.

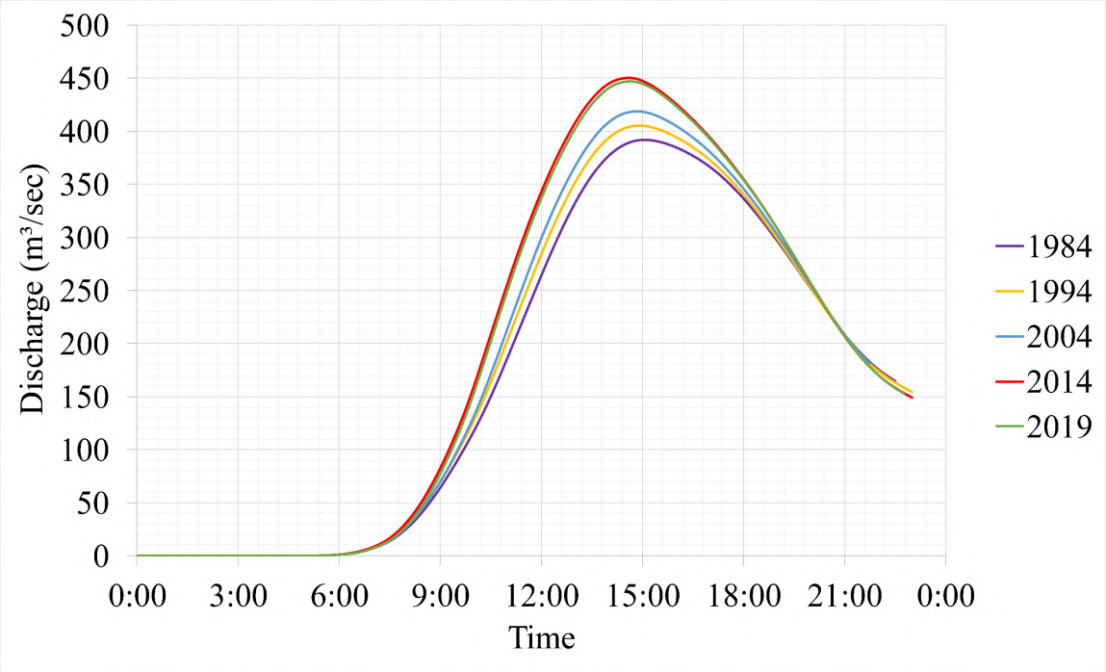

Figure 24. Outflow hydrograph for p = 10% rainfall [141].

The current study, which is backed by research done in the past in this field, reveals that growing urban development in floodplain zones will boost peak discharge, reduce the time to peak, and increase the runoff volume [110,131,155-157]. It is interesting to note that the results, which were published in the first half of the year 2020 [29], predicted that the number of flash floods will increase. The reasoning behind this prediction was that the permeable land that is able to absorb water has decreased, while the impervious areas that are unable to absorb water significantly have increased. Because of this, the rainfalls will directly turn into the runoff. All signs point to the fact that the combined influence of climate change and urban expansion on the current urban flooding issue is one that is indeed serious. However, the beginning point of the solution is not just related to the far future, but it also has a significant amount to do with the present condition, which is that the city does not have an appropriate urban drainage system and enough flood protection.

Within a basin, urbanization will, in general, not only result in an increase in the peak discharge, but it will also lead to an increase in the runoff volume and the extent of the area that is inundated. This predicts an increase in the number of flooded streets and other built-up regions in metropolitan areas. The impact will also be influenced by the topography of the area. The inundation will only be present for a shorter period of time in locations that are steep, but the water velocity will be very high. This can result in the destruction of property caused by the power of the water, as well as the washing away of

vehicles that are parked on the streets. The presence of stagnant water on gentle slopes presents additional risks, including the pollution of water sources.

5.4 Conclusions

The study conducted using multispectral satellite data in Erbil Province, KRI, between 1984 and 2019, aimed to address various research questions related to LULC changes and their impact on flash floods. The findings of the study revealed a steady increase in bare land and built-up areas from 1984 to 2004, while built-up areas increased by almost 245% between 2004 and 2019. Permeable areas like agricultural land and vegetation declined from 1984 to 2019, with vegetation areas only increasing from 2014 to 2019, mainly in the downstream area of the city. The study identified three factors that influenced land use/cover changes, namely economic, social and political factors.

The study investigated the impact of urbanization on flood peak discharge, runoff volume and runoff coefficient, under different urbanization scenarios, with storm rainfall depth of 71.16mm at the probability distribution of 10%. The results showed that urban development considerably aggravates flooding caused by a given storm due to hindrance of natural drainage and decreasing permeability. The study also found that parallel to urban development, the runoff volume and peak discharge increased, thereby increasing the probability of flash floods, which can pose a risk to the quality of life in the city center.

The study highlights the importance of RS and GIS techniques for detecting human activities, especially in third world countries. The study findings are important for policymakers and local authorities in making decisions on how to adapt the city to the current situation and plan for future development. The study results and prepared LULC scenarios will be useful in mitigating flash floods in the studied area.

6. Part III: A Systematic Approach for Choosing the Appropriate Hydrodynamic Model of Urban Flood

6.1 State of Art

Floods and flood modeling are a hot topic in the research field of hydrology and hydrological modeling. Researchers from various continents have investigated the attributes, impacts, and outcomes of intense rainfall incidents that occurred in diverse hydrological conditions [57,158-162]. Furthermore, the rapid transformation of LULC is acknowledged as a significant contributor to the reduction in ground imperviousness, leading to an increase in the volume of surface runoff. In recent times, RS has emerged as an efficient tool for tracking LULC alterations [133,135,136,139,163,164], while the GIS and hydrological modeling packages are widely employed by researchers to identify flood hazards and create flood maps. Although such events are beyond human control or prevention, the frequency and severity of damage could be minimized by implementing techniques such as flood risk mapping, spatial planning, and flood modeling.

The selection of a suitable hydrodynamic model is a critical component of flood modeling. Numerous studies in the literature focus on the application of SWEs to simulate flood inundation in both Full Momentum and simplified models. The Full Momentum model is recommended by scholars, including [165,166]. However, despite the availability of high-resolution topographic data, the lack of observed data limits the ability to adequately evaluate the results of any hydraulic model, as noted by Hunter, *et al.* [167]. Consequently, many researchers have employed the simplified DW model to simulate urban flood events, as seen in works by [168-173]. Recently, the increasing availability of user-oriented computational codes has encouraged the use of two-dimensional (2-D) SWE models, as discussed by Pilotti, *et al.* [174]. Teng, *et al.* [175] reviewed several popular software/models capable of modeling flood inundation, while Néelz and Pender [176] compared the performance of some common 2-D software.

In order to accurately replicate the intricate and multidirectional surface flow paths that arise from urban configurations, the use of two-dimensional (2-D) models is highly recommended in built-up areas. Several studies [177-180] have highlighted the importance of such models. Flood propagation in urban areas is inherently two-dimensional, and its characteristics are shaped by the complex interplay between flow patterns and the configuration of streets and buildings. This interaction results in multiple flow paths at intersections and water flowing around or within buildings, among other things [181].

There are numerous 2-D numerical models and software packages available, each with varying capabilities and from different developers, some of which require purchase and others that are open-source [182]. For this study, the open-source package of HEC-RAS 2-D, which employs both Full Momentum and DW hydrodynamic models, was utilized. As 2-D hydrodynamic modeling is well-suited for flood inundation in urban areas, HEC-RAS was chosen as a widely-used modeling tool for hydraulic engineers. Prior to the 2016 update to version 5.0, HEC-RAS was one-dimensional, and could not directly model the hydraulic effects of cross-section shape changes, bends, and other two- and three-dimensional aspects of flow. However, with the introduction of version 5.0, two-dimensional modeling of flow and sediment transport capabilities were included. Numerous studies have used HEC-RAS 2-D to generate flood inundation maps in urban areas [139,183-191]. Quirogaa, *et al.* [192] demonstrated that HEC-RAS 2-D, a free-surface flow modeling program, performed well in simulating inundation extent during the February 2014 flood event in the Bolivian Amazonia, compared to satellite images. The program is likely to become a standard in this type of modeling, similar to its one-dimensional counterpart. However, different HEC-RAS models have varying mesh representations, capabilities, and data requirements. Costabile, *et al.* [193] assessed the performance and capabilities of HEC-RAS 2-D in basin-scale rainfall-runoff simulations, comparing results obtained using the Full Momentum equations and DWEs options to those obtained using a 2-D Full Momentum model developed by the authors. Other studies have also evaluated the HEC-RAS 2-D model, including Ghimire, *et al.* [194], who assessed its use in predicting flood propagation time and inundation extent for a flood warning system, and Shrestha, *et al.* [195], who compared the suitability of MIKE 21 and HEC-RAS for 2-D floodplain modeling. This study aims to build on this existing literature by exploring the potential and capabilities of the HEC-RAS 2-D model in representing building units in urban flood modeling simulations.

Urban areas, with their large number of buildings, streets, and other manmade features, have distinct characteristics that must be accounted for in flood simulations. Neglecting these features can result in inaccurate results. Soares-Frazão and Zech [196] emphasized that building and street configurations impact flood propagation in urban areas. Jeong, *et al.* [197] conducted two physical experiments and a field study case to numerically analyze the effects of flood waves on urban areas caused by a dam failure. Buildings are one of the most crucial components in urban flood modeling, and their immovability to water flow is a critical factor in urban flooding, as stated by [198]. Proper representation techniques for buildings are also important in urban flood modeling, in addition to the choice of hydrodynamic model. Four techniques, namely BH, BB, BR, and BP, have been commonly

applied to represent buildings in simulations. This part of the study focuses on investigating the application of Building-Block and Building-Resistance techniques, along with HEC-RAS 2-D, for urban flood modeling.

This study aims to investigate the suitability of a 2-D hydrodynamic model (HEC-RAS) for simulating flash flood propagation in urban areas, using different building representation techniques. To assess the model's accuracy, previous experimental tests were utilized, specifically the Toce River physical model data from Testa, *et al.* [199]. The study aims to address gaps in existing literature and contribute to the ongoing debate. The main objectives of this research are to evaluate the potential and capabilities of HEC-RAS 2-D in accurately representing inundation processes within heterogeneous floodplains, compare computational efficiency between models with different grid resolutions and roughness coefficients, and verify different building representation techniques in numerical simulations of urban flooding using results from Szydłowski [200].

The focus of this study is to explore the effectiveness of the BR method, with a high Manning roughness coefficient, for simulating floods in urban areas using HEC-RAS 2-D. Unlike previous work by Beretta, *et al.* [201], which only investigated steady flow, this research examines unsteady flood wave propagation. Additionally, the conclusions drawn about the DW model used for urban flood modeling differ from previous findings. By demonstrating the feasibility of implementing this technique with a low-resolution DEM and open-source software like HEC-RAS 2-D, this study can aid researchers in their urban flood modeling efforts and contribute to a better understanding of numerical modeling and urban flooding. The results of this research part were also published in article [202].

6.2 Materials and Methods

6.2.1 Toce River physical model

The ENEL-CESI hydraulic laboratory in Italy built a physical model of the Toce River to study dam-break flow in its natural valley [199]. The model was made of concrete and was scaled at 1:100 for 5 km of the river. The model was 50 m long and 11 m wide and included water depth gauges at designated locations (see Figure 25a). To simplify the flow structure, the urban zone was separated from the valley borders by two masonry walls positioned parallel to the model's main axis. The urban zone included 15 × 15 cm concrete cubes to represent the urban buildings (see Figure 25b). The model had a digital terrain model of 5 cm, but for this study, the digital terrain model was recreated at a higher resolution of 1 cm, including a modified digital terrain model based on the wall and urban area. The water depth data were recorded using electrical conductivity gauges at 10 locations suspended above

the model, providing high temporal resolution for model validation. The measurement instruments recorded water levels at 0.2 s intervals.

(**a**)

(**b**)

Figure 25. (**a**) The upper part of the original model where the buildings are laid out in the staggered configuration. (**b**) Bathymetric set up by the placement of two masonry walls, where the model city has been located (staggered configuration) [202].

The experiment included the use of 10 electrical gauges, with two located at the entrance point of the flood discharge (P1 and P2) and the remaining eight (P3 to P10) placed beside the concrete blocks to record water depth variations. Two different topographical forms were tested, namely the original

and modified DEM, with the modified DEM simulating only a 7-m-long region at the upstream end of the physical model. In addition, two building layouts in the urban area model were assessed, namely the aligned layout (16 buildings located in rows with a radial direction parallel to the main axis of the valley, but for the original DEM, including 20 buildings) and the staggered layout (14 buildings located in a checkerboard layout, while for the original DEM, including 18 buildings) (see Figure 26).

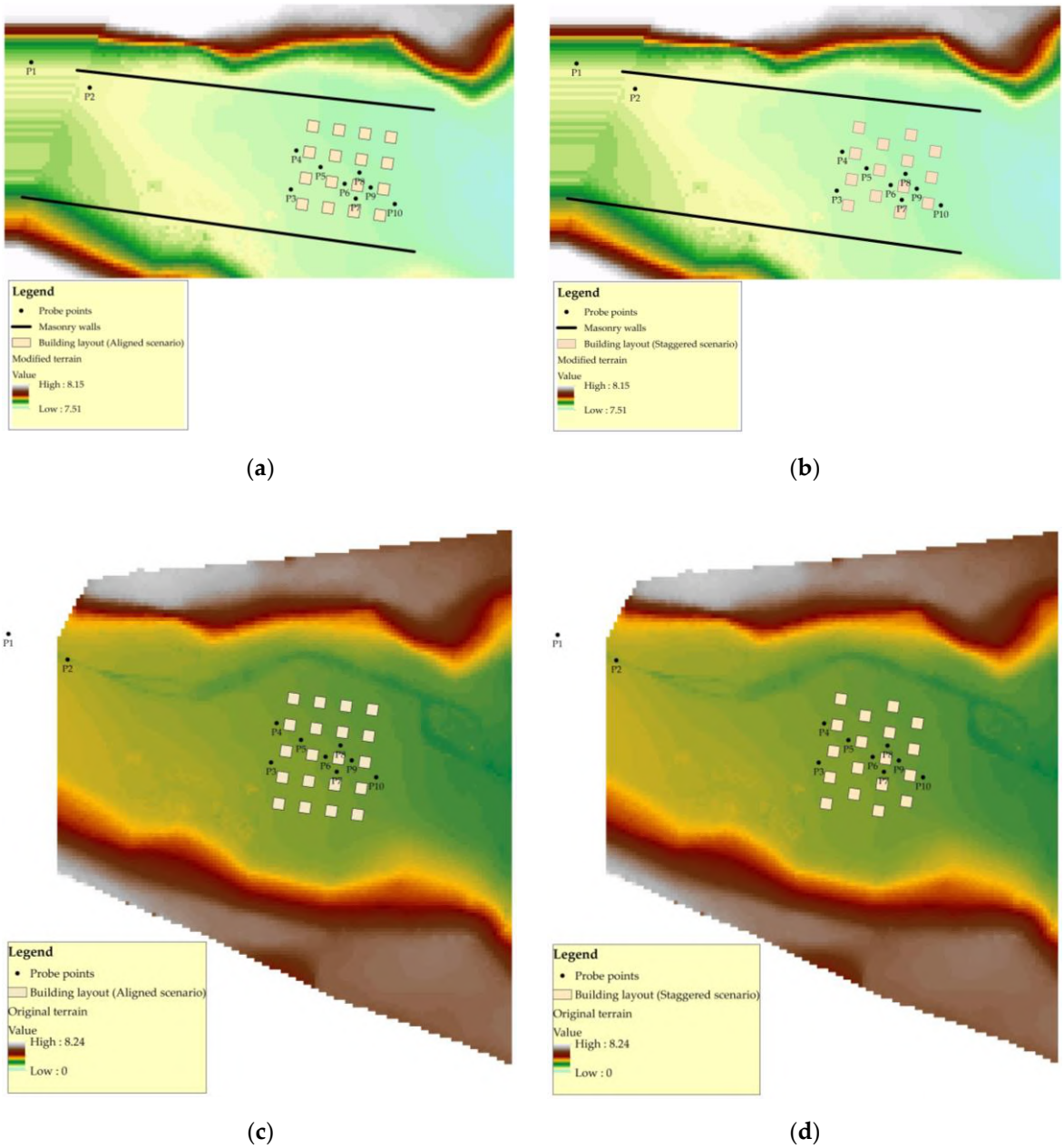

Figure 26. (**a**) The aligned layout of buildings in the modified DEM. (**b**) The staggered layout of buildings in the modified DEM. (**c**) The aligned layout of buildings in the original DEM. (**d**) The staggered layout of buildings in the original DEM [202].

The flood hydrographs recorded as the inflow discharge for both the modified and original DEMs, as well as for the two building layouts, were quite similar with some differences in the flow peak (see Figure 27). The depth variation measurements at points P1 and P2 were used to define the boundary condition at the inflow section, where the flow was subcritical. At the downstream end of the model, the outflow was either sub- or supercritical depending on the actual flow conditions.

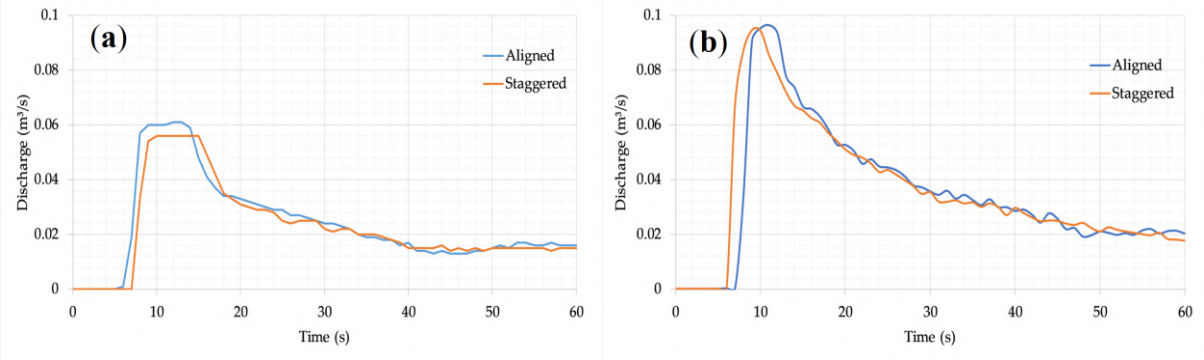

Figure 27. (A) Inflow discharge hydrograph for the modified DEM. (B) Inflow discharge hydrograph for the original DEM [202].

In addition, in order to address the sudden changes in the direction of the flow that occur inside the 2-D flow field, a very fine mesh is required. In this particular investigation, the simulation was carried out using different numerical mesh sizes. In addition, a very fine mesh is required to address the sudden changes in the direction of the flow that occur inside the 2-D flow field. In this particular investigation, the simulation was carried out using different numerical mesh sizes.

6.2.2 Hydrodynamic models of urban flood

In the present study, both model options (the Full Momentum equations and the Diffusion Wave) were considered for HEC-RAS 2-D. The solved 2-D Saint Venant equations in their non-conservative forms are as follows:

$$\frac{\partial H}{\partial t} + \frac{\partial (hu)}{\partial x} + \frac{\partial (hv)}{\partial y} + q = 0 \tag{25}$$

$$\frac{\partial u}{\partial t} + u\frac{\partial u}{\partial x} + v\frac{\partial u}{\partial y} = -\mathrm{g}\frac{\partial H}{\partial x} + v_t\left(\frac{\partial^2 u}{\partial x^2} + \frac{\partial^2 u}{\partial y^2}\right) - c_f u + fv \tag{26}$$

$$\frac{\partial v}{\partial t} + u\frac{\partial v}{\partial x} + v\frac{\partial v}{\partial y} = -\mathrm{g}\frac{\partial H}{\partial y} + v_t\left(\frac{\partial^2 v}{\partial x^2} + \frac{\partial^2 v}{\partial y^2}\right) - c_f v + fu \tag{27}$$

where t is time, u and v are considered as the velocity horizontal components in x and y direction, respectively, and q is a source/sink flux term. H is water surface elevation, h is water depth, g is

gravitational acceleration, $v_t$is the coefficient of horizontal eddy viscosity, c_f is the coefficient of bottom friction, and f is the Coriolis parameter. The Diffusion Wave model can be derived from SWEs by neglecting all terms in the dynamic equations (26) and (27) except for the forces of gravity, friction and hydrostatic pressure. A full explanation of the equations can be found in the HEC-RAS version 5.0 hydraulic reference manual [203].

6.2.3 Building representation techniques

In existing literature, the commonly used building representation techniques for hydrodynamic numerical models in modeling built-up area flooding are four, as previously reported by several authors [171,198,200,204-207]. These techniques are:

- **BB technique:** The building-block technique involves modifying the ground elevation data by increasing the elevation of building units to their real height or a sufficiently high value to prevent water from flowing over them. The entire flow area is meshed as a single grid, ensuring that water flows around the buildings without missing any grids. However, this technique requires grid refinement around the buildings to accurately represent their profiles, and it is recommended to use a fine-structured or unstructured 2-D numerical mesh in HEC-RAS 2-D. The accuracy of the DEM is crucial in creating an accurate hydrodynamic model for built-up areas, as it can limit the quality of the hydraulic model that can be generated [208].

- **BR technique:** The building-resistance technique is a method of assigning different Manning coefficients to each grid in a hydrodynamic model. By setting a high Manning coefficient in simulated building areas, the resistance of the buildings against water flow is artificially increased, resulting in slow water flow velocity. A low Manning coefficient is set for other simulated areas, representing the actual land cover. This technique is useful when obtaining a high-resolution DEM is difficult or costly. It can be applied in HEC-RAS 2-D by creating user-defined polygons where the Manning coefficient n value can be overridden. The user must have a LULC map to utilize the spatially varying Manning n value and specify the user-defined Manning n region.

- **Building-Hole (BH) technique:** This technique involves representing buildings as holes in a numerical mesh that simulates water flow in a given area. The holes are positioned based on the layout of the buildings, with free-slip wall conditions creating a blockage effect that prevents water from flowing over or through the buildings. However, this method can be limited by complex building geometries, which can lead to undesirable mesh refinements that

decrease the efficiency of the model [209-211]. Unfortunately, this technique cannot be applied in HEC-RAS 2-D because the software does not allow cells to be deactivated or holes to be included in the 2-D flow area.

- **Building-Porosity (BP) technique:** This method, which originates from the porous media theory, results in a modification of the Saint-Venant equations [212]. Porosity can be defined in different ways, such as the average volume of pore space in a permeable medium or the average area of pore space in a slice through a permeable medium [213]. Both volumetric and areal porosity can vary spatially in a nonhomogeneous permeable medium, and areal porosity can also exhibit anisotropy, depending on the orientation of the surface over which the areal average is taken. For example, in an urban surface area filled with solid features, the pore space represents the gaps between the solid features, the volumetric porosity indicates the proportion of the land surface that can store water, and the areal porosity represents the portion of space suitable for directionally dependent flood conveyance [214]. However, this method cannot be used in HEC-RAS 2-D, as only the standard Full Momentum (Saint-Venant equations) and DW models are implemented in this software.

6.3 Results and Discussion

The simulation of floods can be carried out using various methods, each with different process representations and numerical models. For this particular study, eight test cases were created for both the original and modified Toce River physical models, involving two types of building configurations (aligned and staggered) and two types of building representations (BB and BR) for each model, as available in HEC-RAS 2-D. The hydraulic conditions used in the numerical simulations were identical to those observed during the physical modeling, although the issue of physical scaling was not analyzed in the modeling process. The full-sized Toce River physical model was used as a hydraulic system for the study. The primary goal of the study was to identify and verify models and techniques. To achieve this, the modified DEM was utilized for the identification stage, while the original DEM was used for the verification stage. All the tests involved unsteady flow analysis, which allowed the study of flood wave propagation. Table 14 provides the naming convention for the test cases.

The delineation of the 2-D flow area in HEC-RAS 2-D involves outlining a polygon within the boundary of the underlying DEM to create a 2-D numerical mesh. To achieve precise simulation of the terrain and profile of buildings, mesh resolutions of 1, 2, and 5 cm were tested and compared using a

0.02 s time step. Mesh resolution is considered a crucial factor in numerical models, as it affects the accuracy of the output mapping and the simulation run time [173,187,215]. The simulation run time and accuracy depend on the model simulation time step and the mesh size. The BB method involved increasing the elevation of the building blocks to create a more realistic simulation. In contrast, the BR method set the Manning coefficient to different values, namely, 0.1, 1, and 10 $m^{-1/3}$.s for the building grids and 0.0162 $m^{-1/3}$.s for other grids. The Manning coefficient value of 0.0162 $m^{-1/3}$.s for the concrete bed was recommended by the experimental team at ENEL-CESI [199].

Table 14. The naming of test cases in the study [202].

Test case	Building layout	DEM	Building representation
1a-BB	Aligned	Modified	BB
1b-BB	Staggered	Modified	BB
1a-BR	Aligned	Modified	BR
1b-BR	Staggered	Modified	BR
2a-BB	Aligned	Original	BB
2b-BB	Staggered	Original	BB
2a-BR	Aligned	Original	BR
2b-BR	Staggered	Original	BR

6.3.1 Analysis of different mesh resolutions in the BB technique

The BB technique is widely recognized as the most realistic method for representing building units in hydrodynamic numerical modeling. Geometric information is the primary factor that influences the outcome of hydrodynamic model simulations. In the BB method, the elevation of the built-up area is increased sufficiently to prevent water from either accumulating or flowing over the buildings in the flow field.

To better understand numerical modeling in composite urban scenarios, the impact of mesh resolution on numerical modeling results is evaluated in detail. In test cases 1a-BB and 1b-BB, a numerical mesh composed of 92,403, 23,014, and 3,641 computational cells was prepared for simulation at mesh sizes of 1, 2, and 5 cm, respectively, to represent the modified DEM (see Figure 26a and b).

Figures 28a-h and 29a-h display the variation in water depth resulting from the hydrodynamic model (Full Momentum) and laboratory measurements for both the aligned and staggered scenarios. The flood wave front hits and passes the first row of buildings almost 11 seconds into the simulation, as evident from the graphs. The water depth predicted by the 5 cm mesh size model was generally lower than the 1 cm and 2 cm grid models in both the aligned and staggered scenarios, with the peak water depth values reflecting the same trend. However, further analysis revealed that the water depth at P5 in the aligned scenario with all grid resolutions was higher than the laboratory measurements (see Figure 28c). This discrepancy may be due to measurement errors that cannot be confirmed at this

stage or may be due to the location of point P5, near which water swelling was observed. The results of the 1 cm mesh resolution were slightly higher than those of the 2 cm mesh resolution. Additionally, the results of the 1 cm grid resolution showed noticeable data oscillation, especially at P9 and P10. This oscillation could be regarded as the model's efficiency and accuracy compared to the 2 cm and 5 cm grid models (see Figure 28g-h and 29g-h).

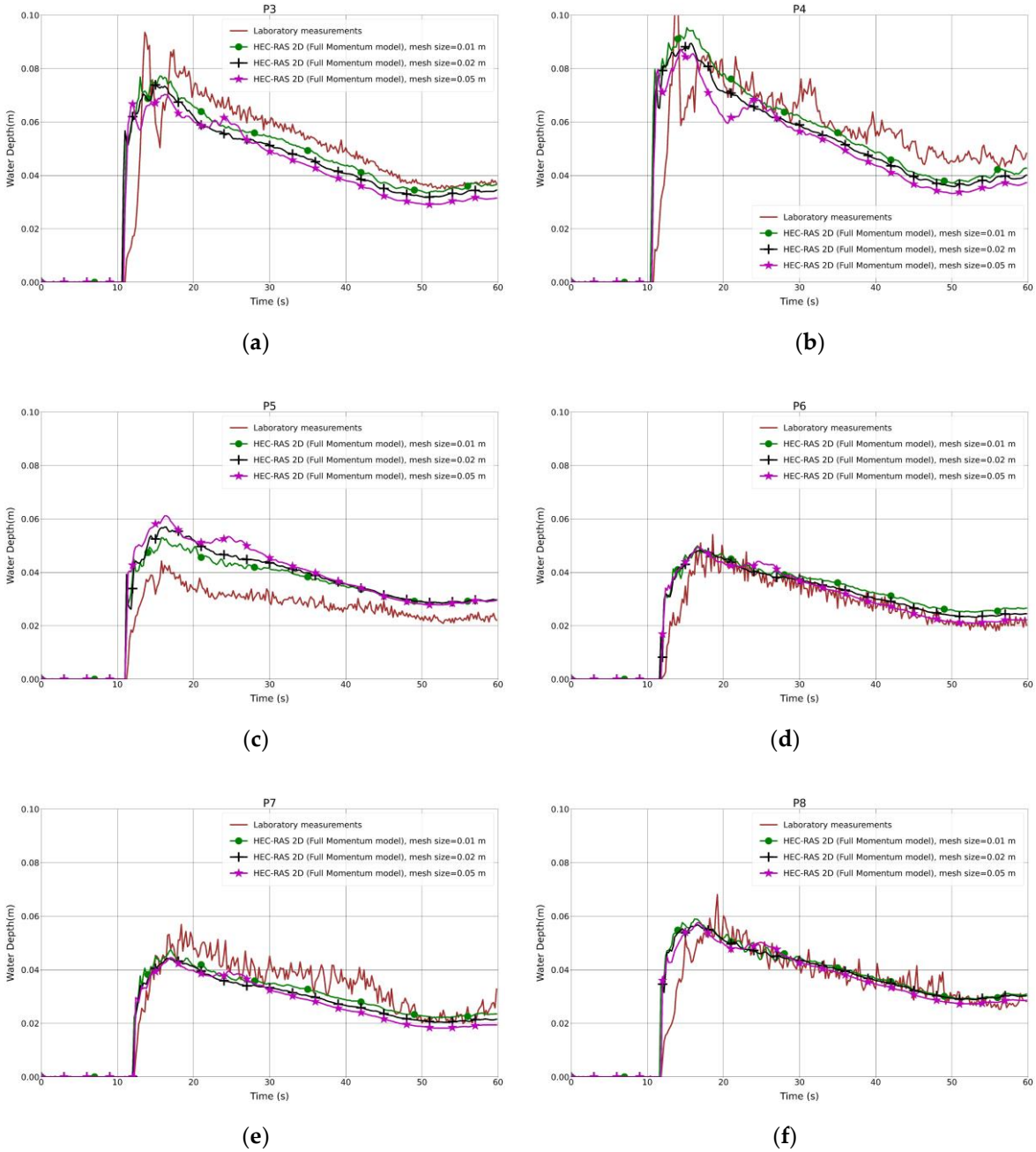

Figure 28. (**a–h**) Analysis of the numerical simulation using different mesh resolutions for the modified DEM with the aligned building layout (1a-BB) [202] (continued on next page).

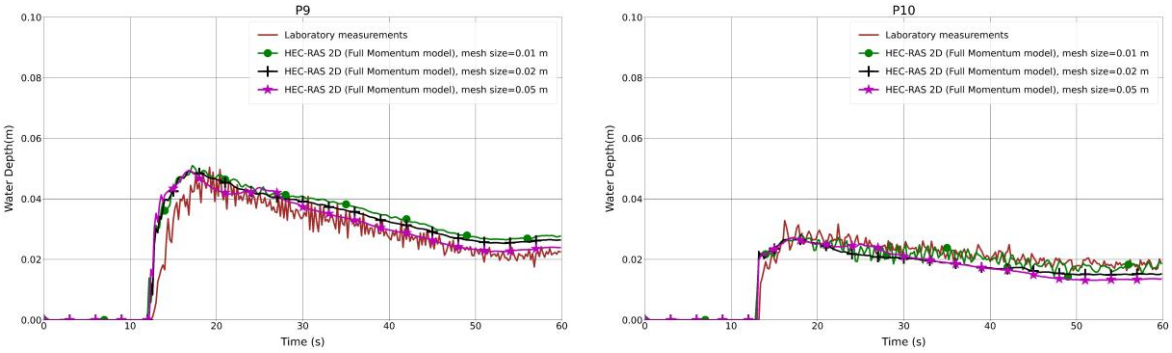

(**g**) (**h**)

Figure 28. (**a–h**) Analysis of the numerical simulation using different mesh resolutions for the modified DEM with the aligned building layout (1a-BB) [202].

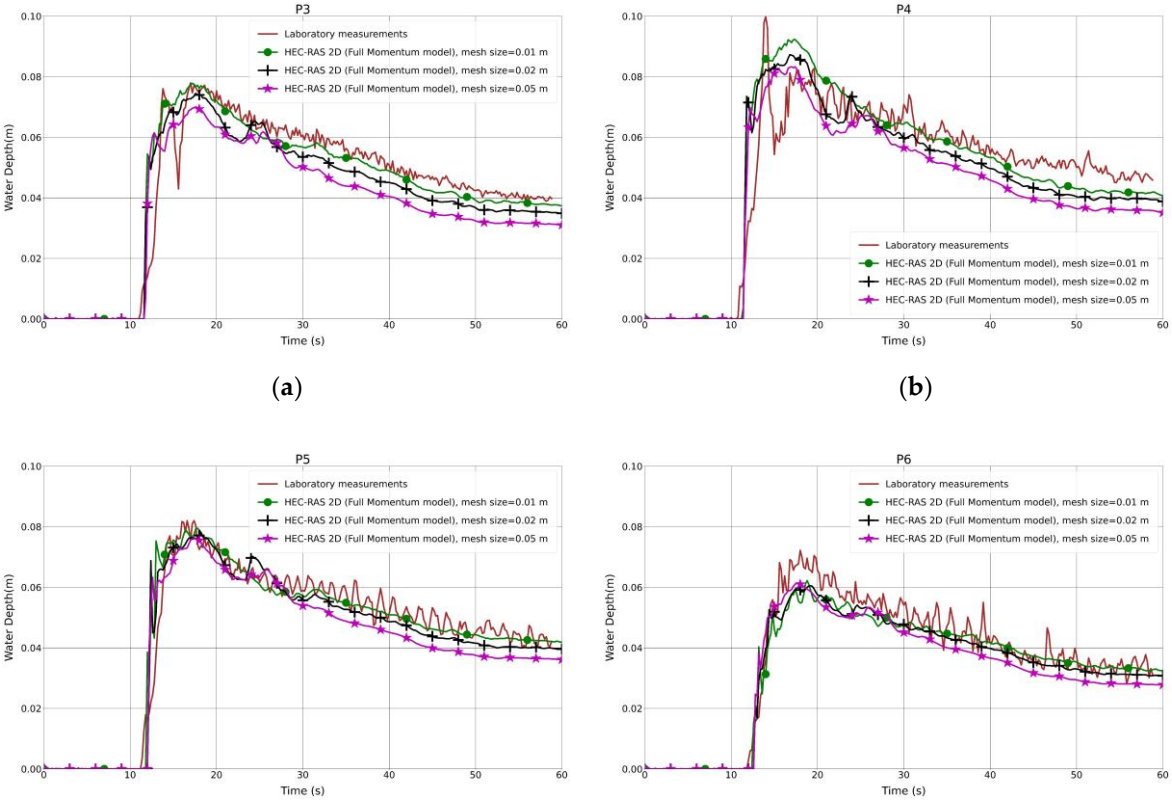

(**a**) (**b**)

(**c**) (**d**)

Figure 29. (**a–h**) Analysis of the numerical simulation using different mesh resolutions for the modified DEM with the staggered building layout (1b-BB) [202] (continued on next page).

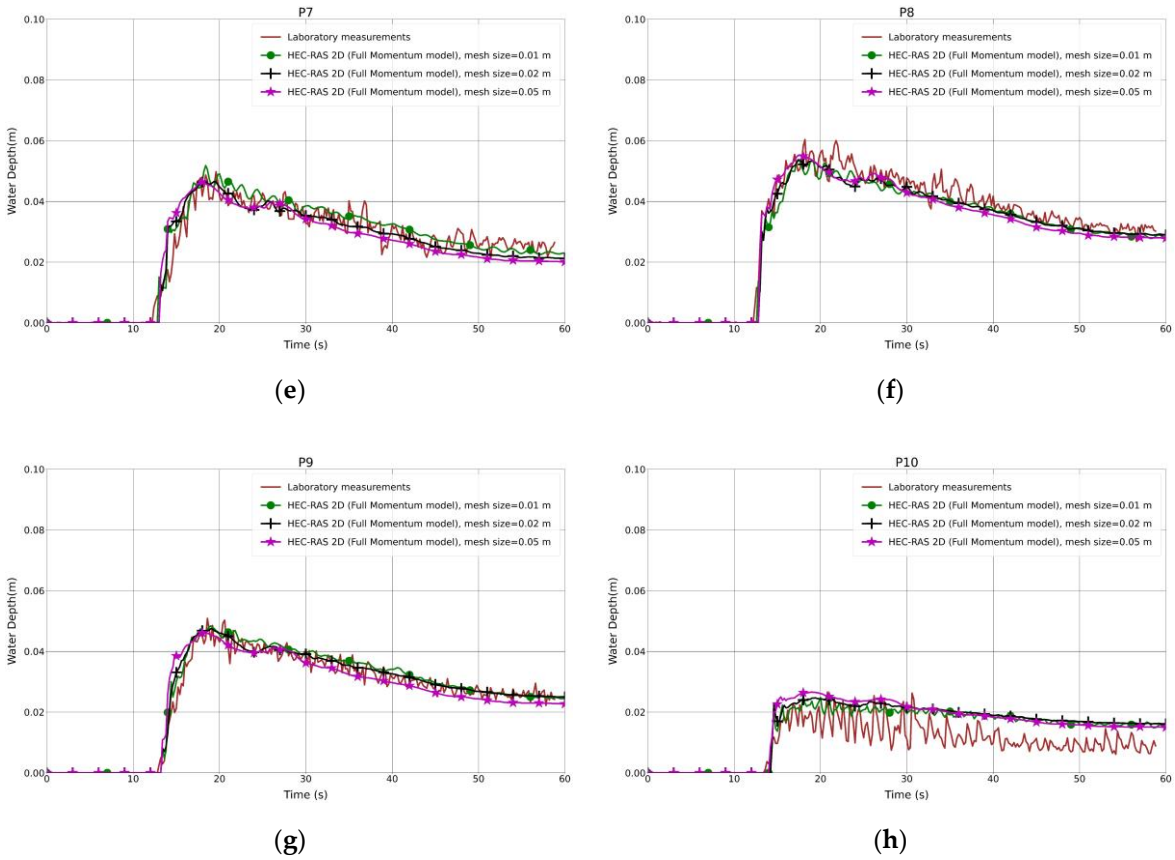

Figure 29. (a–h) Analysis of the numerical simulation using different mesh resolutions for the modified DEM with the staggered building layout (1b-BB) [202].

In the second step of the same test cases (1a-BB and 1b-BB), the 1 cm mesh size and BB representation technique were utilized to compare the results of the Full Momentum and DW models with the laboratory measurements. Figure 30a-h and 31a-h demonstrate that the water depth predicted by the DW model at all probe points was underestimated, except at P10, where the curve fit the laboratory measurement curve. As previously discussed in this section (see Figure 28c), the agreement and discrepancies of the water level at P5 with the laboratory measurements and numerical solutions were explained. Generally, the reason for the DW model's disagreement is that it is a simplified model that cannot accurately calculate the water swelling and dynamics due to no representation of inertia forces in the dynamic equations.

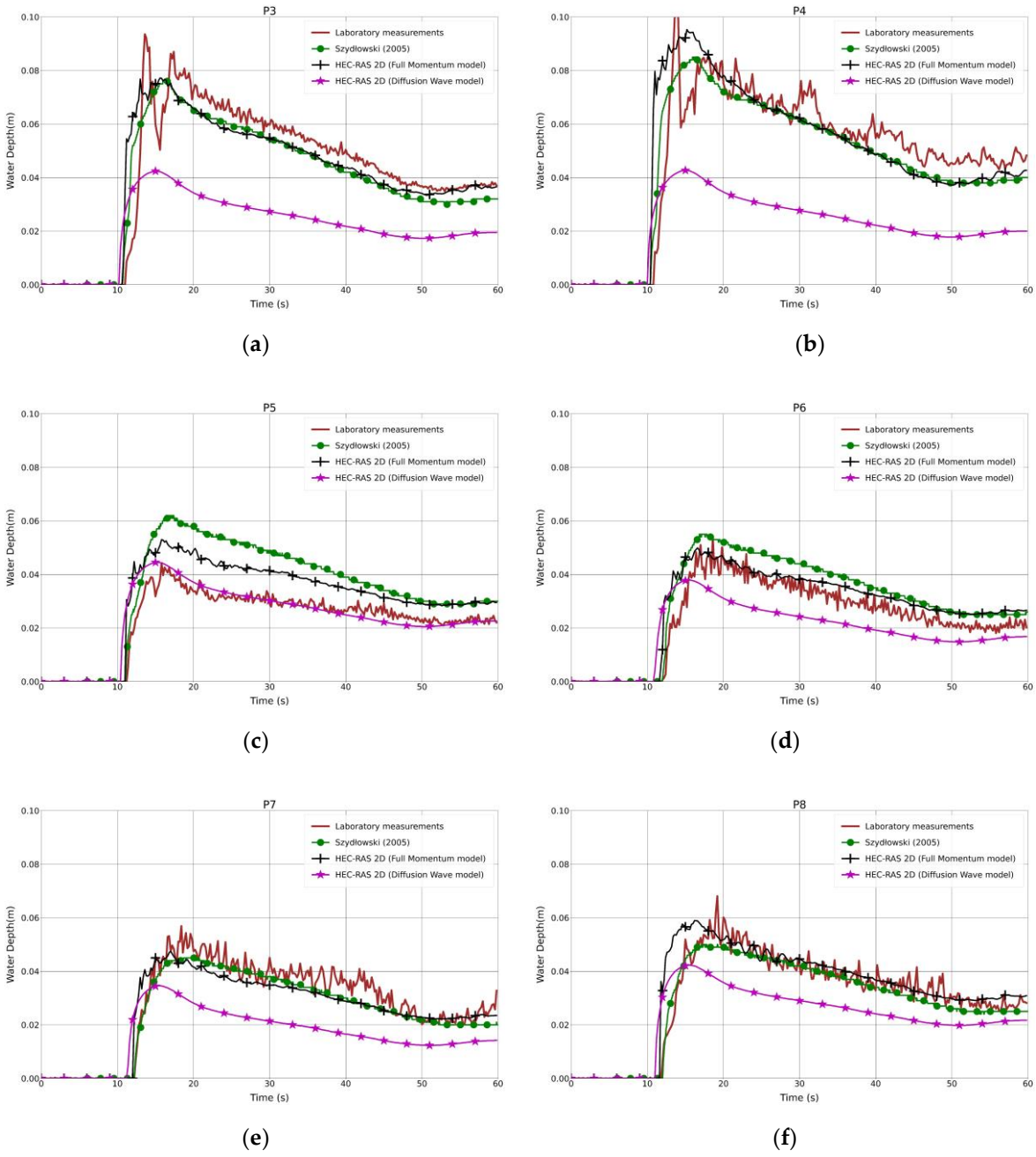

Figure 30. (**a–h**) Laboratory measurements compared to both the Full Momentum model and the DW model, as well as to the solution by Szydłowski [200], for the modified DEM with the aligned building layout (1a-BB) [202] (continued on next page).

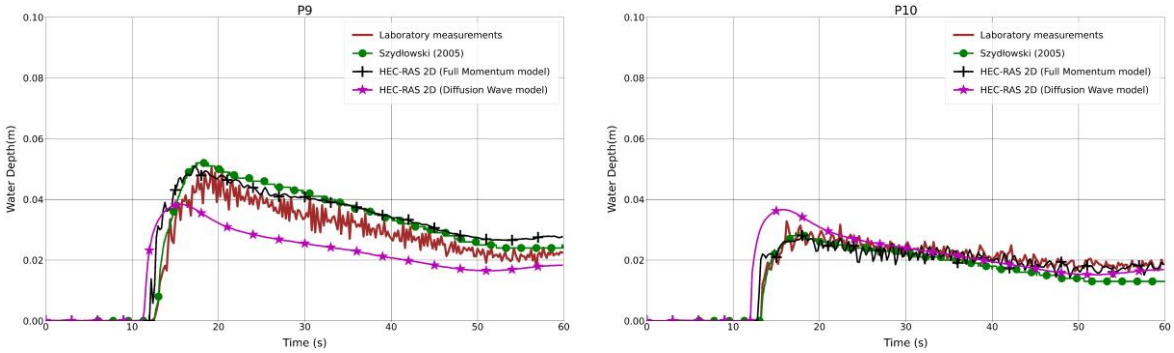

(**g**) (**h**)

Figure 30. (a–h) Laboratory measurements compared to both the Full Momentum model and the DW model, as well as to the solution by Szydłowski [200], for the modified DEM with the aligned building layout (1a-BB) [202].

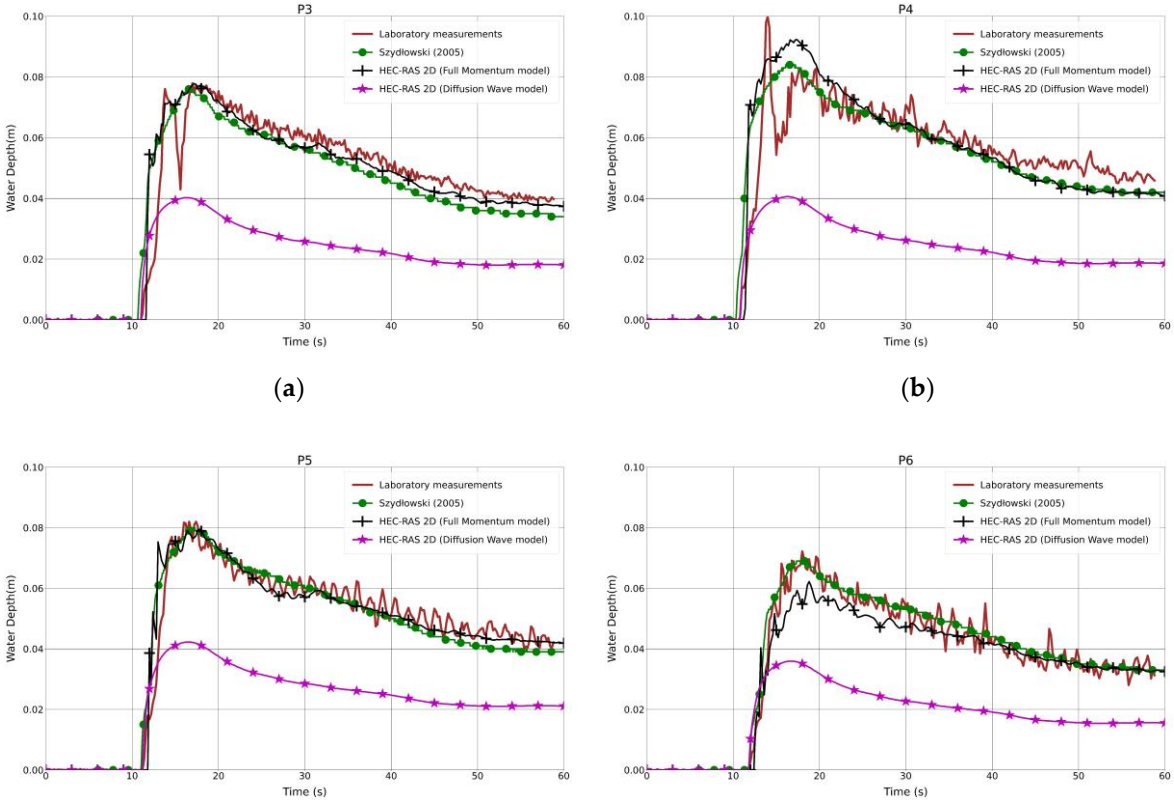

(**a**) (**b**)

(**c**) (**d**)

Figure 31. (**a–h**) Laboratory measurements compared to both the Full Momentum model and the DW model, as well as to the solution by Szydłowski [200], for the modified DEM with the staggered building layout (1b-BB) [202] (continued on next page).

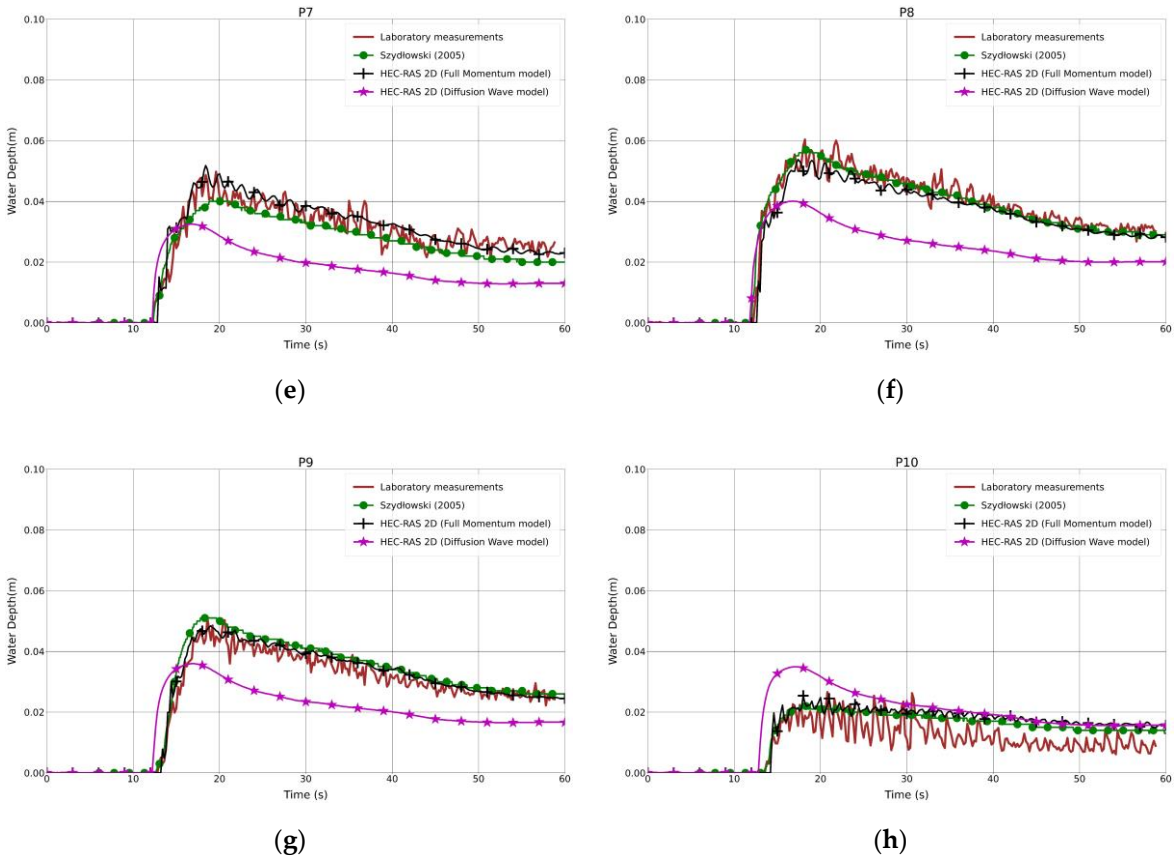

Figure 31. (a–h) Laboratory measurements compared to both the Full Momentum model and the DW model, as well as to the solution by Szydłowski [200], for the modified DEM with the staggered building layout (1b-BB) [202].

While the 2-D DWE simulation was faster, taking only about 45% of the time required to simulate the same model using the Full Momentum model, the results were underestimated compared to the observed laboratory values. For statistical presentation of the outcomes, both Root Mean Square Error (RMSE) and Pearson Product-Moment Correlation Coefficient (PPMCC) were utilized to assess the performance of the models. The performance of the models, including the difference between 1, 2, and 5 cm mesh resolutions, was compared. In both the aligned and staggered building layouts, the highest RMSE was produced by the 5 cm mesh resolution, while the RMSE of the 1 cm mesh resolution was lower than that of the 2 cm resolution overall (see Table 15). The PPMCC of the 1 cm mesh size was the highest compared to the 2 and 5 cm mesh resolutions. However, the difference was minimal. According to Yu and Lane [173], mesh resolution has an impact on model performance, and finer meshes typically produce better results. However, reducing the mesh resolution further may result in data oscillation, affecting the accuracy of the results. Therefore, it is preferable to determine the appropriate mesh resolution based on the building layout, as the 1 cm mesh resolution generally produced results that

were closest to the laboratory measurements compared to the 2 cm and 5 cm resolutions. Furthermore, it was confirmed that the results would not be significantly altered by a simulation with a grid size smaller than 1 cm. Based on Figures 28a-h and 29a-h and Tables 15 and 16, a conclusion can be drawn that the proper grid size for the Toce River physical model is the 1 cm mesh resolution.

Table 15. Calculated RMSE for both building layouts and different grid sizes (cm) (1a-BB and 1b-BB) [202].

Building Layout	Grid Size	P3	P4	P5	P6	P7	P8	P9	P10
Aligned (1a)	1 cm	1.00	1.32	0.92	0.60	0.57	0.72	0.63	0.29
	2 cm	1.13	1.26	1.09	0.53	0.66	0.64	0.56	0.37
	5 cm	1.19	1.38	1.27	0.52	0.73	0.62	0.55	0.40
Staggered (1b)	1 cm	0.83	1.09	0.78	0.68	0.48	0.54	0.43	0.65
	2 cm	0.88	1.08	0.79	0.65	0.47	0.54	0.42	0.71
	5 cm	1.09	1.18	0.91	0.73	0.53	0.54	0.47	0.71

Table 16. Calculated PPMCC for both building layouts and different grid sizes (cm) (1a-BB and 1b-BB) [202].

Building Layout	Grid Size	P3	P4	P5	P6	P7	P8	P9	P10
Aligned (1a)	1 cm	0.92	0.88	0.98	0.96	0.96	0.93	0.97	0.96
	2 cm	0.90	0.90	0.97	0.96	0.96	0.94	0.97	0.96
	5 cm	0.91	0.88	0.96	0.95	0.95	0.94	0.95	0.95
Staggered (1b)	1 cm	0.96	0.94	0.98	0.98	0.98	0.99	0.99	0.87
	2 cm	0.96	0.94	0.98	0.99	0.97	0.99	0.99	0.88
	5 cm	0.95	0.93	0.97	0.98	0.96	0.99	0.97	0.90

6.3.2 Analysis of different Manning coefficients in the BR technique

The coefficient known as the Manning coefficient is used in the field of flow to describe the roughness or friction of a surface and to estimate the average flow velocity. This coefficient is empirical, and its values are often chosen from tables or determined through field measurements. In many flow scenarios, the value of the Manning roughness coefficient significantly affects the computational results. In the BR technique, all the mesh regions representing building blocks (known as user-defined polygons) are assigned three different Manning coefficient values, such as 0.1, 1, and 10 $m^{-1/3}$.s, to evaluate the resistance against the flow. Only one "high" Manning value is used in each simulation run. For the test case 1a-BR and 1b-BR, the model was simulated using a mesh size of 1 cm, consisting of 92,403 computational cells.

Figures 32a–h and 33a–h shows the resulting water depth in the hydrodynamic models and laboratory measurements for both the aligned and staggered scenarios. The flood wave takes nearly 11 s to hit and pass the first building row, which is the same time as in the BB method. In the aligned configuration, the Manning coefficient equal to 0.1 $m^{-1/3}$.s underestimates the water depth at probe

points P3, P4, and P7 compared to laboratory measurements, while P5 and P10 are overestimated. The rest of the points, P6, P8, and P9, correspond well with the experimental results. In the staggered layout, the water depth is overestimated at P10, and at P9, the advantages of the cyan and black lines over the magenta line are minimal. The water depth outputs at the remaining probe points are underestimated. The simulations with the Manning coefficient equal to 1 and 10 $m^{-1/3}$.s fit well with the laboratory measurements, indicating that the building blocks are naturally resistant to water flow. Furthermore, the different Manning coefficient simulation models are compared to the BB technique in all graphs, and the plots show that the simulation model with the Manning coefficient equal to 10 $m^{-1/3}$.s represents the BB case very well.

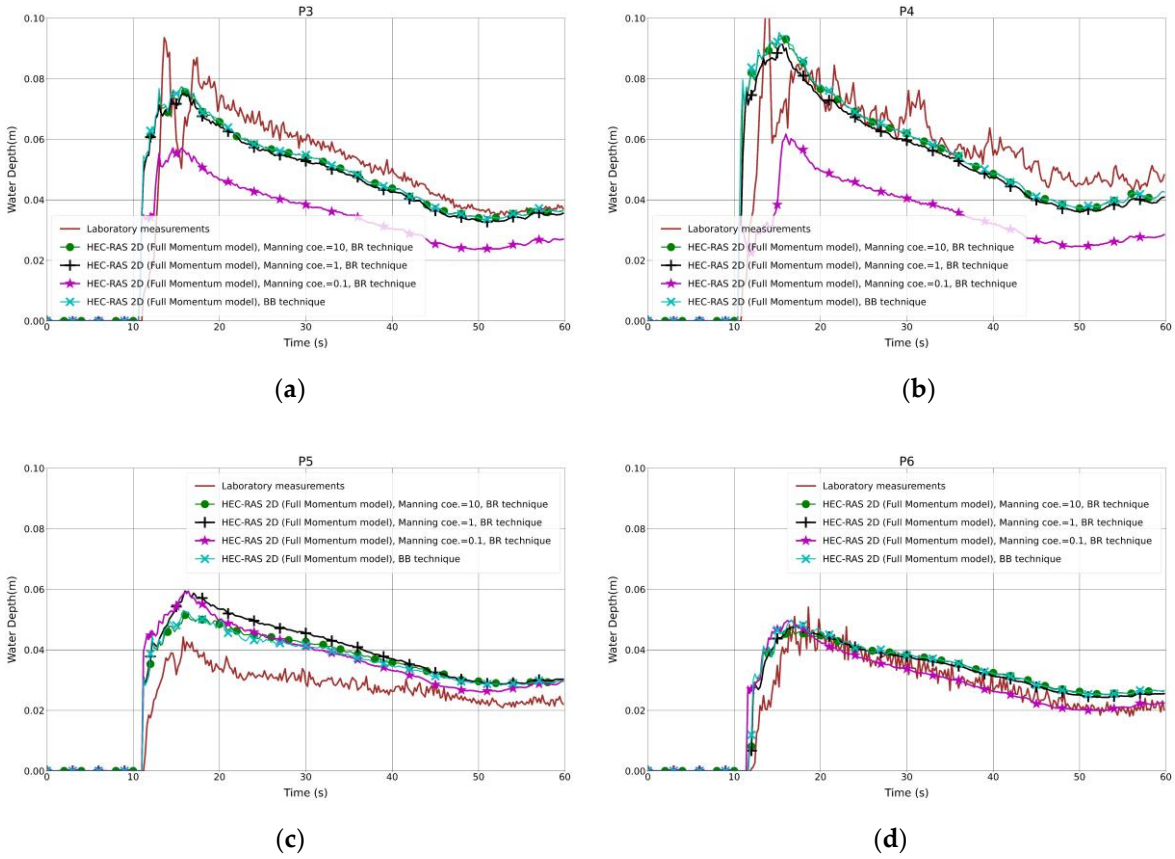

Figure 32. (**a–h**) Analysis of the numerical simulation using different Manning values for the modified DEM with the aligned building layout (1a-BR) [202] (continued on next page).

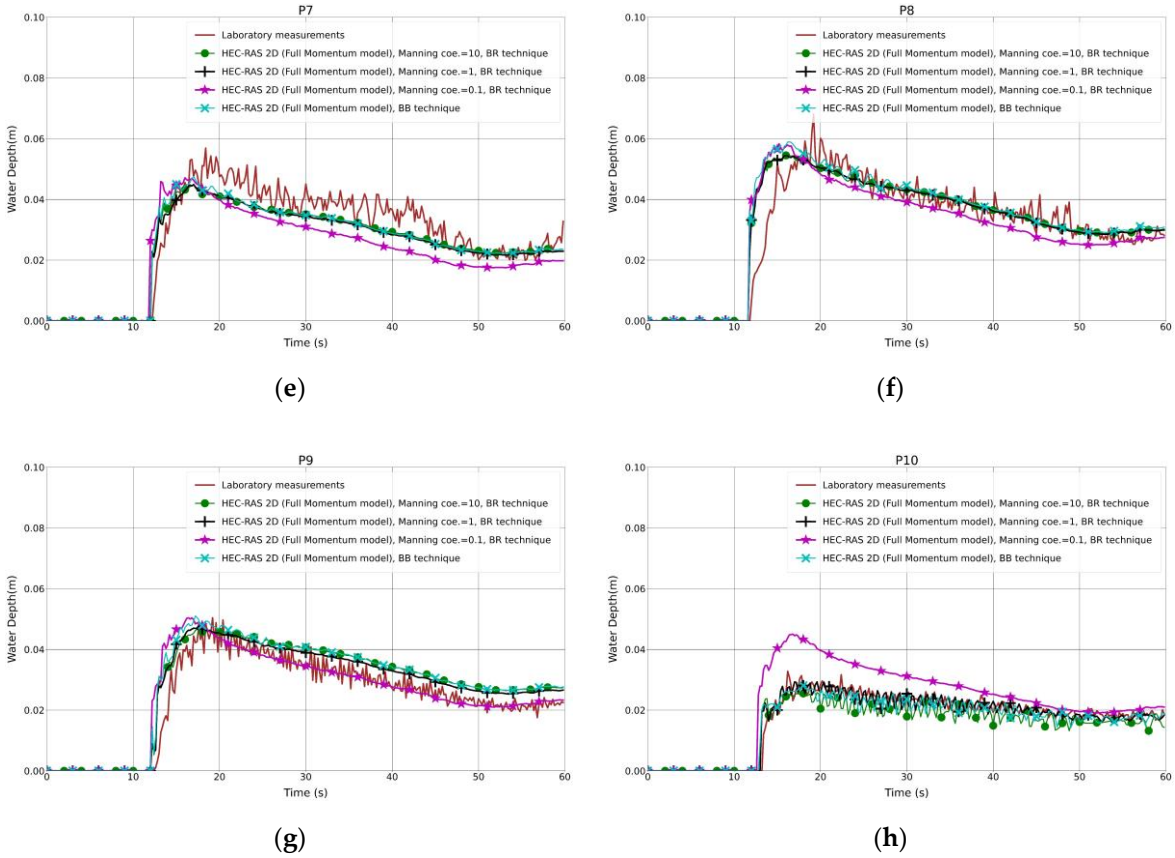

Figure 32. (a–h) Analysis of the numerical simulation using different Manning values for the modified DEM with the aligned building layout (1a-BR) [202].

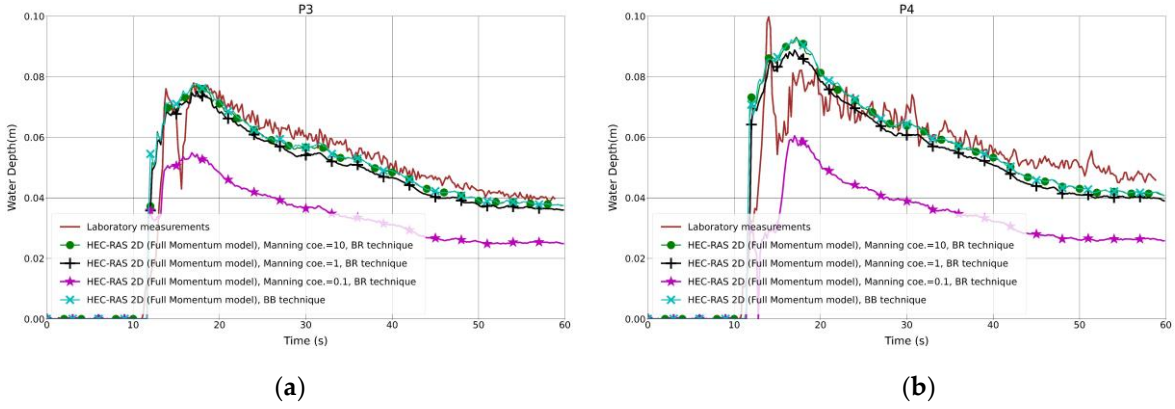

Figure 33. (a–h) Analysis of the numerical simulation using different Manning values for the modified DEM with the staggered building layout (1b-BR) [202] (continued on next page).

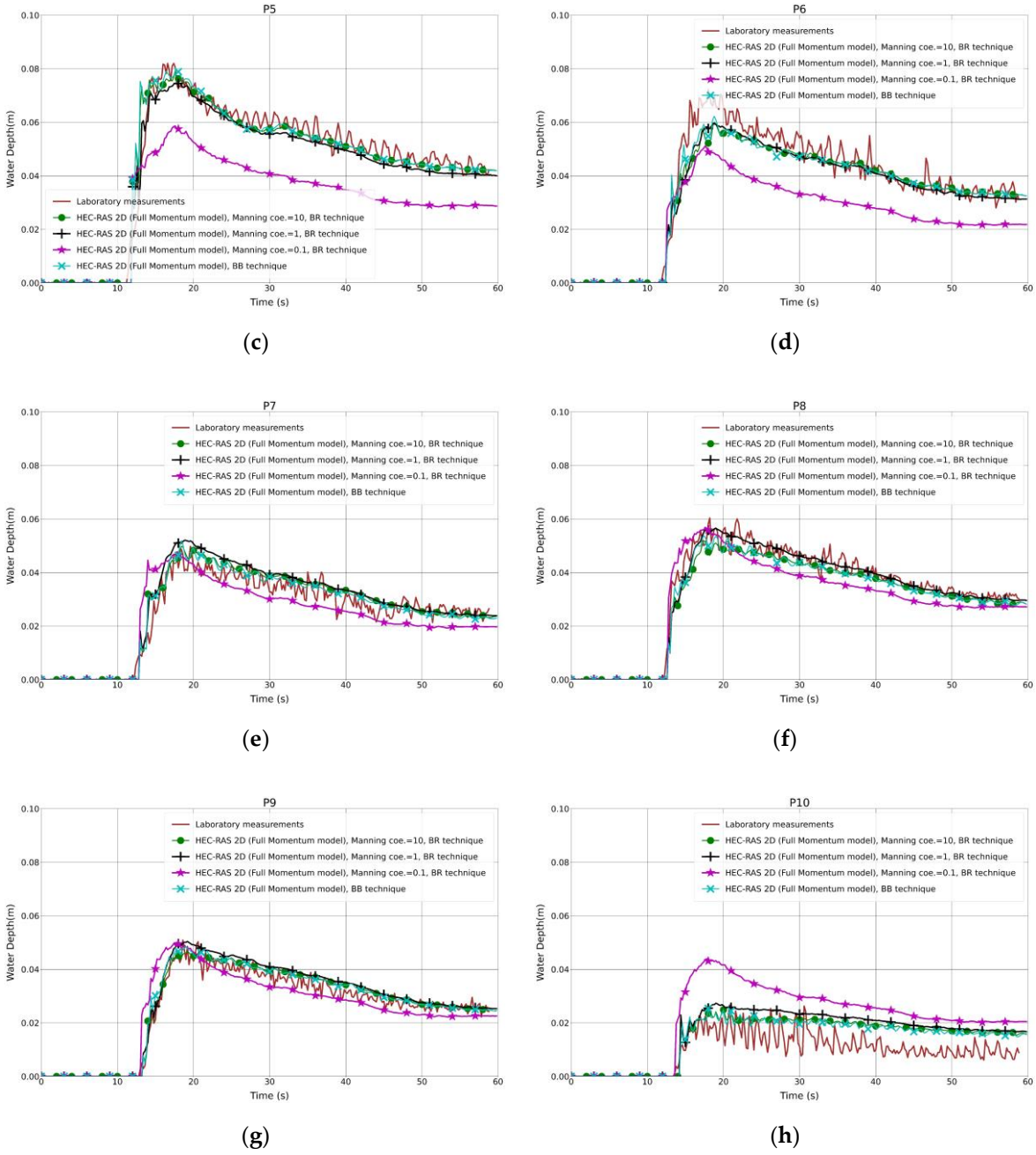

Figure 33. (a–h) Analysis of the numerical simulation using different Manning values for the modified DEM with the staggered building layout (1b-BR) [202].

The Manning coefficient, which describes surface roughness or friction in flow, can significantly impact computational results in many flow cases. In the BR technique, three Manning coefficient values (0.1, 1, and 10 $m^{-1/3}$.s) are assigned to user-defined polygons to examine resistance against flow. Results from the aligned and staggered layouts show that the Manning coefficient of 0.1 $m^{-1/3}$.s underestimates water depth at certain probe points, while coefficients of 1 and 10 $m^{-1/3}$.s fit well with laboratory

measurements (see Table 17). The difference between simulation models with coefficients of 1 and 10 $m^{-1/3}$.s is negligible. The RMSE of the 0.1 coefficient is higher compared to 1 and 10 coefficients in both layouts, while the PPMCC of the 0.1 coefficient is lower but the difference is minimal (see Table 18).

Table 17. Calculated RMSE for both building layouts and different Manning values (cm) (1a-BR and 1b-BR) [202].

Building Layout	Manning Coefficient Value	P3	P4	P5	P6	P7	P8	P9	P10
Aligned (1a)	0.1	1.76	2.32	1.06	0.58	0.87	0.77	0.58	0.79
	1	1.02	1.21	1.21	0.52	0.57	0.62	0.51	0.25
	10	0.97	1.24	0.96	0.55	0.55	0.62	0.56	0.36
Staggered (1b)	0.1	1.84	2.29	1.66	1.42	0.64	0.58	0.51	1.42
	1	0.68	0.88	0.46	0.53	0.46	0.29	0.32	0.80
	10	0.62	0.91	0.48	0.95	0.38	0.40	0.25	0.66

Table 18. Calculated PPMCC for both building layouts and different Manning values (cm) (1a-BR and 1b-BR) [202].

Building Layout	Manning Coefficient Value	P3	P4	P5	P6	P7	P8	P9	P10
Aligned (1a)	0.1	0.93	0.92	0.95	0.92	0.91	0.91	0.93	0.92
	1	0.92	0.90	0.97	0.97	0.97	0.94	0.97	0.97
	10	0.92	0.89	0.98	0.96	0.96	0.94	0.97	0.96
Staggered (1b)	0.1	0.96	0.93	0.97	0.97	0.91	0.97	0.95	0.90
	1	0.97	0.95	0.99	0.98	0.98	0.99	0.99	0.87
	10	0.97	0.94	0.98	0.94	0.98	0.99	0.99	0.86

6.3.3 Verification of the modeling techniques

The aim of this study was to identify suitable models and techniques for the modified geometry of the physical model of the Toce River in the first phase (see Figure 26 a and b). The second phase aimed to verify these models and techniques in the original Toce River physical model (see Figure 26 c and d). After identifying the suitable mathematical representation of unsteady water flow in a built-up area, the Full Momentum model has been selected and determined the optimal modeling parameters, including a mesh resolution of 1 cm and a Manning value of 10 $m^{-1/3}$·s to represent building blocks in the flow field. The models for the original DEM were prepared based on this, in order to verify the modeling techniques.

The investigated building setups in the second step of the work were just the same as previously. The results for both setups and for the BB and BR techniques are shown in Figures 34 a-h and 35 a-h. Generally, the Full Momentum model in the BB technique with a grid resolution of 1 cm fits well with

the laboratory measurements in both building layouts. However, there are some discrepancies, such as an overestimation of the water depth at P5 in the aligned layout (see Figure 34C) and an underestimation of the water depth at P8 in the staggered layout (see Figure 35F). The underestimation of experimental data observed in P8 was previously observed by other authors [216,217].

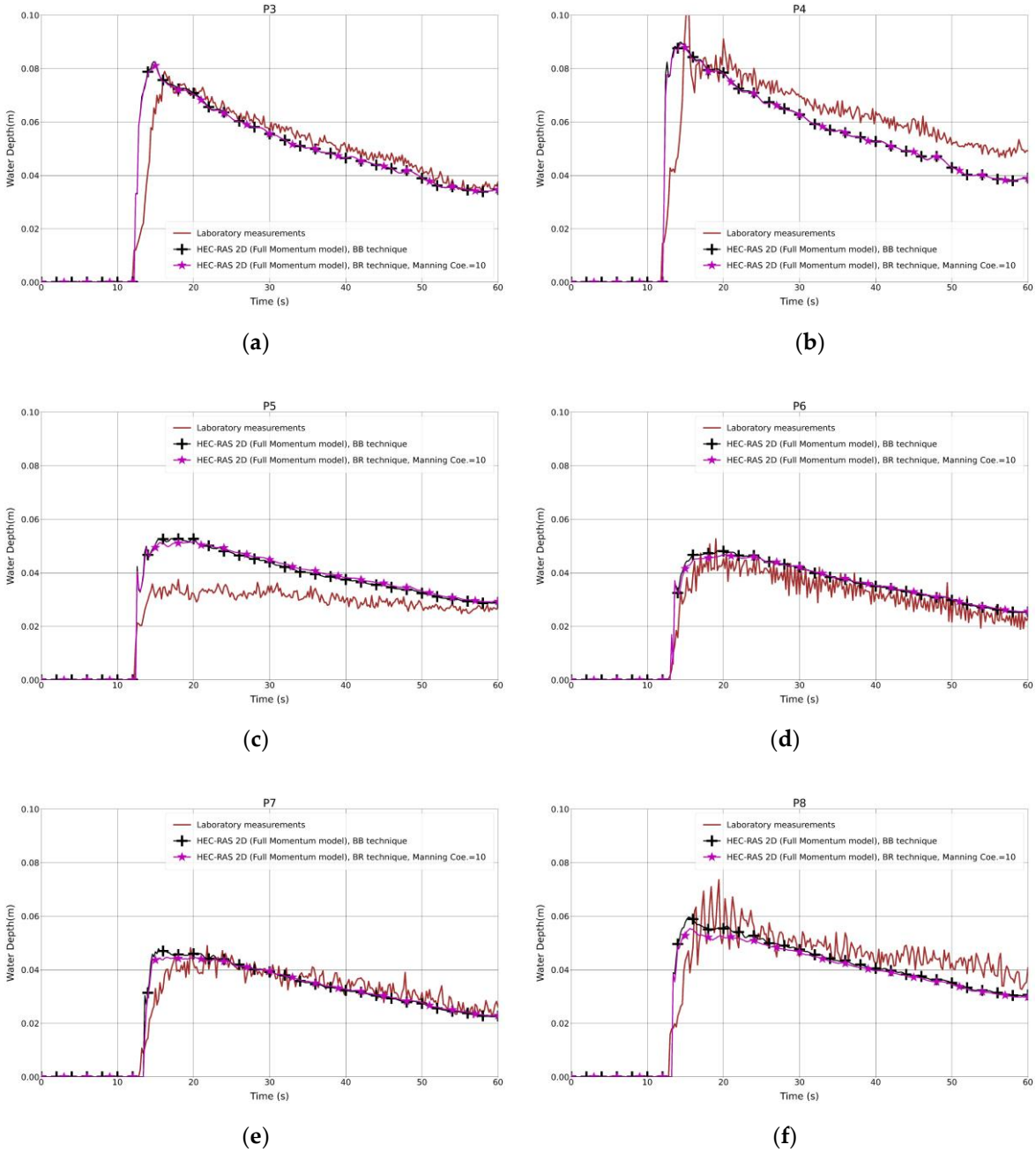

Figure 34. (a–h) Analysis of the numerical simulation using different building representation techniques for the original DEM with the aligned building layout (2aBB and 2a-BR) [202] (continued on next page).

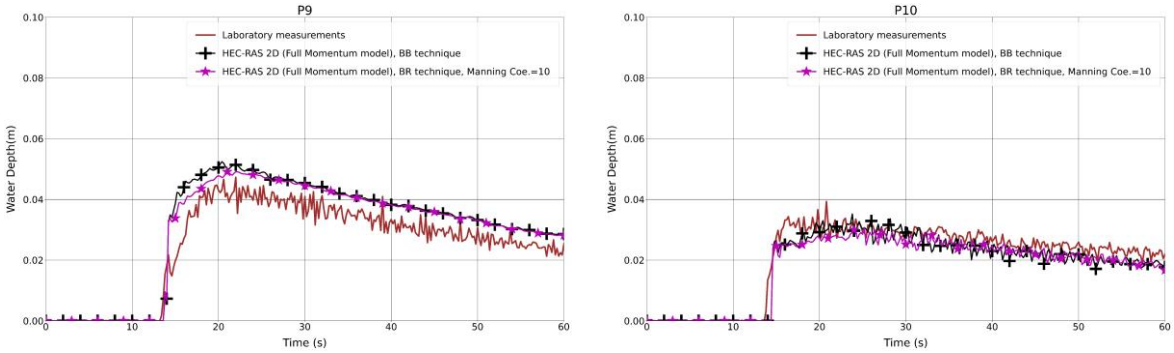

(**g**) (**h**)

Figure 34. (a–h) Analysis of the numerical simulation using different building representation techniques for the original DEM with the aligned building layout (2aBB and 2a-BR) [202].

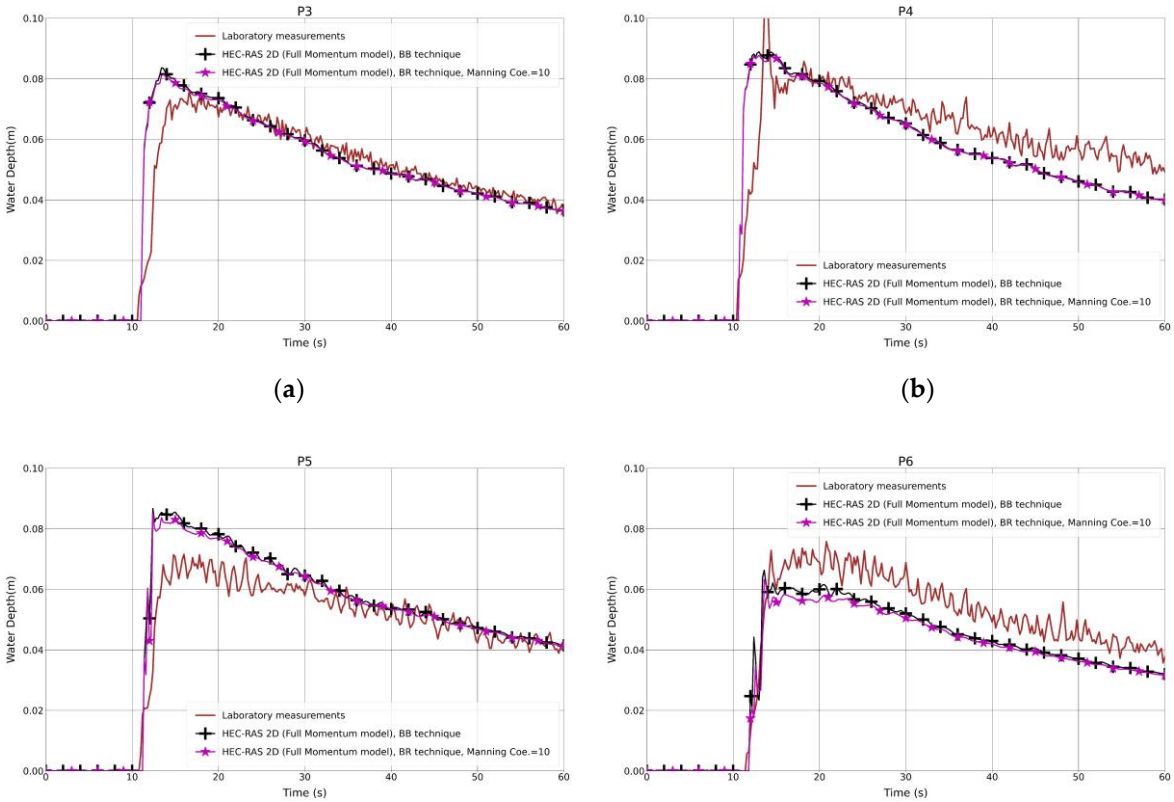

(**a**) (**b**)

(**c**) (**d**)

Figure 35. (a–h) Analysis of the numerical simulation using different building representation techniques for the original DEM with the staggered building layout (2b-BB and BR) [202] (continued on next page).

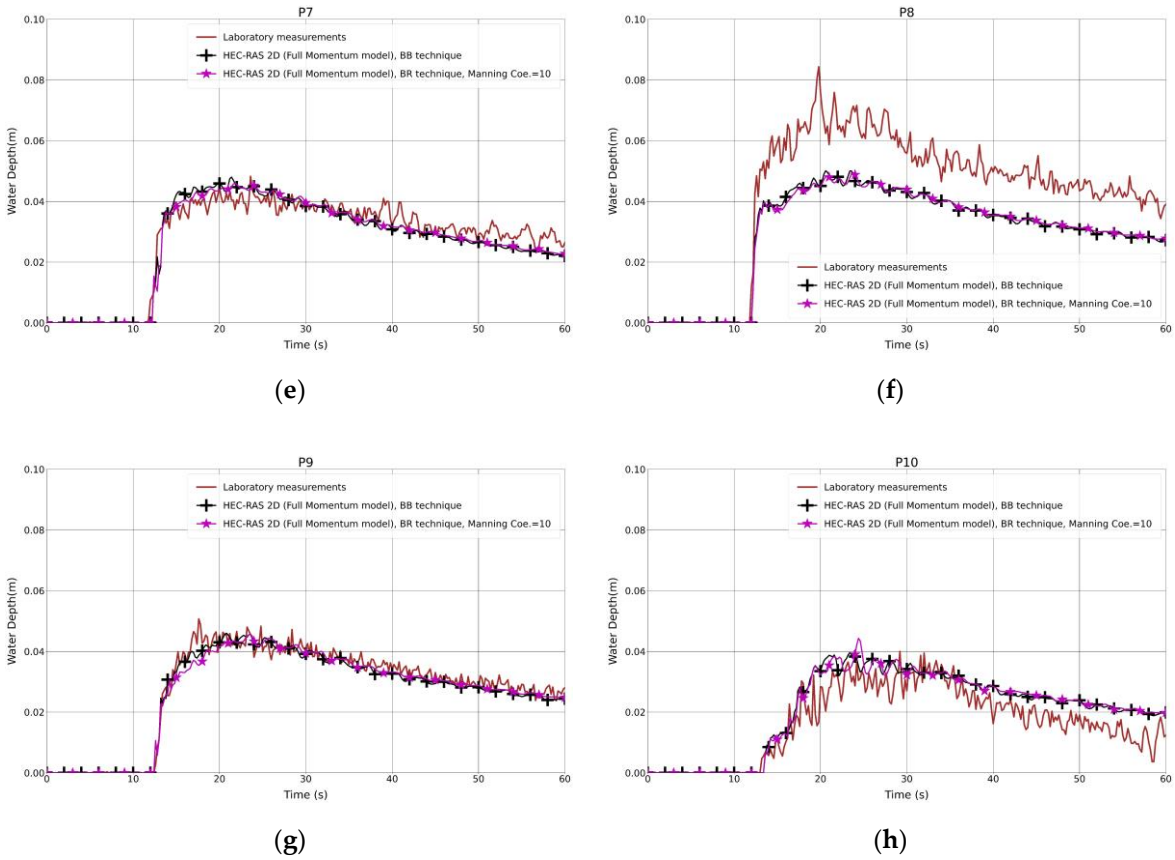

Figure 35. (a–h) Analysis of the numerical simulation using different building representation techniques for the original DEM with the staggered building layout (2b-BB and BR) [202].

Regarding the statistical analysis of water depth outcomes, the RMSE and PPMCC results for both techniques and in both layouts demonstrated strong consistency as shown in Tables 19 and 20. The results were very similar, indicating that both techniques share comparable characteristics. This suggests that the BR technique can be a suitable alternative to the BB technique when dealing with low-resolution DEMs.

Table 19. Calculated RMSE for both building layouts and different building representations (cm) (2a-BB, 2a-BR, 2b-BB and 2b-BR) [202].

Building Layout	Building Representation Technique	P3	P4	P5	P6	P7	P8	P9	P10
Aligned (2a)	BB	0.82	1.15	1.02	0.48	0.47	0.75	0.69	0.36
	BR	0.80	1.13	1.03	0.47	0.40	0.77	0.60	0.38
Staggered (2b)	BB	0.80	1.07	0.92	0.85	0.39	1.46	0.26	0.62
	BR	0.78	1.07	0.81	0.94	0.36	1.46	0.28	0.63

Table 20. Calculated PPMCC for both building layouts and different building representations (2a-BB, 2a-BR, 2b-BB and 2b-BR) [202].

Building Layout	Building Representation Technique	P3	P4	P5	P6	P7	P8	P9	P10
Aligned (2a)	BB	0.94	0.92	0.96	0.98	0.96	0.94	0.98	0.97
	BR	0.94	0.93	0.97	0.98	0.97	0.95	0.98	0.98
Staggered (2b)	BB	0.95	0.93	0.96	0.98	0.97	0.99	0.99	0.94
	BR	0.95	0.93	0.97	0.99	0.97	0.99	0.99	0.94

6.3.4 SWEs vs the DW model

It was observed by Dottori and Todini [169] that the water depths computed inside the urban district by the DW model were unfluctuating in comparison to the observed values. A conclusion was drawn by Costabile, Costanzo and Macchione [168] that the DW model is questionable, particularly in the urban zone, due to the poor prediction of events that can be simulated in the vicinity of the buildings. According to Prestininzi [172], the parabolic approximation is capable of simulating the propagation of such an impulsive wave over complex topography, even though it fails to reproduce some local phenomena such as high frequency oscillation, bores and run-up. The results showed that the water depth at all probe points in the staggered layout, which is most similar to a typical urban layout, was generally underestimated using the DW model. Therefore, it can be concluded that inaccurate results will be produced by using the DW model. Finally, the numerical results are consistent with the previously mentioned results and conclusions that the DW model is not the proper model for urban flood simulation.

6.3.5 Different building representation techniques

The Full Momentum model and DW model test cases, utilizing the BB technique, were compared to Szydłowski [200] solution, which employed the Full Momentum hydrodynamic model and the BH technique to simulate the built-up area, as demonstrated in Figures 30 a-h and 31 a-h. The Full Momentum model implemented in HEC-RAS 2-D correlates well with Szydłowski [200] numerical calculation, and both are in agreement with laboratory measurements in both scenarios. It is worth noting that the BB and BH techniques function similarly in preventing water storage and flow over the building units.

In recent times, the BP model has become a popular technique for modeling urban flooding. Soares-Frazão, Lhomme, Guinot and Zech [217] explored the use of modified shallow-water equations with porosity in conjunction with shock-capturing, Godunov-type algorithms [218]. They concluded that the porosity model can accurately replicate the flow characteristics within and around the urban

area, and that the computational costs are significantly lower than those of classical shallow-water equations solved on a refined mesh. It was observed that the numerical outcomes in both studies demonstrated an earlier arrival time of the wave, which resulted from the defined upstream boundary condition. In terms of agreement with experimental water depth measurements at probe point 5 in the staggered layout, the BR techniques provided better results than the porosity model (SPR) employed in their study.

Jeong, Yoon and Cho [197] developed a two-dimensional unstructured finite volume model based on SWEs and a well-balanced HLLC scheme. They concluded that the water depth in the Toce river physical case was separated into a rapid reduction segment and a slow reduction segment as the flood wave propagated from the front part of the urban area to the rear. They also observed a reduction in the initial arrival time in front of the urban area as the inflow volume increased. This study also noted relatively high-water depth zones and lag phenomena in front of the urban area, which was attributed to the obstacle effects of the building units. Ferrari, *et al.* [219] proposed a porosity-based computational model for the SWEs that utilized an isotropic storage porosity parameter and anisotropic friction. Their anisotropic scheme produced results similar to a high-resolution resolved building model in low-friction regimes, while significantly reducing computational times. Comparing the Anisotropic Porosity (AP) with the BR technique in this study, it was observed similar results in water depth measurements. The findings indicate that the BR technique provides an easier and more simplified approach to modeling urban flooding, while still producing similar quality results to more complex models such as the porosity model. Additionally, Costabile, Costanzo, De Lorenzo and Macchione [181] found that only the SWE model and, to a lesser extent, the Porosity Model (PM) accurately reproduced the hydraulic behavior of the flow without simplifications in the momentum equations. Furthermore, the researchers noted that the Diffusion Model (ZI) was inadequate in providing an accurate depiction of the localized impacts resulting from the interaction between flood flow and hypothetical structures, primarily due to the absence of inertial terms. In the study, the BR technique was visually compared to the PM technique employed in their research, and it was discovered that the BR technique produced water depth measurements at probe points 3 and 4 that were more consistent with experimental results. Comparable outcomes were also observed at other measurement points. The findings from the numerical simulations utilizing the BR technique in HEC-RAS 2-D have substantial implications for simulating urban flooding in a simpler and more straightforward manner than with other models. Despite its simplified nature, the BR technique generates outcomes of comparable quality to more complex models, such as the porosity model.

To compare the BB and BR techniques, the study examined the flow structure in a built-up area by creating maps of Froude number (Fr) (see Figure 36 a and b), velocity field (see Figure 37 a and b), and water depth (see Figure 38 a and b) using HEC-RAS 2-D RAS Mapper tool. The Froude number was defined as the local velocity divided by the square root of the gravitational constant and depth. The maps were created for the staggered layout scenario, which is considered more realistic, and were prepared for both BB and BR techniques after exactly 15 seconds. The maps showed that subcritical (Fr < 1) and supercritical (Fr > 1) flow areas, as well as regions of transcritical flow, were located at the same places for both techniques. Some areas exhibited varying Froude number values, where the flow regime changed from supercritical to subcritical before reaching the buildings, resulting in a hydraulic jump due to flow resistance (see Figure 36 a and b). The flow regimes around the buildings were similar under both BB and BR techniques, with subcritical flow behind the buildings and in a forward flow direction, and subcritical and supercritical flows around the buildings' center and in an onward flow direction. HEC-RAS 2-D demonstrated good performance during the transition from subcritical to supercritical flows.

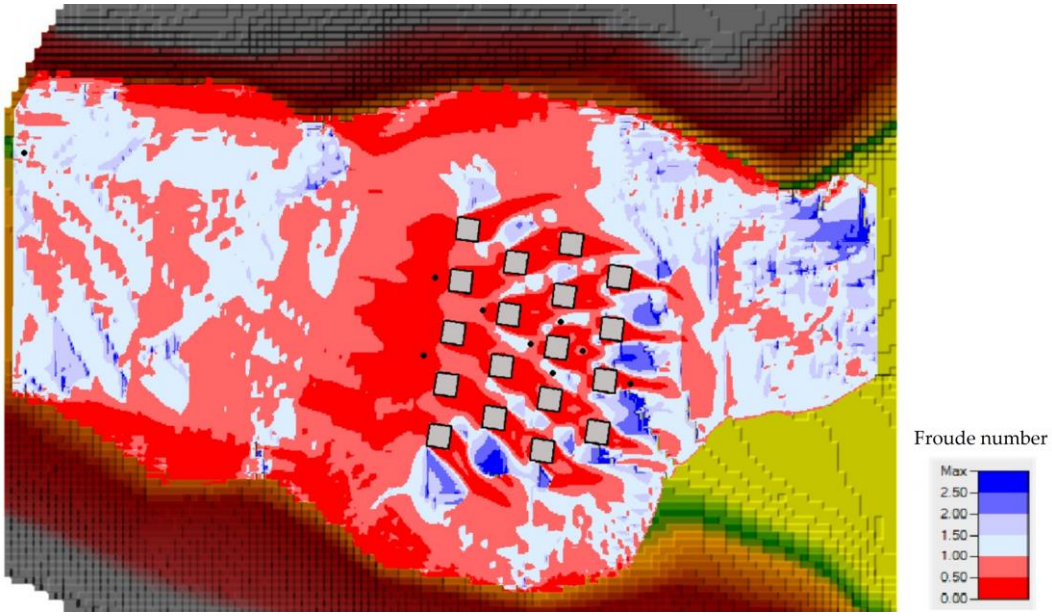

(**a**)

Figure 36. Froude number after 15 s: (a) BB technique with the staggered layout. (b) BR technique with the staggered layout [202] (continued on next page).

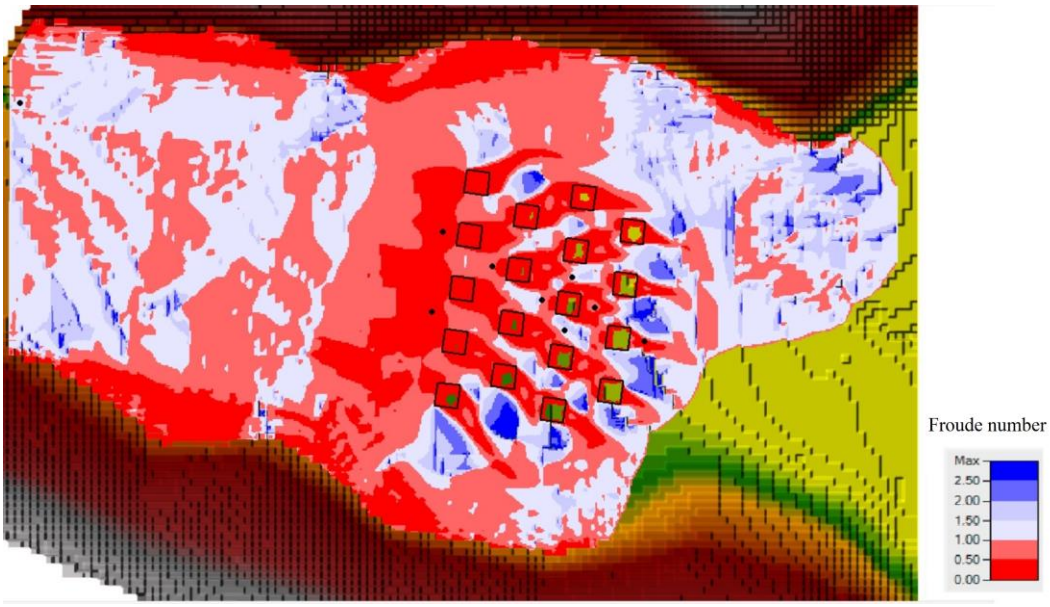

(**b**)

Figure 36. Froude number after 15 s: (**a**) BB technique with the staggered layout. (**b**) BR technique with the staggered layout [202].

Furthermore, velocity maps were created following the same procedure as for the Froude number maps. Figure 37a indicates that in the BB technique, the flow structure around the building varies significantly due to the buildings acting as a barrier to the flow, whereas in the BR technique, the flow structure around the building is relatively uniform (see Figure 37b). Moreover, in the BR technique, a low-velocity value was observed inside the building units, which was attributed to the high Manning coefficient assigned to these specific polygons inside the 2-D flow area in HEC-RAS 2-D.

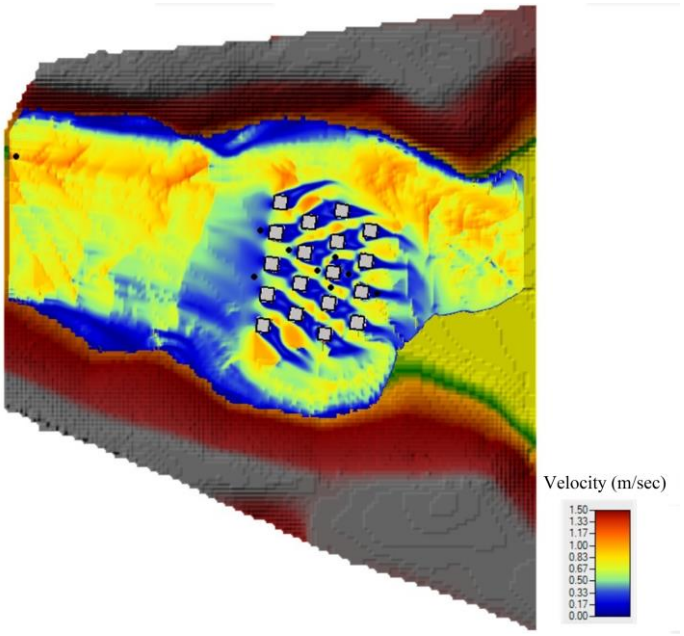

(**a**)

Figure 37. Velocity (m/s) after 15 s: (a) BB technique with the staggered layout. (b) BR technique with the staggered layout (continued on next page).

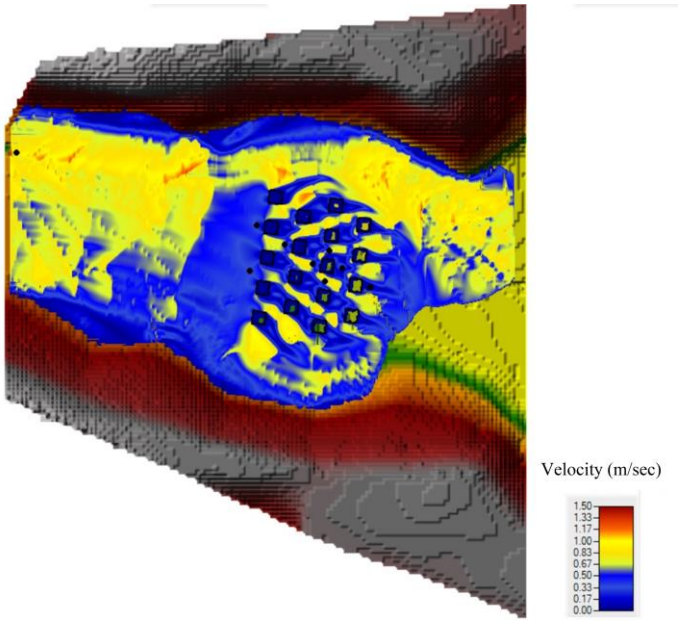

(**b**)

Figure 37. Velocity (m/s) after 15 s: (**a**) BB technique with the staggered layout. (**b**) BR technique with the staggered layout [202].

To gain a better understanding of the two situations, maps were created to depict the extent of the flooded area and water level for both techniques. In Figures 38a and b, the water extent is displayed,

with the color indicating the water depth level, which ranges from 0.01 to 0.1 meters. In general, the water depth levels computed using both techniques within the urban district are very similar. The water depth maps for both techniques show that the hydraulic jump that forms just ahead of the building blocks is accurately reproduced by both techniques. Overall, after 15 seconds of simulation, the total inundated extent is the same for both techniques. However, it should be noted that these techniques were applied to scale models in HEC-RAS 2-D and extreme caution should be exercised when applying them to full-scale models due to scaling issues of various hydrodynamic variables.

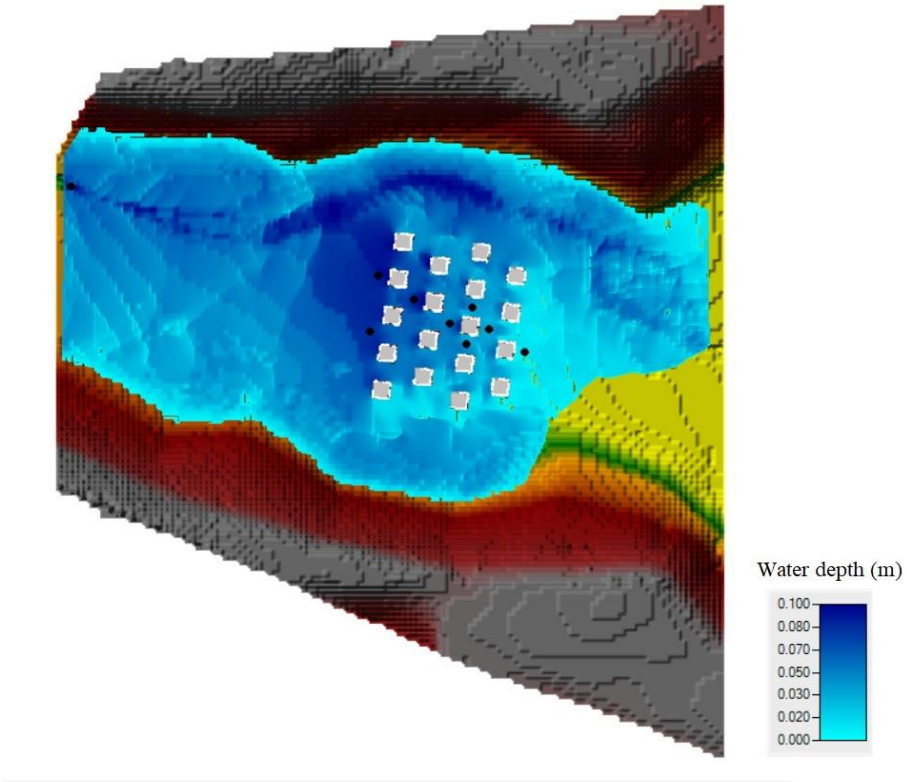

(**a**)

Figure 38. Water depth (m) after 15 s: (a) BB technique with the staggered layout. (b) BR technique with the staggered layout [202] (continued on next page).

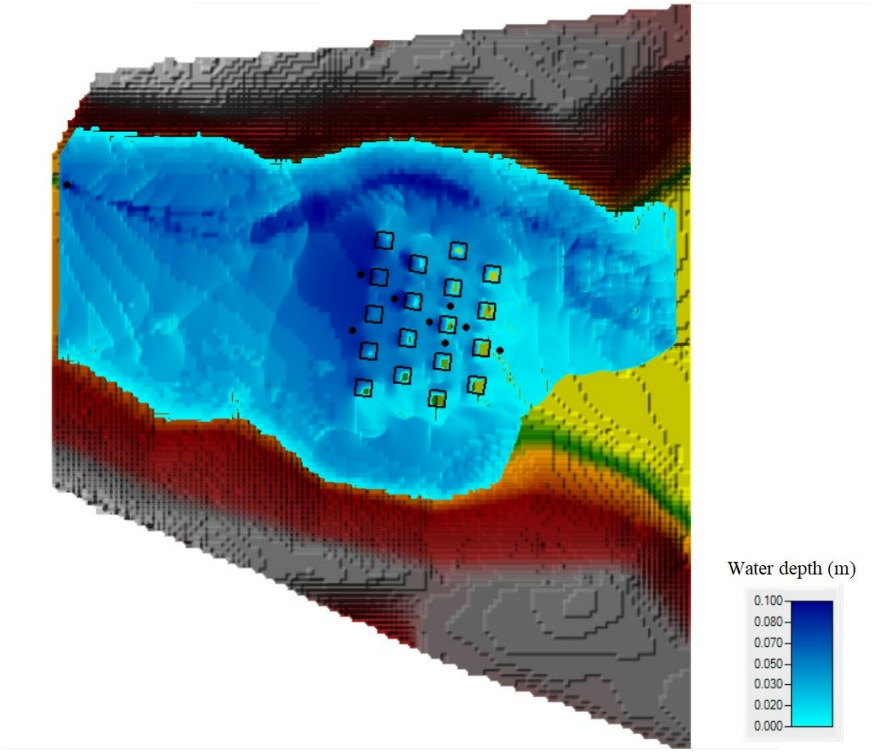

(**b**)

Figure 38. Water depth (m) after 15 s: (**a**) BB technique with the staggered layout. (**b**) BR technique with the staggered layout [202].

6.3.6 The impact of the building layout

In general, the staggered layout displayed higher resistance to flood propagation compared to the aligned layout, resulting in higher flow velocity in the built-up area. The peak value of water depth and time to peak varied depending on mesh sizes. At gauge points P3, P4, and P5, which were directly hit by the flow, the calculated peak water depth values were higher than the measured values compared to other gauge points, regardless of mesh resolution. Regarding water depth, the second and fourth rows of buildings in the staggered layout acted as a barrier to the flow, leading to an increase in water depth and a decrease in velocity upstream of the building. The predicted time of the water depth peak was not significantly affected by mesh resolution, but there was a slight improvement in the 1 cm resolution compared to the 2 and 5 cm resolutions. However, decreasing the mesh size caused data oscillation in the numerical modeling, which had an impact on the accuracy of the results.

6.3.7 The impact of the Manning coefficient

The BR method only applies an artificial increase in the Manning coefficient within the areas of the buildings, not for the entire 2-D flow field. Increasing the Manning coefficient has a significant impact up to a certain value, beyond which further increases appear to have no significant effect on the

outcomes. Therefore, the Manning coefficient is an important parameter in numerical modeling with the BR technique. A Manning coefficient value greater than 1 improves the performance of the numerical model, which is practically significant in such models. As flood modeling processes and the mapping of results, especially in urban areas, require a lot of data such as accurate terrain data, which can be expensive, the BR technique is worthwhile to apply using high Manning coefficients with regards to the resistance effect of buildings.

6.4 Conclusions

To sum up, the study demonstrates that various urban features, such as apartments, houses, business buildings, roads, and man-made infrastructures, have a significant impact on urban flooding. The depth and velocity of water are crucial parameters in mapping flood hazard and calculating damage assessment. The study examines two building layouts: aligned and staggered, using two building representation methods: BB and BR, and uses the HEC-RAS 2-D model to analyze unsteady urban flooding based on the Toce River experimental test case. Eight models were prepared, analyzed, and discussed.

The study concludes that the HEC-RAS 2-D model can simulate unsteady urban flooding using both BB and BR methods, with the BR method being a good representation of building units in numerical simulations using high Manning coefficients. However, the DW model underestimates the water depth at all probe points, except for one point. The value of the Manning coefficient is the crucial parameter in the BR method, as it affects the predictions of velocity and water depth, especially when detailed building geometry data or DEMs are not available. The BR technique is easier to implement and provides fast execution but is less precise than the BB technique, especially with respect to velocity prediction.

The study also shows that a 1 cm mesh resolution is relatively accurate compared to 2 and 5 cm mesh resolutions. However, comprehensive urban flood validation datasets are required for accurate predictive modeling of localized depths and velocities. Furthermore, the applicability of these techniques to real-world case studies should be investigated, given the differences in building layout, roughness, and flow hydrograph in real urban areas. Finally, the validity of the parameters in HEC-RAS 2-D at a larger scale is the subject presented in Part IV of this study.

7. Part IV: Hydrodynamic Modeling of Urban Flood in Erbil

7.1 State of Art

Floods have developed into an event that people in developing countries regard as routine during the rainy season. Flash floods caused by climate change are one of the most common causes of fatalities and property damage in the 21st century.

Building detailed flood inundation maps is typically done through the use of hydrodynamic models. A significant amount of data, time, and computational resources are required for the development of a hydrodynamic model for a large hydrological basin, all of which must be available at the same time [220]. In developing countries, obtaining archived data for rainfall-runoff modelling, high-resolution DEM for topography and accurate LULC for basin characteristics is a challenge. As Loudyi and Kantoush [221] pointed out, a serious challenge for flood risk assessment in the Middle East and North Africa (MENA) region is the unavailability and sometimes unreliability of data, particularly for the calibration and validation of flood models. There are some approaches that could be considered to fill such gaps, for example, as part of hydrological and hydrodynamic modeling of urban floods in Erbil, previously LULC from Landsat satellite images were prepared for the study area [141]. Furthermore, the availability of such data allows a more precise description of hydrological processes occurring in the real world, paving the way for a more numerical approximation of the processes involved in urban flooding. As a result of historical efforts to mitigate flood impacts, flood loss and damage in developed countries, particularly when measured in terms of the number of fatalities, is generally less severe than in developing countries [222].

Rapid urbanization is one of the main causes of flash floods in Erbil. As a result, the patterns of LULC in Erbil have changed significantly over the last two decades, particularly in the urban areas [141]. The most important factor that has a significant impact on creating the danger of flash flooding is the improper use of land for urbanization where the paths of the waterways have been closed. In the aftermath of this, the number of urban flash floods has also increased significantly [29]. Changes and developments to the land surface within cities will have an effect not only on the likelihood of increased flooding, but also on urban water management generally [223]. On the other hand, there have been studies that have linked the increasing frequency of floods to the impact of climate change [224,225]. For applications in urban settings, high temporal resolution of precipitation, such as sub-daily, is required for establishing a relationship between extreme precipitation Intensity–Duration–Frequency IDF [226-228]. When it comes to developing countries such as Iraq, the number and distribution of stations capable of recording rainfall on a shorter time scale are limited. The IMD equation was used to

determine the rainfall data for periods shorter than 24 hr, and IDF curves and empirical IDF formulas for the city of Erbil were developed as a result of these limitations [92]. To assess flood risk, scientists consider the likelihood and severity of a flood in a specific area at a specific time, along with the potential consequences [42,43,229].

From 1950 to 2010, the number of people who died in Iraq as a result of flooding was only 11 [230]. In the fourth quarter of 2021, Erbil was struck by flash floods on October 30 and December 17, the latter of which was particularly devastating, resulting in the deaths of 12 people and the disappearance of the body of a 10-month-old child for almost two months. Another flash flood hit Erbil on January 13, 2022, approximately one month after the previous one. Specifically, this one was located mainly within the study area that was modeled in HEC-RAS 2-D in this part of the thesis. Flash floods are more common in areas with a dry climate and impervious terrain because lack of pervious surface or vegetation allows torrential rains to flow overland rather than infiltrate into the ground. According to the available evidence, the city has experienced three floods in the span of just three months. According to a press release from the province of Erbil, more than 7000 people were declared to be in a state of special calamity [231], and the total flood damage in Erbil was estimated to be $14,5 million [232]. The economic impact of recent flash floods has increased dramatically. Despite the devastation caused by Erbil's flash floods, the study area's summer fresh-water shortage makes flash floods a valuable source of water.

This part of the study addresses a critical issue of urban flash floods in Erbil and presents a new approach to model and identify flood-prone areas using HEC-RAS 2-D hydrodynamic model. Previous studies on stormwater management in Erbil have been lacking, and there is a need to establish sustainable strategies to mitigate the adverse effects of flooding on the society. The study highlights the importance of accurate topographic representation using a DEM of different precision to improve the flood modeling results. The impact of floods on society is also discussed, emphasizing the need for effective management strategies. This study is the first of its kind in the study area, and it is expected to provide valuable insights into developing sustainable urban stormwater management practices.

7.2 Material and Methods

7.2.1 Data availability and processing

In the development and simulation of hydrological and hydrodynamic models, the availability of raw data is the most important factor to be considered. It was necessary to acquire a DEM from the SRTM (http://dwtkns.com/srtm30m/) with a resolution of one arc-second (30 m) in order to delineate the watershed boundary of the study area (see Figure 7a). Li and Wong [233] conducted an analysis to

determine how various DEM data sources may influence the outcomes of hydrologic applications. A DEM with a resolution of 10 m was created using the point clouds of the LIDAR images (the data source was the Erbil municipality, the work date back to 2010). Then, a Feature Manipulation Engine (FME) was used to generate another DEM over the study area, from the layout map of the city, the heights of the buildings were extracted to create a building layer in three dimensions (3-D). From the buildings, a raster with spatial resolution of 1 meter was created. After resampling the DEM of the city (only the area inside 120 m ring road) from 10 m to 1 m, it was then overlaid on the raster accompanied by the buildings. Raster calculation with maximum operation was applied to create a DEM of the city with a resolution of 1 m (see Figure 39).

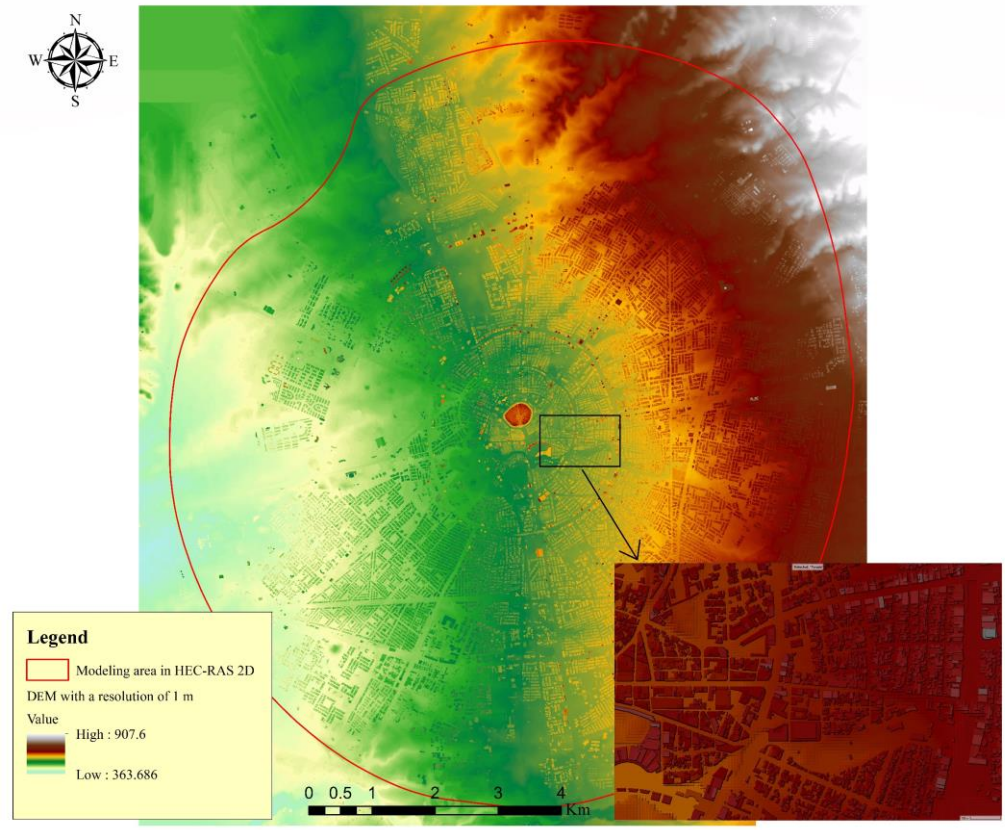

Figure 39. DEM with 1 m resolution for modeling area (BB technique simulations) in HEC-RAS 2-D.

The FAO of the United Nations prepared a digital soil map of Iraq, from which a soil map of the studied area was extracted. Brown soils with deep phases have dominated the soil profile in the area under consideration for 2-D hydrodynamic modeling. The Natural Resource Conservation Service (NRCS) divided soils into four Hydrologic Soil Groups (HSG) based on their runoff potential [234]. A,

B, C, and D are the four HSGs, where A has the least potential for runoff and D have the most. The study area for modelling in HEC-RAS 2-D is in group C [140].

The LULC map was produced by RS data collection. When cloud coverage was less than 5%, an image from the Sentinel-2B satellite (which has been in operation since 2017) was obtained from the Copernicus open access hub platform (https://scihub.copernicus.eu/), operated by the European Space Agency. The image used for analysis was taken on September 13, 2021. The study area was categorized into three groups for the LULC classification: built-up (including residential, industrial, commercial, local streets, roads, and other urban areas), bare land (including uncovered soils, unused areas, and dry river beds), and vegetation (including forests, orchards, vegetable fields, parks, lawns, shrubs, and others) (see Figure 40). The total study area of approximately 102.368 km² is composed of 66.36 km² (64.82%) of built-up areas, 25.038 km² (24.45%) of bare land, and 10.97 km² (10.71%) of vegetated areas.

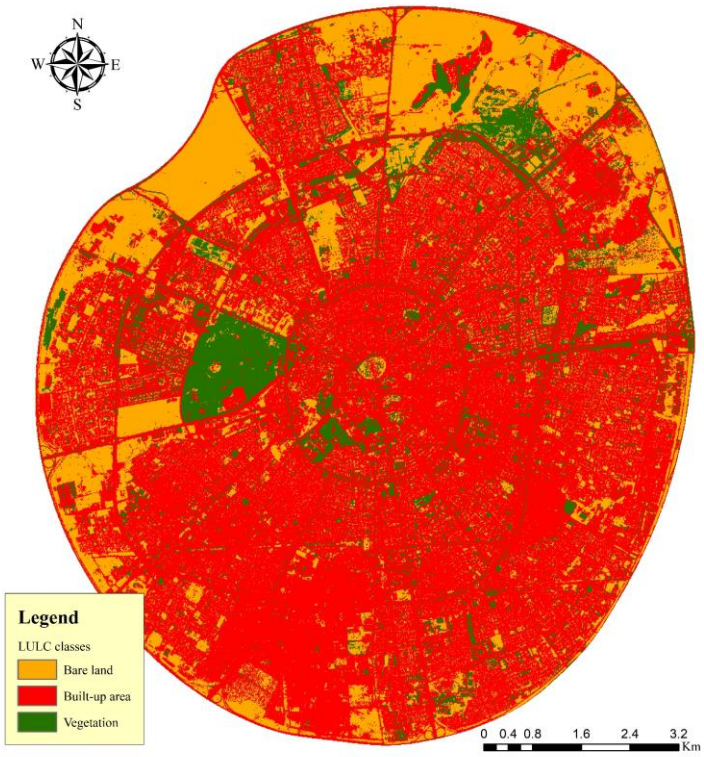

Figure 40. LULC classes inside the modeling area in HEC-RAS 2-D.

7.2.2 HEC-RAS 2-D model setup

HEC-RAS 2-D is an open-source software package developed by the United States Army Corps of Engineers (USACE) [203,208] and is used to model the hydrodynamics of water flow in the area under investigation. In previous section, it was investigated whether HEC-RAS was appropriate for the study's objectives. This was an important result that paved the way for the next stage of

investigation because it demonstrated that both the BB and BR techniques could be used for flood hydrodynamic modeling in urban areas. The Digital Terrain Model (DTM) is responsible for inducing the majority of the topographic characteristics of the study into the HEC-RAS 2-D model. Using a DEM as an input file, HEC-RAS 2-D is capable of creating a DTM within the program. Specifically, a DEM plus buildings with a resolution of 1 m was prepared for use in the generation of the study area's DTM in this case. In the geometric data editor of the software, a 2-D flow area describing the boundary of the assumed flood domain is created by drawing a polygon with the orthophoto as the background layer. Afterwards, an automatically generated computational mesh within the boundary layer is created with a 10×10 m cell size. This results in a total of 1,022,897 grid cells with an average size of 100 m^2. To demonstrate the effects of computational cell size on the model outputs and model run time, two more mesh configurations with 8×8 and 20×20 m are examined. The total number of grid cells in these mesh configurations is 1,598,552 (average cell size = 64 m^2), and 255,501 (average cell size = 400 m^2), respectively. The four building representation techniques that are commonly used to model built-up area flooding in hydrodynamic numerical models are the BB, BR, BH, and BP [171,198,204,206,207]. In the HEC-RAS 2-D, both BB and BR are applicable. BB technique means increasing the ground elevation of building units by modifying distributed ground elevation data, by configuring the buildings to a real height or a sufficiently high artificial elevation value to ensure no water flows over the buildings. Here, the entire simulated flow area should be meshed as a unified grid, so water flows around buildings. In BR, the modeler may give each grid a different Manning coefficient. High Manning coefficients result in high flow resistance and low water flow velocity. In this method, the simulated building areas are given a high Manning n value to increase friction. In other simulated areas, a low value represents the real land cover. Due to the high friction coefficient assigned to the building units, water flows slowly over them but behaves as if there is a high resistance against flow. A detailed description can be found in Part II of the study and [202].

The model's other parameters, which include 2-D surface roughness, CN for LULC classes, boundary conditions, and rainfall data, are also required. Table 21 categorizes the LULC classes, Erbil City center is a densely urbanized area with predominant brown soil and deep phase. Thus, based on imperviousness and soil type, three different Manning's n are selected for the 2-D area [235] (see Table 22). Defining boundary conditions within the HEC-RAS 2-D flow area is required in order to run the 2-D model simulations. Boundary conditions for defined 2-D flow areas can include a variety of features such as flow and stage hydrographs, normal depths, rating curves and precipitation boundary conditions, among other things. In the current study, only 23 outlets of culverts, roads and natural

streams are defined as boundary conditions with normal depth. A time series of rainfall is used as meteorological data in the unsteady flow section for each storm event, and a simulation run is carried out to generate flood inundation for each storm event.

Table 21. CN values [236].

LULC classification	CN for hydrologic soil group			
	A	B	C	D
Built-up area	77	85	90	92
Bare land	68	79	86	89
Vegetation	43	65	76	82

Table 22. Average values of Manning's roughness coefficient based on different LULC classes [235].

LULC classification	Manning's n value
Built-up area	0.013
Bare land	0.03
Vegetation	0.025

Analyzed long-term series of maximum daily rainfall data were used in this study and within them, a theoretical probability distribution of 10, 5, and 1%, which is equal to 71.16, 83.21, and 113.49 mm [29] (see Figure 41 and Part I of this study). The method that was used to prepare the temporal rainfall distribution was based on Huff's second quartile [95]. The reasons for using this method are explained in [29]. Uniform rainfall distribution in space is considered. Unsteady flow routing can be done two-dimensionally with either the SWE or the DWE. To solve the flow over the computational mesh using HEC-RAS, three sets of equations are available: the DWEs; the Shallow Water Equations (SWE-ELM, or Shallow Water Equations, Eulerian-Lagrangian Method) original equations; and a more momentum-conserving Shallow Water Equations solution (SWE-EM, which stands for Shallow Water Equations, Eulerian Method) [203]. In the present study, considering results described in Part III, the original (SWE-ELM) was chosen for HEC-RAS 2-D.

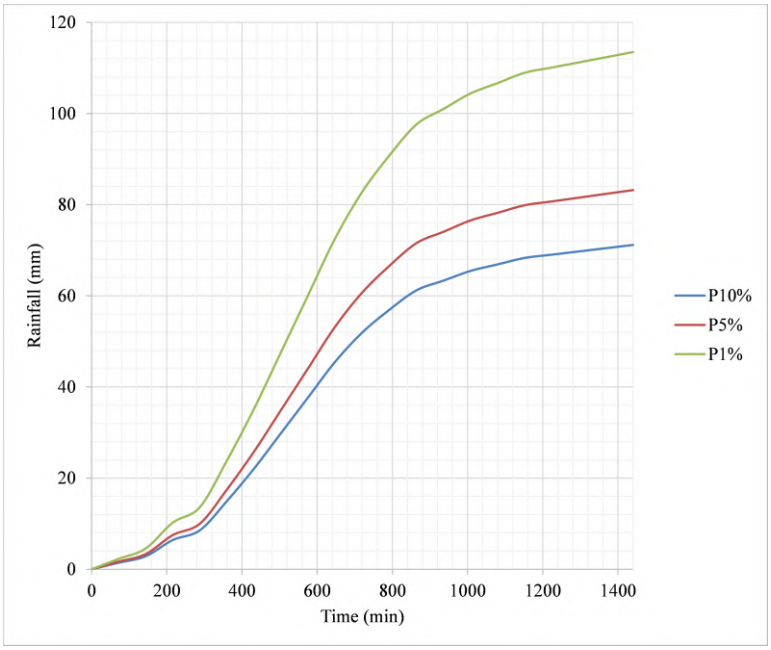

Figure 41. Temporal distribution of rainfall for three probability distributions of 10, 5, and 1 %.

7.2.3 Flood hazard mapping and assessment

Flooding is most commonly caused by intense rainfall occurring when natural rivers and streams are unable to carry the excess water. Similarly, flooding can occur when the stormwater system's capacity is insufficient, resulting in overflow phenomena. Floods create hazardous conditions that humans are particularly susceptible to. The severity of a flood is determined by several factors, including the intensity, volume, timing, and phase of the precipitation that preceded it, as well as the characteristics of the rivers and drainage basins [237]. Floodplains that are left undeveloped and uninhabited could eliminate the risk that flooding poses to a community. It is the interaction of people with the floodplain and their exposure to flood hazards that causes the risk of flooding [238].

Since the work on this dissertation was carried out in stages with the overarching objective in mind, the output of the urban flood model developed can be used to classify hazardous areas using the flood hazard guidelines developed by the Australian Institute for Disaster Resilience. Evaluating and classifying flood hazards requires considering both the depth and velocity of the flood. Understanding the relative degree of hazard and the underlying flood behavior creating the hazard (such as high depth, high velocity, or a combination of depth and velocity) is essential for effective management approaches [238]. To categorize flood hazard areas, the water depth layer is multiplied by the velocity layer using a raster calculator in the ArcMap output. The flood models that utilized the BR technique and a syntactical rainfall probability of 10% were used for this purpose. However, it is important to

consider the assumptions made when developing the flood model and the methodologies used to analyze the results, as they can impact the quality of the results. The modeling approach, model scale and resolution, and the level of topographic data integrated into a model can all influence estimations of flood hazard [238]. As part of the flood research, a flood hazard assessment was conducted to provide preliminary information for urban flood management in Erbil. The analysis classified flood-prone areas inside the 120 m ring road of Erbil according to a general classification of flood hazard [238]. Figure 42 presents a combined set of hazard vulnerability curves for these floodplains [239], based on the guidelines developed by the Australian Institute for Disaster Resilience AIDR.

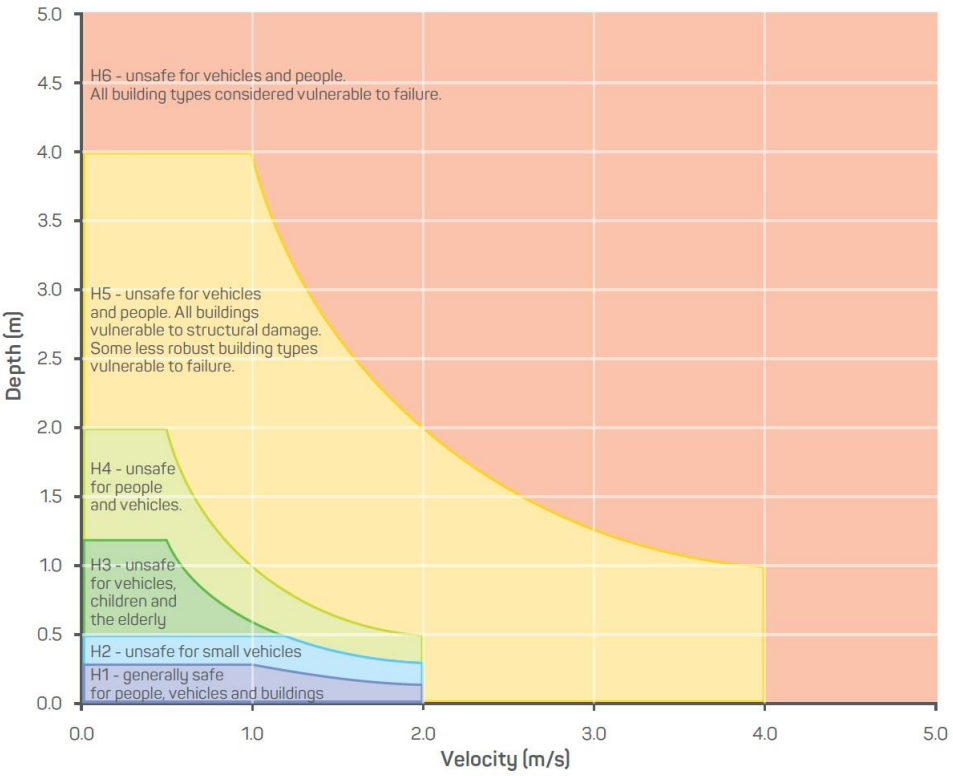

Figure 42. Flood hazard curves according to AIDR [238,239].

Flood risk is determined by the combination of vulnerability to flooding and the total value of assets that could potentially be impacted by flooding. The probability of various flood threats and the value of assets exposed to them are key factors in determining flood risk. The safety of citizens, as well as the infrastructure and developments in a given location, are directly linked to its susceptibility to flooding and the extent of its vulnerability. Understanding the full range of flood behavior is crucial to assessing a community's vulnerability to flooding, which in turn informs flood risk management decisions.

To accurately classify flood-prone areas, it is necessary to define the function of each zone within the study area, such as whether it is primarily residential, commercial, or a mix of both, and the population density. The area may be an agricultural zone, an industrial area, or even focused on tourism or archaeology. This dissertation proposes a simple ranking of hazardous areas, categorized as H1, H2, H3, H4, H5, and H6, to identify high-risk locations.

The combined flood hazard curves presented in Figure 18 provide flood hazard criteria relevant to community susceptibility when interacting with flood-prone areas. The curves are divided into hazard classifications based on specific vulnerability criteria outlined in Tables 23 and 24. Overall, a comprehensive understanding of the vulnerability of a community to flooding is crucial for effective flood risk management. By properly categorizing at-risk areas and implementing appropriate measures, citizens and their assets can be better protected from the devastating impacts of floods.

Table 23. Combined hazard curves – vulnerability criteria [238,239].

Hazard Vulnerability Categorization	**Interpretation**
H1	Generally safe for cars, people, and structures.
H2	Not safe for small cars.
H3	Not safe for cars, kids and the aged.
H4	Not safe for cars and people.
H5	Not safe for both cars and people. All structures are vulnerable to structural damage. Certain less resilient building types are vulnerable to failure.
H6	Not safe for cars and people. All building types are regarded as vulnerable to failure.

Table 24. Combined hazard curves - vulnerability criteria classification limits [238,239].

Hazard Vulnerability Categorization	**Categorization limit (D × V in combination) m²/s**	**Inundation depth (D) m**	**Velocity (V) m/s**
H1	$D \times V \leq 0.3$	0.3	2.0
H2	$D \times V \leq 0.6$	0.5	2.0
H3	$D \times V \leq 0.6$	1.2	2.0
H4	$D \times V \leq 1.0$	2.0	2.0
H5	$D \times V \leq 4.0$	4.0	4.0
H6	$D \times V > 4.0$	-	-

7.3 Results and Discussion

7.3.1 Analysis of flood hydrodynamics in Erbil

Hydrodynamic models are frequently used in the process of creating detailed flood inundation maps. One of the most crucial components of flood modeling is the determination of which hydrodynamic model to use. Because 2-D hydrodynamic modeling is appropriate for analyzing flood inundation in urban areas, the widely used modeling tool for hydraulic engineers, the open-source package of HEC-RAS 2-D has been utilized in this investigation.

7.3.2 Analysis of different mesh resolutions and building representation techniques

This research conducted a comparison of two building representation techniques and evaluated the outcomes of different simulations using both fine and coarse grid sizes. The objective of the study was to analyze the results obtained from modelling floods in urban areas. To accurately simulate the flow on streets, intersections, around houses, and buildings, a fine 2-D grid with a size of less than 5 m is needed. The study initially focused on the BB technique to assess whether the prepared DEM was suitable for numerical simulation. The quality of the prepared DEM was considered acceptable, and the study aimed to determine whether the model would produce satisfactory results. The study used three different grid sizes, starting from 8 m, 10 m, and 20 m, respectively. However, due to the area's size, it was challenging to simulate the flow using a grid size smaller than 8 m. It should be noted that reducing the size of hydrodynamic grid cells results in denser mesh, requiring a longer runtime to complete, leading to a trade-off between simulation accuracy and calculation time. A recent study compared two new methodologies for reducing the processing time of large-scale flood simulations, evaluating their merits and drawbacks to provide effective application advice. Additionally, Yalcin [240] noted that a mesh resolution created at a basin scale with a size greater than 10×10m, known as a "coarse grid," leads to significant errors in the estimated inundation extent due to the inability to capture rapid changes in the terrain geometry.

To investigate the impact of grid size on numerical simulations, multiple simulations were conducted using the BB technique with cell sizes of 8, 10, and 20 m. The results revealed errors in water depth calculations, particularly in front of buildings, which could be due to the difference in street dimensions and cell size (see Figure 43a-c). By decreasing the grid size, water propagation and depth in front of buildings could be improved. The DEM and mesh resolutions are crucial factors in simulating water level dynamics, and the floodplain roughness coefficient must be considered when mapping the extent of a floodplain. Surwase, *et al.* [241] found that the HEC-RAS model is sensitive to the Manning roughness coefficient. However, due to limitations in computer processing capabilities, a

cell size of less than 8 m was not feasible. Therefore, it was concluded that reducing the size of the 2-D flow area would allow for modeling with a grid size of 2×2 m or less, which would be more accurate for abrupt changes in terrain. In conclusion, reducing the grid size can improve simulation accuracy, but there is a trade-off between accuracy and computation time.

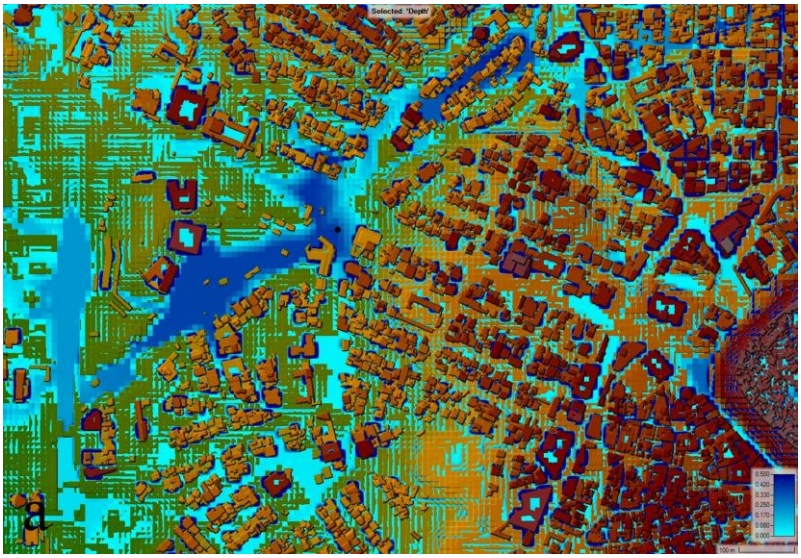

(**a**)

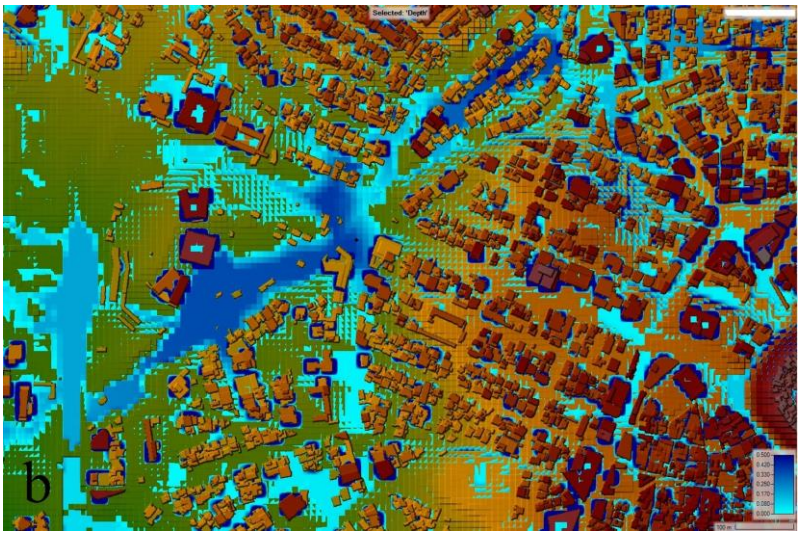

(**b**)

Figure 43. Analysis of the numerical simulation using different mesh resolutions with the BB technique: (a) grid size 8×8 m. (b) grid size 10×10 m. (c) grid size 20×20 m (continued on next page).

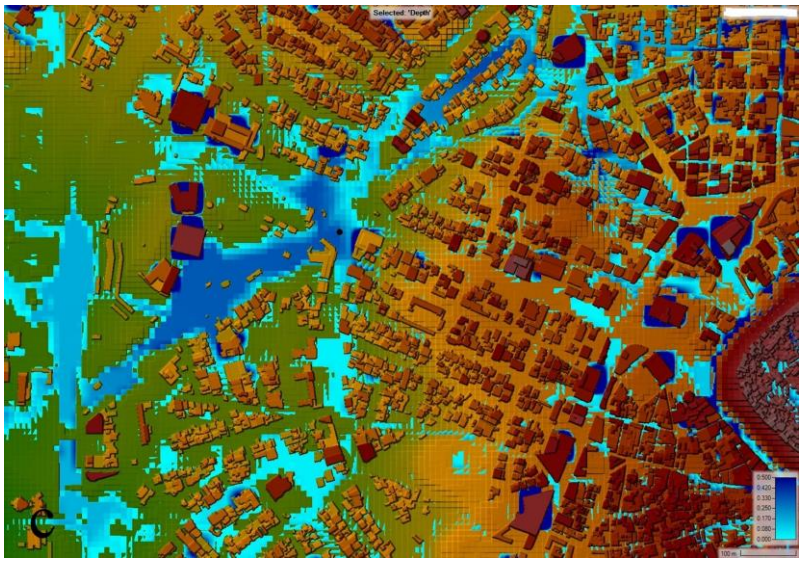

(**c**)

Figure 43. Analysis of the numerical simulation using different mesh resolutions with the BB technique: (**a**) grid size 8×8 m. (**b**) grid size 10×10 m. (c) grid size 20×20 m.

It is the responsibility of researchers to thoroughly investigate all possible avenues and present a conclusion to society. In order to determine the effect of urban flooding within the 120 m ring road in Erbil, the author chose to use the BR technique to model this zone. This method has previously been validated in this thesis in Part III. The BR technique involves assigning Manning coefficient values to mesh regions representing building blocks to examine resistance against flow. This method was found to be more accurate in estimating water depth compared to the BB technique, which models buildings as blocks and does not allow for water to enter them. However, if a high-resolution DEM is used in the modeling and simulation process, the BB technique is expected to provide more accurate results in determining flood extent and the most vulnerable areas. Therefore, the choice of which method is more realistic depends on the specific context and the resolution of the DEM used.

7.3.3 Analysis of flood-affected areas

After realizing the lack of reliable data, it was concluded that the BR technique is effective for analyzing floods in the study area. Therefore, the analyses presented are based on this technique with a 10 m grid size. However, some assumptions had to be made in order to develop the model for the area considered in HEC-RAS 2-D. One of these assumptions was that there is no inflow to the area, although this is not true because there is inflow to the 2-D area through main roads and underground box culverts that cross the 120 m ring road. Despite the lack of recorded data, it was decided to keep

the boundary closed but acknowledge that this assumption may impact the results. Nevertheless, constructing retention basins can prevent flow from outside the studied area from entering. It can be confidently stated that the modeling is accurate to a significant degree because the results were compared with those of known flood-prone areas.

Using two orthogonal components of the flow, 2-D surface flow modeling attempts to predict the maximum inundation area and flow dynamics such as water depth and velocity. Flood accumulation areas are often identified by their low elevation, which indicates their hazard of flooding. Despite changes in the city's layout, the flow movement continues to follow the same path as it did in the past. For example, the source of accumulated water in Tayrawa Street and the main gate of the council of ministers on 30 m street is coming from the northeastern areas of the studied areas, such as the North industrial area and the area near the Family Mall shopping center, according to the findings (see Figure 44a). Similarly, the source of the flow that causes problems in Setaqan quarter on 60 m street and near Nishtiman Bazar comes from the Havalan quarter in the eastern part of the study area, passing through the city via an underground box culvert (see Figure 44b). When the flow rate exceeds the capacity of the box culvert, overflows occur in this zone, and this can be caused by various factors such as the flow from surrounding areas being accumulated there, the inadequacy of the stormwater system, and the accumulation of debris in inlets, manholes, and box culverts, which prevent the system from functioning properly.

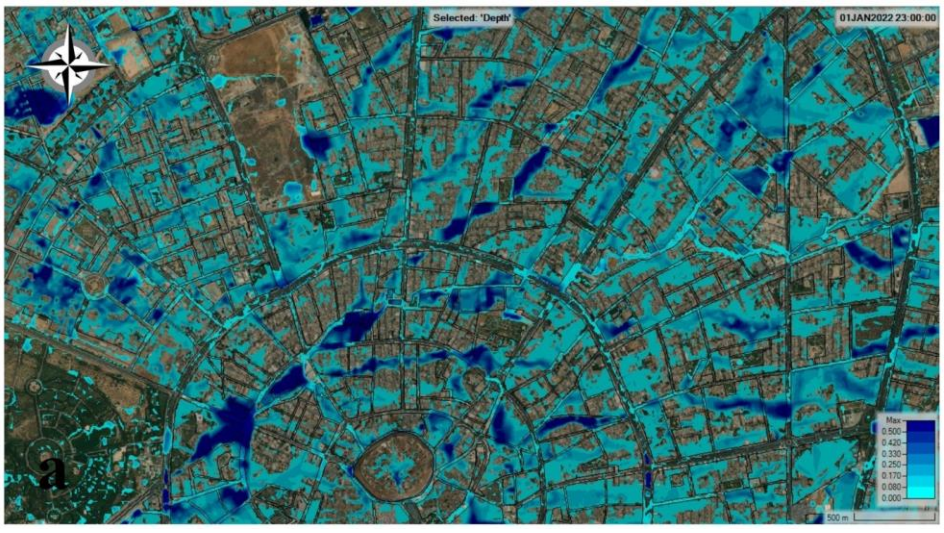

(**a**)

Figure 44. Results of the numerical simulation using BR technique with grid size 10×10 m: (a) upper part of the studied area. (b) the lower part of the studied area (continued on next page).

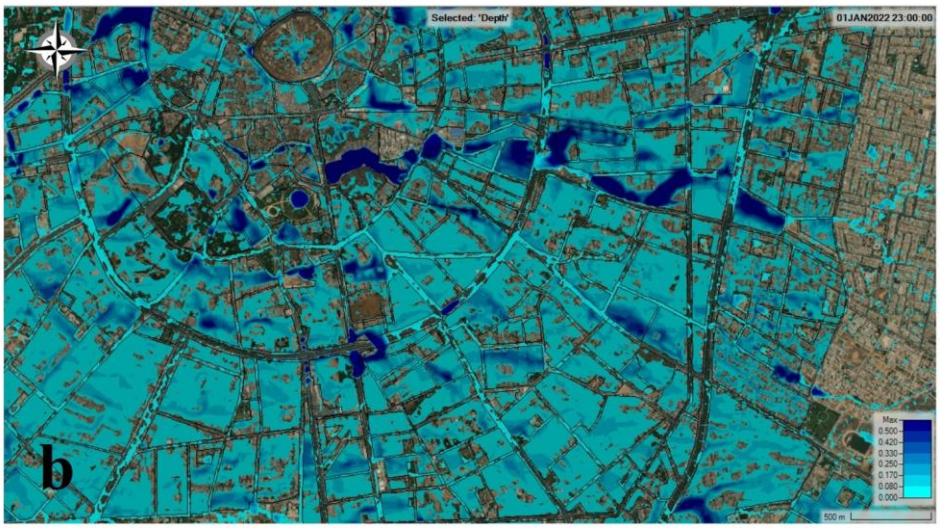

(**b**)

Figure 44. Results of the numerical simulation using BR technique with grid size 10×10 m: (**a**) upper part of the studied area. (**b**) the lower part of the studied area.

The study focuses on flood hazards and the extent of inundation in the Erbil city area. Three simulations based on different probability distributions of rainfall were used to determine the extent of flooding. The focus was on the extent and prone areas of flooding rather than the depth of inundation, as only surface flow data was available during simulations. A vector layer generated using water depth maps at a value of 0.2 m to delineate flood extent in the studied area. Then sorted the vector layer using attribute tables and ignored areas smaller than 500 m^2. The results showed that the amount of rainfall caused the flooded area to expand proportionally (see Figure 45a and b). When the simulation was performed with a rainfall probability of 10%, an area of about 5.725 km^2 was affected by flooding. The size of the affected area increased by about 21.83% when the rainfall probability was increased to 5%, and it resulted in a 71.37% increase in the magnitude of the flood extent when simulated with a rainfall probability of 1% (see Figure 46). The majority of the areas that flood or accumulate water as a result of rainfall are public streets, commercial districts, and residential areas, which have a significant effect on the flow of traffic and cause loss of life and property. The study highlights the need for better distribution of permeable areas to increase infiltration and decrease runoff.

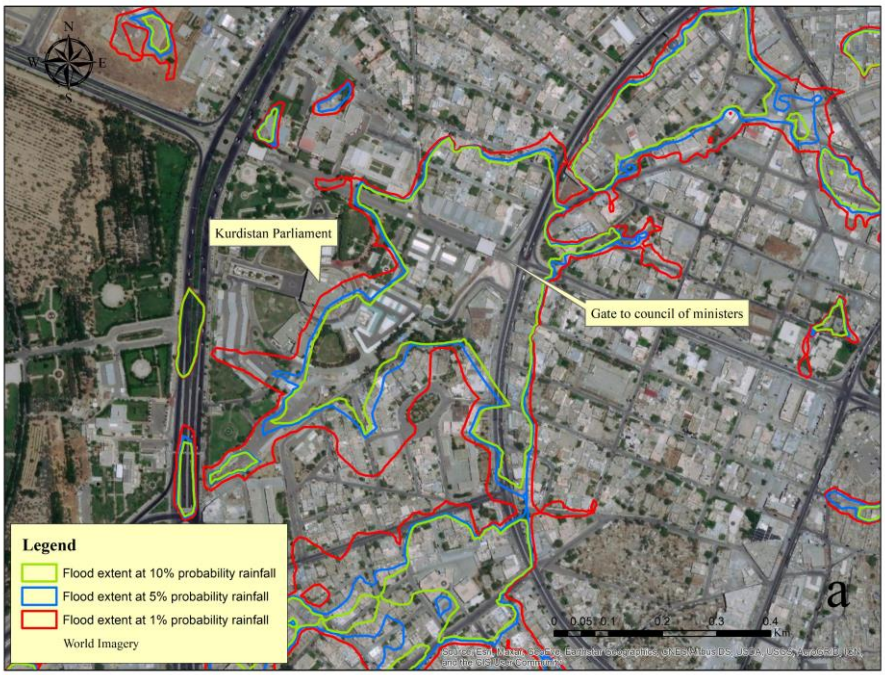

(**a**)

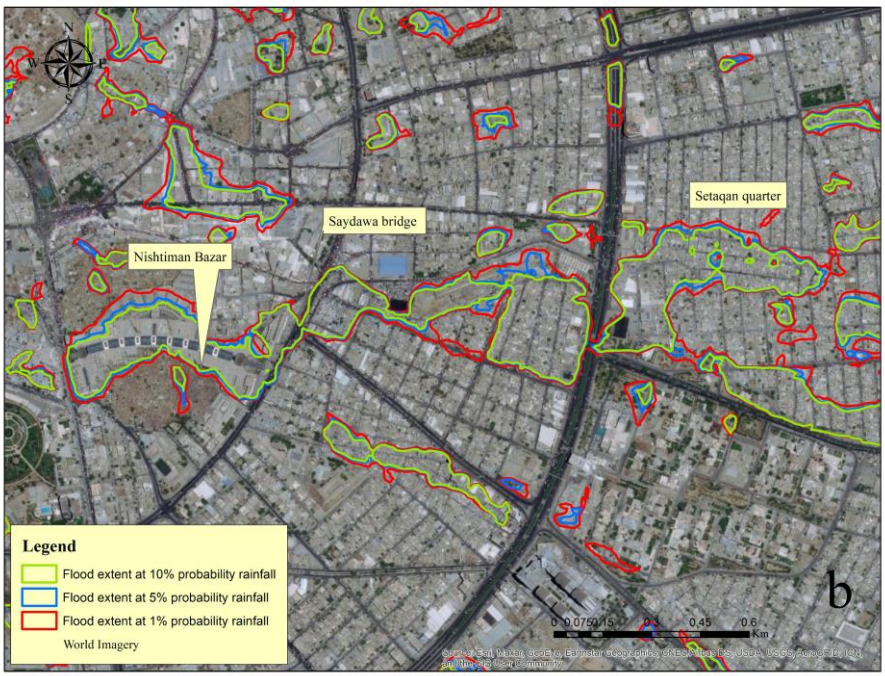

(**b**)

Figure 45. Comparison of the development of flooded areas based on a different rainfall simulation: (**a**) Gate to council of ministers. (**b**) Nishtman Bazar, Saydawa quarter and Setaqan quarter.

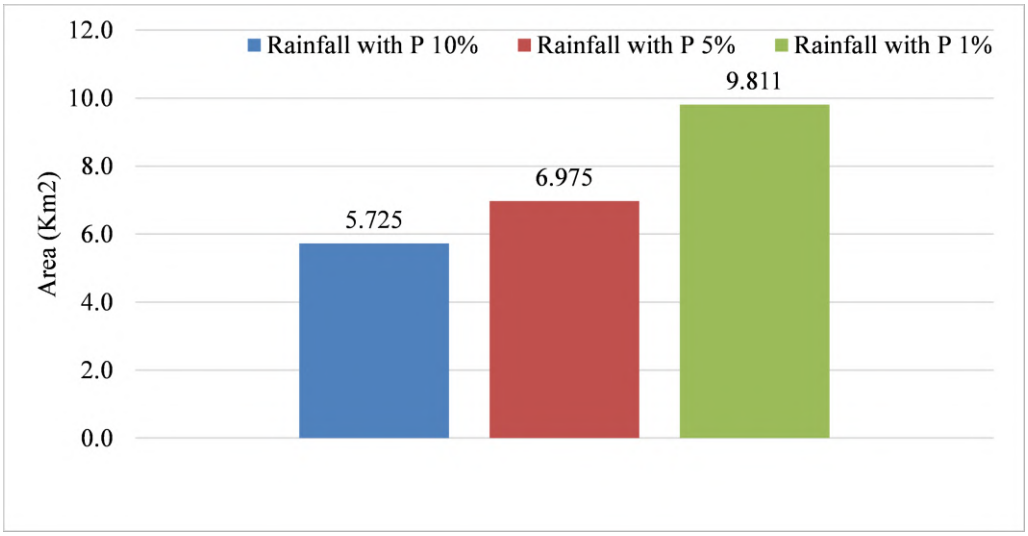

Figure 46. The evolution of inundated areas.

Observing two extraordinary events that occurred at the end of 2021, authorities in Erbil revealed that the flooded area is located on the route of natural and seasonal streams, which occurred outside the area considered in the HEC-RAS 2-D modeling in the current study. The expansion of the city has resulted in the construction of numerous residential and commercial buildings, as well as industrial and manufacturing facilities, along the path of natural flow routes. In this section, the areas at risk of flooding outside of the 120 m ring road were evaluated by using the DEM with a resolution of 30 m to assess flood basins that had been delineated. The route of the natural streams can clearly be seen in Figure 47, which shows that both Zerin city and Korean village are located along the route of the natural streams. According to a media statement issued by the governor of Erbil on October 30, 2021, an amount of 55 mm of rainfall was recorded in the upper part of the city in just two hours on that day. In the northeast, where there is higher topography known as the Tarin heights, crazy flow can flow to the prone areas.

The same can be said for the village of Grd Jutiar, which is located directly adjacent to the natural canal. On that specific day, the capacity of the canal was insufficient to manage the amount of water passing through it. As a result of this, the overflow of canal banks occurred somewhere near the north side of the village, resulting in the catastrophic event. The first phase of a 150 m ring road connecting the main Shaqlawa road with the main Bahrka road was completed in 2021. In an interview with Rudaw TV [34], the project manager for the 150 m ring road stated that the culverts and box culverts that cross the ring road and run along the ring road were only intended to handle stormwater from the surrounding areas and household waters, not the large amounts of water that flow from the natural basin. Erbil city has expanded toward mainly the Northeast and East areas, but detailed hydrologic

studies are absent. Many stormwater and sewer pipes in local areas throughout Erbil have been built without taking the dimensions of water pathways and streams into consideration. It is now possible to experience flash flooding in areas where urban and infrastructure development have taken place.

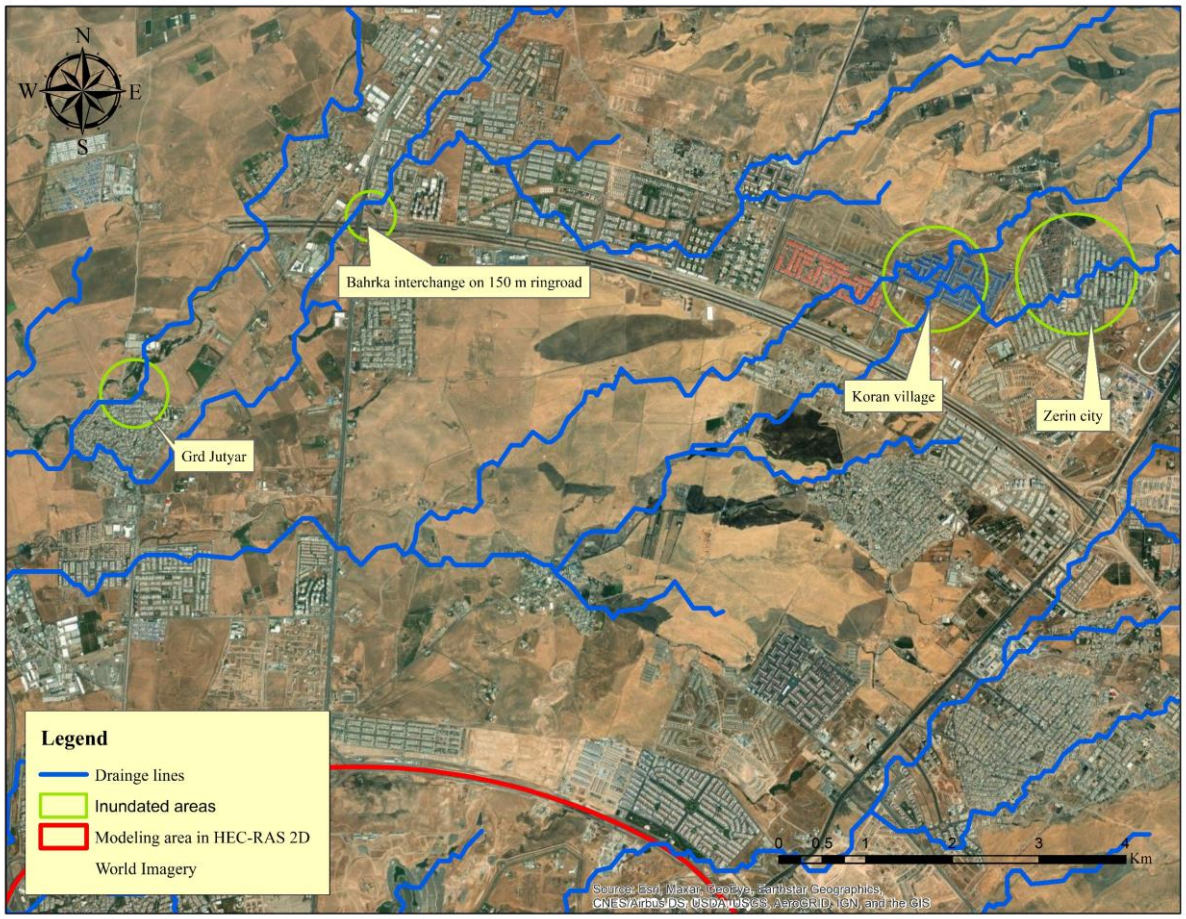

Figure 47. Some inundated areas in Erbil during the storm event of October 30 and December 17, 2021.

Flooding in Erbil ranges from minor incidents, such as inundation of streets and then water entering some houses, to major incidents, such as large areas of the city being submerged for several hours at a time. The event, which took place on December 17, 2021, was primarily focused on the Southeast of the city, specifically the Bnaslawa sub-district and the Roshinbiri quarter (see Figure 48). In reality, this was a catastrophic event that was unprecedented in Erbil's history, because 12 people died. One of them was a 10-month-old child whose body was found approximately 60 days after the event and more than 15 kilometers away from his house. A large number of small-scale local problems are common in most developing cities around the world, primarily because their stormwater systems do not have enough capacity to handle heavy rainstorms [242]. Greater flooding risk exists in areas that

are close to the main channel and accumulation path [243]. There were various contributing factors to this catastrophic event, the first of which was a reduction in the cross-section of streams, with their bed elevations approaching the elevation of the street in some places. The reason for this is that these seasonal streams have not been cleaned in a long time and have become clogged with river sediments and debris (see Figure 49). In addition, a large number of quarries are operating on the river bed on the upstream side of the developed area (Bnaslawa sub-district) to extract sub-base or other materials. According to the locals' speech, those quarries created a dam-like barrier, which collected a large volume of water on that particular day before being breached, causing the flow to become increasingly erratic. As can be clearly seen, a large number of residential areas have been constructed directly adjacent to stream routes, indicating that this type of event is predictable.

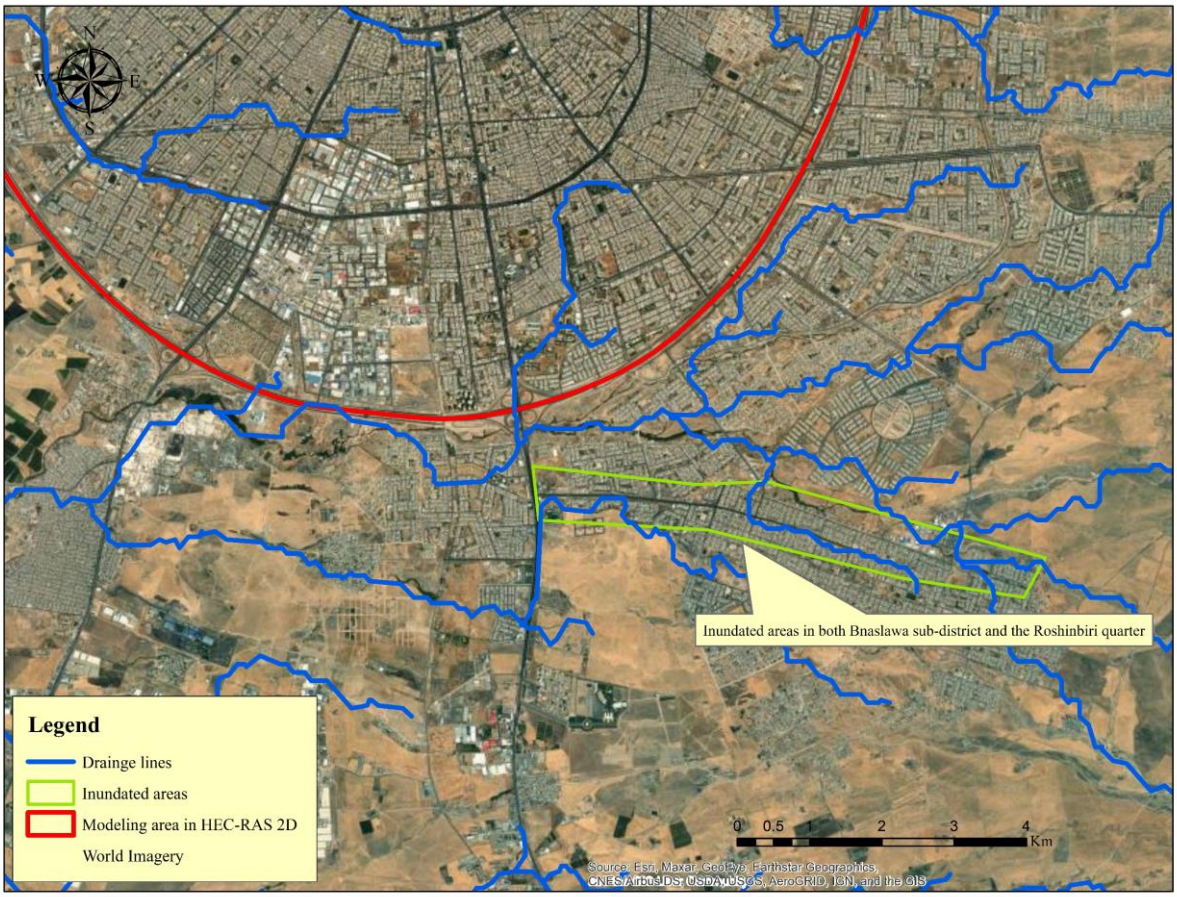

Figure 48. Bnaslawa sub-district and the Roshinbiri quarter inundated in Erbil during the storm event of December 17, 2021.

Figure 49. Debris and waste accumulation inside culverts, sewer pipes, and natural streams.

7.3.4 Flood Hazard Mapping

According to Khaing, *et al.* [244], the process of mapping flood hazards consists of three steps: (1) determining the fundamental problems and situations, (2) collecting the essential data required for flood simulation and inundation mapping, and (3) carrying out flood hazard simulation and mapping. When attempting to evaluate and categorize flood hazards, it is crucial to recognize the relative degree of hazard, as well as the underlying flood behavior that is creating the hazard (for example, high inundation depth, high flow velocity, or depth and velocity combined), as these may require different management strategies. Many stormwater management systems are designed on the assumption that

there is a 10% probability of precipitation occurring. This is because rainfall is more likely to occur with this probability. Therefore, the same idea was adhered to throughout the course of this research. In this study, the results from a simulation using the BR technique with a rainfall probability of 10% have been used to classify flood hazards in the study area. The inundation depth ranges from 0 to 6.05 m, while the flood velocity ranges from 0 to 1.89 m/s. The depth of the inundated areas in the simulations is a crucial factor to consider [245]. Flood inundation mapping has been a significant part of the process of developing sustainable urban planning, preserving human lives and properties, and reducing the likelihood of natural disasters [246-248]. The results indicate that there is a depth of 6.05 m, but it is believed that this is inaccurate because the flood modeling only took into account surface water. This is the case regardless of the amount of water that flows through the stormwater system. In general, the flooded areas that have a depth of 2-3 m are mainly underpasses, whereas the places that have a floodwater depth of 1 m or less are mainly main roads and urban areas. When evaluating the quality of the flood modeling results, it is important not to neglect the quality of the DEM, the numerical techniques that were employed, or the assumptions that were made in the development of the model. Following the execution of the multiplication of (inundation depth × flow velocity), a map was generated, the values of which ranged from 0 to 1.43.

The potential for flooding was then divided into six distinct categories: H1, H2, H3, H4, H5, and H6 vulnerable zones (see Table 23). This classification was based on the Australian flood guide [238,239]. The depth map of the inundated areas, the flow velocity, and the combination of both were categorized according to the same categorization as indicated in the Australian flood guide in order to finally map the flood hazard areas (see Table 24 and Figure 42). Because the resolution of the figures did not allow the full modeled area to be shown on a single map, the decision was made to select certain flood-prone areas that have been inundated in the past. In other words, the locations that have been identified were not chosen at random; rather, they were chosen based on the history of events that have taken place in those places (see Figure 50).

Figure 50. Selected locations to be presented on flood hazard maps.

For instance, during the winter months, every time it rains heavily, water accumulates in Barzani Street in front of the gate to the Council of Ministers, which eventually leads to flooding. Both the locals who live there and the drivers who travel through there will eventually have issues due to the situation (see Figure 51). Detailed explanations of reasons are presented in previous section.

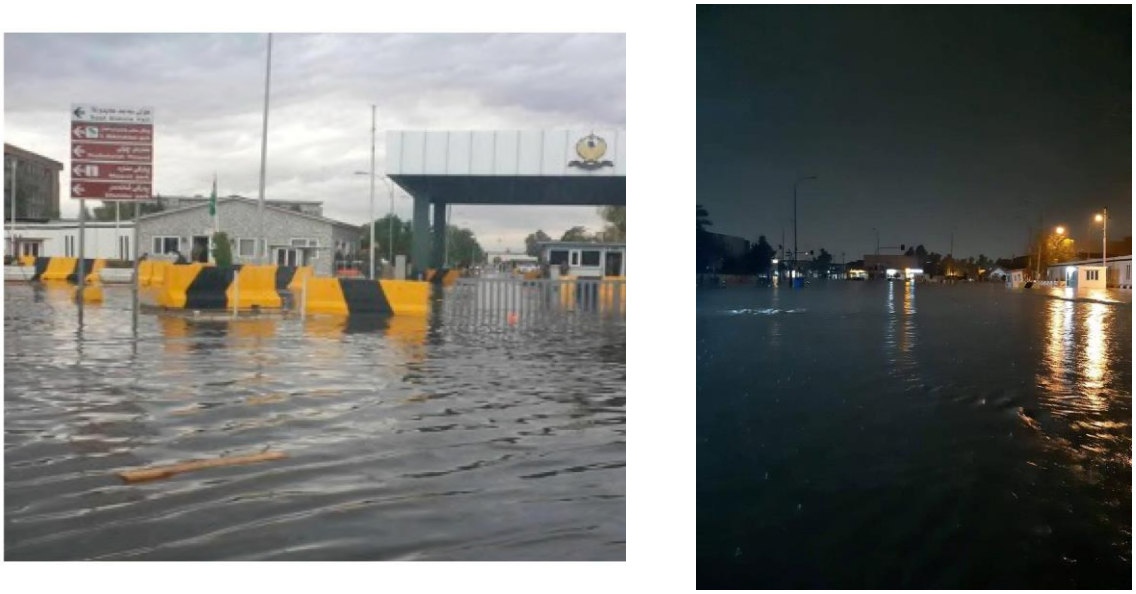

Figure 51. Inundation and water accumulation in Barzani Street in front of the Council of Ministers' gate [30].

Because the inundation depth in the area ranges from 0.3 - 1.2 m, as well as the flow velocity is less than 2 m/s and the combination of inundation and flow velocity is less than 0.3, the zone has been given the H3 classification on the hazard map (Figure 52a, b, c and d). This leads one to believe that the inundation depth was the deciding factor in designating this area as an H3 hazard vulnerability classification. This classification indicates that it is not safe for vehicles, children, and the elderly to be in the area.

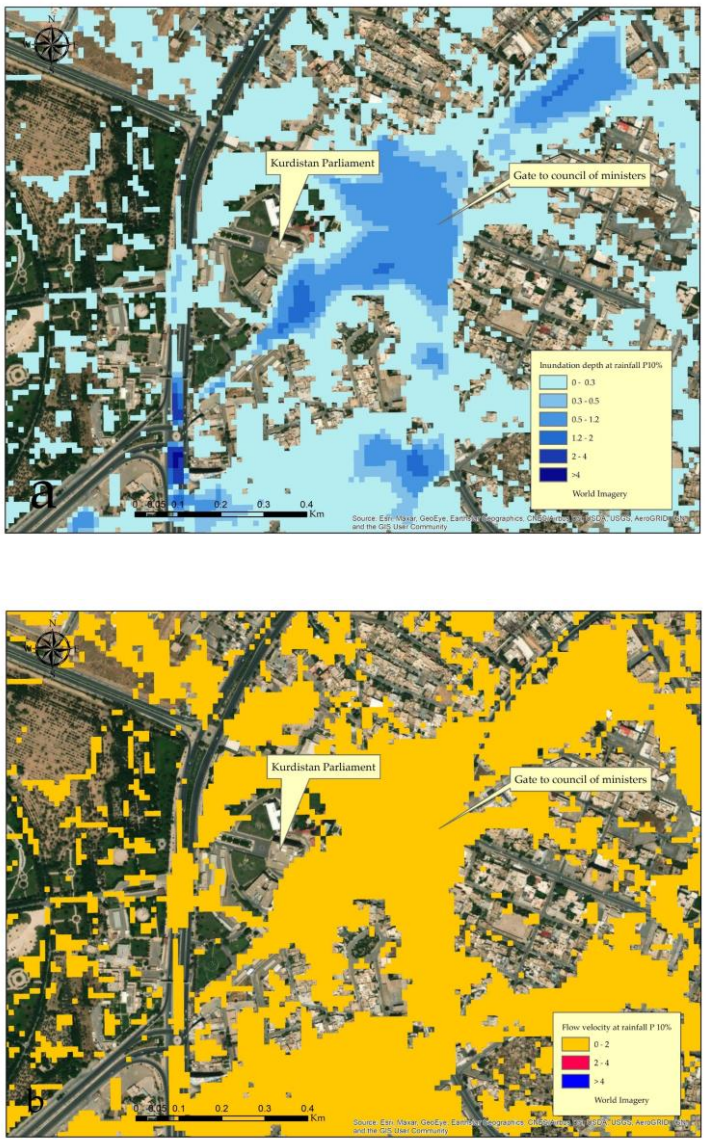

Figure 52. The flood-prone area on Barzani street in front of the gate to the Council of Ministers (a) Inundation depth (m), (b) Flow velocity (m/s), (c) combination of (inundation depth × flow velocity) (d) flood hazard classification map (continued on next page).

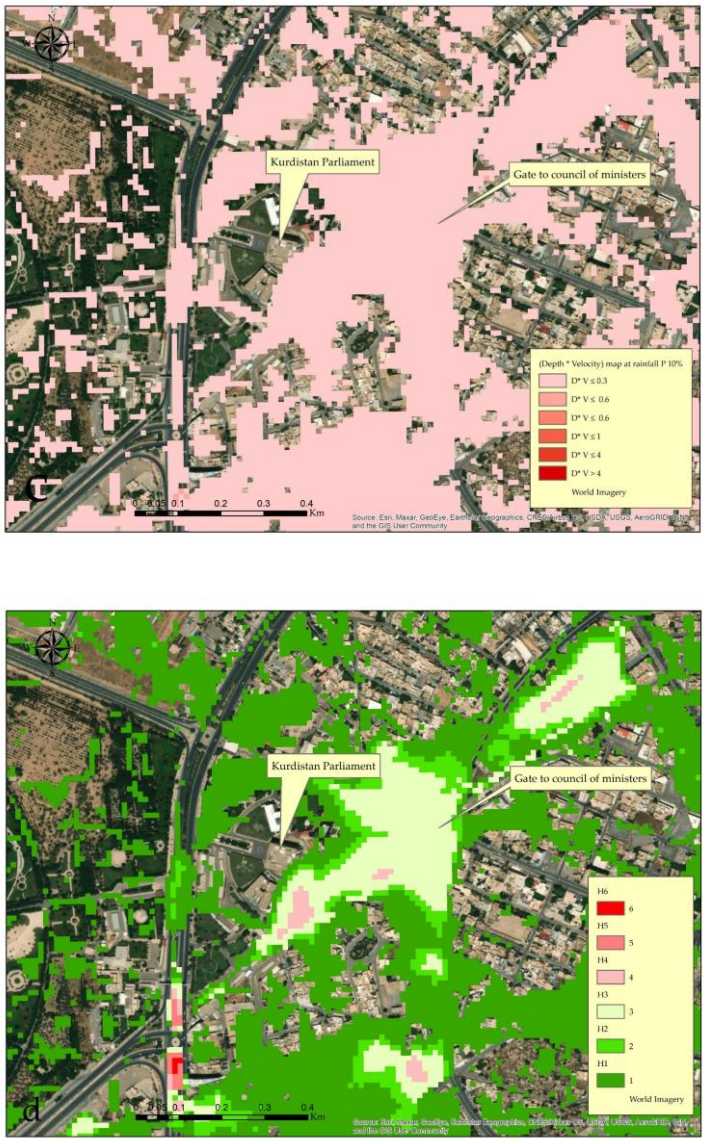

Figure 52. The flood-prone area on Barzani street in front of the gate to the Council of Ministers (**a**) Inundation depth (m), (**b**) Flow velocity (m/s), (**c**) combination of (inundation depth × flow velocity) (**d**) flood hazard classification map.

The repeated flooding that occurred under the Saydawa Bridge is another location that will remain ingrained in the memories of the residents of Erbil, particularly those who live in the Saydawa neighborhood (Figure 53). Previous section provides an in-depth discussion of the factors that led to the accumulation of water at this location. The findings of the flood model reveal that this location is indeed a flood hazard area, and the classification scheme assigns it the H5 category because of this. It is possible to assert that the results of the model are reasonably accurate, as can be seen in Figure 53,

where the depth of the flood is getting close to exceeding 2 meters. This is also evident in Figure 54, which presents a depth map of the areas that were inundated.

Figure 53. Historical flooding and water accumulation under the Saydawa bridge.

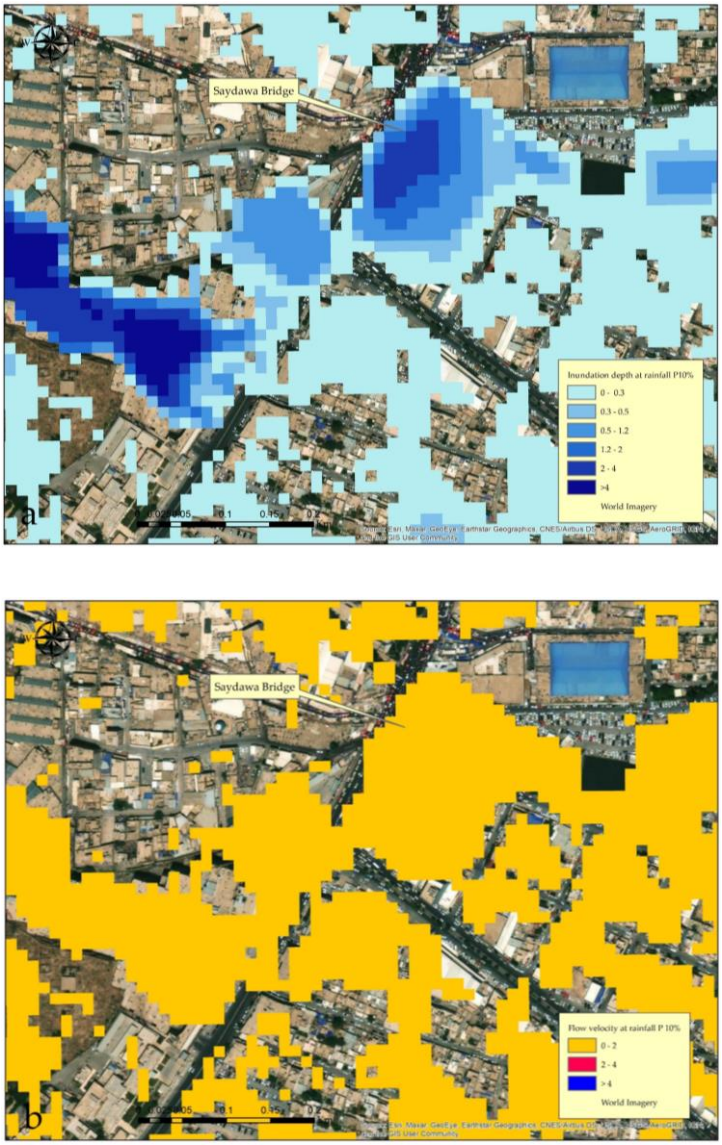

Figure 54. The flood-prone area under Saydawa bridge (a) Inundation depth (m), (b) Flow velocity (m/s), (c) combination of (inundation depth × flow velocity) (d) flood hazard classification map (continued on next page).

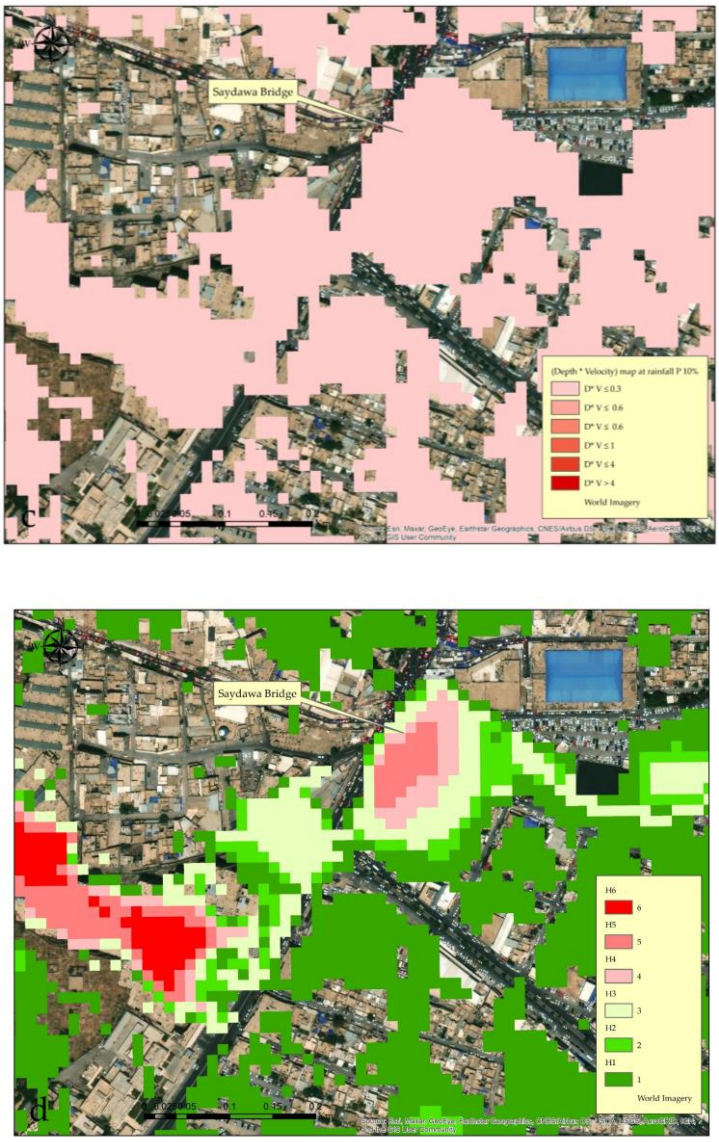

Figure 54. The flood-prone area under Saydawa bridge (**a**) Inundation depth (m), (**b**) Flow velocity (m/s), (**c**) combination of (inundation depth × flow velocity) (**d**) flood hazard classification map

7.4 Conclusions

Climate change is a significant threat to the city of Erbil, as it can cause and exacerbate natural disasters on a large scale, impacting daily life and activities. The previous studies clearly demonstrated the severity of flooding in the area, which is a significant problem in urban areas globally, particularly in developing countries. Flood management is a critical component of water management, and it should be given special attention in the KRI, particularly in the city center of Erbil, where water scarcity solutions are urgently needed. However, due to the city's rapid growth without sufficient funding to

expand and renovate the existing drainage systems, the situation continues to deteriorate. The findings of the study showed that the effects of flash flooding in Erbil are primarily due to the areas' location on waterways. Therefore, serious and practical steps must be taken to mitigate the effects of floods, collect and store runoff water to increase groundwater levels. Currently, some areas of the city face water shortages during warm summer months, and the groundwater level has decreased significantly.

In developing countries, obtaining data for hydrological and hydrodynamic models is a challenging task. Despite facing obstacles and challenges, the study employed the BR technique to construct a hydrodynamic model with cell size (10*10) to prepare for flash floods in areas with a scarcity of data. The observations demonstrated that the BR technique is sufficient for modeling flash floods in regions with limited data. It is essential to recognize the crucial role that data plays in preparing hydrological and hydrodynamic models.

The findings of the study suggest that the Erbil city region is vulnerable to flood hazards, particularly in areas with low-lying topography and high levels of rainfall. The study emphasizes the importance of developing sustainable urban planning and stormwater management strategies to reduce the likelihood of natural disasters and protect human lives and properties.

Overall, the present study contributes to the understanding of flood hazards and their management in urban areas. The study provides insights into the factors that contribute to flood hazards and the strategies that can be employed to manage these risks. The findings of the study have practical implications for urban planners, policymakers, and stakeholders involved in flood risk management in the Erbil city region and beyond.

8. Recommendations and Suggestions for Rain Water Management in Erbil

Certainly, the primary objective of this PhD dissertation was to investigate the factors that have led to an increased likelihood of flooding in Erbil's central district and to determine the root causes of these floods. However, this undertaking also entails pinpointing areas that are vulnerable to such hazards and recommending effective engineering solutions to mitigate the damage caused by previous floods. According to the findings of this study, the suggestions made give priority to the implementation of a strategy for the prevention of flood hazard and the protection of the city and its infrastructure through the maintenance of existing floodwater drainage systems. The following are some of the recommendations that were suggested during the review of the results of the PhD study. These are some of the elements that could be factored into improving the city's drainage system and protecting the city from flooding.

1. Placing a network of automatic meteorological stations across the central district of Erbil and the areas neighbouring it in such a way that they are spatially dispersed in order to better depict the spatial distribution of precipitation across the city.

2. Providing terrain data with a high-resolution DEM in order to re-delineate the hydrological map of the area and draw up realistic sub-basin boundaries. This will significantly affect the identification of topographical factors contributing to flooding.

3. Providing high-resolution satellite imagery so that high-resolution LULC maps can be prepared. It is also useful to recognize and outline all previously flooded areas. Which can be used to create historical flood maps that can be compared with the simulation findings.

4. Placing gauging station, particularly at the outlet of subbasins and the sewer system. This will help hydrologists and environmental scientists in collecting and obtaining data for water resource assessment, planning, development, early flood warning, and river monitoring and hydrologic and hydrodynamic models' validation.

5. Building a network of ponds and reservoirs is one strategy for collecting excess water, which can help prevent or at least delay the onset of flooding. The implementation of a plan to collect water in the north-east and east of the city would make a major contribution to the city's ability to meet the water needs of its residents and agricultural purposes. It would also help in the process of afforestation, which slows down floods and allows them to feed underground reservoirs.

Simultaneously, it would minimize a portion of the floods that are directed towards the city centre. Additionally, to lessen the chaos of the flow and postpone the flow into the city.

6. Cleaning and preserving the width and depth of seasonal streams and drainage lines distributed across the city, particularly in the east, northeast, and southeast areas.

7. A reserve must be established for each stream to prevent development on drainage lines and flood catchments. This reserve must remain in place even after the proposed man-made channels have been constructed. Each project must also include a required analysis of flood risks, including their peaks and catchments, which must be submitted to the proper authorities for approval consideration.

8. More attention should be devoted to the sewer systems, as it is evident that the construction of sewer networks at the city level is not in line with urbanization, population growth, and climate change. This has increased the pressure on the current network. For example, in different places in the city, overflow occurs during rain. This reveals the capacity limitations of the network.

9. The issue of rising runoff has been made worse by the city's uneven distribution of its greenery, which has added to the problem. The rearrangement of the green spaces within the plan of the city is one strategy to decrease the impact that this will have. In this regard, safety measures must to be made in locations that have a higher risk of being flooded.

10. Nature-Based Solutions (NBS) are a type of solution that can be used to increase the capacity of stormwater systems. Some examples of NBS include green roofs, rainwater harvesting systems in the household, permeable surfaces, swales, channels and rills, infiltration trenches, detention and infiltration basins, rain gardens, and retention ponds. All of these solutions can help to reduce the amount of runoff that enters local waterways. Certainty, this decision will be made after analyzing the results of each possible solution using high-resolution models and deciding which alternative is the best fit for the study area.

11. In order to save lives and protect property from the devastation that can be caused by floods, the authorities at the local and regional levels should establish legislation and rules to manage and protect against flooding. It is of the utmost importance to have national policies in place such as these in order to effectively manage flood risk and to increase future flood resilience in areas that are prone to flooding.

12. In the event of flooding, it is crucial that, prior to any wave of rain, especially those that are expected to bring heavy rainfall, officials utilize all available methods of communication with citizens, especially social networks, to alert flood-prone areas. This reduces the potential for loss of life and property.

13. In order to conduct a more precise analysis of urban flooding, the Storm Water Management Model (SWMM) or a coupled model can also be used to evaluate the effectiveness of the current urban drainage system in the city center of Erbil. Due to the absence of GIS-based stormwater lines in Erbil, however, it may be necessary to invest considerable effort. The model is capable of simulating storm events and the subsequent flooding scenarios and will aid the directorate of water and sewer/Erbil in developing an effective drainage system for the city. Filling in the gaps in the current study will result in an entirely new knowledge of the Erbil flooding process in the future, which will assist the government in establishing a more comprehensive flood management and mitigation plan.

14. It is now time to separate the sewage system from the stormwater system. Traditionally, these two systems have been combined in the study area, regarded as an engineering strategy to manage urban drainage.

15. Prepare adaptation and mitigation plans to tackle climate change, not just for floods but also for other natural disasters including drought, water shortages, and heat waves. In actuality, immediate action is required because postponing will incur significantly higher long-term costs.

9. Conclusion

To the best of author's knowledge, this is the first dissertation that has investigated urban flash floods on a systematic level, which means from both a scientific and a practical point of view, in the province of Erbil, and more specifically in the central district. When it is said in a scientific and practical perspective, the scientific intention is to highlight the contributing factors of floods and water accumulation in various areas of the city with each rainfall. Practically, flood hazard maps are necessary to be prepared so that work can be done in collaboration with the authorities to decrease on the possibility of flooding. According to the findings of an analysis of rainfall data, the frequency of extreme rainfalls that have occurred in the past two decades has more than doubled when compared to the previous century. This is evidence that climate change in the region is occurring quickly, and its impacts may be seen clearly. It is also clearly obvious that changes have occurred in the behaviours and distribution of rainfalls as a direct result of climate change. Five of the six events that were investigated were characterized by intense rainfall that lasted for only a short period of time. In situations like these, the requirements for the construction of the sewage system should be revised, and a new synthetic rainfall distribution should be devised. This is because flash floods happened.

The interaction of humans with natural environments frequently enrages the ecosystem, which then responds to this provocation with natural disasters such as floods. Since 2004, Erbil has experienced significant development in terms of both growth and expansion. The residents of the city feel both positivity and concern as a result of this evolution. This expansion is frequently considered to be urban sprawl. In comparison to the previous century, the local's quality of life has improved; nonetheless, the frequency of floods that occur has significantly increased. A significant number of people have the perspective that this is the result of the expansion of the city and that the development in question does not involve the infrastructure of the city, most notably the stormwater system. It was feasible to determine the level of growth in the area by using geospatial techniques, and then show how this type of change affects the hydrological response. This was done so that the area could be better managed. According to the findings, the growth of the city and the increase in the share of built-up areas occurred at the expense of agricultural and green spaces. To put it another way, the expansion of impervious areas has come at the expense of pervious surfaces. As a direct result of this, the probability of flash flooding events is raised, which poses a threat to the overall quality of life in the area that was investigated, particularly in the center of the city.

In order to effectively address the issue of flooding, it is not sufficient to just identify the factors that contribute to the phenomenon; rather, proper scientific and technical solutions need to be

implemented. The application of hydrodynamic models is often required in order to facilitate the process of developing detailed flood inundation maps. The preparation of flood models is not a simple task, as it involves a lot of data, time, and computational resources. However, it faces a large variety of challenges in regions that lack data, particularly in countries that are still developing. For this reason, the utilization of flood modeling techniques that are compatible with the issue of a lack of data and a low quality of the data that is available has been explored as a potential option. There are, in fact, quite a few different software and numerical methods that are used to model urban flooding. However, one must select the type that is suitable for the data that is readily available. It was feasible to test the HEC-RAS 2-D program and determine the mathematical model and building representation technique here by making use of a physical model that had been prepared before, which is known as the Toce River physical model. Unsteady urban flooding can be simulated with the HEC-RAS 2-D model using either one of two different building representation techniques. When it comes to BR technique, the method in question is an accurate representation of building units in numerical simulations that make use of high Manning coefficients. Nevertheless, the BR technique does not provide the same level of accuracy as the BB technique, particularly with regard to velocity prediction. The BR is the technique that is the easiest to apply in comparison to the BB technique, and it is also capable of pretty fast implementation. The work presented here reveals that it is possible to apply the BR technique within the HEC-RAS 2-D to create urban flood models for regions that have a lack of data or poor data quality. This paves the way for the use of DEMs with a lower resolution, such as those that are openly accessible.

A critical challenge that needed to be overcome in order to create an urban flood model for the city of Erbil was the lack of data and resolution of DEMs that were available. However, in light of the findings described in the previous paragraph, a hydrodynamic model of floods in Erbil was developed. Although the results of the model have not been fully validated because there is a lack of necessary data on the outflow hydrographs, it can be said that the results and the locations identified in the model as flood hazard areas are very close to reality. During the preparation of the map of the hazardous areas, it was noticed that the modeling findings are consistent with areas that were flooded or where water accumulated in previous years. The results of a hydrodynamic model that have been prepared should next be interpreted into a map that shows locations that are at vulnerability to flooding. In order to be beneficial to a variety of different groups, including official authorities, insurance companies, and citizens. It is also essential to take special measures to be utilized in future urban design, for example in areas that have a high potential for flooding. Hazardous locations have also been classified with the use of the hazard area categorization that was prepared by the AIDR. It was observed that some

locations within the city were given hazard levels ranging from H1 to H6. This demonstrates that during floods, the city can be hazardous for both its residents and its vehicles and structures.

10. Future Research

This thesis presents a foundation for exploring innovative ideas in the realm of flood dynamics simulations. While the potential opportunities for future research are numerous, some particularly novel areas of exploration include incorporating machine learning techniques to enhance data, developing new methodologies for flood dynamics simulations that utilize alternative data sources (such as satellite imagery or drone footage), and exploring the potential of distributed computing to facilitate more complex simulations.

In addition, research into the effect of microtopography on flood dynamics could also yield significant insights. Incorporating microtopography data, such as DEMs of small-scale features, into flood models has the potential to improve the accuracy and precision of predictions. Moreover, developing a comprehensive understanding of the interaction between microtopography and flood dynamics can also inform better mitigation strategies.

Ultimately, the development of these innovative approaches to flood dynamics simulations has the potential to yield significant advancements in our understanding of flood dynamics and how to mitigate them. By exploring these novel ideas, researchers may be able to develop more comprehensive and accurate models of flood dynamics, which can in turn help communities and policymakers make informed decisions regarding flood risk management.

11. References

1. Leskens, J.; Brugnach, M.; Hoekstra, A.Y.; Schuurmans, W. Why are decisions in flood disaster management so poorly supported by information from flood models? *Environmental modelling & software* **2014**, *53*, 53-61.
2. Parry, M.L.; Canziani, O.; Palutikof, J.; Van der Linden, P.; Hanson, C. *Climate change 2007-impacts, adaptation and vulnerability: Working group II contribution to the fourth assessment report of the IPCC*; Cambridge University Press: 2007; Volume 4.
3. Petit-Boix, A.; Sevigné-Itoiz, E.; Rojas-Gutierrez, L.A.; Barbassa, A.P.; Josa, A.; Rieradevall, J.; Gabarrell, X. Floods and consequential life cycle assessment: Integrating flood damage into the environmental assessment of stormwater Best Management Practices. *Journal of cleaner production* **2017**, *162*, 601-608.
4. CRED. *2021 Distasters in numbers*; Brussels; CRED, 2022; p. 8.
5. Masson-Delmotte, V.; Zhai, P.; Pirani, A.; Connors, S.L.; Péan, C.; Berger, S.; Caud, N.; Chen, Y.; Goldfarb, L.; Gomis, M. Climate change 2021: the physical science basis. *Contribution of working group I to the sixth assessment report of the intergovernmental panel on climate change* **2021**, 2.
6. Kundzewicz, Z.W.; Kanae, S.; Seneviratne, S.I.; Handmer, J.; Nicholls, N.; Peduzzi, P.; Mechler, R.; Bouwer, L.M.; Arnell, N.; Mach, K. Flood risk and climate change: global and regional perspectives. *Hydrological Sciences Journal* **2014**, *59*, 1-28.
7. Winsemius, H.C.; Aerts, J.C.; Van Beek, L.P.; Bierkens, M.F.; Bouwman, A.; Jongman, B.; Kwadijk, J.C.; Ligtvoet, W.; Lucas, P.L.; Van Vuuren, D.P. Global drivers of future river flood risk. *Nature Climate Change* **2016**, *6*, 381-385.
8. CRED. *Natural Disasters 2019: Now is the time to not give up.* ; Brussles: CRED, 2020; p. 8.
9. Fund, I.M. World economic and financial surveys, world economic Outlook database—WEO groups and aggregates information. **2018**.
10. Hu, P.; Zhang, Q.; Shi, P.; Chen, B.; Fang, J. Flood-induced mortality across the globe: Spatiotemporal pattern and influencing factors. *Science of the Total Environment* **2018**, *643*, 171-182.
11. Li, C.-j.; Chai, Y.-q.; Yang, L.-s.; Li, H.-r. Spatio-temporal distribution of flood disasters and analysis of influencing factors in Africa. *Natural Hazards* **2016**, *82*, 721-731.
12. Zarei, M. The water-energy-food nexus: A holistic approach for resource security in Iran, Iraq, and Turkey. *Water-Energy Nexus* **2020**, *3*, 81-94, doi:https://doi.org/10.1016/j.wen.2020.05.004.
13. Al-Ansari, N. Management of water resources in Iraq: perspectives and prognoses. *Engineering* **2013**, *5*, 667-684.
14. Wang, X.; Xia, J.; Dong, B.; Zhou, M.; Deng, S. Spatiotemporal distribution of flood disasters in Asia and influencing factors in 1980–2019. *Natural Hazards* **2021**, *108*, 2721-2738.
15. Ercüment Beyhun, N.; Altintaş, K.m.H.; Noji˙, E.c. Analysis of registered floods in Turkey. *International Journal of Disaster Medicine* **2005**, *3*, 50-54, doi:10.1080/15031430500368485.
16. Bayazıt, Y.; Koç, C.; Bakış, R. Urbanization impacts on flash urban floods in Bodrum Province, Turkey. *Hydrological Sciences Journal* **2021**, *66*, 118-133, doi:10.1080/02626667.2020.1851031.
17. Almazroui, M.; Şen, Z.; Mohorji, A.M.; Islam, M.N. Impacts of Climate Change on Water Engineering Structures in Arid Regions: Case Studies in Turkey and Saudi Arabia. *Earth Systems and Environment* **2019**, *3*, 43-57, doi:10.1007/s41748-018-0082-6.
18. Modarres, R.; Sarhadi, A.; Burn, D.H. Changes of extreme drought and flood events in Iran. *Global and Planetary Change* **2016**, *144*, 67-81, doi:https://doi.org/10.1016/j.gloplacha.2016.07.008.
19. Abdelkarim, A.; Gaber, A.F.D.; Youssef, A.M.; Pradhan, B. Flood Hazard Assessment of the Urban Area of Tabuk City, Kingdom of Saudi Arabia by Integrating Spatial-Based Hydrologic and Hydrodynamic Modeling. *Sensors* **2019**, *19*, 1024.
20. Abdulrazzak, M.; Elfeki, A.; Kamis, A.; Kassab, M.; Alamri, N.; Chaabani, A.; Noor, K. Flash flood risk assessment in urban arid environment: case study of Taibah and Islamic universities' campuses, Medina, Kingdom of Saudi Arabia. *Geomatics, Natural Hazards and Risk* **2019**, *10*, 780-796, doi:10.1080/19475705.2018.1545705.
21. El-Saoud, W.A.; Othman, A. An integrated hydrological and hydraulic modelling approach for flash flood hazard assessment in eastern Makkah city, Saudi Arabia. *Journal of King Saud University - Science* **2022**, *34*, 102045, doi:https://doi.org/10.1016/j.jksus.2022.102045.
22. Elhag, M.; Abdurahman, S.G. Advanced remote sensing techniques in flash flood delineation in Tabuk City, Saudi Arabia. *Natural Hazards* **2020**, *103*, 3401-3413, doi:10.1007/s11069-020-04135-0.

23. Ledraa, T.A.; Al-Ghamdi, A.M. Planning and management issues and challenges of flash flooding disasters in Saudi Arabia: The case of Riyadh City. *J. Archit. Plan* **2020**, *32*, 155-171.
24. Hassan, A.; Albanai, J.A.; Goudie, A. Modeling and managing flash flood Hazards in the State of Kuwait. **2021**.
25. Iraq. Iraqi Constitution. **2005**, 45.
26. Ibrahim, R.I.; Mushatat, S.A.; Abdelmonem, M.G. Erbil. *Cities* **2015**, *49*, 14-25.
27. Gunes, C. *Kurds in a New Middle East*; Springer: 2019.
28. Toperich, S.; Ivanovic, T.; Zagros, N. *Iraqi Kurdistan Region: A Path Forward*; Center for Transatlantic Relations, The Paul H. Nitze School of Advanced: 2017.
29. Mustafa, A.M.; Muhammed, H.; Szydłowski, M. Extreme rainfalls as a cause of urban flash floods; a case study of the Erbil-Kurdistan region of Iraq. *Acta Scientiarum Polonorum Formatio Circumiectus* **2019**, *18*, 113-132.
30. Nanekely, M.; Scholz, M.; Al-Faraj, F. Strategic Framework for Sustainable Management of Drainage Systems in Semi-Arid Cities: An Iraqi Case Study. *Water* **2016**, *8*, doi:10.3390/w8090406.
31. Pirbal, F. *My father's tales*; Bedirxan publisher Erbil, 2007; p. 450.
32. Erbil Govornorate. Erbil history. Available online: https://www.hawlergov.org/app/en/history (accessed on 12.10.2022).
33. Rudaw Meida Network. Flood damages in Erbil. Available online: https://www.rudaw.net/sorani/kurdistan/3010202119 (accessed on April 09, 2022).
34. Rudaw Meida Network. Daily NEWS Available online: https://www.rudaw.net/ (accessed on April 11, 2022).
35. Dottori, F.; Salamon, P.; Bianchi, A.; Alfieri, L.; Hirpa, F.A.; Feyen, L. Development and evaluation of a framework for global flood hazard mapping. *Advances in water resources* **2016**, *94*, 87-102.
36. Grimaldi, S.; Schumann, G.P.; Shokri, A.; Walker, J.; Pauwels, V. Challenges, opportunities, and pitfalls for global coupled hydrologic-hydraulic modeling of floods. *Water Resources Research* **2019**, *55*, 5277-5300.
37. Trigg, M.; Birch, C.; Neal, J.; Bates, P.; Smith, A.; Sampson, C.; Yamazaki, D.; Hirabayashi, Y.; Pappenberger, F.; Dutra, E. The credibility challenge for global fluvial flood risk analysis. *Environmental Research Letters* **2016**, *11*, 094014.
38. Wing, O.E.; Bates, P.D.; Neal, J.C.; Sampson, C.C.; Smith, A.M.; Quinn, N.; Shustikova, I.; Domeneghetti, A.; Gilles, D.W.; Goska, R. A new automated method for improved flood defense representation in large-scale hydraulic models. *Water resources research* **2019**, *55*, 11007-11034.
39. Wing, O.E.; Bates, P.D.; Sampson, C.C.; Smith, A.M.; Johnson, K.A.; Erickson, T.A. Validation of a 30 m resolution flood hazard model of the conterminous U nited S tates. *Water Resources Research* **2017**, *53*, 7968-7986.
40. Sampson, C.C.; Smith, A.M.; Bates, P.D.; Neal, J.C.; Alfieri, L.; Freer, J.E. A high-resolution global flood hazard model. *Water resources research* **2015**, *51*, 7358-7381.
41. Merz, B.; Kreibich, H.; Thieken, A.; Schmidtke, R. Estimation uncertainty of direct monetary flood damage to buildings. *Natural Hazards and Earth System Sciences* **2004**, *4*, 153-163.
42. de Kok, J.-L.; Grossmann, M. Large-scale assessment of flood risk and the effects of mitigation measures along the Elbe River. *Natural Hazards* **2010**, *52*, 143-166, doi:10.1007/s11069-009-9363-6.
43. Gouldby, B. uncertainty and sensitvity analysis method for flood risk analysis. *T24-08-01* **2009**.
44. Oubennaceur, K.; Chokmani, K.; Nastev, M.; Lhissou, R.; El Alem, A. Flood risk mapping for direct damage to residential buildings in Quebec, Canada. *International Journal of Disaster Risk Reduction* **2019**, *33*, 44-54, doi:https://doi.org/10.1016/j.ijdrr.2018.09.007.
45. Dutta, D.; Herath, S.; Musiake, K. A mathematical model for flood loss estimation. *Journal of hydrology* **2003**, *277*, 24-49.
46. Wind, H.; Nierop, T.; De Blois, C.; de Kok, J.-L. Analysis of flood damages from the 1993 and 1995 Meuse floods. *Water resources research* **1999**, *35*, 3459-3465.
47. Meyer, V.; Messner, F. Guidelines for socio-economic flood damage evaluation. **2007**.
48. Gunter, M.M. *Historical dictionary of the Kurds*; Scarecrow Press: 2010; Volume 8.
49. Osman, M. *Kurdistan Region of Iraq Population Analysis Report*; Ministry of Planing, Kurdistan Regional Government: Erbil, 2021; p. 60.
50. Kvočka, D.; Falconer, R.A.; Bray, M. Appropriate model use for predicting elevations and inundation extent for extreme flood events. *Natural Hazards* **2015**, *79*, 1791-1808, doi:10.1007/s11069-015-1926-0.

51. Christensen, J.H.; Christensen, O.B. A summary of the PRUDENCE model projections of changes in European climate by the end of this century. *Climatic Change* **2007**, *81*, 7-30, doi:10.1007/s10584-006-9210-7.
52. Kundzewicz, Z.W.; Mata, L.J.; Arnell, N.W.; DÖLl, P.; Jimenez, B.; Miller, K.; Oki, T.; Şen, Z.; Shiklomanov, I. The implications of projected climate change for freshwater resources and their management. *Hydrological Sciences Journal* **2008**, *53*, 3-10, doi:10.1623/hysj.53.1.3.
53. ten Veldhuis, J.A.E.; Clemens, F.H.L.R.; van Gelder, P.H.A.J.M. Quantitative fault tree analysis for urban water infrastructure flooding. *Structure and Infrastructure Engineering* **2011**, *7*, 809-821, doi:10.1080/15732470902985876.
54. Ashley, R.M.; Balmforth, D.J.; Saul, A.J.; Blanskby, J.D. Flooding in the future – predicting climate change, risks and responses in urban areas. *Water Science and Technology* **2005**, *52*, 265-273, doi:10.2166/wst.2005.0142.
55. Miceli, R.; Sotgiu, I.; Settanni, M. Disaster preparedness and perception of flood risk: A study in an alpine valley in Italy. *Journal of Environmental Psychology* **2008**, *28*, 164-173, doi:https://doi.org/10.1016/j.jenvp.2007.10.006.
56. Szydlowski, M.; Zima, P.; Weinerowska-Bords, K.; Mikos-Studnicka, P.; Hakiel, J.; Szawurska, D. Stormwater and snowmelt runoff storage control and flash flood hazard forecasting in the urbanized coastal basin. In Proceedings of the 14Th International Symposium - Water Management and Hydraulic Engineering 2015, 2015, 2015; pp. 141-150.
57. Arnbjerg-Nielsen, K.; Leonardsen, L.; Madsen, H. Evaluating adaptation options for urban flooding based on new high-end emission scenario regional climate model simulations. *Climate Research* **2015**, *64*, 73-84.
58. Majewski, W. Urban flash flood in Gdansk - 2001. Case study. *Meteorology Hydrology and Water Management* **2016**, *04*, 41-49.
59. Ruin, I.; Lutoff, C.; Boudevillain, B.; Creutin, J.-D.; Anquetin, S.; Rojo, M.B.; Boissier, L.; Bonnifait, L.; Borga, M.; Colbeau-Justin, L.; et al. Social and Hydrological Responses to Extreme Precipitations: An Interdisciplinary Strategy for Postflood Investigation. *Weather, Climate, and Society* **2014**, *6*, 135-153, doi:10.1175/wcas-d-13-00009.1.
60. Smith, B.; Rodriguez, S. Spatial Analysis of High-Resolution Radar Rainfall and Citizen-Reported Flash Flood Data in Ultra-Urban New York City. *Water* **2017**, *9*, doi:10.3390/w9100736.
61. Bisht, D.S.; Chatterjee, C.; Kalakoti, S.; Upadhyay, P.; Sahoo, M.; Panda, A. Modeling urban floods and drainage using SWMM and MIKE URBAN: a case study. *Natural Hazards* **2016**, *84*, 749-776, doi:10.1007/s11069-016-2455-1.
62. Joo, J.; Kjeldsen, T.; Kim, H.-J.; Lee, H. A comparison of two event-based flood models (ReFH-rainfall runoff model and HEC-HMS) at two Korean catchments, Bukil and Jeungpyeong. *KSCE Journal of Civil Engineering* **2014**, *18*, 330-343, doi:10.1007/s12205-013-0348-3.
63. Youssef, A.M.; Sefry, S.A.; Pradhan, B.; Alfadail, E.A. Analysis on causes of flash flood in Jeddah city (Kingdom of Saudi Arabia) of 2009 and 2011 using multi-sensor remote sensing data and GIS. *Geomatics, Natural Hazards and Risk* **2016**, *7*, 1018-1042, doi:10.1080/19475705.2015.1012750.
64. Ávila, A.D.; Carvajal, Y.E.; Justino, F. Representative rainfall thresholds for flash floods in the Cali river watershed, Colombia. *Natural Hazards and Earth System Sciences Discussions* **2015**, *3*, 4095-4119, doi:10.5194/nhessd-3-4095-2015.
65. Al-Amri, N.S.; Subyani, A.M. Generation of rainfall intensity duration frequency (IDF) curves for ungauged sites in arid region. *Earth Systems and Environment* **2017**, *1*, 1-12.
66. Dehghani, M.; Salehi, S.; Mosavi, A.; Nabipour, N.; Shamshirband, S.; Ghamisi, P. Spatial analysis of seasonal precipitation over Iran: Co-variation with climate indices. *ISPRS International Journal of Geo-Information* **2020**, *9*, 73.
67. Dupont, B.; Allen, D.L. *Revision of the Rainfall-intensity Duration Curves for the commonwealth of Kentucky*; University of Kentucky Transportation Center: 1999.
68. Koutsoyiannis, D.; Kozonis, D.; Manetas, A. A mathematical framework for studying rainfall intensity-duration-frequency relationships. *Journal of Hydrology* **1998**, *206*, 118-135.
69. Bell, F.C. Generalized rainfall-duration-frequency relationships. *Journal of the hydraulics division* **1969**, *95*, 311-328.
70. Chen, C.-l. Rainfall intensity-duration-frequency formulas. *Journal of Hydraulic Engineering* **1983**, *109*, 1603-1621.

71. Hershfield, D.M. Estimating the probable maximum precipitation. *Journal of the hydraulics Division* **1961**, *87*, 99-116.
72. Miller, J.; Frederick, R.; Tracey, R. Precipitation frequency atlas of the conterminous western United States (by states). *US National Weather Service NOAA Atlas* **1973**, *2*.
73. Nhat, L.M.; Tachikawa, Y.; Takara, K. Establishment of intensity-duration-frequency curves for precipitation in the monsoon area of Vietnam. *Annuals of Disas. Prev. Res. Inst* **2006**, 93-103.
74. Singh, V.P.; Zhang, L. IDF curves using the Frank Archimedean copula. *Journal of hydrologic engineering* **2007**, *12*, 651-662.
75. Lima, C.H.R.; Kwon, H.-H.; Kim, Y.-T. A local-regional scaling-invariant Bayesian GEV model for estimating rainfall IDF curves in a future climate. *Journal of Hydrology* **2018**, *566*, 73-88.
76. Kristvik, E.; Johannessen, B.G.; Muthanna, T.M. Temporal Downscaling of IDF Curves Applied to Future Performance of Local Stormwater Measures. *Sustainability* **2019**, *11*, 1231.
77. Noor, M.; Ismail, T.; Shahid, S.; Asaduzzaman, M.; Dewan, A. Evaluating intensity-duration-frequency (IDF) curves of satellite-based precipitation datasets in Peninsular Malaysia. *Atmospheric Research* **2021**, *248*, 105203.
78. Ombadi, M.; Nguyen, P.; Sorooshian, S.; Hsu, K.-l. Developing Intensity-Duration-Frequency (IDF) Curves From Satellite-Based Precipitation: Methodology and Evaluation. *Water Resources Research* **2018**, *54*, 7752-7766.
79. Al-Khalaf, H. Predicting short-duration, high-intensity rainfall in Saudi Arabia. King Fahd University of Petroleum and Minerals (Saudi Arabia), 1997.
80. Al-Shaikh, A. Rainfall frequency studies for Saudi Arabia [M. Sc. thesis]. *Riyadh: Civil Engineering Department, King Saud University* **1985**.
81. AlHassoun, S.A. Developing an empirical formulae to estimate rainfall intensity in Riyadh region. *Journal of King Saud university-engineering sciences* **2011**, *23*, 81-88.
82. Dakheel, A.A. Drawing curves of the rainfall intensity duration frequency (IDF) and assessment equation intensity rainfall for Nasiriyah city, Iraq. *University of Thi-Qar Journal* **2017**, *12*, 63-82.
83. Deger, İ.; Yuce, M. Rainfall Intensity-Duration-Frequency Analysis for the City of Gaziantep. In Proceedings of the International Civil Engineering and Architecture Conference, Trabzon, Turkey, 17-20 April 2019, 2019; pp. 760-766.
84. Elsebaie, I.H. Developing rainfall intensity–duration–frequency relationship for two regions in Saudi Arabia. *Journal of King Saud University-Engineering Sciences* **2012**, *24*, 131-140.
85. Hadadin, N.A. Rainfall intensity-duration-frequency relationship in the Mujib Basin in Jordan. *Journal of Applied Sciences* **2005**, *5*, 1777-1784.
86. Hamaamin, Y.A. Developing of Rainfall Intensity-Duration-Frequency Model for Sulaimani City. *Journal of Zankoy Sulaimani* **2017**, *19*, p10634.
87. Hasan, I.F.; Saeed, Y.N. Analysis of Rainfall Data for a Number of Stations in Northern Iraq. *Al-Rafidain Engineering Journal (AREJ)* **2020**, *25*, 105-117.
88. Jalee, L.A.; Farawn, M.A. Developing rainfall intensity-duration-freqency relationship for Basrah City. *Kufa Journal of Engineering* **2013**, *5*.
89. Mahdi, E.S.; Mohamedmeki, M.Z. Analysis of rainfall intensity-duration-frequency (IDF) curves of Baghdad city. In Proceedings of the IOP Conference Series: Materials Science and Engineering, 2020; p. 012066.
90. Majeed, A.R.; Nile, B.K.; Al-Baidhani, J.H. Selection of suitable PDF model and build of IDF curves for rainfall in Najaf city, Iraq. In Proceedings of the Journal of Physics: Conference Series, 2021; p. 012184.
91. Şen, Z. Annual daily maximum rainfall-based IDF curve derivation methodology. *Earth Systems and Environment* **2019**, *3*, 463-469.
92. Kareem, D.A.; M Amen, A.R.; Mustafa, A.; Yüce, M.I.; Szydłowski, M. Comparative Analysis of Developed Rainfall Intensity–Duration–Frequency Curves for Erbil with Other Iraqi Urban Areas. *Water* **2022**, *14*, 419.
93. Dile, Y.T.; Srinivasan, R. Evaluation of CFSR climate data for hydrologic prediction in data-scarce watersheds: an application in the Blue Nile River Basin. *JAWRA Journal of the American Water Resources Association* **2014**, *50*, 1226-1241, doi:10.1111/jawr.12182.
94. Fuka, D.R.; Walter, M.T.; MacAlister, C.; Degaetano, A.T.; Steenhuis, T.S.; Easton, Z.M. Using the Climate Forecast System Reanalysis as weather input data for watershed models. *Hydrological Processes* **2013**, *28*, 5613-5623, doi:10.1002/hyp.10073.

95. Huff, F.A. Time distribution of rainfall in heavy storms. *Water Resources Research* **1967**, *3*, 1007-1019, doi:10.1029/WR003i004p01007.
96. Nascimento, N.d.O.; Balbi, D.A.F.; Naghettini, M. Modeling the Time Distributions of Heavy Storms - Design Hyetographs. In Proceedings of the Building Partnerships, 2004; pp. 1-10.
97. Bezak, N.; Šraj, M.; Rusjan, S.; Mikoš, M. Impact of the Rainfall Duration and Temporal Rainfall Distribution Defined Using the Huff Curves on the Hydraulic Flood Modelling Results. *Geosciences* **2018**, *8*, doi:10.3390/geosciences8020069.
98. Glickman, T.S. *Glossary of meteorology - American Meteorological Society*; American Meteorological Soc.: Boston, Mass., 2000.
99. Weibull, W. A statistical distribution function of wide applicability. *Journal of applied mechanics* **1951**.
100. Banasik, K.; Wałęga, A.; Węglarczyk, S.; Więzik, B. *Metodyki obliczania przepływów i opadów maksymalnych o o sobie prawdopodobieństwo przewysszenia dla zlewni kontrolowanych i niekontrolowanych oraz identyfikacji model transformacji opadu w odpływ (Methods for calculating flows and maximum rainfall, the probability of being exceeded for controlled and uncontrolled catchments and identifying the model of the transformation of precipitation into outflow)*; Warszawa, 2017.
101. Stedinger, J.R. Frequency analysis of extreme events. *Handbook of hydrology* **1993**.
102. Ramaseshan, S. Urban hydrology in different climatic conditions. *Lecture notes of the international course on urban drainage in developing countries, Regional engineering college, Warangal, India* **1996**.
103. Gumbel, E.J. The Return Period of Flood Flows. *The Annals of Mathematical Statistics* **1941**, *12*, 163-190.
104. Gumbel, E.J. *Statistics of extremes*; Columbia university press: 1958.
105. Te Chow, V. *Applied hydrology*; Tata McGraw-Hill Education: 1988.
106. Oyebande, L. Deriving rainfall intensity-duration-frequency relationships and estimates for regions with inadequate data. *Hydrological Sciences Journal* **1982**, *27*, 353-367.
107. Salman, S.A.; Shahid, S.; Ismail, T.; Rahman, N.b.A.; Wang, X.; Chung, E.-S. Unidirectional trends in daily rainfall extremes of Iraq. *Theoretical and applied climatology* **2018**, *134*, 1165-1177.
108. Al-Ansari, N. Topography and climate of Iraq. *Journal of Earth Sciences and Geotechnical Engineering* **2021**, *11*, 1-13.
109. Du, P.; Liu, P.; Xia, J.; Feng, L.; Liu, S.; Tan, K.; Cheng, L. Remote sensing image interpretation for urban environment analysis: methods, system and examples. *Remote Sensing* **2014**, *6*, 9458-9474.
110. Hussein, K.; Alkaabi, K.; Ghebreyesus, D.; Liaqat, M.U.; Sharif, H.O. Land use/land cover change along the Eastern Coast of the UAE and its impact on flooding risk. *Geomatics, Natural Hazards and Risk* **2020**, *11*, 112-130.
111. Duncan, J.; Stow, D.; Franklin, J.; Hope, A. Assessing the relationship between spectral vegetation indices and shrub cover in the Jornada Basin, New Mexico. *International Journal of Remote Sensing* **1993**, *14*, 3395-3416.
112. Fromard, F.; Vega, C.; Proisy, C. Half a century of dynamic coastal change affecting mangrove shorelines of French Guiana. A case study based on remote sensing data analyses and field surveys. *Marine Geology* **2004**, *208*, 265-280.
113. Muttitanon, W.; Tripathi, N. Land use/land cover changes in the coastal zone of Ban Don Bay, Thailand using Landsat 5 TM data. *International Journal of Remote Sensing* **2005**, *26*, 2311-2323.
114. Gautam, N.; Chennaiah, G.C. Land-use and land-cover mapping and change detection in Tripura using satellite LANDSAT data. *International Journal of Remote Sensing* **1985**, *6*, 517-528.
115. König, H.J.; Schuler, J.; Suarma, U.; McNeill, D.; Imbernon, J.; Damayanti, F.; Dalimunthe, S.A.; Uthes, S.; Sartohadi, J.; Helming, K. Assessing the impact of land use policy on urban-rural sustainability using the FoPIA approach in Yogyakarta, Indonesia. *Sustainability* **2010**, *2*, 1991-2009.
116. Swangjang, K.; Iamaram, V. Change of land use patterns in the areas close to the airport development area and some implicating factors. *Sustainability* **2011**, *3*, 1517-1530.
117. Tian, Y.; Yin, K.; Lu, D.; Hua, L.; Zhao, Q.; Wen, M. Examining land use and land cover spatiotemporal change and driving forces in Beijing from 1978 to 2010. *Remote Sensing* **2014**, *6*, 10593-10611.
118. Topaloğlu, R.H.; Sertel, E.; Musaoğlu, N. ASSESSMENT OF CLASSIFICATION ACCURACIES OF SENTINEL-2 AND LANDSAT-8 DATA FOR LAND COVER/USE MAPPING. *International archives of the photogrammetry, remote sensing & spatial Information Sciences* **2016**, *41*.
119. Hansen, M.C.; Loveland, T.R. A review of large area monitoring of land cover change using Landsat data. *Remote sensing of Environment* **2012**, *122*, 66-74.

120. Masek, J.G.; Huang, C.; Wolfe, R.; Cohen, W.; Hall, F.; Kutler, J.; Nelson, P. North American forest disturbance mapped from a decadal Landsat record. *Remote Sensing of Environment* **2008**, *112*, 2914-2926.
121. Thomas, N.E.; Huang, C.; Goward, S.N.; Powell, S.; Rishmawi, K.; Schleeweis, K.; Hinds, A. Validation of North American forest disturbance dynamics derived from Landsat time series stacks. *Remote Sensing of Environment* **2011**, *115*, 19-32.
122. Hussein, S.O.; Kovács, F.; Tobak, Z.; Abdullah, H.J. Spatial distribution of vegetation cover in Erbil city districts using high-resolution Pléiades satellite image. *Acta Geographica Debrecina Landscape & Environment* **2018**, *12*, 10-22.
123. Hamad, R. A remote sensing and GIS-based analysis of urban sprawl in Soran District, Iraqi Kurdistan. *SN Applied Sciences* **2020**, *2*, 24.
124. Houghton, R.A. Revised estimates of the annual net flux of carbon to the atmosphere from changes in land use and land management 1850–2000. *Tellus B* **2003**, *55*, 378-390.
125. Dewan, A.M.; Yamaguchi, Y. Land use and land cover change in Greater Dhaka, Bangladesh: Using remote sensing to promote sustainable urbanization. *Applied geography* **2009**, *29*, 390-401.
126. Dewan, A.M.; Yamaguchi, Y. Using remote sensing and GIS to detect and monitor land use and land cover change in Dhaka Metropolitan of Bangladesh during 1960–2005. *Environmental monitoring and assessment* **2009**, *150*, 237.
127. Jat, M.K.; Garg, P.K.; Khare, D. Monitoring and modelling of urban sprawl using remote sensing and GIS techniques. *International journal of Applied earth Observation and Geoinformation* **2008**, *10*, 26-43.
128. Mundia, C.N.; Aniya, M. Dynamics of landuse/cover changes and degradation of Nairobi City, Kenya. *Land Degradation & Development* **2006**, *17*, 97-108.
129. Aburas, M.M.; Ho, Y.M.; Ramli, M.F.; Ash'aari, Z.H. Monitoring and assessment of urban growth patterns using spatio-temporal built-up area analysis. *Environmental monitoring and assessment* **2018**, *190*, 156.
130. Ali, J.M.; Marsh, S.H.; Smith, M.J. A comparison between London and Baghdad surface urban heat islands and possible engineering mitigation solutions. *Sustainable Cities and Society* **2017**, *29*, 159-168.
131. Wałęga, A.; Radecki-Pawlik, A.; Cupak, A.; Hathaway, J.; Pukowiec, M. Influence of Changes of Catchment Permeability and Frequency of Rainfall on Critical Storm Duration in an Urbanized Catchment—A Case Study, Cracow, Poland. *Water* **2019**, *11*, 2557.
132. Szydłowski, M. Hydraulic analysis of causes of washout of Gdynia-Orłowo sea-shore during the flood in the Kacza river estuary. *Polish Maritime Research* **2019**.
133. Zope, P.; Eldho, T.; Jothiprakash, V. Impacts of land use–land cover change and urbanization on flooding: A case study of Oshiwara River Basin in Mumbai, India. *Catena* **2016**, *145*, 142-154.
134. Abdouli, K.A.; Hussein, K.; Ghebreyesus, D.; Sharif, H.O. Coastal Runoff in the United Arab Emirates—The Hazard and Opportunity. *Sustainability* **2019**, *11*, 5406.
135. Ali, P.; Bohloul, A.; Hosein, M. The effect of the land use/cover changes on the floods of the Madarsu Basin of Northeastern Iran. *Journal of Water Resource and Protection* **2010**, *2010*.
136. Apollonio, C.; Balacco, G.; Novelli, A.; Tarantino, E.; Piccinni, A.F. Land use change impact on flooding areas: The case study of Cervaro Basin (Italy). *Sustainability* **2016**, *8*, 996.
137. Batunacun; Nendel, C.; Hu, Y.; Lakes, T. Land-use change and land degradation on the Mongolian Plateau from 1975 to 2015—A case study from Xilingol, China. *Land Degradation & Development* **2018**, *29*, 1595-1606.
138. Sanyal, J.; Densmore, A.; Carboneau, P. Analyzing the effect of land-use/cover changes at sub-catchment levels on downstream flood peaks: a semi-distributed modeling approach with sparse data. *Catena* **2014**, *118*, 28-40.
139. Sharif, H.O.; Al-Juaidi, F.H.; Al-Othman, A.; Al-Dousary, I.; Fadda, E.; Jamal-Uddeen, S.; Elhassan, A. Flood hazards in an urbanizing watershed in Riyadh, Saudi Arabia. *Geomatics, Natural Hazards and Risk* **2016**, *7*, 702-720.
140. Hameed, H.M. Estimating the effect of urban growth on annual runoff volume using GIS in the Erbil sub-basin of the Kurdistan Region of Iraq. *Hydrology* **2017**, *4*, 12.
141. Mustafa, A.; Szydłowski, M. The impact of spatiotemporal changes in land development (1984–2019) on the increase in the runoff coefficient in Erbil, Kurdistan Region of Iraq. *Remote Sensing* **2020**, *12*, 1302.
142. Eastman, J. *IDRISI Kilimanjaro guide to GIS and image processing. Manual version 14.00*; 2003.

143. Bailly, J.; Arnaud, M.; Puech, C. Boosting: a classification method for remote sensing. *International Journal of Remote Sensing* **2007**, *28*, 1687-1710.
144. Jensen, J.R. Thematic information extraction: pattern recognition. *Introductory Digital Image Processing: A Remote Sensing Perspective* **2005**, 337-406.
145. Liu, X.-H.; Skidmore, A.; Van Oosten, H. Integration of classification methods for improvement of land-cover map accuracy. *ISPRS Journal of Photogrammetry and Remote Sensing* **2002**, *56*, 257-268.
146. Dissanayake, D.; Morimoto, T.; Ranagalage, M.; Murayama, Y. Land-use/land-cover changes and their impact on surface urban heat islands: Case study of Kandy City, Sri Lanka. *Climate* **2019**, *7*, 99.
147. Ranagalage, M.; Wang, R.; Gunarathna, M.; Dissanayake, D.; Murayama, Y.; Simwanda, M. Spatial forecasting of the landscape in rapidly urbanizing hill stations of South Asia: A case study of Nuwara Eliya, Sri Lanka (1996–2037). *Remote Sensing* **2019**, *11*, 1743.
148. Scharffenberg, W.A.; Fleming, M.J. Hydrologic Modeling System-HEC-HMS-User's Manual-Version 2.0. **2000**.
149. NRCS, U. National engineering handbook: Part 630—hydrology. *USDA Soil Conservation Service: Washington, DC, USA* **2004**, 11-15.
150. Mockus, V. National engineering handbook. *US Soil Conservation Service: Washington, DC, USA* **1964**, *4*.
151. Cunge, J. On the subject of a flood propagation computation method (Musklngum method). *Journal of Hydraulic Research* **1969**, *7*, 205-230.
152. Story, M.; Congalton, R.G. Accuracy assessment: a user's perspective. *Photogrammetric Engineering and remote sensing* **1986**, *52*, 397-399.
153. Tung, F.; LeDrew, E. The determination of optimal threshold levels for change detection using various accuracy indexes. *Photogrammetric Engineering and Remote Sensing* **1988**, *54*, 1449-1454.
154. KRG. *Ministry of planning. Regional statistical office. Erbil: Statistic Year Book*; 2013.
155. Huong, H.T.L.; Pathirana, A. Urbanization and climate change impacts on future urban flooding in Can Tho city, Vietnam. *Hydrology and Earth System Sciences* **2013**, *17*, 379.
156. Nirupama, N.; Simonovic, S.P. Increase of flood risk due to urbanisation: a Canadian example. *Natural Hazards* **2007**, *40*, 25.
157. Saghafian, B.; Farazjoo, H.; Bozorgy, B.; Yazdandoost, F. Flood intensification due to changes in land use. *Water resources management* **2008**, *22*, 1051-1067.
158. Ávila, A.; Carvajal, Y.; Justino, F. Representative rainfall thresholds for flash floods in the Cali river watershed, Colombia. *Natural Hazards and Earth System Sciences Discussions* **2015**, *3*, 4095-4119.
159. Rajeevan, M.; Bhate, J.; Jaswal, A.K. Analysis of variability and trends of extreme rainfall events over India using 104 years of gridded daily rainfall data. *Geophysical research letters* **2008**, *35*.
160. Ruin, I.; Lutoff, C.; Boudevillain, B.; Creutin, J.-D.; Anquetin, S.; Rojo, M.B.; Boissier, L.; Bonnifait, L.; Borga, M.; Colbeau-Justin, L. Social and Hydrological responses to extreme precipitations: an interdisciplinary strategy for postflood investigation. *Weather, climate, and society* **2014**, *6*, 135-153.
161. Szpakowski, W.; Szydłowski, M. Evaluating the Catastrophic Rainfall of 14 July 2016 in the Catchment Basin of the Urbanized Strzyza Stream in Gdańsk, Poland. *Polish Journal of Environmental Studies* **2018**, *27*.
162. Yilmaz, A.G. The effects of climate change on historical and future extreme rainfall in Antalya, Turkey. *Hydrological Sciences Journal* **2015**, *60*, 2148-2162.
163. Sanyal, J.; Densmore, A.L.; Carbonneau, P. Analysing the effect of land-use/cover changes at sub-catchment levels on downstream flood peaks: A semi-distributed modelling approach with sparse data. *Catena* **2014**, *118*, 28-40.
164. Shrestha, M.N. Spatially distributed hydrological modelling considering land-use changes using remote sensing and GIS. In Proceedings of the Map Asia Conference, 2003; pp. 1-8.
165. Abderrezzak, K.E.K.; Paquier, A.; Mignot, E. Modelling flash flood propagation in urban areas using a two-dimensional numerical model. *Natural Hazards* **2009**, *50*, 433-460.
166. Cunge, J.A. Of data and models. *Journal of Hydroinformatics* **2003**, *5*, 75-98.
167. Hunter, N.M.; Bates, P.D.; Horritt, M.S.; Wilson, M.D. Simple spatially-distributed models for predicting flood inundation: a review. *Geomorphology* **2007**, *90*, 208-225.
168. Costabile, P.; Costanzo, C.; Macchione, F. Performances and limitations of the diffusive approximation of the 2-d shallow water equations for flood simulation in urban and rural areas. *Applied Numerical Mathematics* **2017**, *116*, 141-156.

169. Dottori, F.; Todini, E. Testing a simple 2D hydraulic model in an urban flood experiment. *Hydrological Processes* **2013**, *27*, 1301-1320.
170. Fewtrell, T.J.; Duncan, A.; Sampson, C.C.; Neal, J.C.; Bates, P.D. Benchmarking urban flood models of varying complexity and scale using high resolution terrestrial LiDAR data. *Physics and Chemistry of the Earth, Parts A/B/C* **2011**, *36*, 281-291.
171. Hunter, N.; Bates, P.; Neelz, S.; Pender, G.; Villanueva, I.; Wright, N.; Liang, D.; Falconer, R.A.; Lin, B.; Waller, S. Benchmarking 2D hydraulic models for urban flooding. In Proceedings of the Proceedings of the Institution of Civil Engineers-Water Management, 2008; pp. 13-30.
172. Prestininzi, P. Suitability of the diffusive model for dam break simulation: Application to a CADAM experiment. *Journal of Hydrology* **2008**, *361*, 172-185.
173. Yu, D.; Lane, S.N. Urban fluvial flood modelling using a two-dimensional diffusion-wave treatment, part 1: mesh resolution effects. *Hydrological Processes: An International Journal* **2006**, *20*, 1541-1565.
174. Pilotti, M.; Milanesi, L.; Bacchi, V.; Tomirotti, M.; Maranzoni, A. Dam-Break Wave Propagation in Alpine Valley with HEC-RAS 2D: Experimental Cancano Test Case. *Journal of Hydraulic Engineering* **2020**, *146*, 05020003.
175. Teng, J.; Jakeman, A.J.; Vaze, J.; Croke, B.F.; Dutta, D.; Kim, S. Flood inundation modelling: A review of methods, recent advances and uncertainty analysis. *Environmental Modelling & Software* **2017**, *90*, 201-216.
176. Néelz, S.; Pender, G. Benchmarking of 2D hydraulic modelling packages. **2010**.
177. Apel, H.; Aronica, G.T.; Kreibich, H.; Thieken, A.H. Flood risk analyses—how detailed do we need to be? *Natural Hazards* **2009**, *49*, 79-98.
178. Mignot, E.; Paquier, A.; Haider, S. Modeling floods in a dense urban area using 2D shallow water equations. *Journal of Hydrology* **2006**, *327*, 186-199.
179. Pina, R.D.; Ochoa-Rodriguez, S.; Simões, N.E.; Mijic, A.; Marques, A.S.; Maksimović, Č. Semi-vs. fully-distributed urban stormwater models: model set up and comparison with two real case studies. *water* **2016**, *8*, 58.
180. Yu, D.; Lane, S.N. Interactions between subgrid-scale resolution, feature representation and grid-scale resolution in flood inundation modelling. *Hydrological Processes* **2011**, *25*, 36-53.
181. Costabile, P.; Costanzo, C.; De Lorenzo, G.; Macchione, F. Is local flood hazard assessment in urban areas significantly influenced by the physical complexity of the hydrodynamic inundation model? *Journal of Hydrology* **2020**, *580*, 124231.
182. Néelz, S.; Pender, G. Benchmarking the latest generation of 2D hydraulic modelling packages. *Environment Agency, Horison House, Deanery Road, Bristol, BS1 9AH* **2013**.
183. Abdelkarim, A.; Gaber, A.F.; Youssef, A.M.; Pradhan, B. Flood Hazard Assessment of the Urban Area of Tabuk City, Kingdom of Saudi Arabia by Integrating Spatial-Based Hydrologic and Hydrodynamic Modeling. *Sensors* **2019**, *19*, 1024.
184. David, A.; Schmalz, B. Flood hazard analysis in small catchments: Comparison of hydrological and hydrodynamic approaches by the use of direct rainfall. *Journal of Flood Risk Management* **2020**, *13*, e12639.
185. Haltas, I.; Tayfur, G.; Elci, S. Two-dimensional numerical modeling of flood wave propagation in an urban area due to Ürkmez dam-break, İzmir, Turkey. *Natural Hazards* **2016**, *81*, 2103-2119.
186. Marko, K.; Elfeki, A.; Alamri, N.; Chaabani, A. Two Dimensional Flood Inundation Modelling in Urban Areas Using WMS, HEC-RAS and GIS (Case Study in Jeddah City, Saudi Arabia). In Proceedings of the Conference of the Arabian Journal of Geosciences, 2018; pp. 265-267.
187. Rangari, V.A.; Umamahesh, N.; Bhatt, C. Assessment of inundation risk in urban floods using HEC RAS 2D. *Modeling Earth Systems and Environment* **2019**, *5*, 1839-1851.
188. Surwase, T.; Manjusree, P. Urban flood simulation-A case study of Hyderabad city. In Proceedings of the National Conference on Flood Early Warning for Disaster Risk Reduction,(June), 2019; pp. 133-143.
189. Syafri, R.R.; Hadi, M.P.; Suprayogi, S. Hydrodynamic Modelling of Juwana River Flooding Using HEC-RAS 2D. In Proceedings of the IOP Conference Series: Earth and Environmental Science, 2020; p. 012028.
190. Szydłowski, M. Hydraulic analysis of causes of washout of Gdynia-Orłowo sea-shore during the flood in the Kacza river estuary. *Polish Maritime Research* **2019**, *26*, 174-182.
191. Yalcin, E. Assessing the impact of topography and land cover data resolutions on two-dimensional HEC-RAS hydrodynamic model simulations for urban flood hazard analysis. *Natural Hazards* **2020**, 1-23.

192. Quirogaa, V.M.; Kurea, S.; Udoa, K.; Manoa, A. Application of 2D numerical simulation for the analysis of the February 2014 Bolivian Amazonia flood: Application of the new HEC-RAS version 5. *Ribagua* **2016**, *3*, 25-33.
193. Costabile, P.; Costanzo, C.; Ferraro, D.; Macchione, F.; Petaccia, G. Performances of the new HEC-RAS version 5 for 2-D hydrodynamic-based rainfall-runoff simulations at basin scale: Comparison with a state-of-the art model. *Water* **2020**, *12*, 2326.
194. Ghimire, E.; Sharma, S.; Lamichhane, N. Evaluation of one-dimensional and two-dimensional HEC-RAS models to predict flood travel time and inundation area for flood warning system. *ISH Journal of Hydraulic Engineering* **2020**, 1-17.
195. Shrestha, A.; Bhattacharjee, L.; Baral, S.; Thakur, B.; Joshi, N.; Kalra, A.; Gupta, R. Understanding Suitability of MIKE 21 and HEC-RAS for 2D Floodplain Modeling. In *World Environmental and Water Resources Congress 2020*; 2020; pp. 237-253.
196. Soares-Frazão, S.; Zech, Y. Dam-break flow through an idealised city. *Journal of Hydraulic Research* **2008**, *46*, 648-658.
197. Jeong, W.; Yoon, J.-S.; Cho, Y.-S. Numerical study on effects of building groups on dam-break flow in urban areas. *Journal of Hydro-Environment Research* **2012**, *6*, 91-99.
198. Li, Z.; Liu, J.; Mei, C.; Shao, W.; Wang, H.; Yan, D. Comparative Analysis of Building Representations in TELEMAC-2D for Flood Inundation in Idealized Urban Districts. *Water* **2019**, *11*, 1840.
199. Testa, G.; Zuccalà, D.; Alcrudo, F.; Mulet, J.; Soares-Frazão, S. Flash flood flow experiment in a simplified urban district. *Journal of Hydraulic Research* **2007**, *45*, 37-44.
200. Szydłowski, M. Numerical simulation of extreme flooding in a built-up area. *Archives of hydro-engineering and environmental mechanics* **2005**, *52*, 321-333.
201. Beretta, R.; Ravazzani, G.; Maiorano, C.; Mancini, M. Simulating the influence of buildings on flood inundation in urban areas. *Geosciences* **2018**, *8*, 77.
202. Mustafa, A.; Szydłowski, M. Application of different building representation techniques in HEC-RAS 2-D for urban flood modeling using the Toce River experimental case. *PeerJ* **2021**, *9*, e11667, doi:10.7717/peerj.11667.
203. Brunner, G.W. *HEC-RAS River Analysis System, 2D Hydraulic reference manual, Version 6.0*; US Army Corps of Engineers—Hydrologic Engineering Center: Davis, 2021.
204. Aronica, G.; Lanza, L. Drainage efficiency in urban areas: a case study. *Hydrological Processes: An International Journal* **2005**, *19*, 1105-1119.
205. Brown, J.D.; Spencer, T.; Moeller, I. Modeling storm surge flooding of an urban area with particular reference to modeling uncertainties: A case study of Canvey Island, United Kingdom. *Water Resources Research* **2007**, *43*.
206. Gallien, T.; Schubert, J.; Sanders, B. Predicting tidal flooding of urbanized embayments: A modeling framework and data requirements. *Coastal Engineering* **2011**, *58*, 567-577.
207. Schubert, J.E.; Sanders, B.F. Building treatments for urban flood inundation models and implications for predictive skill and modeling efficiency. *Advances in Water Resources* **2012**, *41*, 49-64.
208. Brunner, G.W.C.-H. *HEC-RAS river analysis system 2D modeling user's manual*; US Army Corps of Engineers—Hydrologic Engineering Center: Davis, 2021.
209. Mason, D.C.; Horritt, M.S.; Hunter, N.M.; Bates, P.D. Use of fused airborne scanning laser altimetry and digital map data for urban flood modelling. *Hydrological Processes: An International Journal* **2007**, *21*, 1436-1447.
210. Schubert, J.E.; Sanders, B.F.; Smith, M.J.; Wright, N.G. Unstructured mesh generation and landcover-based resistance for hydrodynamic modeling of urban flooding. *Advances in Water Resources* **2008**, *31*, 1603-1621.
211. Tsubaki, R.; Fujita, I. Unstructured grid generation using LiDAR data for urban flood inundation modelling. *Hydrological Processes: An International Journal* **2010**, *24*, 1404-1420.
212. Guinot, V. Multiple porosity shallow water models for macroscopic modelling of urban floods. *Advances in Water Resources* **2012**, *37*, 40-72.
213. Bear, J. Dynamics of fluids in porous media Dover Publications. *INC, New York* **1988**.
214. Kim, B.; Sanders, B.F.; Famiglietti, J.S.; Guinot, V. Urban flood modeling with porous shallow-water equations: A case study of model errors in the presence of anisotropic porosity. *Journal of Hydrology* **2015**, *523*, 680-692.
215. Horritt, M.S.; Bates, P.D. Effects of spatial resolution on a raster based model of flood flow. *Journal of Hydrology* **2001**, *253*, 239-249.

216. Kim, B.; Sanders, B.F.; Schubert, J.E.; Famiglietti, J.S. Mesh type tradeoffs in 2D hydrodynamic modeling of flooding with a Godunov-based flow solver. *Advances in Water Resources* **2014**, *68*, 42-61.
217. Soares-Frazão, S.; Lhomme, J.; Guinot, V.; Zech, Y.J.J.o.H.R. Two-dimensional shallow-water model with porosity for urban flood modelling. **2008**, *46*, 45-64.
218. Godunov, S.K. A difference scheme for numerical computation of discontinuous solutions of fluid dynamics. *Mat. Sb* **1959**, *47*, 271-306.
219. Ferrari, A.; Viero, D.P.; Vacondio, R.; Defina, A.; Mignosa, P. Flood inundation modeling in urbanized areas: A mesh-independent porosity approach with anisotropic friction. *Advances in water resources* **2019**, *125*, 98-113.
220. Galasso, C.; Senarath, S.U.S. A Statistical Model for Flood Depth Estimation in Southeast Europe. In *Vulnerability, Uncertainty, and Risk*; 2014; pp. 1415-1424.
221. Loudyi, D.; Kantoush, S.A. Flood risk management in the Middle East and North Africa (MENA) region. *Urban Water Journal* **2020**, *17*, 379-380, doi:10.1080/1573062X.2020.1777754.
222. Doocy, S.; Daniels, A.; Murray, S.; Kirsch, T.D. The human impact of floods: a historical review of events 1980-2009 and systematic literature review. *PLoS currents* **2013**, *5*.
223. Löwe, R.; Mair, M.; Pedersen, A.N.; Kleidorfer, M.; Rauch, W.; Arnbjerg-Nielsen, K. Impacts of urban development on urban water management–limits of predictability. *Computers, Environment and Urban Systems* **2020**, *84*, 101546.
224. Gizaw, M.S.; Gan, T.Y. Possible impact of climate change on future extreme precipitation of the Oldman, Bow and Red Deer River Basins of Alberta. *International Journal of Climatology* **2016**, *36*, 208-224, doi:https://doi.org/10.1002/joc.4338.
225. Jiang, R.; Gan, T.Y.; Xie, J.; Wang, N.; Kuo, C.-C. Historical and potential changes of precipitation and temperature of Alberta subjected to climate change impact: 1900–2100. *Theoretical and Applied Climatology* **2017**, *127*, 725-739, doi:10.1007/s00704-015-1664-y.
226. Courty, L.G.; Wilby, R.L.; Hillier, J.K.; Slater, L.J. Intensity-duration-frequency curves at the global scale. *Environmental Research Letters* **2019**, *14*, 084045.
227. Noor, M.; Ismail, T.; Chung, E.-S.; Shahid, S.; Sung, J.H. Uncertainty in Rainfall Intensity Duration Frequency Curves of Peninsular Malaysia under Changing Climate Scenarios. *Water* **2018**, *10*, 1750.
228. Shahabul Alam, M.; Elshorbagy, A. Quantification of the climate change-induced variations in Intensity–Duration–Frequency curves in the Canadian Prairies. *Journal of Hydrology* **2015**, *527*, 990-1005, doi:https://doi.org/10.1016/j.jhydrol.2015.05.059.
229. Bouwer, L.M.; Bubeck, P.; Aerts, J.C.J.H. Changes in future flood risk due to climate and development in a Dutch polder area. *Global Environmental Change* **2010**, *20*, 463-471, doi:https://doi.org/10.1016/j.gloenvcha.2010.04.002.
230. Ritchie, H.; Roser, M. Natural disasters. *Our World in Data* **2014**.
231. Relifeweb. Iraq: Flash Floods - Dec 2021. Available online: https://reliefweb.int/disaster/fl-2021-000208-irq (accessed on 31.01.2022).
232. Erbil Govornorate. Media Statement. Available online: https://www.hawlergov.org/app/ku/node/2146 (accessed on 31.01.2022).
233. Li, J.; Wong, D.W. Effects of DEM sources on hydrologic applications. *Computers, Environment and urban systems* **2010**, *34*, 251-261.
234. NRCS, U. Chapter 7–Hydrologic Soil Groups in: NRCS–National Engineering Handbook (NEH), Part 630–Hydrology. *USDA NRCS, Washington, DC* **2009**, 7.1-7.5.
235. Chow, V.T. Open-channel hydraulics. *McGraw-Hill civil engineering series* **1959**.
236. Cronshey, R. *Urban hydrology for small watersheds*; US Department of Agriculture, Soil Conservation Service, Engineering Division: 1986.
237. UNISDR. *Words into Action Guidelines, National Disaster Risk Assessment – Governance Systems, Methodologies and Use of Data*; United Nations Office for Disaster Risk Reduction: Geneva, 2017.
238. AIDR. Managing the Floodplain: A Guide to Best Practice in Flood Risk Management in Australia. **2017**, *Guidline 7-3*, 30.
239. Smith, G.P.; Davey, E.K.; Cox, R.J. *Flood Hazard Guideline, Technical report 2014/07*; Water Research Laboratory, University of New South Wales: Australia, Manly Vale, 2014.
240. Yalcin, E. Assessing the impact of topography and land cover data resolutions on two-dimensional HEC-RAS hydrodynamic model simulations for urban flood hazard analysis. *Natural Hazards* **2020**, *101*, 995-1017.

241. Surwase, T.; SrinivasaRao, G.; Manjusree, P.; Begum, A.; Nagamani, P.; JaiSankar, G. Flood inundation simulation of Mahanadi River, Odisha during September 2008 by using HEC-RAS 2D model. In Proceedings of the Proceedings of International Conference on Remote Sensing for Disaster Management, 2019; pp. 851-863.
242. Sissakian, V.K.; Al-Ansari, N.; Adamo, N.; Abdul Ahad, I.D.; Abed, S.A. Flood Hazards in Erbil City Kurdistan Region Iraq, 2021: A Case Study. *Engineering* **2022**, *14*, 591-601.
243. Gigović, L.; Pamučar, D.; Bajić, Z.; Drobnjak, S. Application of GIS-interval rough AHP methodology for flood hazard mapping in urban areas. *Water* **2017**, *9*, 360.
244. Khaing, Z.M.; Zhang, K.; Sawano, H.; Shrestha, B.B.; Sayama, T.; Nakamura, K. Flood hazard mapping and assessment in data-scarce Nyaungdon area, Myanmar. *PLoS One* **2019**, *14*, e0224558.
245. Merz, B.; Thieken, A.; Gocht, M. Flood risk mapping at the local scale: concepts and challenges. In *Flood risk management in Europe*; Springer: 2007; pp. 231-251.
246. Luo, P.; Mu, D.; Xue, H.; Ngo-Duc, T.; Dang-Dinh, K.; Takara, K.; Nover, D.; Schladow, G. Flood inundation assessment for the Hanoi Central Area, Vietnam under historical and extreme rainfall conditions. *Scientific reports* **2018**, *8*, 1-11.
247. Pinos, J.; Timbe, L. Performance assessment of two-dimensional hydraulic models for generation of flood inundation maps in mountain river basins. *Water science and engineering* **2019**, *12*, 11-18.
248. Zin, W.W.; Kawasaki, A.; Win, S. River flood inundation mapping in the Bago River Basin, Myanmar. *Hydrological Research Letters* **2015**, *9*, 97-102.